Variability and Changes of Hydrography and Circulation in the Subpolar Southern Ocean

Matthis Auger

THÈSE DE DOCTORAT
DE SORBONNE UNIVERSITÉ

Spécialité : Océanographie Physique

École doctorale : “Sciences de l’Environnement d’Île-de-France”

réalisée au

Laboratoire d’Océanographie et du Climat
Expérimentations et Approches Numériques

présentée par

Matthis AUGER

pour obtenir le grade de

DOCTEUR DE SORBONNE UNIVERSITÉ

Variability and Changes of Hydrography and Circulation in the Subpolar Southern Ocean

date de soutenance prévue le 31 Janvier 2022

devant le jury composé de

Pr. Damien CARDINAL	Sorbonne Université, LOCEAN, Paris	*Président*
Pr. Sarah GILLE	Scripps Insitution of Oceanography, San Diego, California	*Rapportrice*
Pr. Andrew THOMPSON	California Institute of Technology, Pasadena, California	*Rapporteur*
Dr. Rosemary MORROW	Université Paul Sabatier, LEGOS, Toulouse	*Examinatrice*
Pr. Michael MEREDITH	British Antarctic Survey, Cambridge	*Examinateur*
Dr. Pierre PRANDI	Collecte Localisation Satellite, Toulouse	*Examinateur*
Dr. Jean-Baptiste SALLEE	CNRS, Sorbonne Université, LOCEAN, Paris	*Directeur de thèse*

Acknowledgements

During this Ph.D., I have met lots of people without whom the work presented here wouldn't have been possible.

I am first very grateful to Jean-Baptiste Sallée, my main supervisor, for trusting me since the beginning of this Ph.D. Thank you JB, for your scientific help and pertinence, your motivational speeches. Thank you for the discussions we had and the way you always managed to help me refocus on the important things when I was spreading myself too thin. I am also very grateful to Pierre Prandi, my co-supervisor. Thank you, Pierre, for your patience when I was frequently showing up at your desk seeking help and the way you supported me back when I was at CLS. Thank both of you for always being there when I needed, and for the way you constantly promoted my work. I could not have hoped for better supervisors.

I would also like to thank the members of the "Team Polaire". I am so glad to have been part of this group of very enthusiastic people. Thank you for these Thursday science meetings where we would not ever talk about science. Thank you Lucie, Etienne, Yona, Amélie, Sara, Camille, Audrey, Kenza, Saurabh, Linus. Thank you more broadly to the people of the LOCEAN, where I spent my last two years of Ph.D. Considering the context of these two years, I'm glad to still have had the opportunity to meet and collaborate in any way with many of you.

Thank you to the people of CLS, and particularly to the Earth Observation team. Thank you Yannice, Antoine, Maxime, Guillaume, Marie-Isabelle, Jean-Christophe, Fanny, for your help during this first year of my Ph.D. at CLS.

I am very grateful as well to my Master thesis supervisors, Rosemary Morrow and Elodie Kestenare. Thank you, Rosemary, for everything you have done for me, from recommending me to JB for this thesis or making me sail to Antarctica. Elodie, it all started with a call with you. Thank you for trusting me since the beginning and for having been so available and helpful back when I was at the LEGOS. I am also grateful to Alberto Naveira Garabato for being a member of my Ph.D. committee with Rosemary. Thank you for your always valuable inputs.

I would like to aknowledge the CNES as well, for funding my thesis and supporting my work along the years. Thank you Anne, Gerald, Nicolas, Amandine for the interesting discussions.

Finally, I would like to thank Sarah Gille and Andrew Thompson for accepting to review the manuscript, Rosemary Morrow and Michael Meredith for accepting to be examinators, and Damien Cardinal for being the president of the jury of my Ph.D. Thanks to all of you.

Remerciements

Je voudrais d'abord remercier ma famille qui m'a soutenu au cours de cette thèse et dans tous les choix que j'ai fait jusqu'ici. Merci à ma mère, et à mon père, qui m'ont toujours persuadé que je pourrais atteindre mes objectifs et croire en moi. Merci à tous les deux de me pousser à faire ce que je dois faire tout an me motivant à faire ce que j'ai envie de faire. Merci pour tout ce que vous faites pour me rendre la vie plus facile.

Merci Cloé d'être toujours présente pour moi, que ce soit pour être ma reliseuse officielle ou pour tout et n'importe quoi ! Merci de faire le lien entre la famille et moi quand je commence a m'enfermer un peu trop dans mon truc. Je suis content qu'on ait pu se retrouver à Paris ces deux dernières années et j'espère qu'on continuera à le faire malgré nos futurs vagabondages ! Merci au reste de la famille pour leur soutient sans réserve.

Merci aux djeuns LOCEAN. Bravo à Lucie de m'avoir fait perdre un maximum de temps de thèse (la recherche : dé-stonks) mais de la meilleure des manières. Meilleure décision de squatter ton bureau, on a bien rigolé. J'ai à mon tour fait perdre énormément de temps de thèse à Léa : merci de m'avoir accueilli dans ton bureau dans mes moments de saturation (quand tu n'es pas en mer, soit à peu la moitié de l'année). Merci à Antoine pour les improbables sessions cigare/whisky/Ritz, Sarah pour les jeudis tant pis et les excès de vitesse sur l'autoroute du rire. Merci à Coco pour les débriefs du matin et les potins. Merci à Lucile petit ange de la fast-ice partie trop tôt, et Clément petit ange des fronts parti trop souvent. Merci à Amélie de récupérer toutes mes secondes mains, à Etienne pour ton enthousiasme, tout le temps, partout et pour n'importe quoi ! Sara, vivement notre duo krill/manchot, je n'en peux plus d'attendre. Melissa, tu ne fais pas partie du LOCEAN mais un peu quand même, j'attends impatiemment l'écriture de notre recueil de citations. Damien, tes perfomance de hula hoop resteront gravées à jamais dans ma tête. Yoyo, ma jumelle de thèse, merci d'avoir souffert et rigolé avec moi. Merci à Gaston de supporter mon addiction chronique aux fléchettes. Pas merci à Clovis pour son café mais merci pour le reste. Merci à Camille pour le compte rendu quasi-quotidien de la météo en Haute-Savoie et 1 an de photos de montagnes (!). Merci à Chabert pour les discussions intelligentes et celles qui le sont beaucoup moins. 7 ans qu'on se suit, et je sais pas trop comment mais j'espère que ça va continuer. C'est marrant évoluer avec toi m'a aussi aidé à me comprendre mieux moi-même. Merci au GGK (Gina, Georges, Kenza) pour le bureau avec le plus d'ambiance au LOCEAN (ambiance avec le GGK : + + + / ambiance sans le GGK : - - -). Merci aussi à Robin, Diego, Léa, Yang, Brady, Léo, Sara, Yang, et tous ceux que je n'ai pas cité. Merci également à JB encore, Juliette, Martin, Jean-Benoit, Gilles, Jacqueline, Matlab, Christophe, Patrice.

Merci encore à l'équipe CLS, Pierre, Yannice, Maxime, Fred, Guillaume, Marie-Isabelle, Elodie, Philippe, Jean-François, Jean-Christophe, Thibault, pour les pauses cafés et les sessions course à pied sur le canal du midi.

Merci également à tous ceux qui n'ont pas été directement lié à ma thèse, mais dont la présence pendant ces trois années m'a permis de me sentir soutenu et entouré. Merci à Julien, Tristan, Hugo. 11 ans qu'on se connait et tout est toujours pareil qu'au premier jour ! Théo, Sam, Maxime, Fannack, Arthur, Pasto, Dorian, toujours là depuis si longtemps bateau. Merci à Estelle d'avoir toujours tant à raconter et de me maintenir au courant de toute la vie de la communauté Illacaise. Merci à l'Enstafari et plus largement la communauté Brestoise et ses week-ends qui font tout oublier. Merci à Bazar, Razo, Caro, Roro, Valentin, Léo, Jean, Amélie, Rémy, Marie, Quentin, Sanchez, Tim, Antoine, Vincent, Babeth, Kekette, Enora, Marc Marc, Patxi Marine, Cléo, Elliot, Clothilde, Charles, Julia et tous les autres. Merci à Caroline pour tout.

Enfin, merci à tous ceux que je n'ai pas cité mais que j'ai pu croiser au fil des années.

Scientific activities during the Ph.D.

Publications in peer-reviewed scientific journals

[1] **Auger M.**, Morrow, R., Kestenare, E., Sallée JB., Cowley R. (2021) *Southern Ocean in-situ temperature trends over 25 years emerge from interannual variability*, Nature Communications, DOI : 10.1038/s41467-020-20781-1

[2] **Auger, M.**, Prandi, P., Sallée, JB., *Southern Ocean Sea Level Anomaly in the Sea Ice Covered Sector From Multimission Satellite Observations* [In review at Scientific Data]

[3] **Auger, M.**, Sallée, JB., Prandi, P., Naveira Garabato, A.C., *Southern Ocean Seasonal Variability in the Sea Ice-Covered Sector From Multi-mission Satellite Observations of Sea Level Anomaly* [In review at Journal of Geophysical Research : Oceans]

[4] **Auger, M.**, Sallée, JB., Prandi, P., Pauthenet, E., *Southern Ocean Ice-Covered Eddy properties from satellite altimetry* [In preparation]

[5] Lauber, J., Hattermann, T., de Steur, L., Darelius, E., **Auger, M.**, Sallée JB., Prandi, P., *Observed inflow of warm water below Fimbulisen from 2016 to 2019 explained by large-scale atmospheric and oceanic variability* [In preparation]

Datasets Published

[1] **Auger M.**, Morrow, R., Kestenare, E., Sallée JB., Cowley R. (2021) Vertical sections of in-situ temperature over 25 years in the Southern Ocean Data set, SEDOO. DOI : 10.6096/11

[2] **Auger, M.**, Prandi, P., Sallée, JB., Daily Southern Ocean Sea Level Anomaly And Geostrophic Currents from multimission altimetry, 2013-2019 Data set, SEANOE. DOI : 10.17882/81032

Also available as

[2] **Auger, M.**, Prandi, P., Sallée, JB., Gridded Sea Level Heights and Geostrophic Currents - Antarctic Ocean, AVISO, available at https ://www.aviso.altimetry.fr/en/data/products/sea-surface-height-products/regional/antarctic-ocean-gridded-sea-level-heights.html

Summer School

Fluid Dynamics of Sustainability and the Environment, at the *Ecole Polytechnique*. 39h of courses, 24 hours of projects. Summer 2019.

Courses

Club de Lecture, *LOCEAN* (10h)

Seminar "Changement climatique : science, politique, société", *Ecole Normale Supérieure* (24h)

MOOC "Monitoring Atmospheric Composition", *EUMETSAT* (15h)

MOOC "Communiquer efficacement à l'écrit", *ED 129* (18h)

Activities in the Laboratory

Implementation of the PhD students seminars at the LOCEAN ; consisting in monthly sessions with two presentations from PhD students destinated to all the members of the laboratory. Started in 2021.

Oceanographic Expedition

December 2021 : SURVOSTRAL ; 20 days onboard of *l'Astrolabe*. From Hobart (Tasmania) to Dumont d'Urville (Antarctica). Responsible for TSG and XBTs.

Scientific Communications

Outreach :

[1] L'Océan Austral Se Réchauffe en Profondeur, Matthis Auger, *Les Echos Planète*, Outreach paper, 2021.

Press Coverage :

[1] Southern Ocean waters are warming faster than thought, threatening Antarctic ice, *The Washington Post*, Journal Article, 2021.

[2] Antarctique : les scientifiques observent « un réchauffement rapide et marqué des eaux en profondeur.», *Futura Sciences*, Journal Article, 2021.

[3] L'Antarctique se réchauffe et fait craindre la fonte de la calotte glaciaire, *Natura Sciences*, Journal Article, 2021.

[4] Réchauffement dans les profondeurs de l'Antarctique, *RTS (Radio Télévision Suisse)*, Radio Podcast and Interview, 2021.

[5] En Antarctique, l'océan se réchauffe plus vite que prévu, *France Culture*, Radio Podcast, 2021.

[6] The Earth Observer, *NASA The Earth Observer*, p15-16, on the satellite altimetry data processing, 2021.

Seminars :

Auger M., Sallée JB., Prandi P., *New Insights Into The Ice-Covered Southern Ocean Circulation From Multi - Altimeter Combination* (Oral Session) SO-CHIC general assembly, 2020, Online.

International Conferences :

Auger M., Prandi P., Sallée JB. *Multi-altimeter combination for the retrieval of sea surface height in the ice-covered Southern Ocean* (Oral Session) 51st International Liege Colloquium on Ocean Dynamics, 2019, Liège, Belgium.

Auger M., Prandi P., Sallée JB. *Sea Level Anomaly from a Multi-Altimeter Combination in the Ice-Covered Southern Ocean* (Keynote Oral Session) Ocean Surface Topography Science Team Meeting 2019, Chicago, USA.

Auger M., Sallée JB., Prandi P., *New Insights Into The Ice-Covered Southern Ocean Circulation From Multi - Altimeter Combination* (Oral Session) Ocean Sciences Meeting 2020, San Diego, USA.

Auger M., Sallée JB., Prandi P., *New Insights Into The Ice-Covered Southern Ocean Circulation From Multi - Altimeter Combination* (Keynote Oral Session) European Polar Science Week 2020, Online.

Auger M., Sallée JB., Prandi P., *New Insights Into The Ice-Covered Southern Ocean Circulation From Multi - Altimeter Combination* (Oral Session) Cryosat 10th Anniversary, 2021, Online.

Auger M., Sallée JB., Prandi P., *New Insights Into The Ice-Covered Southern Ocean Circulation From Multi - Altimeter Combination* (vPICO Presentation) EGU General Assembly 2021, Online.

Abstract

The Southern Ocean is central to the global oceanic circulation and climate. This region is however on the frontline of human-induced climate change, through intense uptake of anthropogenic heat and carbon. Consequently, the Southern Ocean has experienced important changes in its hydrography and circulation over the last decades. Its subpolar part, south of the Antarctic Circumpolar Current, hosts large circulation systems of importance for the production of water masses and their associate heat and carbon content, for ocean interactions with sea-ice and ice-shelves, and consequently for global mean sea level. Observations are still sparse in that region, particularly in wintertime when it is covered by sea ice. Thus, the regional response of the subpolar Southern Ocean hydrography and circulation to interactions with the atmosphere, cryosphere, and background circulation at various spatial and time scales is still under active research.

In this thesis, I contribute to observing the variability and long-term changes of the hydrography and circulation of the subpolar Southern Ocean, and to unveil the mechanisms driving their variability. I first observe the long-term temperature changes in the upper layer of the Southern Ocean, from repeated ship-based measurement transects over 25 years. Besides previously documented trends, I refine the monitoring on the still poorly observed warming and shallowing of the warm subsurface water of the Southern Ocean. The long term warming is stronger than interannual variability, and the shallowing rate is 3 to 9 times the previously estimated one. In a second part, I develop and exploit an ocean topography dataset, spanning six years of measurements over the whole Southern Ocean south of 50°S. This dataset allows me to explore the variability of the subpolar Southern Ocean circulation, particularly the seasonal cycle of the large-scale circulation and the mesoscale variability under sea ice. At the seasonal scale, the circulation of the Weddell and Ross gyres, and the Antarctic Slope Current are mainly dictated by three modes of variability, principally linked to the surface stress of the wind on the surface of the ocean and its modulation by the sea ice. The mesoscale variability is weak outside the energetic Antarctic slope current in the pack ice, while the marginal ice zone seems to be a region with enhanced cyclonic eddies generation. The implications of these results on the physical processes of the Southern Ocean and its long-term changes are discussed.

Keywords : Southern Ocean, Subpolar circulation, temperature trends, long term changes, satellite altimetry, seasonal variability, mesoscale variability, ocean-atmosphere-cryosphere interactions.

Résumé

L'océan Austral est une région centrale pour la circulation océanique globale et le climat. Il est cependant également en première ligne du changement climatique, notamment par son absorption importante de chaleur et de carbone anthropique. Par conséquent, l'océan Austral a connu de grands changements dans sa structure hydrographique et sa circulation dans les dernières décennies.

Sa région subpolaire, au sud du courant circumpolaire Antarctique, abrite une circulation grande échelle importante pour la production des masses d'eau et leur contenu de chaleur et de carbone, pour les interactions océaniques avec la banquise et les plateformes glaciaires, avec des conséquences sur l'élévation du niveau de la mer. C'est également une région très peu observée, en particulier en hiver lorsque celle-ci est couverte par la banquise. Par conséquent, la réponse locale de la circulation et de la structure hydrographique de l'océan Austral subpolaire à des interactions avec l'atmosphère, la cryosphère et la grande échelle est toujours sujette à de nombreuses recherches.

Dans cette thèse, je contribue à observer la variabilité et les changements à long terme de l'hydrographie et de la circulation de l'océan Austral subpolaire, et à documenter les mécanismes qui contrôlent leur variabilité. J'observe d'abord les changements à long terme de la température de la couche supérieure de l'océan Austral, à partir de transects répétés par bateau pendant 25 années. En plus des changements déjà bien documentés, je montre le réchauffement et la remontée des eaux chaudes de subsurface, à une vitesse plus importante qu'estimée auparavant et de façon plus forte que la variabilité interannuelle. Je présente ensuite un jeu de données de hauteur de mer, qui consiste en six années de mesures sur l'ensemble de l'océan Austral au sud de 50°S. Ce jeu de données me permet d'explorer la variabilité de la circulation de l'océan Austral subpolaire, et notamment sur le cycle saisonnier de la circulation grande échelle et de l'activité méso-échelle sous la glace. À l'échelle saisonnière, la circulation des gyres de Weddell, de Ross et le courant de pente Antarctique sont principalement dictés par trois modes de variabilités, reliés à la tension de vent en surface et sa modulation par la glace de mer. La circulation de méso-échelle est faible sous la banquise hors du courant de pente Antarctique, alors que la zone marginale de glace semble favoriser la génération de tourbillons cycloniques. Les implications de ces résultats pour les mécanismes physiques de l'océan Austral et ses changements à long terme sont discutées.

Mots-clés : Océan Austral, circulation subpolaire, tendances de température, changements à long terme, altimétrie satellitaire, variabilité saisonière, variabilité méso-échelle, interactions océan-atmosphère-cryosphère.

Table of contents

General Introduction

Sommaire

1 Preamble

Ocean circulation plays a central role in regulating climate and supporting marine life by transporting heat, carbon, oxygen, and nutrients throughout the world's ocean. By absorbing heat and carbon from the atmosphere, the ocean also helps to mitigate human-induced climate change. From 1971 to 2010, around 91% of Earth's excess energy was converted into warming the oceans (Masson-Delmotte et al., 2021).

The Southern Ocean is at the heart of the global oceanic circulation (Figure .1). It links the three main oceanic basins (Pacific, Atlantic, and Indian) and exchanges salt and heat between basins through the global overturning circulation. The Southern Ocean allows the ventilation of the deep water in its southern part, and the subduction of surface waters at intermediate depths in its northern part. For these reasons, it has taken up to 43% of anthropogenic carbon and 75% of anthropogenic heat that has been absorbed by the world ocean since the 1860s (Frölicher et al., 2015). As a consequence, strong and rapid changes of the Southern Ocean properties have been observed in the past decades (Meredith et al., 2019).

From strong warming observed in the north of the Southern Ocean (Gao et al., 2018; Häkkinen et al., 2016) to a slight surface cooling in the south (Rye et al., 2020; Haumann et al., 2020), important multidecadal temperature changes have been observed. Both of these trends are associated with atmospheric changes and intimately linked with changes in the cryosphere, having an important impact on global sea level rise (Meredith et al., 2019). However, the complex feedback mechanisms between the ocean, atmosphere, and cryosphere in the Southern Ocean remain poorly understood (Meredith et al., 2019; Masson-Delmotte et al., 2021), and ocean observational coverage in many areas remains extremely limited.

The Southern Ocean is one of Earth's least observed regions. Its remoteness and harsh climatic conditions make ship observations difficult. Sea ice, which covers millions of square kilometers of the ocean each winter, prevents ocean observation from satellites and makes it difficult for scientific ships to reach the subpolar Southern Ocean. Despite the development of innovative observation methods (e.g. instrumented marine mammals, ice-capable autonomous assets), significant gaps in the observation system still remain, and in particular in the sea ice-covered regions and at depths lower than 2000 meters (Newman et al., 2019).

My approach in this Ph.D. is that more can be extracted from existing observations. In particular, in this thesis, I propose to revisit a long time series of repeated in situ ship-transects observations to investigate if observed temperature changes in the upper ocean actually emerge over interannual variability. I also revisit existing remote sensing satellite altimetry observations of the sea ice-covered Southern Ocean to propose a new estimate of sea level anomaly of the region, at unprecedented spatial and temporal coverage. From this set of observations, I aim to investigate some of the processes governing the changes and driving the dynamics of the subpolar Southern Ocean.

In this general introduction, I first present the dynamics and variability of the Southern Ocean at various spatial scales. I then outline the ocean and cryosphere changes that have occurred in the past decades. Finally, I introduce the observation methods of the Southern Ocean, with a specific focus on XBT measurements and satellite altimetry observations that are used in this thesis.

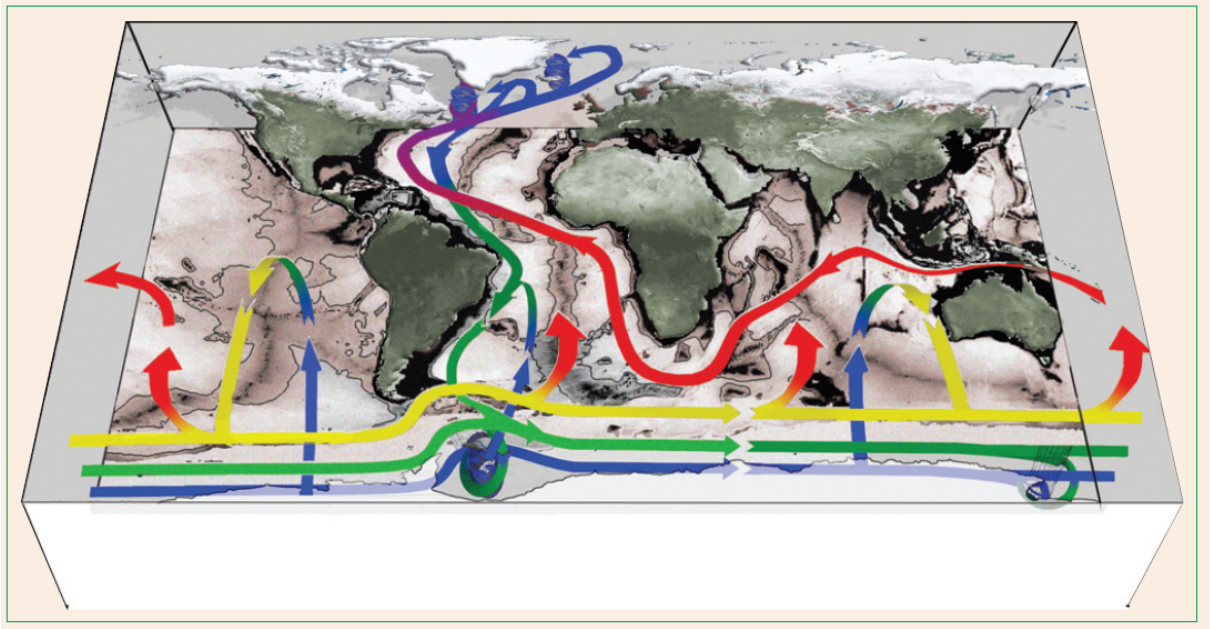

FIGURE .1: Idealised Meridional Overturning Circulation, from Marshall and Speer (2012). Denser waters are indicated by cooler colors, ranging from bottom water in blue to surface and thermocline water in red.

2 The Southern Ocean circulation and water-masses

From the basin-wide circulation features to the smaller mesoscale eddies, the Southern Ocean circulation results from a variety of processes across a large range of spatial and temporal scales. All these processes are interacting together to transport physical, chemical, or biological properties and create the Southern Ocean circulation structure.

2.1) Large, basin-scale circulation

Horizontal circulation and transport in the Southern Ocean

From the Antarctic Circumpolar Current in its northern part to the gyres, coastal, and slope currents in its subpolar part, the Southern Ocean has a complex dynamical structure dictated by bathymetry, as well as mechanical and buoyancy forcings. In this section, I describe these Southern Ocean dynamical structures, from north to south.

The Southern Ocean has a singular topography strongly the regional atmospheric and ocean circulation system. From 55°S to 65°S, there is no continental barrier, which allows the establishment of a strong energetic current flowing circumpolarly around Antarctica (Figure .1) called the Antarctic Circumpolar Current (ACC). The ACC is the most powerful oceanic currents of the planet (Hodel et al., 2021), with a transport estimated at 173 ± 8.7 Sv (1 Sv = 10^6 m^3s^{-1}) at the Drake Passage between the South American and Antarctic continents (Donohue et al., 2016). It transports water mass properties zonally around the Antarctic Continent, across the main oceanic basins (Pacific, Indian and Atlantic, Figure .1 Rintoul et al., 2001). The ACC is composed of

a series of jets (Sokolov and Rintoul, 2009a,b). These jets coincide with the presence of oceanic fronts, which are sharp separations between water masses with different hydrographic properties. The main fronts are, from north to south, the SubTropical Front (STF), the SubAntarctic Front (SAF), and the Polar Front (PF), and the Southern Antarctic Circumpolar Front (SACCF). A schematic of the positions of the southern fronts is shown in Figure .2 (Orsi et al., 1995; Thompson et al., 2018). While circumpolar contours have been used as a convenient proxy to define Southern Ocean fronts in past studies (Sallée et al., 2008; Sokolov and Rintoul, 2009a,b), Southern Ocean fronts are actually complex small-scale jets interacting with each other and the bathymetry, and evolving rapidly (Hughes and Ash, 2001; Chapman et al., 2020). There is therefore no single definition of Southern Ocean fronts, and their characterisation is still a subject of active debate (Chapman et al., 2020).

Variations in the ACC transport and position have long been described to mainly respond to winds variations (Allison et al., 2010). Its northern part was thought to follow northern annual wind stress curl variations, while its southern part was linked to both semi-annual and annual cycles of the amplitude of cyclonic subpolar gyres (Peterson, 1988). Later, the influence of wind on the ACC transport and position was found to be weaker than expected (Gille, 2014). In fact, buoyancy only has an impact on ACC transport variations rather than wind stress (Hogg, 2010), through the bottom or deep water production in the Southern Ocean (Gent et al., 2001) or in the northern hemisphere through interhemispheric influence (Fučkar and Vallis, 2007). The role of eddies in the ACC transport and its change will be discussed later in this general introduction.

Some parts of the ACC may have a strong or a growing influence on the Antarctic ice shelves. In some regions, the ACC can be localized only hundreds of kilometers away from the ice shelves, directly impacting the rates of regional ice melt (Gille et al., 2016). South of the ACC, the subpolar ocean circulation has even more direct links to Antarctica's cryosphere. This part of the Southern Ocean is seasonally ice-covered and contains several dynamical structures (Figure .2), such as cyclonic gyres and coastal and slope currents.

The subpolar Southern Ocean contains three cyclonic gyres : The Weddell Gyre, located at the eastern side of the Antarctic Peninsula, the Ross Gyre, in the Pacific sector, and the Australian-Antarctic gyre in East Antarctica.

The largest of these circulation features is the Weddell gyre. It is located in the Atlantic sector of the Southern Ocean (Figure .2). The Weddell Gyre is constrained south by the continental slope, west by the Antarctic Peninsula at 60°W, and north by the ACC (Deacon, 1979). Its eastern boundary is not clearly identified. It was first evaluated to be roughly around 30°E (Deacon, 1979), then 57°E (Park et al., 2001) or even at 70°E in Vernet et al. (2019). Its transport has been evaluated to be 45 ± 7 Sv in its northern branch, and 56 ± 8 Sv in its southern branch (Klatt et al., 2005), with a zonal gyre strengh away from the ice shelf edge of 32 ± 5 Sv (Reeve et al.). The structure of the Weddell Gyre is maintained by the cyclonic wind field over the Weddell basin and the bathymetry of the sector (Armitage et al., 2018), but also by buoyancy forcings (Colin de Verdière, 1989). There are still lots of uncertainties with the physical mechanisms that control the Weddell gyre. Vernet et al. (2019) listed multiple research priorities to investigate in the coming years, such as the connections to the rest of the Southern Ocean, the cross-shelf processes, or the variability of the Antarctic Slope Front (ASF).

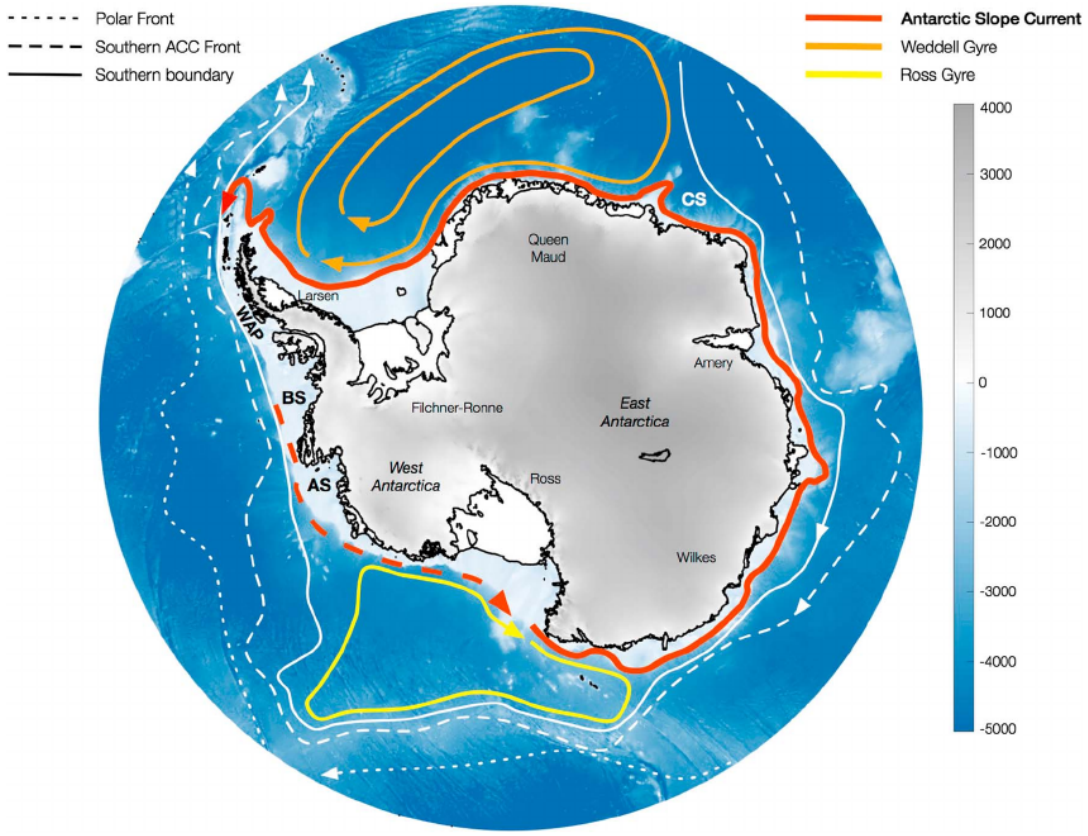

FIGURE .2: Schematic circulation of the Antarctic margins. The Antarctic Slope Current (ASC), in ref, is depicted as a near-circumpolar, anticyclonic (westward) feature appearing at the shelf break in East Antarctica and the Weddell Sea. Uncertainty regarding the initiation of the ASC is indicated by the dashed line in the Bellingshausen and Amundsen Seas (BS, AS) in West Antarctica, as well as the western Ross Sea. Along the West Antarctic Peninsula (WAP), a slope current flows eastward, along with the southern boundary of the Antarctic Circumpolar Current (ACC). Interactions with the Weddell (orange) and Ross (yellow) Gyres, as well as the southern fronts of the ACC (white), are highlighted by their proximity to the ASC in various locations around the Antarctic margins, (e.g., east of the Cosmonauts Sea, CS). The color gives the topography : depth for the open ocean and elevation for ice shelves and ice sheets (Schaffer et al., 2016). Positions of the ACC fronts are based on Orsi et al. (1995) ; gyre circulations are based on Armitage et al. (2018) ; the ASC is plotted along the 1000-m isobath. Figure and caption from Thompson et al. (2018).

The Ross Gyre, while being smaller than the Weddell Gyre, is still one of the main current systems of the Southern Ocean transporting from 17 Sv in the Summer to 30 Sv in the winter (Dotto et al., 2018). It is located between longitudes 170°E and 215°E (Figure .2), with a meridional extent going from the Antarctic continent to 55°S (Dotto et al., 2018). As for the Weddell Gyre, it is highly influenced by the interannual variability of the winds (Armitage et al., 2018), which are mainly linked to the Antarctic Oscillation and the Amundsen Sea Low (Dotto et al., 2018).

Lastly, the Australian Antarctic gyre is not often represented in Southern Ocean circulation schematics (Figure .2), but has a substantial westward flow of 76 ± 26 Sv in its southern branch, with a position located from 80°E to 150°E, from the Antarctic continental shelf to up to 55°S for its northern branch (McCartney and Donohue, 2007). This gyre is in fact a combination of multiple subgyres, bounded by the local bathymetry (Yamazaki et al., 2020).

In the southern branch of these gyres and in most regions around the Antarctic continent, the Antarctic Slope Front (ASF) separates relatively warm waters north of the continental slope from cold water on the continental shelf (Figure .2). It is therefore associated with a strong meridional gradient in physical and chemical properties (Jacobs, 1991; Whitworth et al., 1985). The cross-slope density gradient, maintained by the wind regime over the continental shelf, is associated with a westward, surface-identified flow, located on the continental slope, named the Antarctic Slope Current (ASC). Its velocity varies between 10 and 30 cm.s^{-1} (Thompson et al., 2018). The ASC is thus forced by the winds influence on the ASF, but also regionally by tides and eddies (Stewart et al., 2019).

The variability of the subpolar ocean circulation systems is poorly known. Yet, the increasing amount of wintertime observations is slowly shedding light on subpolar ocean circulation variability, especially on a seasonal timescale. Over the entire subpolar Southern Ocean, Garabato et al. (2019) presented two dynamical responses to the seasonal cycles of the winds and sea ice forcings. Direct sea-level signals show an exchange of mass between the continental shelf and the offshore part of the Southern Ocean, and a 2-month delayed transfer of mass between the offshore subpolar Southern Ocean and the subtropics to the north. The former leads to strong seasonal signals in the dynamics of the subpolar Southern Ocean, with maximum westward velocity anomalies reaching 1 cm.s^{-1} in the ASC in May-July, and 0.3 cm.s^{-1} eastward velocity anomalies north of the subpolar Southern Ocean. Such ASC seasonal mode is consistent with other modelling studies (Mathiot et al., 2011) and analyses using satellite altimetry (Armitage et al., 2018). From moorings, Núñez-Riboni and Fahrbach (2009) found a slight delay between ASC speed seasonal increase north of the slope and on the shelf, with a maximum velocity reached in May on the shelf, and June offshore. The details of the seasonality of the ASC are still under debate, but it is already known that this seasonality has important consequences on regional climate and the ice-shelves (Silvano et al., 2019). The variability of the Weddell and Ross gyres is phased with the seasonality of the ASC, with a larger seasonal cycle in the Weddell gyre (Armitage et al., 2018) and a specific semi-annual intensification in the Ross Gyre (Dotto et al., 2018).

The continental shelf and slope circulation variability are also associated with the *Southern Mode*, which corresponds to rapid propagating waves along the continental shelf break all around Antarctica (Kusahara and Ohshima, 2009). This Southern Mode is responsible for propagating the SSH response to localized wind forcing all around Antarctica (Spence et al., 2017) . For instance, there is a large response in the western Antarctic peninsula to wind changes localized in East Antarctica. SSH anomalies are transported by coastal Kelvin waves and induce a change in the barotropic current even thousands of kilometers away from the initial perturbation (Spence et al., 2017).

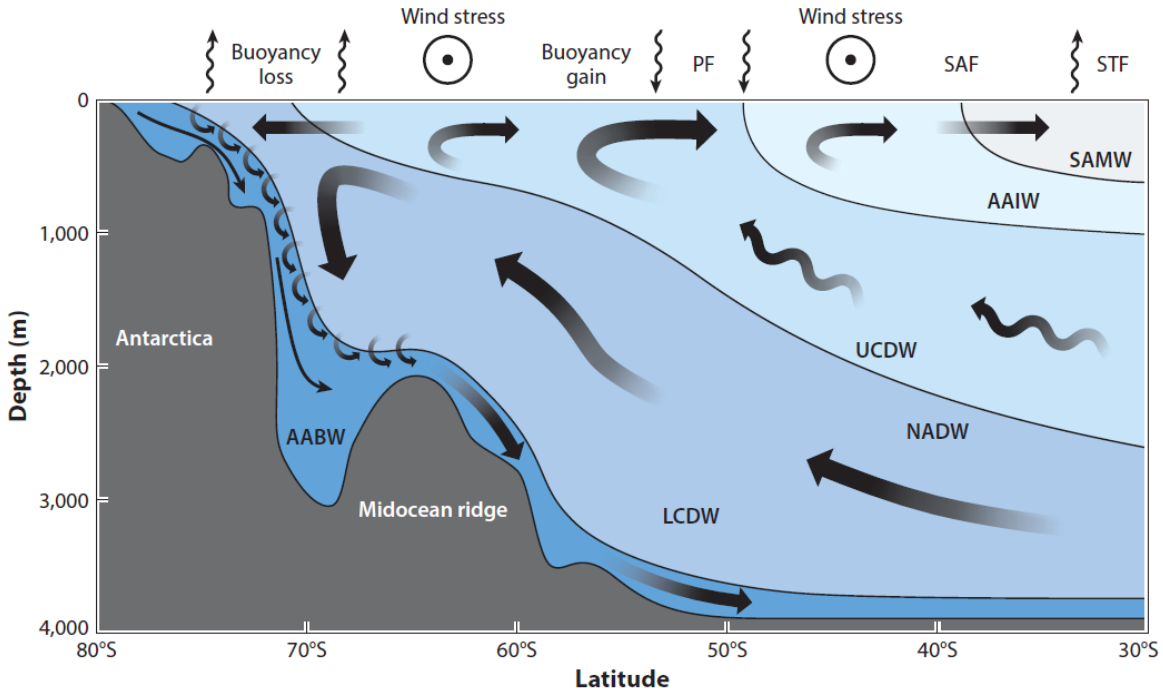

FIGURE .3: Zonally averaged Southern Meridional Overturning Ciruclation main paths, from (Gent, 2016), adapted from Speer et al. (2000).

All of these horizontal ocean circulation systems are part of the wider tridimensional circulation of the Southern Ocean.

Large scale tridimensional circulation

The Southern Ocean hosts a Southern Meridional Overturning Circulation (SMOC) associated with water-mass formation, transformation, and export. In this section, I present the meridional and vertical transport associated with the SMOC. I then list the main water masses and their properties and associated processes. Finally, I display the main meridional structures of the Antarctic continental shelf.

The meridional hydrographic structure of the Southern Ocean reflects the SMOC, associated with the upwelling, sinking, and poleward or equatorward transport of Southern Ocean water masses (Figure .3 ; Gent, 2016). It is an important part of the global Meridional Overturning Circulation (MOC), organized as a tridimensional circulation system, which globally redistributes physical and biogeochemical ocean properties (Orsi et al., 1995; Rintoul and Naveira Garabato, 2013; Naveira Garabato et al., 2014). The SMOC is associated with large water mass formation. It has been estimated that 55% of the total global ocean's volume has been formed in the Southern Ocean (DeVries and Primeau, 2011), therefore playing an essential role in ventilating the global ocean.

The SMOC is organized in two circulation cells, converting deep water into either lighter surface water, or heavier bottom water (Figure .3 ; Speer et al., 2000; Marshall and Speer, 2012; Pellichero et al., 2018).

In the subsurface Southern Ocean, warm and saline Circumpolar Deep Water (CDW) coming from the northern hemisphere is transported southward (Speer and Marshall, 2012). It spirals southeastward and upward through the ACC, and reaches the mixed layer south of the ACC (Orsi et al., 1995; Tamsitt et al., 2017), due to the southward decrease in zonal wind stress (Speer and Marshall, 2012). In the subpolar Southern Ocean, Circumpolar Deep Water (CDW) is warmer than the surface layer and is the main heat source of the region (Orsi et al., 1995; Stewart et al., 2018).

The upper cell is associated with the upwelling and northward transport of the deep water. When reaching the surface, the upper branch of the CDW interacts with the atmosphere and sea ice which transforms them into lighter water (Meijers et al., 2010; Pellichero et al., 2017a; Abernathey et al., 2016). There, the fresh and cold surface water is advected northward by the strong westerlies through Ekman transport and subducted on the northern side of the ACC into SubAntarctic Modal Water (SAMW) and Antarctic Intermediate Water (AAIW) (Sallée et al., 2012).

The lower cell is associated with the deeper layer of the CDW that is deeper than 2000m depth under the ACC. This water mass reaches the surface close to the continental slope (Gordon and Huber, 1990; Thompson et al., 2018). There, sea ice forms, which rejects salt brines in the surface layer. The strong increase in the salinity of the surface layer drives the densification of the surface water that sinks, entrains the CDW and flows in the seabed along the continental shelf slope as Antarctic Abyssal Water (AABW) (Orsi, 2010; Drucker et al., 2011; Ohshima et al., 2013; Akhoudas et al., 2021). It is then transported northward and ventilates the abyss of the world's oceans (Orsi et al., 1999; Johnson, 2008).

The meridional cells that have been described hide a heterogeneous meridional structure. For example, for the lower cell, close to the Antarctic continent, Thompson et al. (2018) listed three main regimes at the continental shelf break, associated with the ASF strength and shape. They are influenced by the wind regime, heat, and freshwater fluxes, and impact the ASC velocity. They are represented in figure .4 :

— The Fresh shelf regime (Figure .4ad) is the most common and is dominant in East Antarctica. On a Fresh shelf, strong coastal easterly winds induce a positive Sea Surface Height (SSH) toward the continent, and a strong westward flowing ASC. The ASC velocity is high enough to hamper cross-slope exchanges, separating the cold shelf waters with the warm CDW (Meijers et al., 2010; Thompson et al., 2018). Fresh shelves are not associated with dense or bottom water formation.
— The dense shelf regime (Figure .4be) relates to the regions associated with bottom water production, which are located in the Weddell sea (Meredith et al., 2014), Ross sea (Assmann and Timmermann, 2005), the Somov and Adélie seas (Williams et al., 2008), and in the Cosmonaut sea (Ohshima et al., 2013). In these regions, the export of cold and salty bottom water creates "V-shaped" cross slope isopycnals, associated with a local ASC on the slope (Meijers et al., 2010; Ohshima et al., 2013).

— Lastly, the Warm shelf regime (Figure .4cf) is mostly found in the Amundsen-Bellingshausen seas and is associated with weaker easterlies or even westerlies at the continental slope, no or weak ASF (Pauthenet et al., 2021), and intrusions of warm CDW on the continental shelf (Wåhlin et al., 2010; Nakayama et al., 2014).

These hydrographic structures are associated with the zonal circulation of the ASC, but they also control the amount of cross slope transport from direct advection or eddies. This supply of relatively warm CDW on the shelf is key in the ice shelves basal melt and important for modulating the formation and export of dense water on the shelf (Nicholls et al., 2009; Hattermann et al., 2014; Morrison et al., 2020), which influences the tridimensional circulation of the Southern Ocean.

2.2) Mesoscale dynamics

Generalities

The ocean is a turbulent system, therefore favorable for mesoscale instabilities to develop (Morrow and Le Traon, 2012). Mesoscale variability stands for eddies, meandering currents or fronts, and filaments of spatial scales from tens to several hundreds of kilometers, and temporal scales of tens to hundreds of days. In this thesis, I focus on the eddies, which are coherent vortex, often with different physical properties than their surrounding areas (Bonaduce et al., 2021), ubiquitous in the open ocean (Ducet et al., 2000) and present in the sea ice regions. Mesoscale eddies have strong impacts on the thermodynamics of the oceans, due to their ability to mix, diffuse and trap ocean contents (McWilliams, 1985; Chelton et al., 2011; Morrow and Le Traon, 2012). They play a role in the energy budget of the ocean as well, by converting potential energy stored by the oceans to kinetic energy and transferring it at spatial scales (Visbeck et al., 1997; Stammer, 1998). Eddies not only impact the large-scale circulation of the ocean, but they also influence on the wind field, clouds, and precipitation (Chelton, 2013).

Most of the studies I cited to introduce the mesoscale eddies have been conducted from satellite altimetry data (Ducet et al., 2000; Chelton et al., 2007, 2011; Morrow and Le Traon, 2012), one of the preferred ways to investigate those eddies in large regions. On high-resolution Absolute Dynamic Topography datasets, their signature is either positive (anticyclonic) or negative (cyclonic eddies) closed contours of ocean topography (Chelton et al., 2007). Automatic detection and tracking are great tools to investigate those features (Mason et al., 2014), and may be complemented by in-situ measurements such as from the Argo network to establish the various kind of eddies of a circulation system (Pegliasco et al., 2015) or evaluate the integrated global zonal mass transport by eddies (30-40 Sv ; Zhang et al., 2014).

As addressed in the previous sections, the dynamics and fronts of the Southern Ocean are essentially zonal. That means that eddies are necessary for the cross-frontal transport in both the ACC and the subpolar part of the basin, and are expected to play a major role in the dynamics of the region.

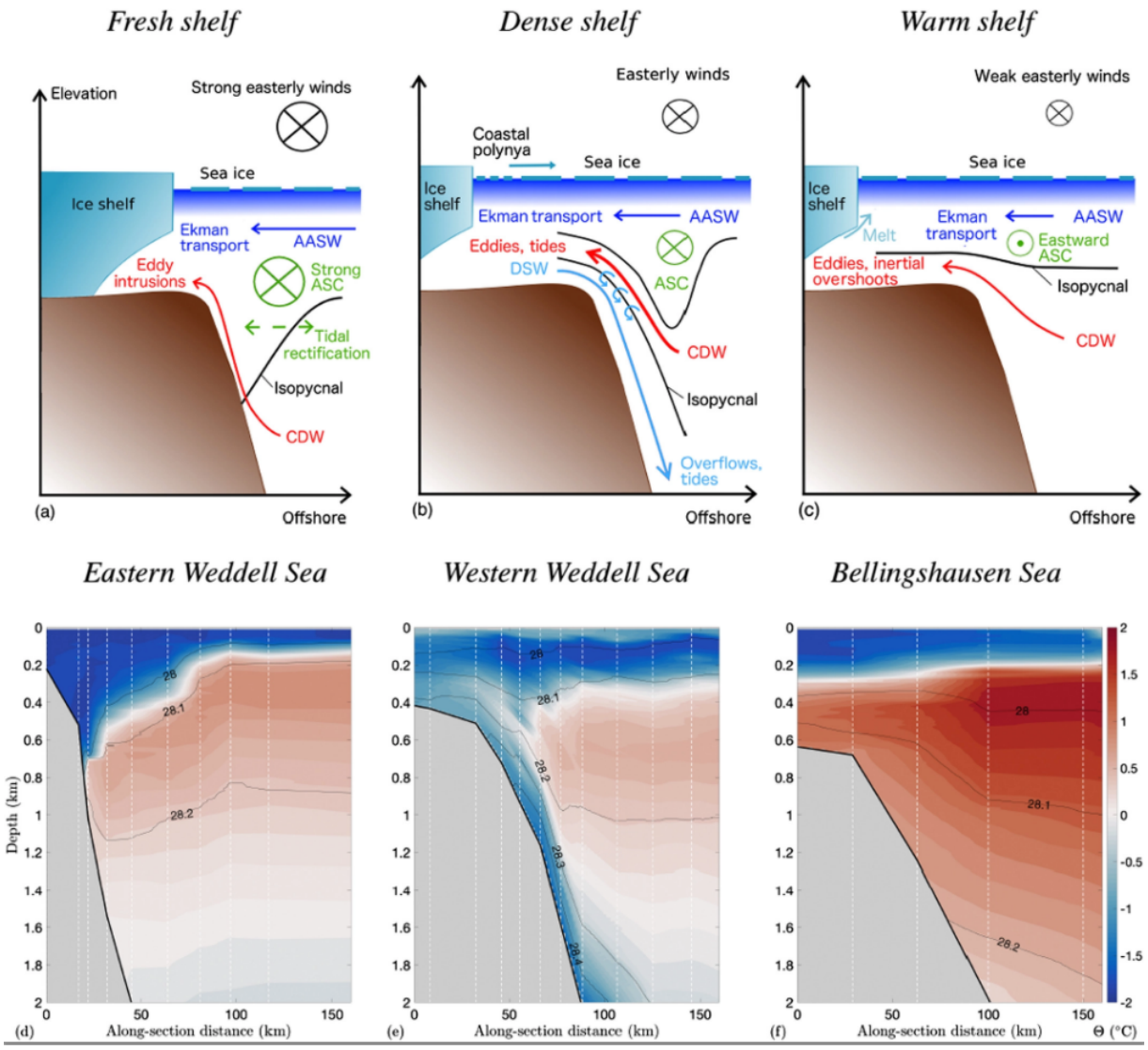

FIGURE .4: Antarctic Slope Current (ASC) regimes : (a–c) Key water masses, along- and across-slope flows and supporting mechanisms in the (a) Fresh shelf, (b) Dense shelf, and (c) Warm shelf Antarctic Slope Current (ASC) regimes defined in this article. (d–f) Measurements of conservative temperature (colors) and neutral density (black contours) across the ASC in locations corresponding to each ASC regime : (d) the eastern Weddell Sea (Heywood and King, 2002), (e) the western Weddell Sea (Thompson and Heywood, 2008),and (f) the Bellingshausen Sea (Orsi and Whitworth, 2005). Section locations are shown in Figure 6, and white dashed lines indicate locations at which hydrographic casts were taken. The following water masses are identified : Antarctic Surface Water (AASW), Circumpolar Deep Water (CDW), Dense Shelf Water (DSW). Figure and caption from Thompson et al. (2018).

Eddies in the Antarctic Circumpolar Current

In the ACC, the eddy field is very energetic and plays a central role in the Southern Ocean dynamics and water transport (Speer et al., 2000; Rintoul, 2018). Both eddies and the ACC depend on each other : steep isopycnals within the ACC are important reservoirs of potential energy for eddies to develop (Hogg et al., 2017), and in turn, eddies set the ACC momentum balance between the surface winds and the bottom (Gille, 1997; Rintoul et al., 2001; Ivchenko et al., 2008).

Southward eddy heat flux crosses the ACC and balances high latitude heat loss (Rintoul, 2018). More broadly, eddies crossing the ACC jets allow the establishment of a meridional transport of water masses (Speer et al., 2000; Marshall, 2003; Ivchenko et al., 2008). In the acc system, eddies are rather concentrated in eddy hot spots, in the lee of the main bathymetric features (Chelton et al., 2007; Thompson and Sallee, 2012; Mashayek et al., 2017). There, mesoscale eddies are an essential component of the Southern Meridional Overturning Circulation (SMOC) through their ability to link the surface layer with water masses at depth (Speer et al., 2000; Rintoul et al., 2001), or to allow the upwelling of water masses within the ACC system (Tamsitt et al., 2017).

The observed properties of the eddies in the ACC are not uniform but follow the distribution of the main jets : local maxima in mean amplitude and radius are in the most energetic parts of the ACC (Chelton et al., 2011). In the rest of the ACC and northern part of the Southern Ocean, the global distribution of the eddy radius decreases with latitude, consistent with the Rossby radius (Chelton et al., 1998, 2011).

Eddies in the subpolar Southern Ocean

The properties of the eddies and their impact on the subpolar Southern Ocean system are still largely unknown due to the few observations available. Yet, modelling studies estimate that they are an important part of the processes governing the regional circulation of heat and freshwater transport (Nøst et al., 2011; Stewart and Thompson, 2015; Stewart et al., 2018). As in the ACC, the eddies are intimately linked to the local circulation. One of the main circulation features of the subpolar Southern Ocean is the ASC. Locally, the ASC is driven by the mesoscale eddies (along with coastal winds, sea ice and tides ; Stewart et al., 2019). The ASC and the associated ASF, represent dynamic and hydrographic barriers preventing intrusions of warmer off-shelf waters on the continental shelf break (Jacobs, 1991). Yet in the subpolar basin too, the eddies contribute to the southward, cross-front, or cross-shelf transport of the warm intermediate layers (Thompson et al., 2014). In fact, while the shoreward surface transport is due to winds, the eddies might be an efficient mechanism to bring heat on the continental shelf (Stewart and Thompson, 2015), at hotspots regions of warm water intrusions with large bathymetry features (Nakayama et al., 2014) or in dense water formation regions (Stewart and Thompson, 2015). Eddy stirring is also a contributor to this cross-shelf heat transport (Stewart et al., 2018). In the end, the eddy activity was observed to impact the reservoirs of heat and salt on the shelf (Foppert et al., 2019) and drive the local ice shelves basal rates (Nøst et al., 2011).

The issue of having rather few observational studies on eddies on the subpolar Southern Ocean also affects the Arctic but to a lesser extent. In that context, results drawn from studies in the Arctic may transfer to the subpolar Southern Ocean to some degree. There, several studies focused on the effect of the sea ice on mesoscale eddies. Within the sea ice region, Meneghello et al. (2020), pointed at a quasi-deletion of surface eddy kinetic energy at the surface in winter, caused by a strong dissipation of eddies by the overlying sea ice. At depth, however, they observed an intense year-long eddy activity in the halocline as well, in a study combining modelling and observations Meneghello et al. (2020). Consistently, Timmermans et al. (2008); Zhao et al. (2014, 2016) detected numerous anticyclonic eddies in the Arctic halocline between 50 and 250 meters depth, mostly cold-core anticyclones. These were observed from Ice Tethered Profilers,

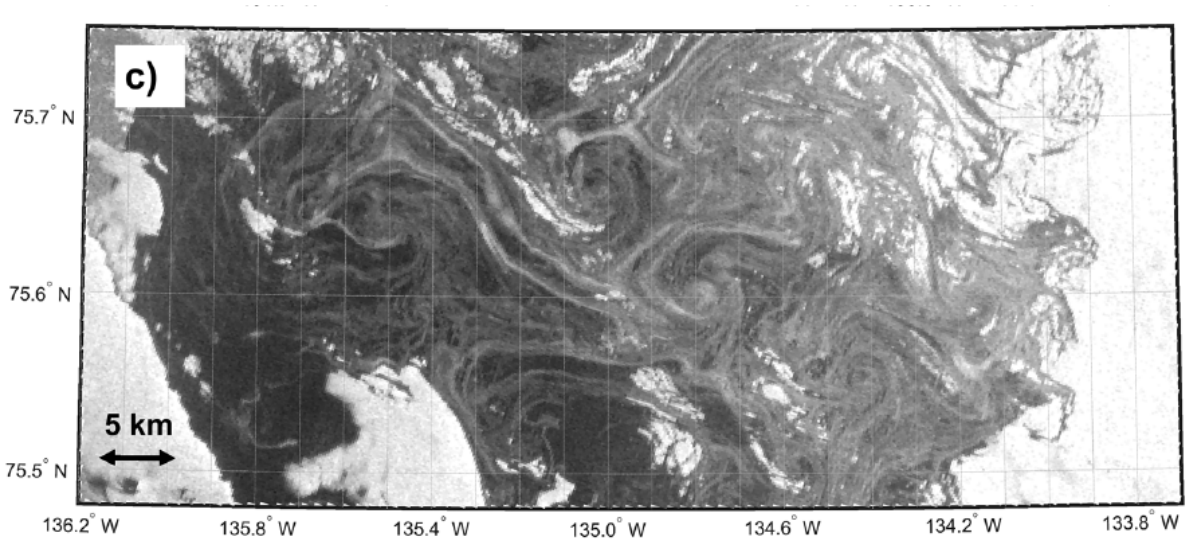

FIGURE .5: Eddies signature on drifting ice, observed in the marginal ice zone on ALOS2 Palsar2 images, from Kozlov et al. (2019)

in both Canadian and Eurasian basins. They have been observed far from their generation region and their radius is of the order of 10-20 km (Timmermans et al., 2008; Zhao et al., 2014, 2016). Those eddies may be generated at surface oceanic fronts (Manucharyan and Timmermans, 2013), making the Marginal Ice Zone (MIZ) one of the best candidates for generating these anticyclonic eddies. Indeed, at the floe edges, melting sea ice drives horizontal density gradients that create instabilities (Horvat et al., 2016; Manucharyan and Thompson, 2017). The ice-induced surface stress pattern and interactions with the local ice edge jet may enhance the instabilities as well (Häkkinen, 1986; Thomas, 2008; Lu et al., 2015). Eddies at the marginal ice zone can be observed by satellite imagery (Figure .5 Kozlov et al., 2019), as the cyclonic features may trap and advect sea ice outside of the sea ice zone (Manucharyan and Thompson, 2017).

This link between sea ice and eddies was also investigated using dedicated modelling. In the leads, which are open water channels in the sea ice regions, local refreezing produces salt fluxes that create sharp fronts, favorable for instabilities and genesis of oceanic eddies (Cohanim et al., 2021). The resulting eddies are dependent on the lead width and duration, and the magnitude of the buoyancy forcing (Smith et al., 2002). They contain most of the salt rejected by the ice formation, are mostly anticyclonic, and can survive in the subsurface up to one month after the closure of the lead (Matsumura and Hasumi, 2008). While most of these modelling studies were set up with conditions specific to the Arctic, Cohanim et al. (2021) modeled the effect of thermohaline fluxes in the leads in Antarctic conditions. Consistently with previous results in the Arctic, the instabilities generated in the leads show a dominance of anticyclonic eddies (Cohanim et al., 2021). In this case, the modeled anticyclones were growing in size reaching from 10 to 20km after 50 days, and contributed to populate the halocline. Therefore, the ice covered halocline may be a preferred location for the eddies generated in the MIZ and in the leads.

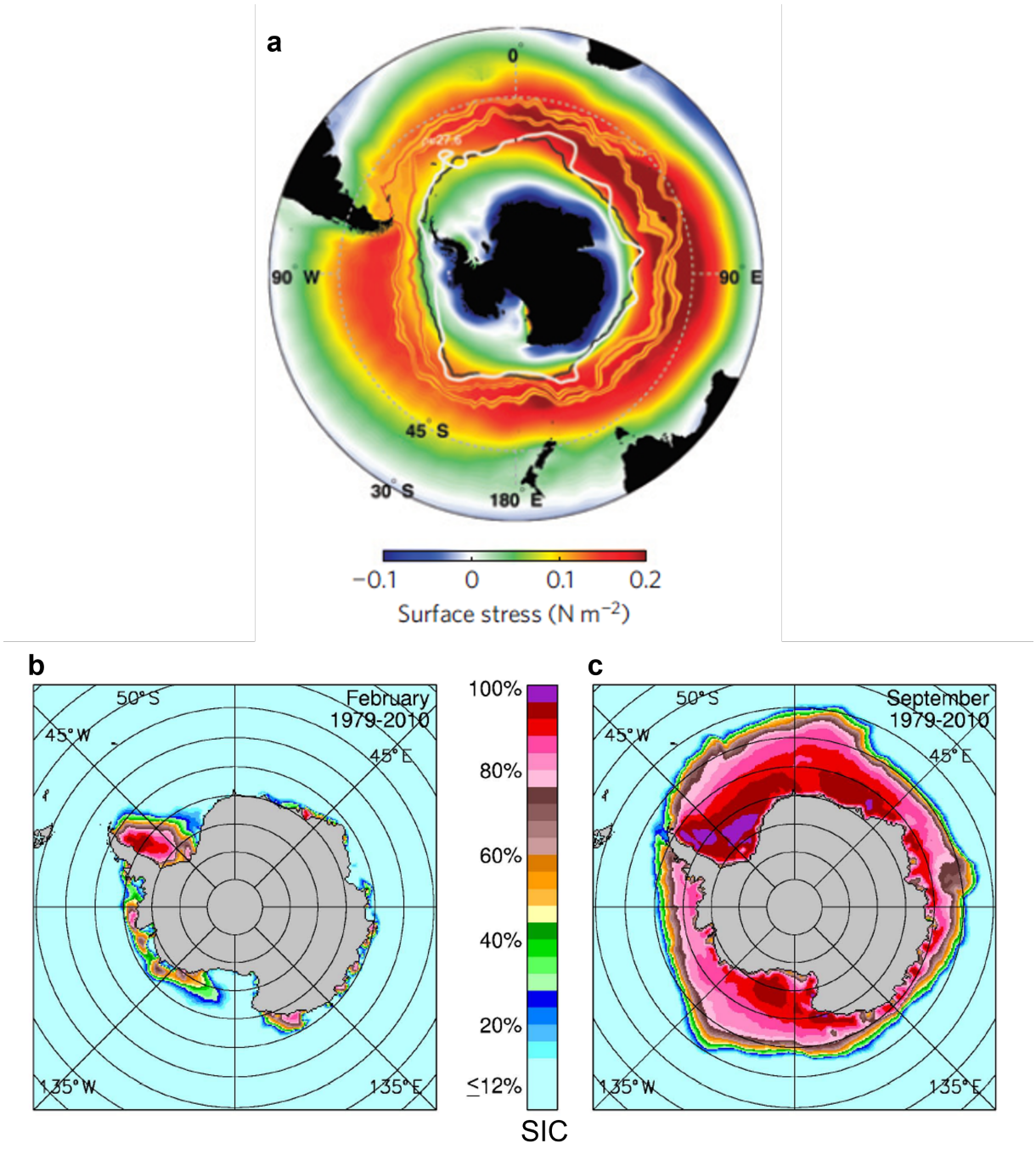

FIGURE .6: Southern Ocean forcings. (a) Mean zonal wind stress at the surface of the ocean for the period 1980-2000. Subantarctic and polar fronts are marked in orange. The winter ice edge is marked by the black line and the 27.6 $kg.m^{-3}$ outcrop by the white line. From Marshall and Speer (2012). (b) Mean February and (c) September Sea Ice Concentration from 1979-2010 data, from Parkinson and Cavalieri (2012).

2.3) Main forcings of the Southern Ocean Circulation

In this section, I briefly introduce the main forcings of the circulation at each of the Southern Ocean interfaces, from wind mechanical forcing to the Antarctic ice shelves, and via sea ice and air-sea heat and freshwater fluxes.

Air-sea heat and freshwater fluxes

Through precipitation, evaporation, and heating, the atmosphere impacts the properties of the surface of the Southern Ocean. The properties may propagate in the subsurface and impact its hydrography.

The atmospheric contribution to freshwater fluxes at the ocean surface results from the combination of precipitation and evaporation (hereafter, P-E flux). In the Southern Ocean, the sparse observation of precipitation and evaporation limit our ability to monitor these fluxes. Atmospheric reanalysis can be used to estimate these fluxes and their change but such reanalysis is poorly constrained so large discrepancies exist between the different reanalysis products (Bromwich et al., 2011; Trenberth, 2011). However, the large-scale spatial distribution of the climatology of the P-E fluxes is generally robust across different data sources, and displays overall larger precipitation over evaporation in the northern part of the Southern Ocean, north of the ACC, and larger evaporation over precipitation south of the ACC (Akhoudas, 2019).

As for freshwater fluxes, the lack of observation hinders the monitoring of air-sea heat fluxes in the Southern Ocean, especially in autumn and winter, or in the seasonally ice-covered regions (Swart et al., 2019). This results in strong disparities between heat fluxes reanalysis, illustrated by (Swart et al., 2019), but with an overall pattern showing intense heating in the vicinity of the ACC ($\approx$ 80 0W.m^{-2}), lower in the gyres ($\approx$ 20 0W.m^{-2}), and heat loss at the coast of Antarctica ($\approx$ -20 0W.m^{-2}).

Winds

Southern Hemisphere winds organize in a zonally banded structure, with peak westerlies at mid-latitude around 40-60°S, and peak easterlies along the Antarctic continental shelf (Figure .6a ; Marshall and Speer, 2012). Winds are a strong forcing of ocean circulation by transferring momentum at the ocean surface through wind stress (Trenberth et al., 1990). In the ACC, the momentum acquired at the ocean surface provides energy to the current, which is partially released by baroclinic instability and bottom stress after being transferred at depth by mesoscale eddies (Rintoul et al., 2001). North and south of the ACC, the large wind-stress curls are thought to drive subtropical and subpolar gyres (Sverdrup, 1947; Pedlosky, 2013; Armitage et al., 2018).

The zonal structure and strength of wind stress and associated curl has also a large impact on the meridional overturning circulation of the Southern Ocean (Gent, 2016). In the region of the ACC, westerly winds drive a net northward Ekman transport in the surface layer of the Southern Ocean (Speer et al., 2000). South of the ACC, the curl created by the mid-latitude westerlies and high latitude easterlies induces an Ekman divergence and associated upwelling (Marshall and Speer, 2012) of CDW. Over the Antarctic continental slope, winds help to maintain a strong density gradient over the slope and to sustain the Antarctic Slope Current (Thompson et al., 2018).

The dominant mode of variability of surface winds in the Southern Hemisphere is associated with the so-called Southern Annular Mode (SAM) of variability (Thompson and Wallace, 2000). The SAM index is associated with marked variability in atmospheric Sea Level Pressure (SLP), surface temperature, and winds variability (Marshall, 2003; Thompson and Wal-

lace, 2000). It is defined as the pressure difference between 40°S and 65°S. When the SAM is positive, SLP gradient between 40°S and 65°S is increased (more negative than average), which results in a strengthening and poleward shift of the westerlies (Hall and Visbeck, 2002). Other climate modes also have a great regional influence on the Southern Ocean atmospheric surface pressure and winds : e.g. the Amundsen Sea low (ASL) or El Niño – Southern oscillation (ENSO)(Karoly, 1989; Turner et al., 2013; Dotto et al., 2018; Li et al., 2021).

Sea Ice

Large parts of the Southern Ocean are covered by a thin sea ice layer (about 1 meter on average) floating over the ocean (Parkinson and Cavalieri, 2012). Several parameters describe the sea ice state, such as its thickness or freeboard above the flotation line. The Sea Ice Concentration (SIC) is defined as the percentage of ice-covered ocean within a defined geographical domain. Sea ice coverage can be expressed by its extent or area (SIE or SIA). The SIE is conventionally defined as the sum of the area of the grid cells with a SIC higher than 15%, while the SIA is the sum of the cells with a SIC higher than 15% times the SIC of the corresponding cell (Parkinson and Cavalieri, 2012).

In the Southern Ocean, the sea ice extent is associated with a large seasonal cycle ranging from $3.110^6 km^2$ in February to $18.510^6 km^2$ in September (Figure .6bc, Parkinson and Cavalieri, 2012). Sea ice mostly forms close to the continental shelves, where the wind and currents generate an ice divergence, allowing the apparition of latent heat polynyas (Morales Maqueda et al., 2004). Polynyas are ice-free coastal regions that allow a greater ice formation by enabling direct exchanges between the cold atmosphere and the sea surface. Ice formed in the coastal polynyas is then advected northward by the winds, where it melts at lower latitude (Holland and Kwok, 2012) in summer. From both its role in acting as a barrier damping the momentum transfer from the wind toward the surface of the ocean (Tsamados et al., 2014; Martin et al., 2016) and modifying heat and freshwater fluxes (Pellichero et al., 2017a), sea ice is one of the main forcings of the Southern Ocean circulation.

By modulating the surface stress induced by winds, sea ice directly impacts the dynamical forcing of the subpolar Southern Ocean. When the ocean is ice-covered, the momentum applied to the surface is controlled by winds, ocean currents, and sea ice shape, velocity, and concentration. These interactions are extremely complex, and their representation in models is still a matter of active research (Tsamados et al., 2014; Martin et al., 2016). Computing such ice-covered ocean surface stress from atmospheric reanalysis and ocean and sea ice observations is also a challenge in the absence of large-scale observations of top and bottom sea ice surface roughness (Martin et al., 2016). To first order, observation-based analyses suggest that considering the contribution of sea ice to the surface stress allows a better description of the subpolar Southern Ocean seasonal variability (Garabato et al., 2019; Núñez-Riboni and Fahrbach, 2009).

Sea ice has also a large impact on ocean circulation through its thermodynamic forcing at the surface ocean interface. More precisely, the freshwater fluxes associated to sea ice have a much larger impact than the heat flux, with a ratio estimated between 2 to 5 higher for the freshwater contribution (Pellichero et al., 2018). When sea ice melts, it releases freshwater (or water with very low salinity compared to the ocean salinity) into the ocean surface layer (Aa-

gaard and Carmack, 1989). In contrast, when sea ice forms in winter, there is a rejection of salt brines in the surface layer also associated with large density flux, triggering intense convection (Allison, 1981). sea ice melt and formation are therefore associated with a large seasonal cycle of the density of the mixed-layer and associated vertical structure of the ocean (Chaigneau et al., 2004; Pellichero et al., 2017a). But maybe more importantly, because sea ice forms and melts in different locations (predominantly forms at high latitude, and melts at lower latitude), the sea ice seasonal cycle creates a meridional gradient of density flux at the ocean surface, which is a central piece of water-mass formation and transformation associated with the meridional overturning circulation of the Southern Ocean (Pellichero et al., 2018; Abernathey et al., 2016). This seasonality has a large impact on the Southern Ocean dynamics and hydrography (Chaigneau et al., 2004; Hattermann, 2018).

The sea ice is not a continuous surface, but is rather composed of ice platforms, the flows. Divergence in the drift of the flows may create openings in the sea ice, which are the leads (Smith IV and Morison, 1993). I already presented their impact on the mesoscale dynamics in the "Eddies Under Sea Ice" section, but sea ice leads can also impact the hydrography of the water column under the sea ice, from their ability to act as small polynyas. Sea ice leads are also important in the observability of the ocean conditions in the sea ice regions, as it will be presented in the last part of this general introduction.

Antarctic Ice Shelves

The Antarctic Ice Shelves are ice platforms attached to the Antarctic land on the one side, but floating over the ocean for its largest part, bounded by an ice cliff with a height between 2 and 50 meters on its seaward side (Jackson, 2005). These shelves create cavities over the continental shelf, where their bottom side is in contact with the ocean and exchanges heat and freshwater fluxes with the underlying water masses (Fahrbach et al., 1994). Meltwater fluxes may enhance sea ice production, by accumulating relatively low density, cold, and fresh water in the surface layer (Price et al., 2008; Bintanja et al., 2013). But meltwater fluxes may also suppress the bottom water formation, by compensating the salt fluxes from ice formation, with salinity values reaching levels not high enough for the bottom water production (Fahrbach et al., 1994).

3 Long term changes in the Southern Ocean

The Southern Ocean has an important role in mitigating human-induced climate change. It is estimated that the Southern Ocean has absorbed 75% of the excess of heat in the atmosphere that has been caused by anthropogenic forcing in the past 160 years (Frölicher et al., 2015). In parallel, it is also acting as one of the main anthropogenic carbon sinks of the global oceans (Frölicher et al., 2015). These carbon and heat uptakes have an important influence on global mean surface temperature (Winton et al., 2013). In counterpart, the Southern Ocean circulation and water-masses (hydrography and chemical properties) are rapidly changing (Gille, 2002, 2008; Schmidtko et al., 2014), which has indirect impact on sea ice and ice shelves (Bintanja

et al., 2013; Eayrs et al., 2021). Other changes such as modifications in the atmospheric regime due to ozone depletion and increasing greenhouse gasses concentration also drive long-term changes in the Southern Ocean system (Swart et al., 2018).

This section aims at summarizing some of the main long-term changes that have been observed over the past decades in the atmospheric surface winds, in the Southern Ocean circulation and hydrography, and in the cryosphere.

3.1) Change in surface winds, heat fluxes, precipitation, and evaporation

The Southern Hemisphere storm tracks and associated westerly winds have migrated polewards over recent decades, especially in the austral summer and autumn, associated with a trend towards more positive phases of the Southern Annular Mode (SAM) over the instrumental period and particularly since the 1970s (Gulev et al., 2021; Lee et al., 2021). Stratospheric ozone depletion and increase in GreenHouse Gases (GHGs) in the atmosphere have been identified as the two main causes for this positive SAM trend (Thompson et al., 2011; Abram et al., 2014). ChloroFluoroCarbons have been responsible for ozone loss since the 1970s, itself inducing a cooling of the Antarctic lower stratosphere and directly impacting the SAM index (Thompson and Wallace, 2000; Marshall, 2003). While the onset of Antarctic ozone hole recovery has been observed in past years as a response to the lowering of CFCs emissions (internationally agreed as part of the Montreal Protocol; (Banerjee et al., 2020)), increasing greenhouse gas concentrations are now dominating the positive SAM trend (Swart et al., 2018). In the 21st century, under high emission scenario, the last IPCC report assessed likely that Southern Hemisphere mid-latitude jet would continue strengthening and shifting poleward (Lee et al., 2021). However, strong future mitigation scenarios are associated with relative stability of the mid-latitude jet (Bracegirdle et al., 2020).

Direct observation of changes in the heat fluxes is made extremely difficult due to the lack of direct measurements (Swart et al., 2019). However, the Southern Ocean absorbed a tremendous part of the human-induced excess of heat in the atmosphere : 75 ± 22 % of the anthropogenic of the excess of heat absorbed by the world oceans was absorbed in the Southern Ocean (estimated from a modelling study; Frölicher et al., 2015). The Southern Ocean heat content increases rapidly, with a rate that has increased in the last decade compared to previous decades (Meredith et al., 2019).

Last decade changes in freshwater fluxes of the Southern Ocean are consistent with an intensification of the global hydrological cycle (Held and Soden, 2006). Thus, precipitation is thought to have increased in regions where it was already dominating over evaporation, and evaporation is thought to have increased where it was already dominating over precipitation (Trenberth, 2011). Consequently, P-E tends to decrease in the northern part of the Southern Ocean and to increase ACC, but which is however not found by all the available reanalyses (Bromwich et al., 2011). These changes are not well observed but are consistent with the basin-scale observed change in surface salinity (Durack et al., 2012). At a more local scale, a direct relationship between change in surface salinity and P-E flux is more difficult to assess. While Aoki et al. (2013) proposed that increase in precipitation fluxes have contributed to a freshening of the surface layer off Adélie Land, Morrow and Kestenare (2014, 2017) found in the same

region no correlation between the long term trends of precipitations and surface salinity. Instead, a significant correlation with sea ice interannual variability was established (Morrow and Kestenare, 2014). At high latitude, intricate feedbacks between surface salinity, sea ice, and precipitation make it difficult to disentangle processes at play. For instance, an increase in precipitation can have an impact on sea ice, as it was modelled to increase the sea ice cover along with the surface freshening (Purich et al., 2018).

3.2) Hydrographic and circulation changes

Circulation changes

In contrast to observed changes in atmospheric westerlies, the ACC has not shown any significant transport or position change in the past decades (Chidichimo et al., 2014; Gille, 2014; Donohue et al., 2016; Gille et al., 2016). Instead of changing the mean current, increase in winds seem cause an increased eddy-activity (Meredith and Hogg, 2006; Hogg et al., 2015; Martínez Moreno et al., 2020). The response of the Southern Ocean to wind stress change has been discussed within the framework of two concepts called eddy saturation and eddy compensation (Rintoul, 2018), which respectively relate to change in ACC transport and in the MOC strength.

In an eddy saturation regime, an increase in wind stress which tends to steepen southern ocean isopycnals in the , is counterbalanced by an enhanced eddy activity releasing the added potential energy into eddy kinetic energy (Meredith and Hogg, 2006; Patara et al., 2016). As a result, the ACC transport does not increase. From in situ observations, Böning et al. (2008a) found no steepening of the isopycnals that would be associated with an increase in ACC transport, while the wind stress was strengthening in the previous decades due to the positive trend in the SAM. From satellite altimeters, Meredith and Hogg (2006) showed that increasing winds were associated with a 2-3 year delayed increase of the Southern Ocean eddy activity, consistent with an ACC in eddy saturation states. Numerical models have been instrumental to refine our understanding of ACC response to winds (Hallberg and Gnanadesikan, 2006; Farneti et al., 2010; Dufour et al., 2012). From not eddy-resolving models, the response of the ACC to increasing wind stress is an intense acceleration of the flow (Hallberg and Gnanadesikan, 2006). When improving the resolution of eddies, they act to counteract the effects of the increasing winds, so that the ACC transport increase is more subtle (Hallberg and Gnanadesikan, 2006). This increase in eddy activity due to stronger winds is not uniform around the Southern Ocean, as the response seems to be more consistent with the wind changes in the Pacific and Indian sectors (Patara et al., 2016; Meredith, 2016).

In an eddy compensation regime, strengthening winds tend to accelerate the wind-driven overturning circulation. But the increase in eddy activity discussed above also enhances the eddy-induced overturning circulation, which compensates the wind-driven overturning intensification (Abernathey et al., 2011; Gent, 2016; Rintoul, 2018). The compensation is however only partial, and not over the same depth range, so the increase in winds is thought to be associated with a changing upper cell of the Southern Ocean MOC (Farneti et al., 2010; Dufour et al., 2012; Hogg et al., 2017). This upper cell acceleration as a response to wind strengthening is consistent with observation-based estimates of change in water-mass age (Waugh et al., 2019).

Observation-based estimates of mode water subduction in the past decade tend to concur with an increased upper cell of the SMOC over this period (Gao et al., 2018). In the future, these changes are expected to continue as winds continue increasing and shifting southward (for all future emission scenarios except strong mitigation scenario ; Meredith et al., 2019; Fox-Kemper et al., 2021). By modelling the response of the water masses' ideal age under strengthening and shifting winds, Waugh et al. (2019) show that SAMW ideal age decrease linearly with increasing and shifting winds.

But other drivers than winds may have an influence on the changes in the ACC transport. In fact, changes in surface buoyancy from intensification of the global hydrological cycle and heating (Trenberth, 2011; Frölicher et al., 2015) may drive the acceleration of the ACC, by increasing the density gradient across the ACC (Shi et al., 2020).

In the lower cell of the SMOC, the main change in the tridimensional circulation is a decline of the volume and a warming of the dense Antarctic Abyssal Water (AABW) (Purkey and Johnson, 2012), suggestive of a lowering of the cell and a slowdown of the bottom limb (Desbruyères et al., 2016). This trend has been observed in all the major bottom water production sites, such as the Weddell Gyre (Jullion et al., 2013; Abrahamsen et al., 2019), in the Ross sea (Jacobs and Giulivi, 2010), or in Adélie Land (Aoki et al., 2005; Rintoul, 2007). Several source of numerical evidence have shown that this change is consistent with increased glacial meltwater flux in the high latitude ocean, which would reduce the density of bottom waters, and will eventually reach a point where shelf water of all sectors of the Southern Ocean will become too light to sink in the abyss (Bronselaer et al., 2018; Golledge et al., 2019; Lago and England, 2019; Moorman et al., 2020). However, a number of new observation-based studies have recently reported possible recovery of the Antarctic Abyssal Water (AABW) in a few sectors of Southern Ocean (Abrahamsen et al., 2019; Castagno et al., 2019; Gordon et al., 2020; Silvano et al., 2020). In the future, the IPCC AR6 concludes with medium confidence that the lower cell will continue decreasing in the 21st century as a result of increased basal melt from the Antarctic Ice Sheet.

Past decades and future change in the horizontal circulation of the subpolar ocean remains unclear due to observational and numerical challenges in this part of the ocean. The circulation response to an idealized southward shift of the winds might be a decrease in Ekman southward transport close to Antarctica and a reduction of the downward Ekman pumping at the coast Spence et al. (2014). This would also lead to a weakened ASF associated with slower coastal currents Spence et al. (2014). But it remains unclear whether coastal easterlies are projected to shift consistently with the mid-latitude westerlies (Bracegirdle et al., 2020).

Temperature and salinity changes

Significant temperature changes have been observed in different parts of the Southern Ocean over the last decades, from ship-based observations, floats, and bathythermographs (Gille, 2002, 2008; Sallée, 2018). These trends reflect that the Southern Ocean accounted for 35–43% of the total heat gain in the upper 2000 m global ocean between 1970 and 2017, with a share that has increased to 45–62% between 2005 and 2017 (Meredith et al., 2019). A schematic of the distribution of the temperature trends in the Southern Ocean is shown on the left part of Figure .7.

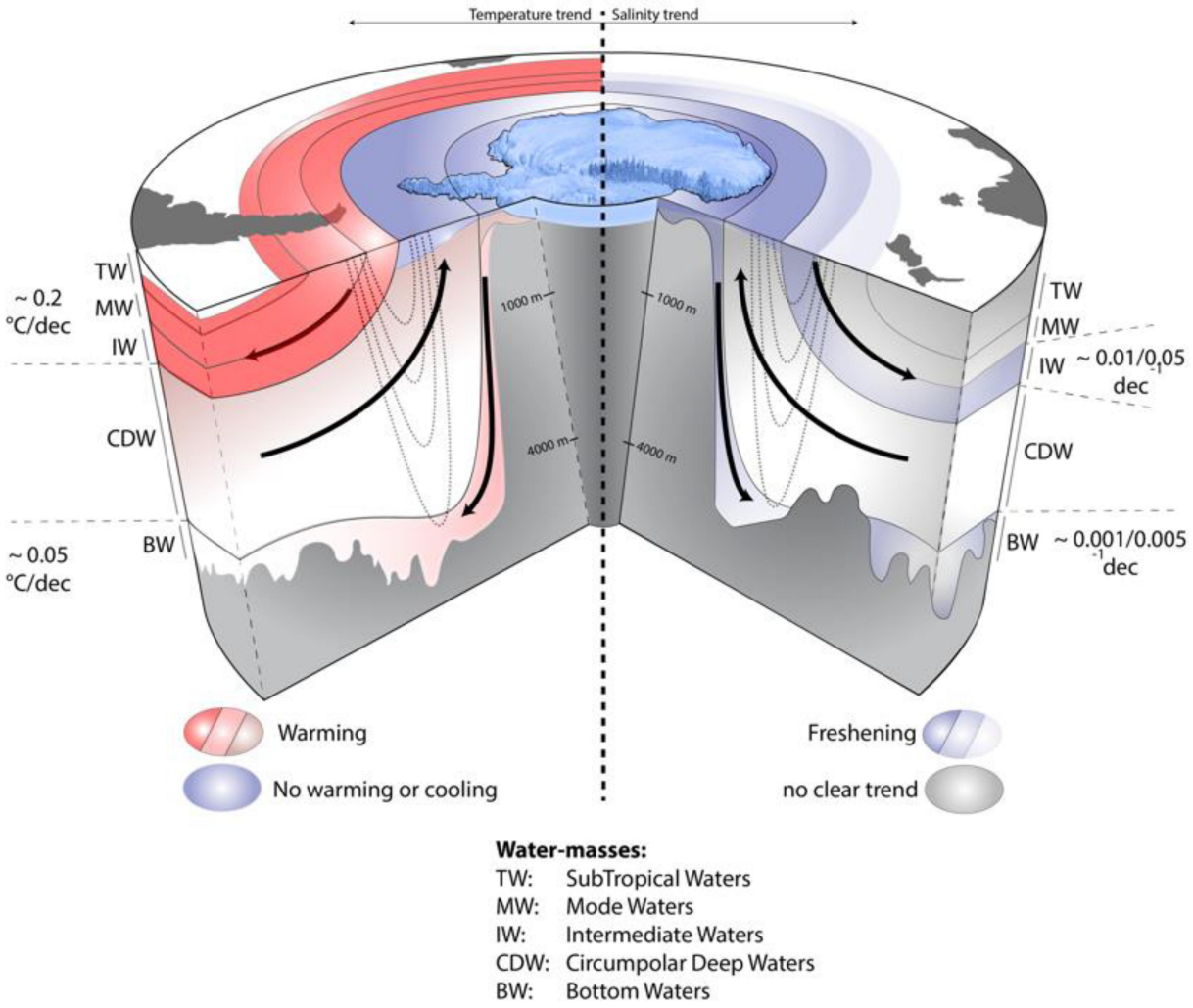

FIGURE .7: Schematic showing temperature and salinity trends in different layers of the Southern Ocean. The layers are defined as main water masses of the Southern Ocean : subtropical water (TW), mode water (MW), intermediate water (IW), circumpolar deep water (CDW), and bottom water (BW). Black arrows show the main overturning pathways in the basin, and the dashed black contours show a vertical slice of the deep-reaching Antarctic Circumpolar Current circulating clockwise around the Antarctic continent. Adapted from (Sallée, 2018), Figure and caption from Palmer et al. (2019).

The major part of the excess of heat stored in the SO is concentrated north of the ACC, in the latitude band 30–50°S. In this sector, in the upper 2000 m, the SAMW and the Antarctic Intermediate Water (AAIW) have experienced strong warming and thickening over the past decades (Sprintall, 2008; Giglio and Johnson, 2017; Gao et al., 2018; Swart et al., 2018). These trends are consistent with increasing surface heat flux and local wind stress curl increasing the downwelling north of the ACC. South of the ACC, in the surface layer, the ocean has experienced a slight cooling trend over the past decades. Its cause is still under debate. This summertime cooling might be driven by summertime wind anomalies associated with the SAM trends, transferring heat from the surface layer downward (Doddridge et al., 2021). Other studies associated this cooling with changes in freshwater fluxes. While Haumann et al. (2020) present changes in the sea ice dynamics as the main driver of this cooling, Rye et al. (2020) concludes that an increased meltwater discharge primarily drives it. Both of these studies argue that increased freshwater

flux would have stratified the ocean (Sallée et al., 2021), which would tend to isolate the surface layer from the warmer CDW, reducing heat transfer toward the mixed-layer. The upper layer of the CDW has experienced slight warming and shallowing close to the Antarctic continent, representing a potential threat for the stability of Antarctic ice shelves (Schmidtko et al., 2014). This warming is consistent with the increased stratification of the upper Southern Ocean and the surface cooling.

Salinity trends over the last decades have been driven mostly by surface forcing from cryosphere (Rye et al., 2020; Haumann et al., 2016) and air-sea freshwater fluxes changes (Held and Soden, 2006) inducing the observed freshening of the surface layer (Aoki et al., 2013; Morrow and Kestenare, 2014). Salinity anomalies are then transported by the mean flow, inducing a freshened subsurface (Durack and Wijffels, 2010). At the Antarctic continental shelf, the shelf waters in bottom water formation regions have been freshening (Jacobs and Giulivi, 2010; Jullion et al., 2013; Meredith et al., 2014; Palmer et al., 2019). This freshening is associated with a warming trend, consistent with the changes in the water freezing point (Jacobs and Giulivi, 2010). Consequently, the abysses of the Southern Ocean are warming and freshening (Rintoul, 2007; Shimada et al., 2012; Purkey and Johnson, 2013). While a rebound of the shelf water salinities has been reported in the Ross sea (Castagno et al., 2019), the latest projections show that the freshening and decrease in the volume of bottom water formation will continue in the future (Fox-Kemper et al., 2021).

Freshening at the surface has also been propagated northward, dominating a large part of the Southern Ocean south of 45°S (Swart et al., 2018), and can also be found in the subsurface waters such as the samw and AAIW (Durack and Wijffels, 2010) due to the subduction of the subsurface anomalies (Figure .7 ; Palmer et al., 2019).

3.3) Cryosphere changes

Sea Ice

In contrast to the dramatic sea ice decline that has been observed in the last decades in the Arctic (Comiso et al., 2017), the Antarctic sea ice area has not experienced statistically significant change (Fox-Kemper et al., 2021). This overall weak change actually hides a much more pronounced and regionally contrasted change in sea ice cover. Regional sea ice trends are larger but are heterogeneous circumpolarly (Figure .8cd. ; Eayrs et al., 2021) and differ according to the time period of observation.

From 1979 to 2015, there was a SIC gain in most parts of the subpolar basin, except in Amundsen-Bellingshausen seas and east of the Weddell Sea (Figure .8ac. ; Eayrs et al., 2021). This regional pattern may result from regional wind variability associated with climate modes variability (Holland and Kwok, 2012; Sigmond and Fyfe, 2014; Haumann et al., 2014). Overall, Antarctic sea ice extent has been slightly increasing from 1979 to 2014 (Figure .8a.). Using a model forced with atmospheric reanalyses, Holland (2014) estimated that the Antarctic sea ice volume has been increasing with a rate of 0.4% per year over 1992-2010, with sea ice thickness trends regional distribution consistent with the SIC trends. These trends may result from changes in the Southern Ocean winds, but also from spring changes of mid-latitude westerlies,

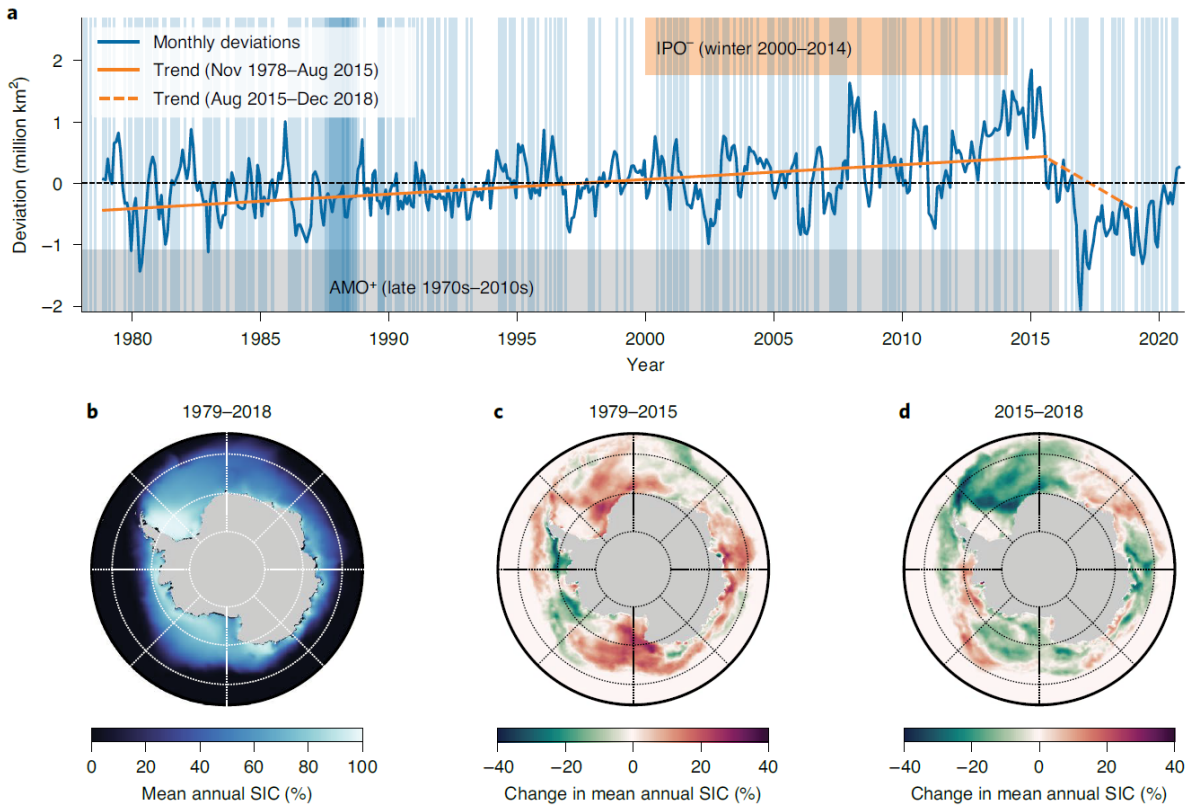

FIGURE .8: Variability in Sea Ice Concentration (SIC) and Sea Ice Concentration (SIC) from passive microwave remote sensing. (a) Monthly mean SIE anomalies since 1979 with respect to the 1979–2018 climatology (blue line) ; trend lines (orange ; dashed orange) calculated through the monthly anomalies. Orange shading shows the IPO and grey shading shows the AMO+. Blue shading shows months with weakened westerlies (SAM-). (b) Mean annual SIC 1979-2018. (c) Mean annual SIC changes from 1979 to 2015. (d) Mean annual SIC changes from 2015 to 2018. Figure and caption from Eayrs et al. (2021).

allowing an increased advection of atmospheric heat in the subpolar Southern Ocean (Eayrs et al., 2021). However, wind and atmospheric heat changes are not the only forcings responsible for modifications in sea ice distribution and volume. From the 1970s, a surface freshening of the Southern ocean has been highlighted by several studies (Durack et al., 2012; de Lavergne et al., 2014). From a model with preindustrial conditions and no wind trends, Purich et al. (2018) was able to accurately reproduce the observed regional sea ice trends, only by adding freshwater at the ocean surface calling for a reconsideration of the main drivers of the sea ice changes.

From 2014 onward and for the first time in 30 years, Antarctic sea ice extent experienced a strong and abrupt decrease (Figure .8ad. ; Turner et al., 2017; Meehl et al., 2019; Eayrs et al., 2021). Reasons for this drop in sea ice cover and extent remain unclear, but several plausible explanations have been put forward. On the one hand, Meehl et al. (2019) highlight a warm temperature anomaly in the southern ocean due to teleconnections with the Indian and western Pacific oceans, which might have caused unprecedented melting of the sea ice. On the other hand, Wang et al. (2019) bring out the role of the combination of the most negative SAM

since the 1960s in November 2016 with an anomalously deep ASL (Turner et al., 2017). These extremely low sea ice anomalies continued in 2017, reaching another minimum in sea ice and staying extremely low in 2018 (Figure .8a ; Parkinson, 2019; Eayrs et al., 2021).

Continental Ice

Antarctic mass loss has been accelerating over the last decades, reaching 252±26 Gt per year over 2009-2017, more than 6 times the mass loss trend over 1979-1990 (Figure .9 : Rignot et al., 2019). This increasing mass loss is primarily caused by CDW inflow on the continental shelf, bringing relatively warm water toward the ice shelves and accelerating the basal melt (Cook et al., 2016).

As for sea ice extent change, ice shelves mass trends are regional. The most important mass loss are located in the Amundsen-Bellingshausen seas (Milillo et al., 2019), the Wilkes Land (Shen et al., 2018), and West and Northeast Antarctic Peninsula (Wouters et al., 2015; Cook et al., 2016). In the Amundsen and Bellingshausen seas, ice shelf basal melt has been increasing dramatically and is accelerating (Paolo et al., 2015).Indeed, changing ocean currents bring warmer CDW to the west Antarctica continental shelf, subsequently melting the ice shelves from below (Nakayama et al., 2018). It is estimated that between 0.3 and 0.4 Sv of CDW enters the continental shelf through a localised bathymetry channel (Wåhlin et al., 2010).

While other parts of the Antarctic have not experienced such large changes in recent years, some of them may possibly experience increasing melting rates in the 21st century in response to climate change. For instance, in the Weddell sea, changes in the ASC caused by modifications in sea ice cover can be responsible for introducing a larger amount of warm water under the Filchner-Ronne ice shelf (Darelius et al., 2016), that would dramatically increase melt rate of this large ice-shelf (Hellmer et al., 2012).

Since 1971, Antarctic mass loss has contributed to 6.8 (66% probability range : -3.9 to 17.5 mm) to the sea level rise (Fox-Kemper et al., 2021). In the future, continuing ice shelves and glaciers melting might eventually threaten the Antarctic ice cap stability, inducing an increase in ice discharge in the ocean (Mouginot et al., 2014). While many uncertainties remain on the future of the Antarctic Ice Sheet (Edwards et al., 2021), some long-term simulations have shown that Antarctica ice loss may contribute up to 14 centimeters to sea level rise by 2100 in a high greenhouse gas emission scenario (Golledge et al., 2019). Part of the future Antarctic Ice Sheet depends on the still unclear positive feedback between increasing mass loss rates and subsurface ocean warming (Bronselaer et al., 2018).

4 In situ and satellite ocean observation in the seasonally ice-covered Southern Ocean

Coordinated international efforts to monitor Antarctic climate began in the International Geophysical Year of 1957/58 (Jones et al., 2016). Since then, the ever-increasing ocean observing capacities of the Southern Ocean has remained, but has not been homogeneous. While the number of both in-situ measurements and remote sensing capacities has dramatically risen

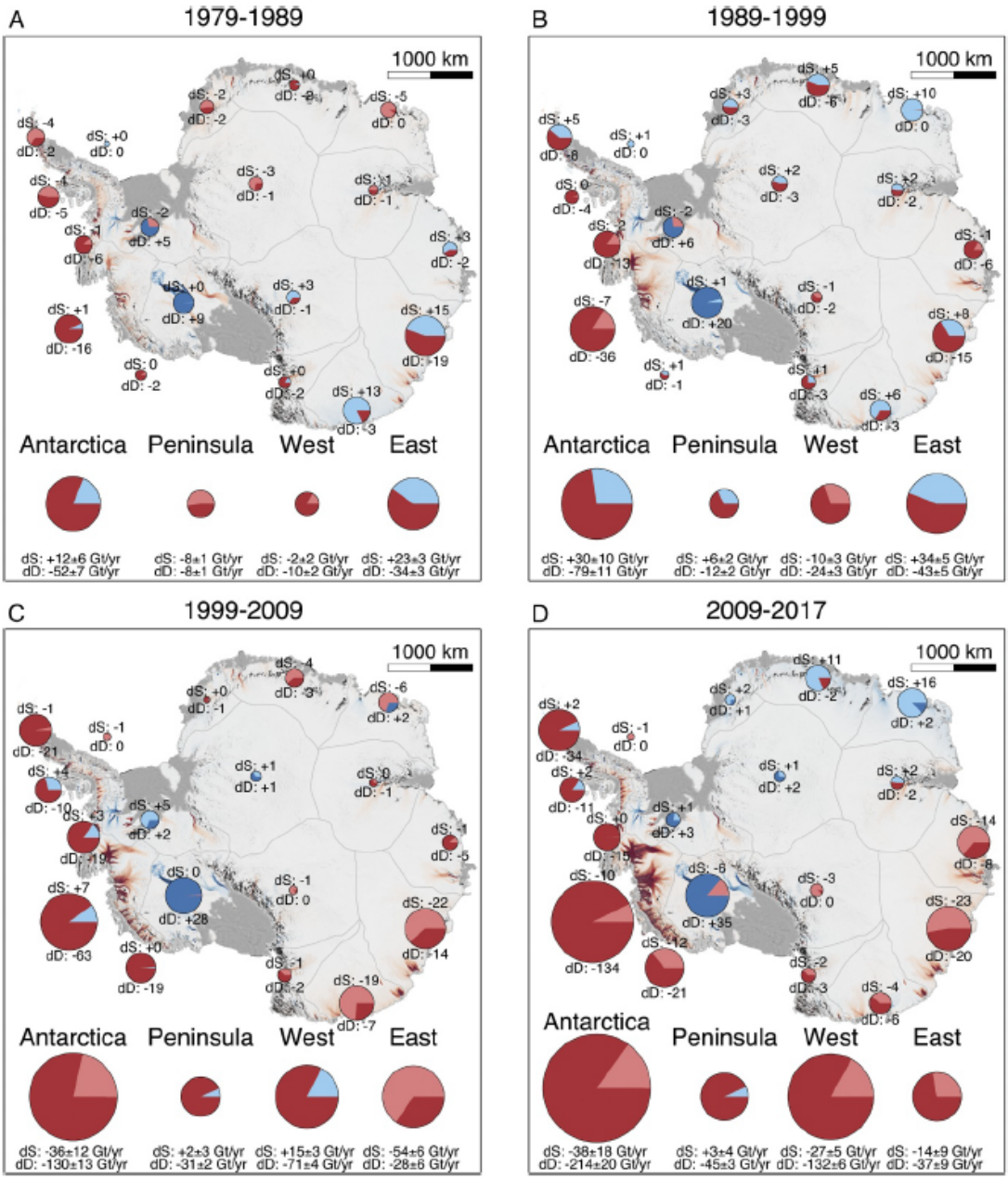

FIGURE .9: Ice mass balance of Antarctica using the component method (SMB, on grounded ice minus ice discharge, D, at the grounding line) for (a) 1979–1990, (b) 1989–2000, (c) 1999–2009, and (d) 2009–2017. The size of the circle is proportional to the absolute magnitude of the anomaly in D ($dD = SMB_{1979-2008}D$) or SMB ($dSMB = SMBSMB_{1979-2008}$). The color of the circle indicates loss in dD (dark red) or dSMB (light red) versus gain in dD (dark blue) or dSMB (light blue) in billions of tons (10^{12} kg) per year. Dark color refers to dD ; light color refers to dSMB. Plots show totals for Antarctica, Antarctic Peninsula, West Antarctica, and East Antarctica. Background is the total mass balance spread into the drainage basins color-coded from red (loss) to blue (gain). Figure and caption from Rignot et al. (2019)

over the ACC and more generally over the ice-free ocean, observation coverage remains poor in the seasonally ice-covered region (Newman et al., 2019). This lack of observation remains one of the main limits for our understanding of the subpolar Southern Ocean processes. The lack of observation arguably results from a compound of specific characteristics of the Southern

Ocean that makes its observation challenging : (i) it is a very vast ocean, and remote for most of the inhabited region ; (ii) its hostile climate conditions makes any expedition a challenge in itself ; (iii) the presence of sea ice required technology to be specifically adapted : autonomous assets (all type of gliders, buoy, or floats) that have helped observe a large part of the global ocean cannot be readily deployed ; ocean observing satellite are blocked by the presence of sea ice ; ship expeditions require ice-breaker and are both costly and challenging.

In this section, I present the various types of observation capacities for measuring the Southern Ocean water-mass properties and circulation, both at short and long timescales. In a large part of my thesis, I propose to revisit radar altimetry treatment to recover observations and physical understanding of the Southern Ocean in sea ice-covered regions. Then, I introduce the basics of the radar altimetry technique and its application in both open ocean and ice-covered oceans.

4.1) In situ measurements

Ship-based observations

Most of the in-situ temperature and salinity profile observations available in the subsurface Southern Ocean before 2004 were sampled from ship platforms. Ship-based observations remain the gold standard in terms of in situ data quality, so it represents a key part of the observing system if one aims to investigate long-term changes of the hydrography. However, ship observations remain very sparse in the Southern Ocean (especially when considering its vast area). That makes it difficult to evaluate long-term change, and in particular, Southern Hemisphere heat content and temperature changes over the decades prevailing the autonomous float measurements (Gille, 2008). Ship observations of the Southern Ocean hydrography are made mainly from three types of instruments : eXpandables BathyThermographs (XBTs), bottle data (OSD), and Conductivity Temperature Depth (CTD) probes.

One of the key programs that have contributed to increasing Southern Ocean observations is the World Ocean Circulation Experiment (WOCE) program. The WOCE program consisted of repeated hydrographic sections sampling temperature, salinity, and chemical properties in the whole Earth oceans, including multiple sections in the Southern Ocean. From repeated transects crossing the whole Southern ocean in the 1990s, it allowed the monitoring of long term subsurface temperature changes (Chaigneau et al., 2004; Gille, 2002, 2008) or ACC transport (Cunningham et al., 2003) over various parts of the Southern Ocean. The WOCE program has since been continued by the GO-SHIP international program (Sloyan et al., 2019). From these international programs, both the hydrography structure and the tridimensional circulation of the Southern Ocean has been examined (e.g. Sloyan and Rintoul, 2001; Talley, 2003; Naveira Garabato et al., 2014), including specific estimates of bottom water production (e.g. Orsi et al., 1999; Shimada et al., 2012).

A myriad of other in situ observations programs has also helped sample the Southern Ocean with specific process-understanding strategies (rather than long-term monitoring). I would not be able to cite all of them, but such programs helped in particular to observe large parts of the Antarctic continental shelf and slope with various instruments and strategies.

Moorings

Moorings are devices that sample ocean properties for an extended period, from an instrument attached to a line moored to the seafloor. They consist of an anchor positioned at a defined location, and a cable linked to a float higher in the water column. Instruments are positioned along this cable and sample dynamics, physics, and/or chemistry at various depths.

Transects of moorings can be established across the Southern Ocean main currents, to estimate their transport. In the Drake passage, moorings were used to compute the mean volume transport of the ACC and its evolution, by combining with satellite altimetry (Koenig et al., 2014) or with Bottom Pressure Recorders (Chidichimo et al., 2014).

Moorings measurements provide very valuable observations to study the ice-covered oceans. They can be deployed in the summer, and sample the subpolar Southern Ocean in winter even when it is ice-covered. For instance, from hydrographic and CTD moorings deployed on the Antarctic Peninsula in 2009-2010 and 2012-2013, Flexas et al. (2015) established the role of the tides on the ASF and ASC. Mooring observation were also used to first uncover seasonal variability and its forcing of the ASF in the Weddell Sector (Núñez-Riboni and Fahrbach, 2009; Chavanne et al., 2010).

Floats

Autonomous profiling floats are extensively used to measure the hydrography, dynamics, or chemistry of the global oceans. Floats drift with the oceanic currents and sample the ocean from the surface to a prescribed depth by changing its buoyancy. When reaching the surface, they communicate their measurements by satellite which allows real-time observation of the global oceanic properties at depth.

The Argo program is a broad-scale array of autonomous floats sampling the global ocean (Roemmich and Gilson, 2009) and marks a strong step for a transition from an opportunistic observation system of the upper layer of the Ocean to a dedicated observation system. Deployment of the floats started in 1999, with 3000 floats sampling the global ocean in 2007 (Johnson et al., 2022).

In the Southern Ocean, Argo floats measurements were a huge step forward towards a better coverage of the first 2000 meters of the ocean. In one year in the Southern Ocean, the Argo dataset provided more profiles than acquired in the preceding 100 years (Riser et al., 2016).

Outcomes of the Argo program in the Southern Ocean were numerous. In the northern part of the Southern Ocean, it to documented the increasing heat storage between latitudes 40°S-60°S (Llovel and Terray, 2016; Böning et al., 2008b; Giglio and Johnson, 2017; Gao et al., 2018), decrease in salinity (Giglio and Johnson, 2017),and the position of the ACC fronts (Sokolov and Rintoul, 2009a).

Autonomous floats are riskier to use in the subpolar Southern Ocean. As they need to reach the surface to transmit their data to satellites, the sea ice represents an important issue to their deployment and transmission. Several programs worked to unlock this main constraint so that

now, autonomous floats routinely sample the ice-covered Southern Ocean (Klatt et al., 2007). But because of the risk and the added technological complexity, the observation density remains much lower than in the open ocean regions.

Others

Other in-situ measurements dedicated to the Southern Ocean have been developed. One of them is the increasing number of instrumented marine mammals, with the MEOP program (Treasure et al., 2017), generating a large number of hydrographic profiles in the polar oceans. Instrumented elephant seal data exists since 2004, and reaches depths of 2000 meters (Roquet et al., 2014) and have been used for instance to describe the seasonal variations of the Antarctic Slope Front (Pauthenet et al., 2021).

Ice-capable profiling gliders or Autonomous Underwater Vehicle (AUV) have also sampled the ice-covered ocean, some at very high latitude, and in ice cavities (Dowdeswell et al., 2008; Barker and Whitcomb, 2016; Heywood et al., 2014). Profiling gliders are autonomous vehicles that can be commanded remotely and use multiple sensors to measure ocean properties and dynamics (Eriksen et al., 2001). AUV are similar to gliders but are propelled and can carry a larger pack of sensors (Wynn et al., 2014). Both are increasingly used in ice-covered regions to investigate ocean-ice interactions.

4.2) Radar altimetry technique and its application to polar oceans

Radar altimetry principle

Satellite altimetry has proved to be a very successful solution to observe the solid earth and the surface ocean geostrophic dynamics. Over the ocean, satellite radar altimetry consists in retrieving the ocean topography by measuring the orbit of the satellite from a reference surface (H) and the distance between the satellite and the surface of the ocean (D). The Sea Surface Height (SSH) is then computed as

$$SSH = H - D. \tag{4.1}$$

Orbit determination lies on the Precise Orbit Determination (POD) system, which lies on the combination of an orbit modelling, onboard sensors, and an earth reference (Stammer and Cazenave, 2018). The distance between the satellite and the sea surface is retrieved from an onboard radar instrument. The instrument emits a radar wave at the nadir (local vertical below the instrument) toward the sea surface. The wave travels through the atmosphere and is backscattered toward the satellite. The two-way travel time between the emission and the reception, which is corrected from the atmosphere effects on the wave and the ocean state, allows retrieving the distance between the satellite and the sea surface.

Historically, while the method has been investigated since the 1970s, it reached its scientific maturity in the early 1990's, with the launch of ERS-1 (1991 Sandwell and Smith, 1997) and TOPEX-POSEIDON (1992 ; Fu et al., 1994). The satellite constellation has been constantly improving, with GEOSAT Follow-On (1998-2008), the Jason series (3 satellites from 2001 to nowadays), and others such as Envisat or AltiKa. Throughout these years, great progress has been

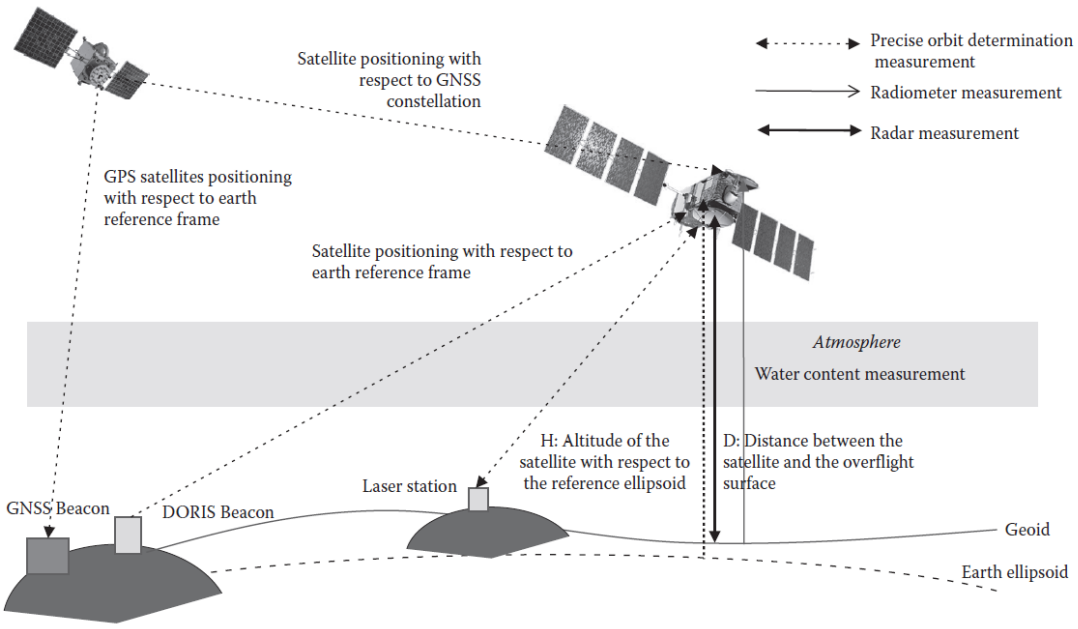

FIGURE .10: Satellite radar altimetry measurement principle : The main sensor used to compute the distance between the satellite and the targeted surface is a radar ; however, to obtain the appropriate measurement accuracy, one needs a radiometer to measure the quantity of water that impacts the atmospheric propagation of the radar signal. To compute the altitude of the satellite with respect to an in situ network that constitutes the Earth reference, sensors onboard the satellite are used in combination with modelling of satellite trajectory to perform the Precise Orbit Determination (POD) of the spacecraft. Figure and caption from Stammer and Cazenave (2018)

made on the accuracy and spatial resolution of satellite measurements. New instruments have also been developed to increase the capacities of satellite altimeters. Cryosat-2 (2010-) is carrying a Synthetic Aperture Radar Altimeter (SRAL), including a Delay-Doppler mode (or SAR mode, Synthetic Aperture Radar mode) over the sea ice regions, allowing a better along-track resolution (Wingham et al., 2006). It also includes a SAR-In (SAR-Interferometric) that improves the across-track resolution. SAR altimeters are increasingly more used on new satellites, and classic Low Resolution Mode (LRM) altimeters are expected to disappear in the future. Other great improvements will be undoubtedly made by the interferometric Radar and its even higher resolution, such as onboard the soon launched SWOT satellite (Biancamaria et al., 2016; Morrow et al., 2019).

Determination of geostrophic currents

The flow of geophysical fluids is described by the Navier-Stokes equation, describing the equilibrium of a Newtonian, incompressible fluid (Pedlosky, 2013). The Navier Stokes equation can be written as :

$$\rho \frac{\partial(\mathbf{u})}{\partial t} + \rho \mathbf{u}.\nabla \mathbf{u} = -\nabla p + \mu \nabla^2 \mathbf{u} + \mathbf{F}, \tag{4.2}$$

where **u** is the velocity vector of the fluid, ρ is its density, p is its pressure, μ is the viscosity of the fluid, and **F** are the external forces applied to the fluid. The terms of this equation (Eq. 4.2) refer, from left to right, to the acceleration of the fluid, the advection term, the pressure gradient, the viscosity and the other forces applied to the fluid.

Estimating ocean current from gridded Sea Level Anomalies requires the use of the geostrophic approximation. In this approximation, it is considered that the horizontal pressure gradient and the Coriolis force balance each other (Pedlosky, 2013). This approximation is possible for large features with Rossby number well below unity :

$$R_o = \frac{v}{f.L_c} << 1, \tag{4.3}$$

with v the speed of the fluid, L_c the spatial scale of the dynamical feature, and f the Coriolis parameter ($f = 2\Omega \sin \Phi$, with Ω the Earth rotation speed and Φ the latitude).

Under the geostrophic approximation, and from the Navier-Stokes equation, the geostrophic balance writes as :

$$v_g = \frac{1}{f\rho} p_x, \tag{4.4}$$

$$u_g = -\frac{1}{f\rho} p_y, \tag{4.5}$$

where u_g and v_g are respectively the zonal and meridional components of the geostrophic currents. This last set of equation can be rewritten by introducing η, the dynamic topography of the ocean, as :

$$v_g = \frac{g}{f} \eta_x, \tag{4.6}$$

$$u_g = -\frac{g}{f} \eta_y. \tag{4.7}$$

From these equations, it appears that only the slope of the dynamic topography is needed to compute the ocean currents under the geostrophic approximation. Therefore, geostrophic currents can be computed from satellite altimetry observations.

Radar Altimetry application in the open ocean

Since 1992, satellite altimetry has been used to map global ocean geostrophic circulation through high precision sea level measurements, thereby allowing a big step forward in our understanding of the ocean circulation, its variability, and its response to climate change (Morrow and Le Traon, 2012). The number of satellites sampling the ocean is now larger than ever, creating new possibilities in terms of combination and sea level mapping resolution (Taburet et al., 2019). Daily and global multi-mission products such as the Data Unification and Altimeter Combination System (DUACS ; Taburet et al., 2019) reach a horizontal resolution of 100 km at high latitude (Ballarotta et al., 2019). However, these products do not include the seasonally ice-covered regions of the global oceans (Figure .11a), even though conventional satellite altimetry can help to understand the open ocean parts of the polar oceans (Prandi et al., 2012).

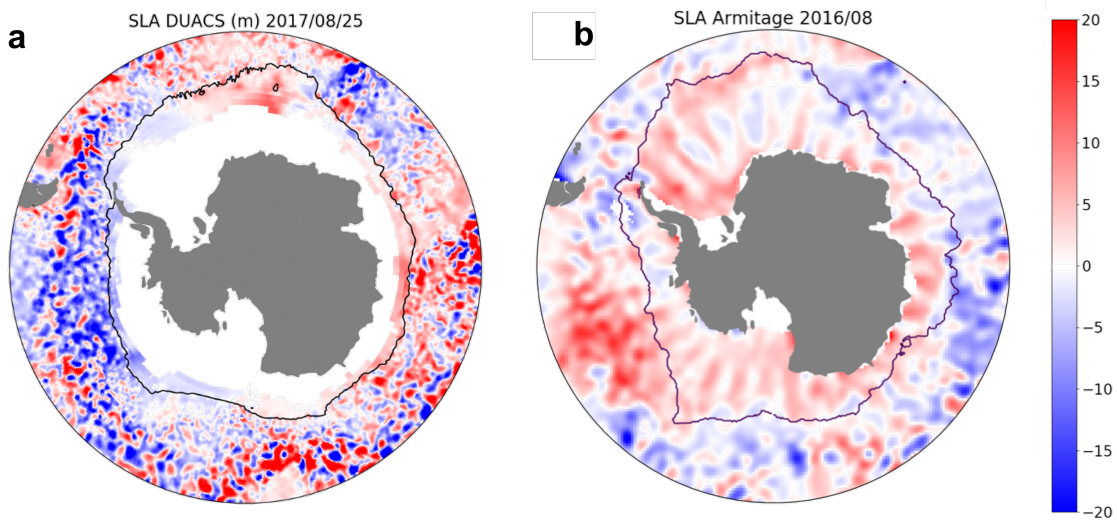

FIGURE .11: Snapshots of existing SLA products over the Southern Ocean. a. SLA snapshot from the DUACS global product in the open ocean (Taburet et al., 2019). b. SLA snapshot from Armitage et al. (2018) monthly product constructed from Cryosat-2.

Dedicated processing needs to be used over ice-covered areas : one of the aims of my thesis is to explore the impact of new dedicated processing in the seasonally ice-covered area of the Southern Ocean.

Sea Surface height determination in the ice-covered oceans

The radar altimetry technique has long been considered as a potential way to observe ocean dynamics under sea ice. Drinkwater et al. (1991) found that it was possible to identify the leads from the floes in the ice-covered regions with no other information than the waveform transmitted back to the altimeter. It led to numerous studies both in the Arctic and the Southern Ocean (See **Chapter II**). However, despite the high number of satellites sampling the Southern Ocean in the last decades, all studies conducted in the past years have used only one satellite (Armitage et al., 2018; Dotto et al., 2018). This results in relatively low spatial and temporal resolution of the currently existing products (Figure .11b), but also in lower accuracy as more satellites provide more calibration methods between each other. Methods for merging multiple satellites into one product exist (Taburet et al., 2019), but none dedicated to the Southern Ocean have been implemented yet.

5 Main scientific questions

In this introduction, I attempted to present the state of the art of our knowledge in the mean Southern Ocean physical state, and in its variability across various temporal and spatial scales : from the large-scale oceanic features down to the mesoscale. While processes at various scales and their forcings have been presented separately in this introduction, they in fact interact with each other over the whole spectra. These interactions shape the Southern Ocean circulation as we know it, and have a determining role in the global and regional climate. I also introduced some of the changes occuring in the Southern Ocean. These changes are highly coupled to changes in the atmosphere and in the cryosphere. The understanding of these couplings and feedbacks remains incomplete and hinders the understanding of how the Southern Ocean system will continue to change in the future (Meredith et al., 2019; Fox-Kemper et al., 2021). One important caveat for our progress is the availability of observations in the Southern Ocean in general, but particularly, at great depth and in the seasonally ice-covered regions.

Vernet et al. (2019) recently reviewed the remaining barriers to an improved understanding of the Weddell sea mechanisms. Those are in many ways relevant to the wider subpolar Southern Ocean. Among the processes that may be given priority of study : the connections of the subpolar gyre with the rest of the Southern Ocean ; the changes in air-sea-ice interactions ; the cross-continental shelf processes ; and the subpolar water masses variability and export. Most of these areas of study are limited by the scarce wintertime observations and our lack of understanding of ocean-cryosphere coupling. For instance, the ocean-ice shelf coupling represents a key obstacle to understanding and projecting future ice shelves melt and ice sheet mass loss. We also remain unable to fully describe the processes controlling CDW intrusions on Antarctica's continental shelf. Several processes that require improved description for a better understanding of the Antarctic Slope Current (ASC) variability have been listed in Thompson et al. (2018). They include the link between the interior density changes and remotely observed variability ; the connectivity of the ASC with the ice shelves ; or the response of abrupt changes in warm CDW inflows on the continental shelf. Thompson et al. (2018) also emphasized the need for a better theoretical understanding of the links between ASC, winds, buoyancy forcings, eddies, and tides, but also the need for more observation and higher modelling capacities able to model accurately the full circumpolar ASC. Finally, several obstacles remain for accurate modelling of the future changes of the ASC, such as the understanding of the decadal internal variability of the temperature changes of the water masses, the changes in surface forcings, but also the potential feedback mechanisms between the cryosphere, the winds, the warm water intrusions and the along slope and cross-slope dynamics of the ASC.

While this thesis is motivated by these knowledge gaps, I certainly do not have the (unrealistic) ambition to resolve and document all of these processes. The objective I set for my thesis is to deepen the observation of the changes affecting the Southern Ocean, and to explore the variability of the large-scale and mesoscale processes and their role in regulating the circulation system of the Southern Ocean and driving its changes. I also aim at examining the forcings of these variabilities and changes. I focus on three distinct scales of importance, from the larger to

the smaller : long-term multi-decadal and basin-scale change ; seasonal variability of the main horizontal circulation features, i.e. mostly focusing on gyres and slope current ; and mesoscale activity in the subpolar ice-covered region.

This thesis is motivated by the following scientific questions :

How have the circulation and hydrography of the Southern Ocean changed over the past several decades and are documented changes a significant departure compared to interannual variability ?

In this general introduction, I emphasized the importance of the Southern Ocean in the global oceanic circulation system, and how this region is impacted by climate change. Understanding the changes at stake goes through their accurate description. Yet, despite the increasing capacities of the observation system of the Southern Ocean, the monitoring of its changes is constrained by the limited long-term measurements. This is particularly true in the subpolar region of the Southern Ocean. As documented above in the Introduction, many changes of the Southern Ocean have been described in past studies, but it remains unclear how much of the described changes are significant departures from interannual variability, and whether they are caused by internal variability, or long-term forced climate change.

What mechanisms drive the variability and changes of Southern Ocean circulation and hydrography ?

Arguably at least as important as describing the change themselves, understanding the processes governing Southern Ocean variability and changes is central to our understanding of the Southern Ocean system. Processes may depend on time scales of interest (long term, decadal, interannual, seasonal, monthly, daily) and may probably involve interactions between multiple elements of the climate. Today, we are only starting to understand the seasonal variability of the subpolar ocean and its importance for setting large-scale circulation. Additional work development of more diverse observational and methodological frameworks remains required to progress our understanding of processes dominating seasonal, interannual, and long-term variability of the Southern Ocean.

How do we expect the Southern Ocean circulation and hydrography to change in the future ?

Lack of understanding of past change and governing processes hinders our understanding of future change of the Southern Ocean system. In this regard, the recent IPCC reports are unambiguous and assessed that almost all future Southern Ocean changes are known with low confidence (e.g. Meredith et al., 2019; Fox-Kemper et al., 2021). This thesis does not enter the realm of future Southern Ocean climate change as simulated by climate models. It is, however, motivated by furthering our understanding of plausible futures from improved process understanding. Given the current lack of understanding of governing Southern Ocean processes, and given the known limitations of climate models in simulating the Southern Ocean, identifying main order processes may allow to first, better evaluate current climate models, second, to discuss potential change of individual processes.

To these aims, I attempt to use the best-fitted observations for each purpose. Identifying fit-for-purpose observation-based datasets represent the initial founding step of my thesis. I propose to base my work on two essential datasets that I contributed to revamp and better

reprocess for the specific aim of my thesis : a 25-year long repeated temperature observation at one choke-point across the Southern Ocean basin ; a 6-year set of gridded observations from three satellites that have sampled the subpolar Southern Ocean. In consequence, a side (but important) objective of this thesis is to recover these existing measurements in the Southern Ocean, and to propose new processing to obtain original and valuable sources of information freely distributed as a service to the community.

In **Chapter I**, I present the temperature trends in the upper 800 meters of the Southern Ocean from a 25-year transect between Hobart (Tasmania) and Dumont d'Urville (Adelie Land). This results from the integration of thousands of XBT profiles, processed specifically to retrieve these trends. Some of the observed trends were found to overcome interannual variability. I also find that some subsurface warming and warm water shallowing trends have been underestimated in the past, with potential threats for the downstream ice shelves. There are however two main limitations for drawing conclusions on this study. First, it lacks spatial context : it is difficult to know how this transect integrates into the larger Southern Ocean. Second, the processes driving the Southern Ocean variability at various scales are still hardly known. Therefore, we still don't know their contribution to the response of the Southern Ocean system to climate change.

The following parts of this thesis rely on a newly developed satellite altimetry dataset. This product may be one of the best tools currently available to tackle both of these issues, as it covers the whole Southern Ocean and may be able to detect large-scale to mesoscale signals at the surface of the ocean. We have produced a new ocean surface topography dataset from satellite altimetry in the Southern Ocean in the context of this thesis. This dataset is described in **Chapter II**. We also present the dedicated processing needed to convert raw along-track waveforms into a gridded high-resolution ocean topography dataset. The dataset is then validated with independent data sources and the range of error is estimated. In **Chapter III**, I use this new product to document the seasonal cycle of the zonal geostrophic currents in the subpolar Southern Ocean. The dynamics of the Weddell Gyre, Ross Gyre, and Antarctic Slope Current are investigated and linked with the potential drivers of the variability. In **Chapter IV**, this same product is further explored to investigate mesoscale activity from an eddy identification and tracking procedure applied to the ice-covered Southern Ocean. Eddy properties are investigated, described, and the impacts of the drivers of the variability found in **Chapter III** on the eddies are explored. I conclude and discuss my results in the last chapter of this manuscript, including a discussion of potential future change.

CHAPITRE

I

Southern Ocean In-Situ Temperature Trends Over 25 Years Emerge from Interannual Variability

Sommaire

1 Preamble

In the general introduction, I presented the Southern Ocean, its circulation, properties, and changes. The amplitude and the multiplicity of Southern Ocean long-term changes are relatively well established. However, due to observation limitations, it remains unclear how much long-term change estimates are impacted by interannual to decadal variability. In that context, I aim in this chapter to revisit temperature change in the Southern Ocean, while trying to delineate long-term change and interannual variability.

Up to now, long term temperature change in the Southern Ocean has been assessed from multiple evidences, including analyses of Argo and ship-based CTD profiles (e.g. Schmidtko et al., 2014; Gao et al., 2018; Aoki et al., 2005; Gille, 2008; Sprintall, 2008) or CMIP models (e.g. Armour et al., 2016; Frölicher et al., 2015; Swart et al., 2018). Argo and model results are however limited by the low spatial resolution of the dataset used, the widely spread locations of the measurements, or the limits of modelling in the polar regions. The ship-based studies, on the other hand, can also be sensitive to irregular sampling throughout the years and seasons.

Still, these studies allowed the establishment of several temperature trends among various regions and water masses of the Southern Ocean. A strong warming trend north of the ACC was associated with the positive SAM index trends (Gille, 2008; Giglio and Johnson, 2017; Gao et al., 2018; Swart et al., 2018). At the same time, the increase in wind forcing, potentially associated with a sea ice and ice shelves induced increase of freshwater fluxes caused a surface cooling in the subpolar Southern Ocean (Schmidtko et al., 2014; Haumann et al., 2020; Rye et al., 2020; Doddridge et al., 2021; Armour et al., 2016). Under the surface, the CDW have been found to be warming and rising toward the surface at a slow rate (Schmidtko et al., 2014).

In this chapter, I evaluate the emergence of temperature trends of the upper layer of the Southern Ocean from interannual variability. This is done using in situ measurements, from 25-years of eXpandables BathyThermographs (XBTs) sampling across the Southern Ocean between 1992 and 2017, between Hobart (Tasmania) and Dumont d'Urville (Antarctica). This dataset covers the entire meridional extent of the Southern Ocean 6 times a year for 25 years. It represents a unique opportunity for revisiting observation of temperature trends and allows for the first time to estimate how the computed trends compare to interannual variability. It also allows to properly remove the impact of the seasonal cycle on the observed Southern Ocean trends.

2 Southern Ocean In-Situ Temperature Trends Over 25 Years Emerge from Interannual Variability

nature COMMUNICATIONS

ARTICLE

https://doi.org/10.1038/s41467-020-20781-1 OPEN

Southern Ocean in-situ temperature trends over 25 years emerge from interannual variability

Matthis Auger [1,2]✉, Rosemary Morrow[3], Elodie Kestenare [3], Jean-Baptiste Sallée[1] & Rebecca Cowley [4]

Despite playing a major role in global ocean heat storage, the Southern Ocean remains the most sparsely measured region of the global ocean. Here, a unique 25-year temperature time-series of the upper 800 m, repeated several times a year across the Southern Ocean, allows us to document the long-term change within water-masses and how it compares to the interannual variability. Three regions stand out as having strong trends that dominate over interannual variability: warming of the subantarctic waters (0.29 ± 0.09 °C per decade); cooling of the near-surface subpolar waters (−0.07 ± 0.04 °C per decade); and warming of the subsurface subpolar deep waters (0.04 ± 0.01 °C per decade). Although this subsurface warming of subpolar deep waters is small, it is the most robust long-term trend of our section, being in a region with weak interannual variability. This robust warming is associated with a large shoaling of the maximum temperature core in the subpolar deep water (39 ± 09 m per decade), which has been significantly underestimated by a factor of 3 to 10 in past studies. We find temperature changes of comparable magnitude to those reported in Amundsen–Bellingshausen Seas, which calls for a reconsideration of current ocean changes with important consequences for our understanding of future Antarctic ice-sheet mass loss.

[1] Sorbonne Université, CNRS, LOCEAN, Paris, France. [2] CNES, Toulouse, France. [3] LEGOS, CNRS/IRD/CNES/University of Toulouse III, Toulouse, France. [4] CSIRO Marine and Atmospheric Research, Hobart, Tasmania, Australia. ✉email: matthis.auger@locean-ipsl.upmc.fr

The Southern Ocean has been rapidly changing over the past decades with widespread consequences for the global climate. It has stored an outsized amount of heat associated with climate change that has been extracted from the atmosphere and stored in its subsurface water-masses[1,2]. The Southern Ocean alone has stored 35–43% of the global upper 2000 m ocean heat gain from 1970 to 2017, and an even greater proportion in recent years, with an estimate of 45–62% from 2005 to 2017[2]. This heat storage, as well as concomitant change in its vertical stability due to change in surface salinity[3–5], translates into significant warming of subsurface water-masses[6]. The overall water-mass warming since 1970 is composed of significant warming north of, and within, the eastward flowing Antarctic Circumpolar Current[7–9] (ACC), and slight cooling observed in the surface subpolar waters[10]. Some regions show slight warming and uplifting of the subpolar Upper Circumpolar Deep Waters (that lie directly offshore the Antarctic continental shelf), threatening to invade onto the continental shelves with drastic potential consequences for the melt of Antarctic Ice Shelves and subsequent global sea level rise[11].

Despite those emerging results, there are inherent limitations in our past and current observation system that pose a strong limitation in our confidence of any of these climate-scale changes that occurred in the Southern Ocean[12,13]. For most changes in the Southern Hemisphere, it remains unclear whether the natural and interannual variability can cause the observed change or overwhelms the forced response[13]. A recent study based on numerical simulations suggests that warming north of the Antarctic Circumpolar Current is largely human induced and overwhelms the natural variability[14]. But this remains one study using one single climate model, and our limited confidence in the representation of subpolar Southern Ocean processes in climate models drastically hampers our confidence at higher latitude[2]. Observations are needed, more than in any other region, to shed more light on long-term ocean trends and understand how they compare to natural and interannual variability.

In this paper, we unlock these limitations by presenting an observation dataset of the most frequently repeated and longest time-series of a temperature section across the Southern Ocean in the upper 800 m, from its northern boundary to Antarctica. The temperature section, referred to as Section IX28, is the longest of the three long-term high-resolution repeat upper ocean XBT temperature monitoring lines that have made observations of the seasonal heating cycle across the Southern Ocean[15]. IX28 has been repeated several times a year since 1992 at 140°E, from Hobart, Tasmania to Antarctica (Fig. 1a), providing us with a unique 25-year temperature time-series to robustly estimate summer temperature changes consistently across an entire meridional section, and document from observations how temperature changes compare to typical interannual variability.

Results

25-year Climatological state and long-term change. Based on the 148 repeats of the same section, we construct a summer temperature climatological mean over the 25 years (since November 1992), which shows the main Southern Ocean water-masses and the fingerprints of the main fronts associated with the Antarctic Circumpolar Current (Fig. 1b; see "Methods"). The warmest water-masses on the section, the Subtropical Water (STW) and SubAntarctic Mode Water (SAMW) are located in the northern part of the transects. Their southern extent is limited by the Subtropical Front (11 °C at 150 m[16]) and the Subantarctic Front (strongest temperature gradient between 3 and 8 °C at 300 m depth[17]), respectively. SAMW is found down to 600 m depth, beneath the summer mixed layer, consistent with previous studies[18,19]. Antarctic Surface Waters (AASW) are located in the upper 250 meters of the Southern Ocean and south of the Polar Front (most northern extent of the subsurface 2 °C water[20]). AASWs are composed of a remnant subsurface tongue of cold water produced in winter[21,22] (Winter Water), and warmer surface waters produced in summer[23,24]. Below the Winter Water tongue lies the less-dense Upper Circumpolar Deep Water (UCDW), then the denser Lower Circumpolar Deep Water (LCDW), that rises beneath the WW layer south of the Antarctic Divergence around 63°S. These Circumpolar Deep Waters are advected at depth around the Southern Ocean, and partly originate from North Atlantic Deep Waters[25].

We are interested in how this temperature structure is changing over time on a multi-decadal timescale. Over the past decades, the temperature has been warming overall across the section, but with a structure showing marked patterns, which are related to the different water-masses of the region. The largest warming reaching 0.4–0.8 °C per decade is observed on the northern end of the section, north and within the ACC (region A in Fig. 2b) in the subtropical waters and subantarctic Mode Waters. In contrast, on the southern end of the section, a cooling trend of 0.1–0.3 °C per decade is observed in the coolest water-mass of the region (region B in Fig. 2b), extending from the surface to about 200 m, in a region where the interannual variability has similar magnitude. Hints of cooling trends are also apparent in the surface layer further north, but the trends are dominated by interannual variability north of ~61°S in the surface layer. Deeper in the water column, the Upper Circumpolar Deep Water layer (region C in Fig. 2b) shows subtle warming trends of around 0.05 °C per decade from 62.5°S to 52°S, but here, the interannual variability is weak.

The temperature change structure shown across the section concurs well with past studies that have investigated long-term temperature trends in the Southern Ocean (ref. [6], and references therein). Here, we however bring an important step forward in our understanding of past changes by showing that Southern Ocean water-mass temperature trends is robust over a 25-year period. But more importantly, we are able to estimate the typical interannual variability (referred to here as noise) to better interpret the observed trends over a 25-year period (referred to here as signal; see Methods). In other words, from observations in the Southern Ocean, we are able to estimate whether the signal of temperature change has emerged above the interannual variability noise. A latitude-vertical section of this trend signal-to-noise ratio is shown in Fig. 2c. The three regions highlighted above clearly stand out, experiencing temperature changes that emerge above the background interannual variability over the past 25 years. Counter-intuitively, it is in the Upper Circumpolar Deep Water layer, where the long-term change amplitude is the lowest of the section, that the signal-to-noise ratio is the largest because interannual variability is actually very weak. This clearly pinpoints that, while subtle, the observed temperature increase in the Upper Circumpolar Deep Water represents a radical deviation from its mean state. In other water-masses with a more recent surface connection, the 25-year trends are weaker compared to the typical interannual variability. A signal-to-noise ratio lower than one does not mean trends are insignificant; rather it remains unclear whether the measured long-term change reflects a robust change departing from its typical interannual variability. A robust long-term trend might be hidden behind a low signal-to-noise ratio, but one would have to accumulate more years of repeat observations to observe its emergence above the interannual noise.

Water-mass temperature time-series and forcing. We next compute time-series and associated trends, averaged over the three regions identified above where trends overcome both their

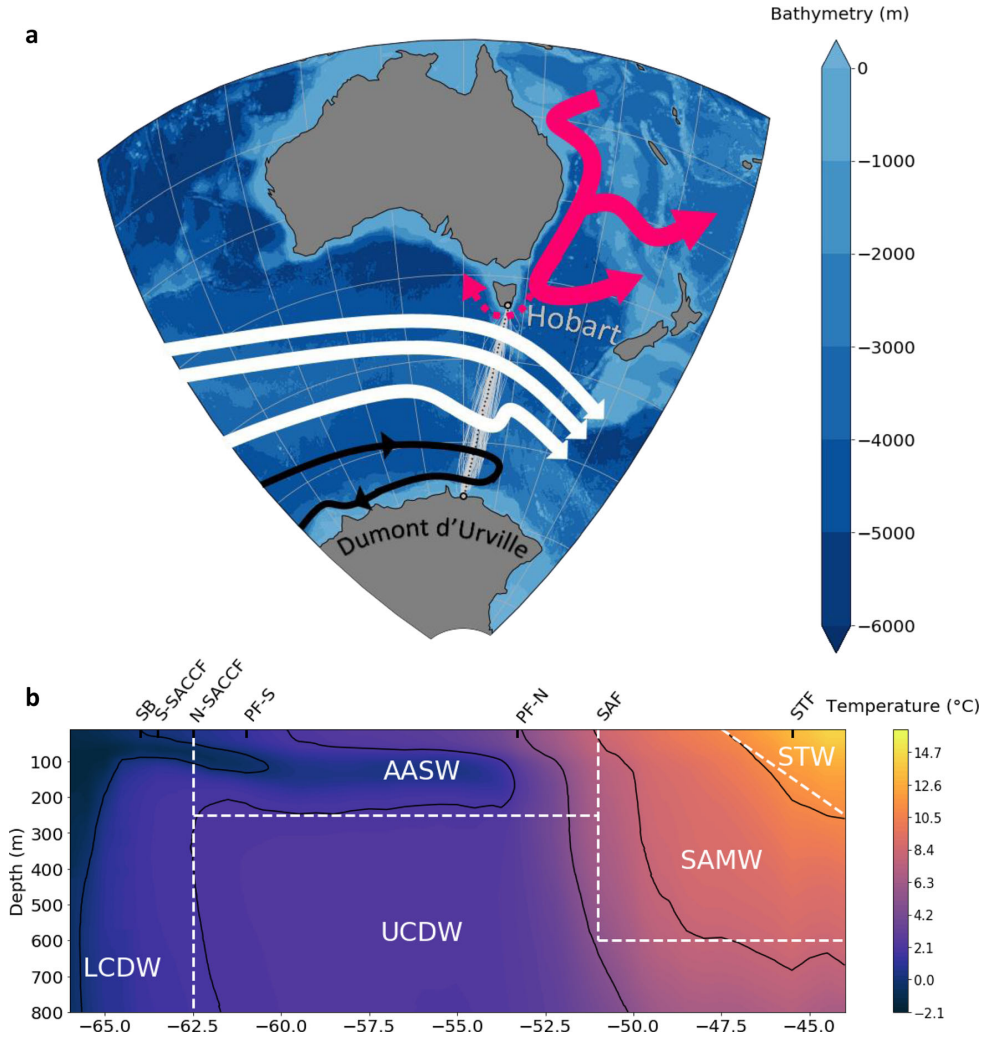

Fig. 1 SURVOSTRAL program transects and summer mean temperature section. a SURVOSTRAL observations over 25 years between Hobart and Dumont D'Urville (DDU), and bathymetry of the region. The mean trajectory is in dashed black. Data used in this study are in gray. A schematic circulation is represented. White, black, and red arrows are respectively the Antarctic Circumpolar Current, the Antarctic Slope Current and Australian-Antarctic Basin gyre, and the East Australian Current. **b** 25-year average of the summer (NDJF) temperature sections. Average position of the fronts (SB: Southern Boundary, S-SACCF: Southern Branch of the Southern Antarctic Circumpolar Current Front, N-SACCF: Northern Branch of the Southern Antarctic Circumpolar Current Front, PF-S and PF-N are the Southern and Northern branches of the Polar Front, SAF: SubAntarctic Front, STF: SubTropical Front) and principal water-masses positions are indicated (LCDW: Lower Circumpolar Deep Water, UCDW: Upper Circumpolar Deep Water, AASW: Antarctic Surface Water, SAMW: SubAntarctic Modal Water, STW: SubTropical Water). Black contours show the mean isotherms.

standard error, and the typical interannual variability: in the subantarctic and subtropical region north of 52.5°S (region A); in the near-surface subpolar region, in the upper 200 m, south of 61°S (region B); and in the subsurface Upper Circumpolar Deep Water, deeper than 250 m, and between 62.5°S-55°S (region C).

When averaged over the entire Subantarctic and Subtropical Mode Water region (region A), the temperature has increased significantly by 0.29 ± 0.09 °C per decade, with a 25-year signal to noise ratio of 2.40, indicating a trend much greater than the estimated interannual noise (Fig. 3a). Locally the trend can be as high as 0.8 °C per decade (Fig. 2b), with the strongest warming organized in deep-reaching localized vertical bands. These structures may be related to more prevalent warm-core eddies or small meanders towards the end of the time series. We note that the computed warming is similar when analyzed in streamwise coordinates following altimetric-derived meanders or in geographical coordinates[26].

Based on a shorter 13-yr time-series, Morrow et al.[27] proposed that this warming was due to the southward movement of both the STF and the SAF, reflecting the consensus when the study was published that ACC fronts were shifting southward. After a decade of scientific debate, a new consensus emerges that on a circumpolar average, the SAF has been shown to be stable and not moving meridionally in the last decades[2,28] and that the warming might instead be due to increased heat uptake from the ocean surface[19,29]. While the warming trend is relatively constant

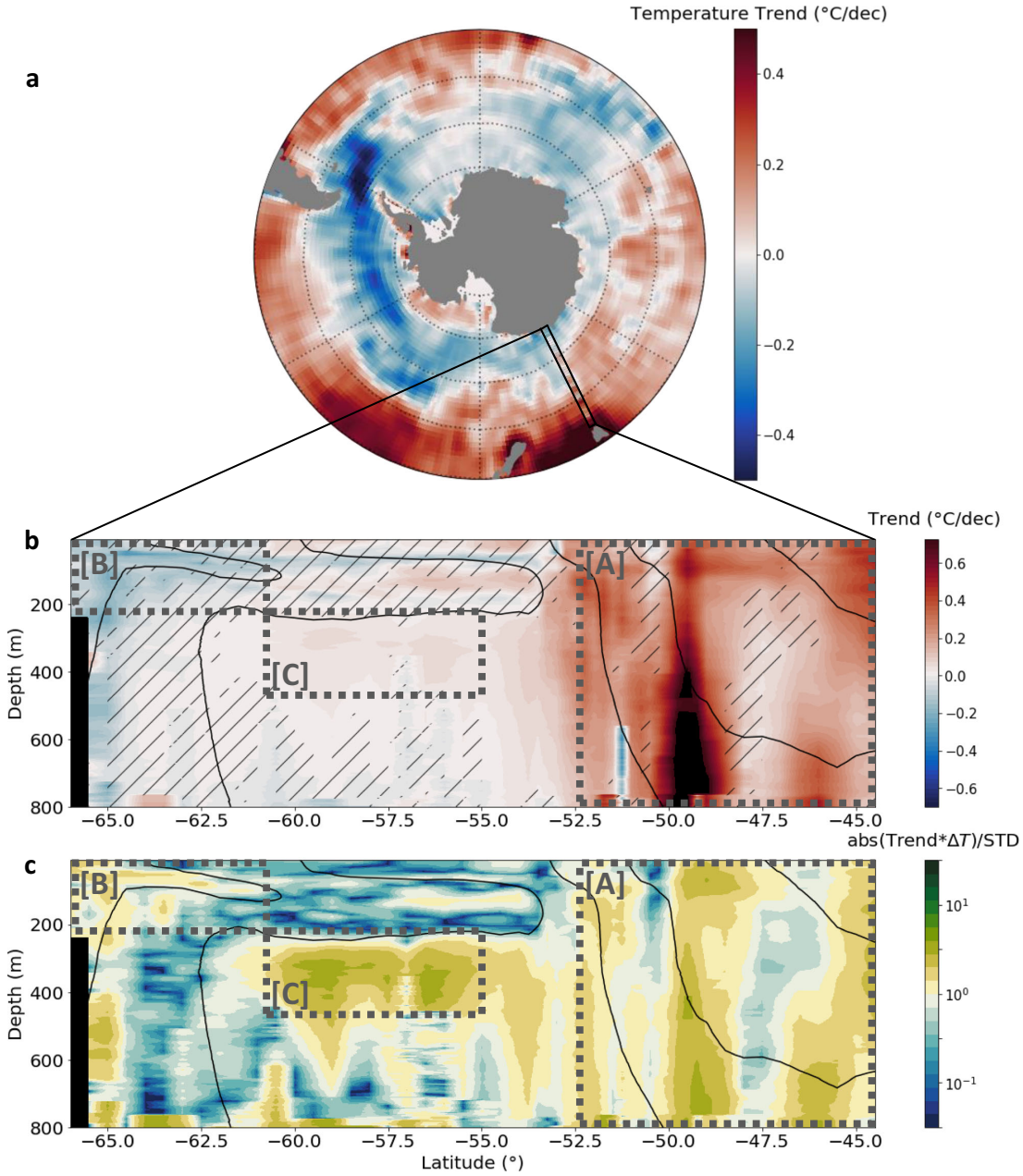

Fig. 2 Temperature trend section and its ratio with interannual variability. a Summer Reynolds SST Trends (°C/dec) from 1993 to 2017 (NDJF). Black box indicated the region of SURVOSTRAL transects. **b** Temperature trends (°C/dec) from SURVOSTRAL XBT data. Hatched data represent zones where abs(Trends*ΔT)/STD < 1, ΔT being the length of the record; i.e., where the trends are smaller than the interannual variability over the 25 years of measurements. **c** Ratio between the trend signal and interannual variability. Position of zones [A], [B], and [C] discussed in this study is represented by the dotted boxes in (**b**, **c**).

over the 25-year period, there are periods of distinct cooling, for example, in 1996 and 2005, and stronger warming in 2001–2002 and in 2014–2016. Similar interannual variability is also evident in the sea-surface temperature fields, with a correlation of 0.63 between SST and the Region A temperature time series, and a slightly lower 25-yr trend of 0.15 ± 0.09 °C per decade, consistent with the trend distribution within the zone (Fig. 2b). Part of the observed interannual variability might be due to intermittent incursions of subtropical waters carried by the Tasman Sea extension south of Tasmania, impacting the extent of STW, as well as local eddy activity around the SAF[30–32] (See Supplementary Fig. 1).

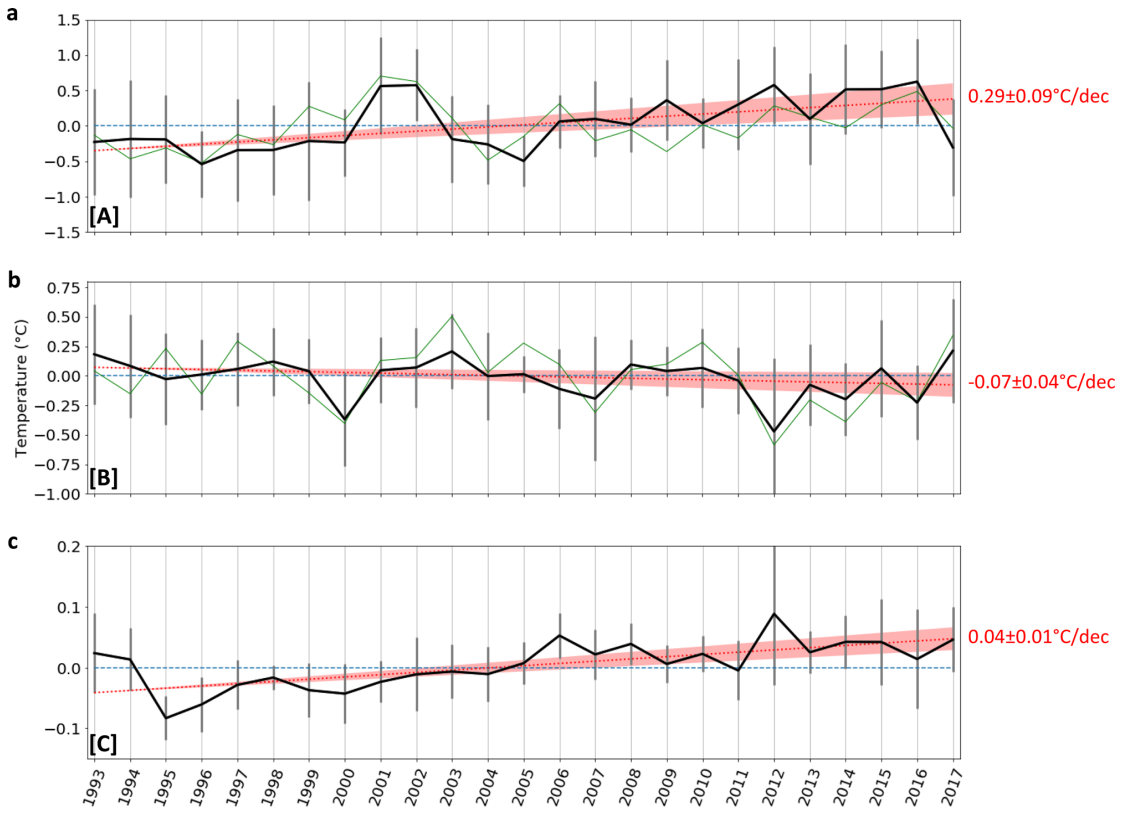

Fig. 3 Temperature anomalies time-series and trend per sector. **a**–**c** Show the evolution (black line) and trend (red line) of the temperature anomalies within zones [A], [B], and [C], respectively. Green line is the NDJF SST Reynolds anomalies interpolated onto the SURVOSTRAL line for each zone. Errors bars are the standard deviation of the mean anomalies for each grid point within the zone.

The overall cooling in the surface subpolar waters close to Antarctica, from the surface to 200 m and from 66°S to 61°S (region B), has a non-significant trend of −0.07 ± 0.04 °C per decade (Fig. 3b, *p*-value 0.07), with a signal-to-noise ratio of 1.16. The cooling appears mostly associated with the coolest waters in the regions (Fig. 2b); Figs. 1b and 2b, c both show water-mass cooler than 0 °C as standing out at the southern edge of our section, with consistent long-term change. When subjectively isolating only data points cooler than 0 °C, the cooling is significant and slightly more marked (−0.09 ± 0.05 °C per decade, signal-to-noise ratio of 1.49; Fig. 4a). This cooling of subpolar waters is also accompanied by a freshening of the surface waters over the same period, as well as an increase in sea-ice cover[5]. Region B has a lower signal-to-noise, and the interannual variability in temperature, SSS and sea-ice is impacted by local coastal circulation changes and increased ice flow from 2011 onwards, following the Mertz Glacier calving just upstream[33–35]. Such high-latitude cooling over the upper 200 m in region B is also consistent with local sea surface cooling observed from satellite SST observations (Fig. 3b, correlation $r = 0.80$), and more generally with the surface cooling of a large part of the Southern Ocean that have been observed from observations in the subpolar waters over the past three decades[10,13,36]. This cooling has been explained by the increased stratification associated with freshening of the surface layer which would tend to reduce mixing with the slightly warmer underlying Lower and Upper Circumpolar Deep Water[4,10,37–39]. Indeed, a trend in surface water freshening has been observed over the same period near 140°E[5]. This has been linked to increased sea-ice cover, particularly after the Mertz Glacier calving in 2010 and enhanced by a large-scale northward shift of the zero-zonal wind position from 1999 onwards, that increased the Ekman-driven sea-ice convergence near the coast[5].

Interestingly the winter water tongue extending further north does not show a similar cooling. Small pockets of cooling exist but the WW trend signals are dominated by interannual variability (0.22 signal to noise ratio). Even when focusing only on the temperature of the core of the Winter Water layer, defined as the layer with temperature colder than 2 °C between 55°S and 61.5°S, the large interannual variations overwhelm any long-term change, with peak-to peak temperature ranging from 0.40 to 0.65 °C (Fig. 4b). These temperature variations within the Winter Water core are positively correlated ($r = 0.70$) with the sea surface temperature of the previous winter further upstream in the subpolar Australian-Antarctic basin (120–145°E; 57–61°S) (Fig. 4b), where the Winter Waters were modified at the surface (see Supplementary Note 1).

The upper layer of the Upper Circumpolar Deep Water from 61°S to 55°S, and over 250–450 m depth (region C) exhibits a small but significant overall warming trend of 0.04 ± 0.01 °C per decade (significant, Fig. 3c), associated with a high signal to noise ratio of 2.58. Consistently, the time-series show relatively weak interannual variability, but a steady warming of the layer. The maximum temperature increase sits directly below the seasonally variable surface layer, in the upper and warmer part of the

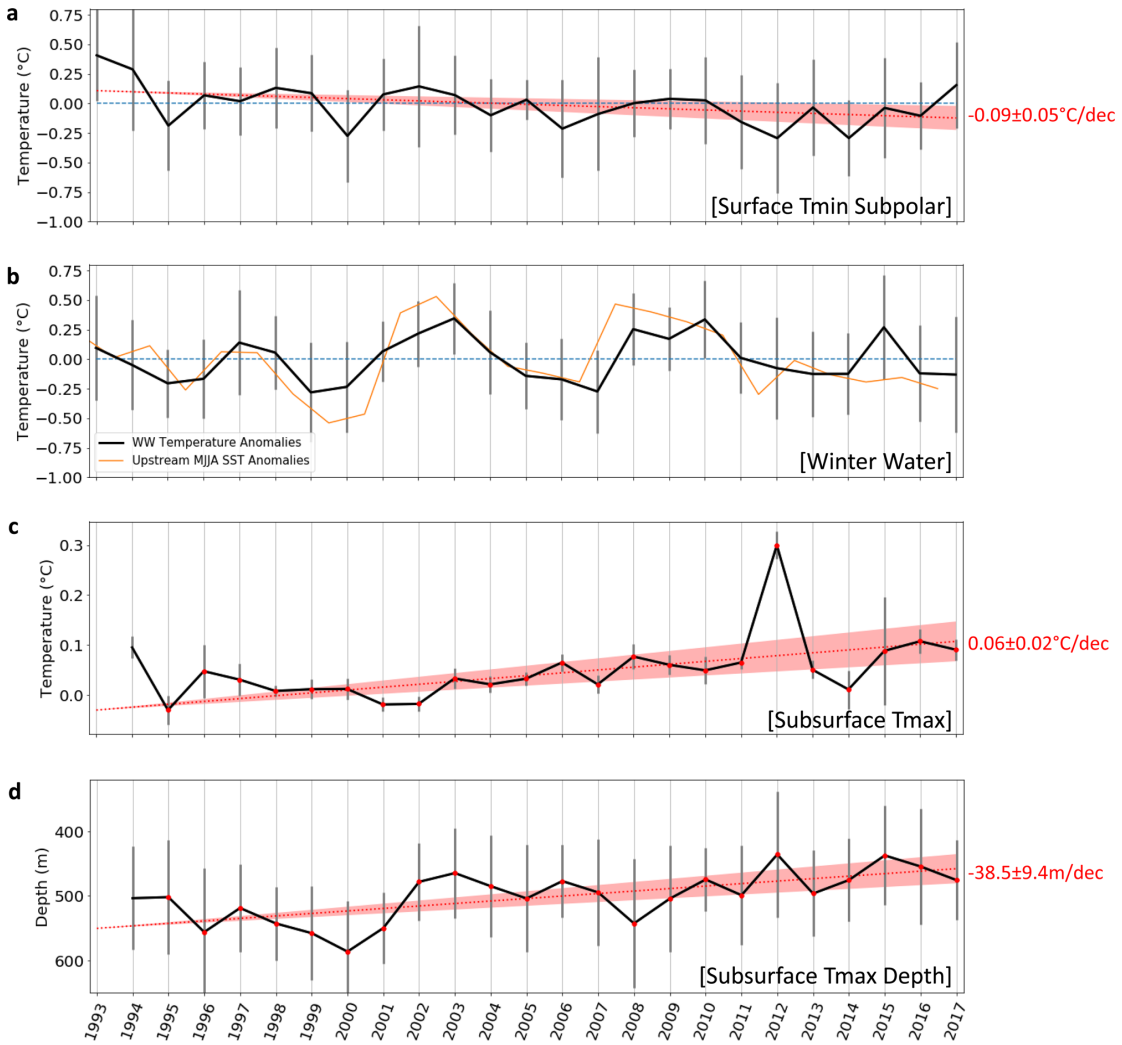

Fig. 4 Time-series of temperature and characteristics of specific water mases. a Zone [B] anomalies, restricted to the gridpoints where the 25 years-mean temperature transect <0. **b** Black line is the WW temperature anomalies from SURVOSTRAL XBTs between 54 and 61.5°S, restricted to the Tmin gridpoints where the 25 year-mean temperature transect is less than 2 °C. Yellow line is the MJJA SST anomalies upstream of SURVOSTRAL WW, between (120–145°E and 57–61°S). **c** CDW maximum temperature evolution (see "Methods"). Red dots are the years the linear trend is computed on; i.e., years when there is at least 2 months with data on average for each grid point for NDJF months. **d** CDW maximum temperature depth (see "Methods"). Errors bars are the standard deviation of the mean temperature anomalies (depth for panel **d**) for each grid point within the zone.

water-mass around 300–550 m (Fig. 2b). When the temperature time-series is computed in this core of temperature maximum, the warming trend is even greater, reaching 0.06 ± 0.02 °C per decade, with a signal to noise ratio of 2.44 (when excluding 2012 which appears as a clear warm outlier, the trend is the same as in the full region C, being 0.04 °C ± 0.01 °C per decade, but with a higher signal to noise ratio of 3.79). Previous authors have suggested the warming of the Upper Circumpolar Deep Water might be driven by increased stratification at the base of the Winter Water layer due to freshening, which would reduce mixing between the two layers and heat removal from the Upper Circumpolar Deep Water to the atmosphere[10,40,41]. Since we have only temperature profiles, the role of the salinity stratification cannot be verified directly. However, in accordance with this hypothesis, we observe larger warming in the upper part of the layer, directly underlying a near-surface water mostly affected by interannual variability (Fig. 4b) but with a few hints of local cooling (Fig. 2b). In addition to the warming of Upper Circumpolar Deep Water, the depth of the core of maximum temperature is observed to shoal at a significant rate of 39 ± 9 m per decade (Fig. 4d), three to ten times higher than previously reported (5–10 m per decade[11]), and within the error envelope of the rate observed in West Antarctica (50 ± 18 m per decade[11]). The cause of the shoaling of the maximum temperature layer remains unclear. It could be related to long-term changes in Ekman pumping[11], but using the atmospheric reanalysis ERA-5, we find only a very subtle long-term trend in local upward Ekman pumping, which is not statistically significant. Other potential mechanisms, e.g., associated with turbulence-driven shoaling of the surface layer, remain to be tested in a future study.

Discussion

Our findings carry important implications for our understanding of Southern Ocean temperature change, a region of the world that remains poorly observed and understood, though with a pivotal role in global climate. Using a unique observation time-series repeated several-times per year over the past 25 years across the Southern Ocean, we document the temperature trend over the upper 800 m, and shed light on three main regions where the temperature change dominates over typical interannual variability. Interestingly, only the subtropical region, north of the Antarctic Circumpolar Current (region A) has been shown to be associated with a human-induced forced signal that emerges over natural variability[14], though recent work suggests that forced warming in the sub-surface subpolar ocean does emerge over natural variability by the end of the 20th century or early decade of the 21st[42]. We note that these studies are based on climate models with significant limitations in their representation of the Southern Ocean[2], hence it is important to provide robust observational targets for future improvement.

The repeat meridional temperature sections used in this study cross a Southern Ocean region of inter-ocean exchange, where waters from the Pacific can flow south of Tasmania into the Indian Ocean[30,43]. The northern part of the IX28 section exhibits strong interannual variations in the temperature data, impacted by ENSO/SAM climate modes and eddy movements across 140°E[44]. Despite this, our 25-year trend calculations have a strong signal-to-noise, with the upper ocean warming trend exceeding the interannual variations. The warming of 0.29 ± 0.09 °C per decade north of the ACC is in accordance with previous studies[7–9] and with other parts of the Southern Ocean[45]; Southern Ocean circulation being essentially zonal, subsurface trends are expected to be zonally consistent all-around Antarctica. Close to the Antarctic continent, during the austral summer heating cycle, our temperature profiles confirm that the widespread surface cooling around Antarctica observed with satellite SST data extends to around 200 m depth at 140°E.

One of the most important results of our study is the large warming and shoaling of the subsurface temperature maximum in the subpolar Southern Ocean, in the Upper Circumpolar Deep Water. This water-mass sits directly below the surface layer and mostly flows eastward, feeding the Pacific basin, where major increase of basal melt has long been identified further downstream in the Amundsen–Bellingshausen sector[46]. In addition, we note that some of the water-masses at the southern end of the section, though probably south of the maximum Upper Circumpolar Deep Water warming we observe, might be part of a cyclonic Australian-Antarctic gyre[47], with direct influence on the Wilkes basins that has recently been shown to be associated with important mass loss of many glaciers of this region[46,48–50]. Our 25-year study confirms two major threats (significant warming and shoaling of Upper Circumpolar Deep Water) that may enhance the ice-shelf melting downstream, with potential dramatic impacts for future global sea-level. Both of these changes that we observed at 140°E have been substantially underestimated in this part of the Southern Ocean until now and must imperatively be taken into account in future ice-sheet modeling predictions[51], and more generally when developing future climate change narratives. Our observational study provides a basis for validating such models and contributing toward these developments.

Methods

SURVOSTRAL Program. The dataset of temperature used in this study consists of 25 years (November 1992 to February 2017) of XBT profiles on a section from Hobart (Tasmania, 42.9°S, 147.3°E) to Dumont d'Urville (Adelie Land, 66.6°S, 140.0°E), as part of the SURVOSTRAL project (Fig. 1a, https://doi.org/10.18142/172). Measurements are taken from the French Antarctic resupply vessel *L'Astrolabe*, with about six transects per year between late October and early March. Depending on ice and weather conditions, XBT measurements are sampled every 35 km, with 18 km sampling across the energetic polar frontal region. Temperature profiles extend down to 900 meters depth with a vertical resolution of about 0.7 meters. The XBT temperature profile accuracy is +0.1 °C. XBT profiles over the entire series have been corrected for temperature and depth biases depending on the probe type, following refs. [52,53]. Corrected XBT measurements are available here: http://thredds.aodn.org.au/thredds/catalog/IMOS/SOOP/SOOP-XBT/PRODUCTS/BiasCorrectedData_ChengEtAl_2014/Line_IX28_Dumont-d-Urville-Hobart/catalog.html.

Gridding process. In order to compute anomalies and trends, 10238 XBT profiles are interpolated onto a regular line from North to South, following the mean path of the Astrolabe's transect, with 0.5° resolution in latitude (increasing to 0.25° in the polar frontal zone from 49 to 54°S), with 2 m depth resolution down to 800 m depth. Results are robust when changing the vertical resolution and interpolation type. XBT profiles sampled further than 3° in longitude from the mean path of the Astrolabe are removed from the analysis. In the following sections, we will discuss three types of products on this regular grid.

1. Climatological monthly mean temperature sections are calculated for each month during the austral summer ONDJFM period and averaged over 25 years. Since the sections are not evenly distributed within a given month, each monthly temperature section is assigned to the median sampling day of all profiles in the month. These values are then linearly interpolated onto daily values before calculating temperature anomalies.
2. Temperature anomaly profiles are constructed by subtracting the corresponding climatological daily value at each latitude and depth from each measurement. These anomalies allow us to construct a gridded section of interannual temperature anomalies and the temperature anomaly trends for the 25-year observation period.
3. Annual austral summer (NDJF) mean temperature sections are constructed for each year from 1993 to 2017 (Supplementary Fig. 2). This product is only used in this study to locate the CDW temperature maximum zone.

The data distribution and the main data processing techniques for these three products are provided in the supplementary information. The monthly mean temperature sections from October to March (Supplementary Fig. 3) calculated from the 25-year time series are consistent with those calculated by ref. [23] based on only 8-years of SURVOSTRAL data. This highlights that the seasonal warming cycle is quite stable in this region on a long-term average. The water-masses with the strongest seasonal changes are at the surface: the Antarctic Surface Waters (AASW) south of the Polar Front show the largest monthly mean variations over the summer warming cycle with coolest waters observed in sampled months closest to winter, late Oct–Nov. In the north of the section, there is a seasonal southward and deepening expansion of Subtropical waters throughout the summer season. We note that even if measurements are sampled only in summertime, computed trends can be considered as annual trends. Indeed, the main seasonal variations are in the surface layer, and XBT temperature profiles' surface values are consistent with satellite SST values. Finally, SST trends computed on NDJF months are coherent with SST trends computed on full year. This shows that for the surface layer, there are no wintertime trends that are counteracting the summer trends, and observed trends are consistent for the whole year for the full time series.

Trend section and zone trends. The temperature trend latitude-depth section is constructed by computing a linear trend using the anomalies available at each grid point. Each profile is associated with one latitude in the grid and is interpolated onto the depth grid. No interpolation was made in latitude to avoid interpolation of anomalies over large data gaps (e.g., during storms), so trends are robust to varying data distribution. The yearly anomalies are weighted by 1/std of all of the anomalies obtained during the corresponding season. The number of measurements used to compute the 25-year trends for each grid point is represented on Supplementary Fig. 4. Each grid point is sampled by between 3 and 10 profiles per year. With an XBT accuracy of 0.1 °C, it translates into a standard error from the mean of ~0.03–0.06 °C, allowing us to resolve changes over 25 years of 0.001–0.002 °C per year, or 0.01–0.02 °C per decade. This value is lower when computing trends over larger regions A, B, and C. Surface trends are consistent with SST Reynolds[54] product trends on summer NDJF periods (Fig. 2a, $r = 0.70$), and SST Reynolds[54] full year trends ($r = 0.70$). Trends averaged over zones [A], [B], and [C] are computed in the same way, but all anomalies available in each zone are averaged for each season. The trend significance is computed using a Mann-Kendall test. Trends with p-value lower than 0.05 are considered significant, and their confidence interval is computed as their standard error.

CDW maximum temperature values and their depths are computed by selecting the warmest 10% temperature grid points on each austral summer temperature section within zone [C]. The mean depth of these selected grid points is then the depth of maximum CDW temperature, and the mean anomalies of these selected grid points gives the evolution of the temperature maximum. CDW maximum temperature value and depth trend is computed only on the years when there is at least 2 out of 4 months with measurements on average for the summer NDJF mean

for all the subset grid points. Missing data in 1993 occurs since data is available in less than 10% of the grid subset.

Trend (signal) to interannual variability (noise) ratio. The amplitude of the trend compared to the strength of the interannual variability is evaluated for each zone and grid point, by computing the signal to noise ratio. Our signal is the temperature evolution following the linear trend over the 25 years, and our noise is the standard deviation of the error between the trend and the measured temperature:

If T is the temperature evolution throughout the $\mathrm{ny} = 25$ years, and $ax + b$ its linear regression, the signal to noise ratio S is computed as:

$$S = \frac{\mathrm{ny} * a}{\mathrm{STD}(ax - T)} \quad (1)$$

S represents the ratio between the trend and the interannual signal: if $S > 1$, the trend signal is dominant compared to the interannual variation.

External data. We use NOAA monthly optimum interpolation (OI) satellite and in-situ[54] surface temperature data to verify the consistency of our XBT observations to surface changes in temperature.

ECMWF ERA5 monthly surface turbulent wind stress product is used to investigate the effect of the wind on the temperature trends and variations (DOI: 10.24381/cds.f17050d7).

Data availability

Corrected XBT measurements are available here: http://thredds.aodn.org.au/thredds/catalog/IMOS/SOOP/SOOP-XBT/PRODUCTS/BiasCorrectedData_ChengEtAl_2014/Line_IX28_Dumont-d-Urville-Hobart/catalog.html. The datasets generated during the current study are available with the DOI: 10.6096/11.

Received: 19 June 2020; Accepted: 14 December 2020;
Published online: 21 January 2021

References

1. Frölicher, T. L. et al. Dominance of the Southern Ocean in anthropogenic carbon and heat uptake in CMIP5 models. *J. Clim.* **28**, 862–886 (2014).
2. Meredith, M. et al. in *IPCC Special Report on the Ocean and Cryosphere in a Changing Climate* (eds Pörtner, H.-O. et al.) (2019).
3. de Lavergne, C., Palter, J. B., Galbraith, E. D., Bernardello, R. & Marinov, I. Cessation of deep convection in the open Southern Ocean under anthropogenic climate change. *Nat. Clim. Change* **4**, 278–282 (2014).
4. Haumann, F. A., Gruber, N., Münnich, M., Frenger, I. & Kern, S. Sea-ice transport driving Southern Ocean salinity and its recent trends. *Nature* **537**, 89–92 (2016).
5. Morrow, R. & Kestenare, E. 22-year surface salinity changes in the Seasonal Ice Zone near 140 degrees E off Antarctica. *J. Mar. Syst.* **175**, 46–62 (2017).
6. Sallée, J.-B. Southern Ocean Warming. *Oceanog* **31**, 51–62 (2018).
7. Gille, S. T. Decadal-scale temperature trends in the Southern Hemisphere Ocean. *J. Clim.* **21**, 4749–4765 (2008).
8. Böning, C. W., Dispert, A., Visbeck, M., Rintoul, S. R. & Schwarzkopf, F. U. The response of the Antarctic Circumpolar Current to recent climate change. *Nat. Geosci.* **1**, 864–869 (2008).
9. Giglio, D. & Johnson, G. C. Middepth decadal warming and freshening in the South Atlantic. *J. Geophys. Res.: Oceans* **122**, 973–979 (2017).
10. Armour, K. C., Marshall, J., Scott, J. R., Donohoe, A. & Newsom, E. R. Southern Ocean warming delayed by circumpolar upwelling and equatorward transport. *Nat. Geosci.* **9**, 549–554 (2016).
11. Schmidtko, S., Heywood, K. J., Thompson, A. F. & Aoki, S. Multidecadal warming of Antarctic waters. *Science* **346**, 1227–1231 (2014).
12. Newman, L. et al. Delivering sustained, coordinated, and integrated observations of the Southern Ocean for global impact. *Front. Mar. Sci.* **6**, 433 (2019).
13. Jones, J. M. et al. Assessing recent trends in high-latitude Southern Hemisphere surface climate. *Nat. Clim. Change* **6**, 917–926 (2016).
14. Swart, N. C., Gille, S. T., Fyfe, J. C. & Gillett, N. P. Recent Southern Ocean warming and freshening driven by greenhouse gas emissions and ozone depletion. *Nat. Geosci.* **11**, 836–841 (2018).
15. Goni, G. J. et al. More than 50 years of successful continuous temperature section measurements by the global expendable bathythermograph network, Its integrability, societal benefits, and future. *Front. Mar. Sci.* **6**, 452 (2019).
16. Nagata, Y., Michida, Y. & Umimura, Y. in *Antarctic Ocean and Resources Variability* (ed. Sahrhage, D.) 92–98 (Springer, 1988).
17. Belkin, I. M. & Gordon, A. L. Southern Ocean fronts from the Greenwich meridian to Tasmania. *J. Geophys. Res.: Oceans* **101**, 3675–3696 (1996).
18. Sallée, J.-B., Wienders, N., Speer, K. & Morrow, R. Formation of subantarctic mode water in the southeastern Indian Ocean. *Ocean Dyn.* **56**, 525–542 (2006).
19. Gao, L., Rintoul, S. R. & Yu, W. Recent wind-driven change in Subantarctic Mode Water and its impact on ocean heat storage. *Nat. Clim. Change* **8**, 58–63 (2018).
20. Botnikov, V. N. Geographical position of the Antarctic Convergence Zone in the Antarctic Ocean. *Soviet Antarctic Exped.* 324–327 (1963).
21. Helm, K. P., Bindoff, N. L. & Church, J. A. Changes in the global hydrological-cycle inferred from ocean salinity. *Geophys. Res. Lett.* **37**, 18 (2010).
22. Aoki, S. et al. Widespread freshening in the Seasonal Ice Zone near 140°E off the Adélie Land Coast, Antarctica, from 1994 to 2012. *J. Geophys. Res.: Oceans* **118**, 6046–6063 (2013).
23. Chaigneau, A., Morrow, R. A. & Rintoul, S. R. Seasonal and interannual evolution of the mixed layer in the Antarctic Zone south of Tasmania. *Deep Sea Res. Part I: Oceanographic Res. Pap.* **51**, 2047–2072 (2004).
24. Pellichero, V., Sallée, J.-B., Schmidtko, S., Roquet, F. & Charrassin, J.-B. The ocean mixed layer under Southern Ocean sea-ice: Seasonal cycle and forcing. *J. Geophys. Res.: Oceans* **122**, 1608–1633 (2017).
25. Orsi, A. H., Whitworth, T. & Nowlin, W. D. On the meridional extent and fronts of the Antarctic Circumpolar Current. *Deep Sea Res. Part I: Oceanographic Res. Pap.* **42**, 641–673 (1995).
26. Auger, M., Morrow, R. & Kestenare, E. *Étude de la variabilité de l'océan Austral à partir de 25 ans de mesures SURVOSTRAL*. https://zenodo.org/record/4094960#.X5BPM9AzY2x (2018).
27. Morrow, R., Valladeau, G. & Sallee, J.-B. Observed subsurface signature of Southern Ocean sea level rise. *Prog. Oceanogr.* **77**, 351–366 (2008).
28. Chapman, C. C., Lea, M.-A., Meyer, A., Sallée, J.-B. & Hindell, M. Defining Southern Ocean fronts and their influence on biological and physical processes in a changing climate. *Nat. Clim. Change* **10**, 209–219 (2020).
29. Häkkinen, S., Rhines, P. B. & Worthen, D. L. Warming of the global ocean: spatial structure and water-mass trends. *J. Clim.* **29**, 4949–4963 (2016).
30. Morrow, R., Donguy, J.-R., Chaigneau, A. & Rintoul, S. R. Cold-core anomalies at the subantarctic front, south of Tasmania. *Deep Sea Res. Part I: Oceanographic Res. Pap.* **51**, 1417–1440 (2004).
31. Pilo, G. S., Oke, P. R., Rykova, T., Coleman, R. & Ridgway, K. Do East Australian current anticyclonic eddies leave the Tasman Sea? *J. Geophys. Res.: Oceans* **120**, 8099–8114 (2015).
32. Morrow, R. & Kestenare, E. Nineteen-year changes in surface salinity in the Southern Ocean south of Australia. *J. Mar. Syst.* **129**, 472–483 (2014).
33. Campagne, P. et al. Glacial ice and atmospheric forcing on the Mertz Glacier Polynya over the past 250 years. *Nat. Commun.* **6**, 6642 (2015).
34. Tamura, T., Williams, G. D., Fraser, A. D. & Ohshima, K. I. Potential regime shift in decreased sea ice production after the Mertz Glacier calving. *Nat. Commun.* **3**, 826 (2012).
35. Massom, R. A. & Stammerjohn, S. E. Antarctic sea ice change and variability—physical and ecological implications. *Polar Sci.* **4**, 149–186 (2010).
36. Bindoff, N. L. et al. in *Climate Change 2013: The Physical Science Basis* (eds Stocker, T. F. et al.) Ch. 10 (IPCC, Cambridge Univ. Press, 2013).
37. Bintanja, R., van Oldenborgh, G. J., Drijfhout, S. S., Wouters, B. & Katsman, C. A. Important role for ocean warming and increased ice-shelf melt in Antarctic sea-ice expansion. *Nat. Geosci.* **6**, 376–379 (2013).
38. Haumann, F. A., Gruber, N. & Münnich, M. Sea-ice induced Southern Ocean subsurface warming and surface cooling in a warming climate. *AGU Adv.* **1**, e2019AV000132 (2020).
39. Rye, C. D. et al. Antarctic glacial melt as a driver of recent Southern Ocean climate trends. *Geophys. Res. Lett.* **47**, e2019GL086892 (2020).
40. Marshall, J. et al. The ocean's role in the transient response of climate to abrupt greenhouse gas forcing. *Clim. Dyn.* **44**, 2287–2299 (2015).
41. Lecomte, O. et al. Vertical ocean heat redistribution sustaining sea-ice concentration trends in the Ross Sea. *Nat. Commun.* **8**, 258 (2017).
42. Silvy Y., Guilyardi E., Sallée J.-B., & Durack P. J. Human-induced changes to the global ocean water-masses and their time of emergence. *Nat. Clim. Change* **10**, 1030–1036 (2020)
43. Speich, S. et al. Tasman leakage: a new route in the global ocean conveyor belt. *Geophys. Res. Lett.* **29**, 55-1–55-4 (2002).
44. Meredith, M. P. & Hogg, A. M. Circumpolar response of Southern Ocean eddy activity to a change in the Southern Annular Mode. *Geophys. Res. Lett.* https://doi.org/10.1029/2006GL026499 (2006).
45. Sprintall, J. Long-term trends and interannual variability of temperature in Drake Passage. *Prog. Oceanogr.* **77**, 316–330 (2008).
46. Rignot, E. et al. Four decades of Antarctic Ice Sheet mass balance from 1979–2017. *Proc. Natl Acad. Sci. USA* **116**, 1095 (2019).
47. McCartney, M. S. & Donohue, K. A. A deep cyclonic gyre in the Australian–Antarctic Basin. *Prog. Oceanogr.* **75**, 675–750 (2007).
48. Frezzotti, M., Cimbelli, A. & Ferrigno, J. G. Ice-front change and iceberg behaviour along Oates and George V Coasts, Antarctica, 1912-96. *Ann. Glaciol.* **27**, 643–650 (1998).

49. Miles, B. W. J., Stokes, C. R. & Jamieson, S. S. R. Simultaneous disintegration of outlet glaciers in Porpoise Bay (Wilkes Land), East Antarctica, driven by sea ice break-up. *Cryosphere* **11**, 427–442 (2017).
50. Shen, Q. et al. Recent high-resolution Antarctic ice velocity maps reveal increased mass loss in Wilkes Land, East Antarctica. *Sci. Rep.* **8**, 4477 (2018).
51. Seroussi, H. et al. ISMIP6 Antarctica: a multi-model ensemble of the Antarctic ice sheet evolution over the 21st century. The Cryosphere Discussions 1–54, https://doi.org/10.5194/tc-2019-324 (2020).
52. Cheng, L., Zhu, J., Cowley, R., Boyer, T. & Wijffels, S. Time, probe type, and temperature variable bias corrections to historical expendable bathythermograph observations. *J. Atmos. Ocean. Technol.* **31**, 1793–1825 (2014).
53. Cowley, R., Wijffels, S., Cheng, L., Boyer, T. & Kizu, S. Biases in expendable bathythermograph data: a new view based on historical side-by-side comparisons. *J. Atmos. Ocean. Technol.* **30**, 1195–1225 (2013).
54. Reynolds, R. W., Rayner, N. A., Smith, T. M., Stokes, D. C. & Wang, W. An improved in situ and satellite SST analysis for climate. *J. Clim.* **15**, 1609–1625 (2002).

Acknowledgements

XBT temperature data were obtained with the support of the French Institut Polaire Emile Victor (IPEV), the LEGOS, IMOS (Australia's Integrate Marine Observing System) and the CSIRO Marine and Atmospheric Research. We wish to thank the crew of the Astrolabe and the many volunteers who helped with these observations over 25 years. XBT data processing was performed by Rebecca Cowley of CSIRO, and the XBT technical assistance by Matt Sherlock and Craig Hanstein, CSIRO. This project is supported through funding from the Earth Systems and Climate Change Hub of the Australian Government's National Environmental Science Program. This analysis was financed by the French TOSCA program. M.A. and J.B.S. have received funding from the European Union's Horizon 2020 research and innovation program under grant agreement N° 821001. M.A. was funded through a CNES/CLS scholarship. Data were sourced from Australia's Integrated Marine Observing System (IMOS)—IMOS is enabled by the National Collaborative Research Infrastructure strategy (NCRIS). It is operated by a consortium of institutions as an unincorporated joint venture, with the University of Tasmania as Lead Agent.

Author contributions

All analysis for this paper was performed by M.A. and supervised by R.M., E.K., and J.-B.S. The study was designed by R.M. Observational data were validated and calibrated by R.C. and E.K. All authors contributed to interpreting the results and writing the manuscript.

Competing interests

The authors declare no competing interests.

Additional information

Supplementary information is available for this paper at https://doi.org/10.1038/s41467-020-20781-1.

Correspondence and requests for materials should be addressed to M.A.

Peer review information *Nature Communications* thanks Andrea Storto and other, anonymous, reviewers for their contributions to the peer review of this work. Peer review reports are available.

Reprints and permission information is available at http://www.nature.com/reprints

Publisher's note Springer Nature remains neutral with regard to jurisdictional claims in published maps and institutional affiliations.

Supplementary Information for Southern Ocean *in-situ* temperature trends over 25 years emerge from interannual variability by Auger et al.

Supplementary Note 1: Definition of Winter Water Upstream Zone:

In our study, Winter Water is defined as the water-mass with a temperature lower than 2°C between 54°S and 61.5°S. To find the winter origin of this Winter Water along the mean SURVOSTRAL line near 140°E, we used backward-flowing Lagrangian trajectories derived from surface altimetric currents on the first day of November, December, January and February between 1993 and 2003. We found that 90% of SURVOSTRAL WW particles at 140°E could be located within the surface mixed layer upstream in the previous winter (May to August) in the region centered at 57 - 61°S and 119°E and 146°E.

Supplementary Note 2: Zone A Interannual variations in SST and Subtropical water extent

Supplementary Figure 1b shows how the extent of subtropical waters crossing our section (waters warmer than 11°C) varies in direct relation to the interannual upper ocean temperature changes in Zone A (correlation r=0.58).

Cool anomalies in the Subantarctic zone were noted in SURVOSTRAL data during 1994-1995, due to the persistence of cold-core eddies near 140°E separated from the SAF (Morrow et al., 2004), whereas the 1996 cool anomalies are influenced by a weaker input of STW from the Tasman Sea (Supplementary Figure 1b; Morrow and Kestenare 2014). Stronger warming events in 2001-2002 and in 2014-2016 have anomalously warm SST (Supplementary Figure 1a). These years may be influenced by incursions of subtropical waters carried by the Tasman Sea extension south of Tasmania following large La Nina events, impacting the extent of STW crossing 140°E, as well as more warm-core eddies propagating through the region (Pilo et al., 2015; Morrow and Kestenare, 2014).

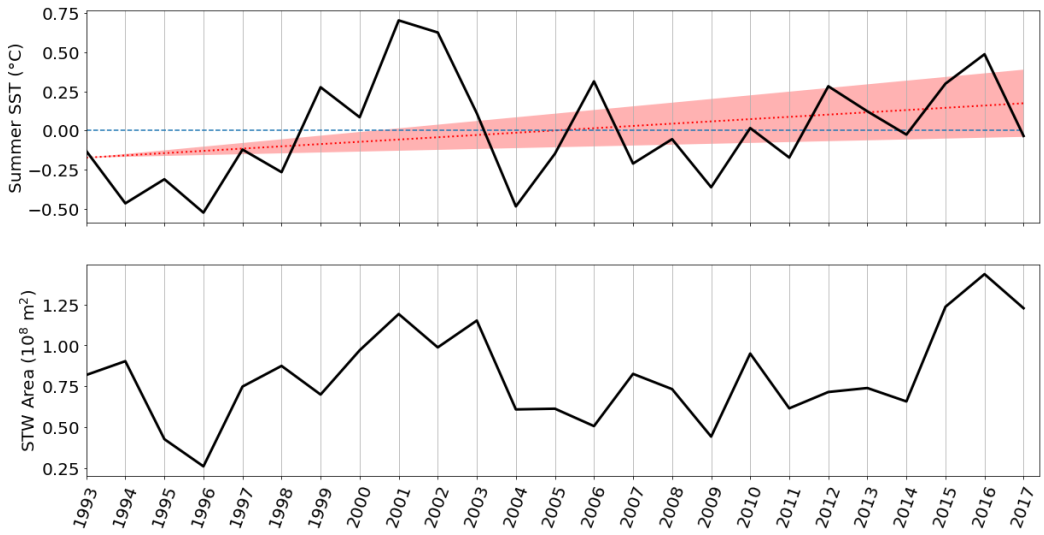

Supplementary Figure 1: Interannual variations in Sea Surface Temperature and Subtropical water extent. a. NDJF Mean sea surface anomalies on the SURVOSTRAL line within zone A bounds. b. Subtropical Water area within the transect.

Supplementary Note 3: Austral summer mean temperature sections

Mean temperature sections are calculated for each austral summer, from November to February (NDJF). A monthly mean section is calculated for each month and for each year, and the four monthly values of NDJF are then averaged to obtain the austral summer temperature section. This reconstruction was chosen since there are certain years with more missing data in one month than another (Supplementary Figure 5). The available profiles for each year are impacted by the distinct seasonal changes seen in Supplementary Figure 3. For example, a simple austral summer average of all available profiles but with points missing in November would show an annual warming compared to the average NDJF conditions. To reduce the effects of this sampling bias, we replace the missing values at each point in the monthly section with the 25-yr monthly mean value. Note that this step is not applied for the anomalies.

Supplementary Figure 2 shows the austral summer mean temperature sections for each year from 1993 to 2017. Black regions have no data available for the entire austral summer, which occurred during the early voyages in 1992-1993 as the XBT system was being established, and south of 66°S. Hatched regions have only 2 out of 4 months with good observations, and the other months are filled with the 25-year mean monthly value.

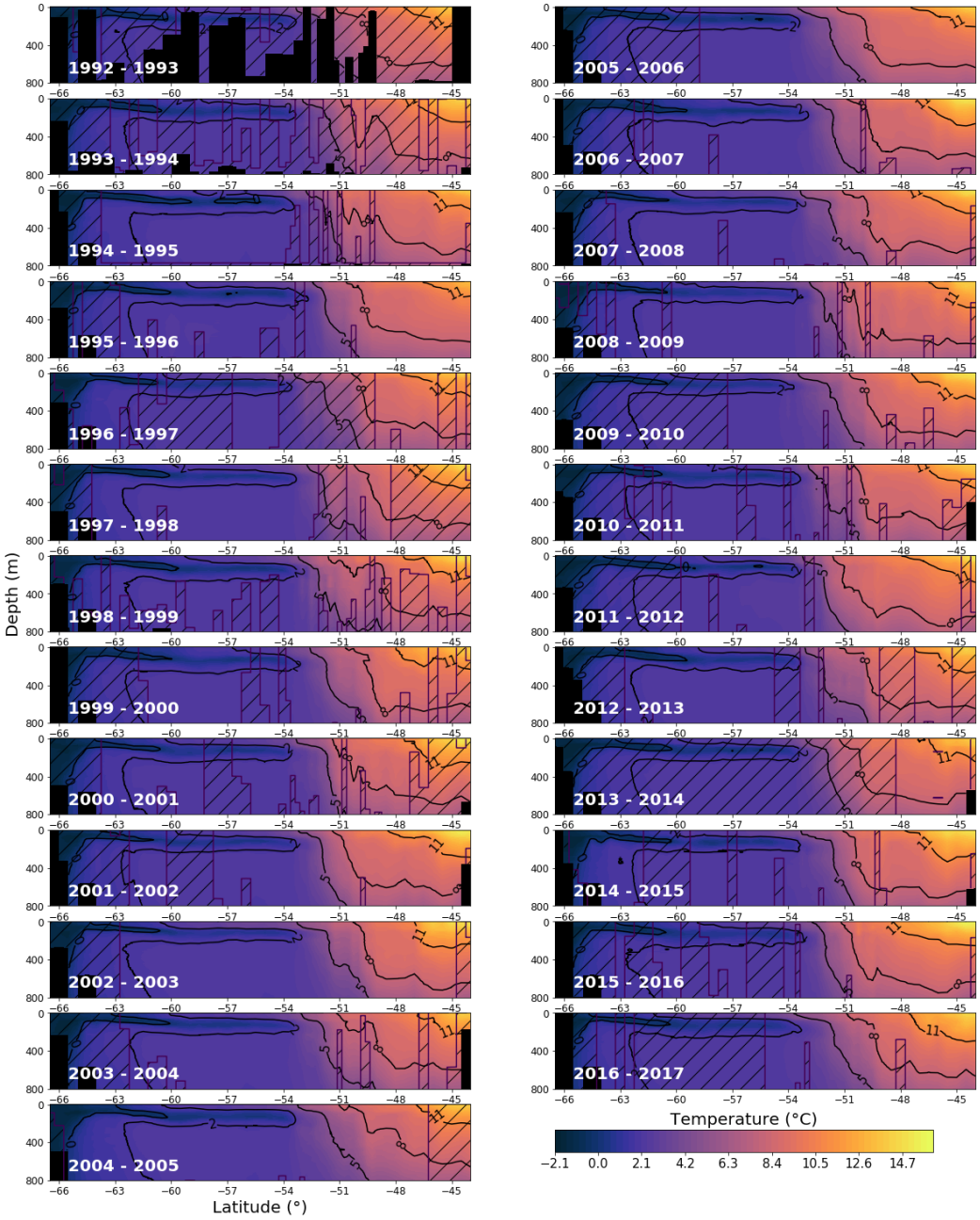

Supplementary Figure 2: Austral summer mean temperature transects. Austral summer mean temperature structure from 1993 to 2017 based on SURVOSTRAL profiles from the months NDJF. Hatched areas are where climatological monthly mean had to be added at least

twice to compute the summer mean. Black contours show the mean isotherms of 0, 2, 5, 8 and 11°C.

Supplementary Note 4: Calculating monthly mean temperature sections

Monthly mean XBT temperature sections are computed between October and March from the 25 years of Austral Summer data (Supplementary Figure 3), following a similar method to that used in Morrow et al. (2008). XBT profiles are associated to a latitude box and interpolated linearly on the depth range of the study grid (see Methods), then all profiles available each month are averaged within a latitude-depth grid box.

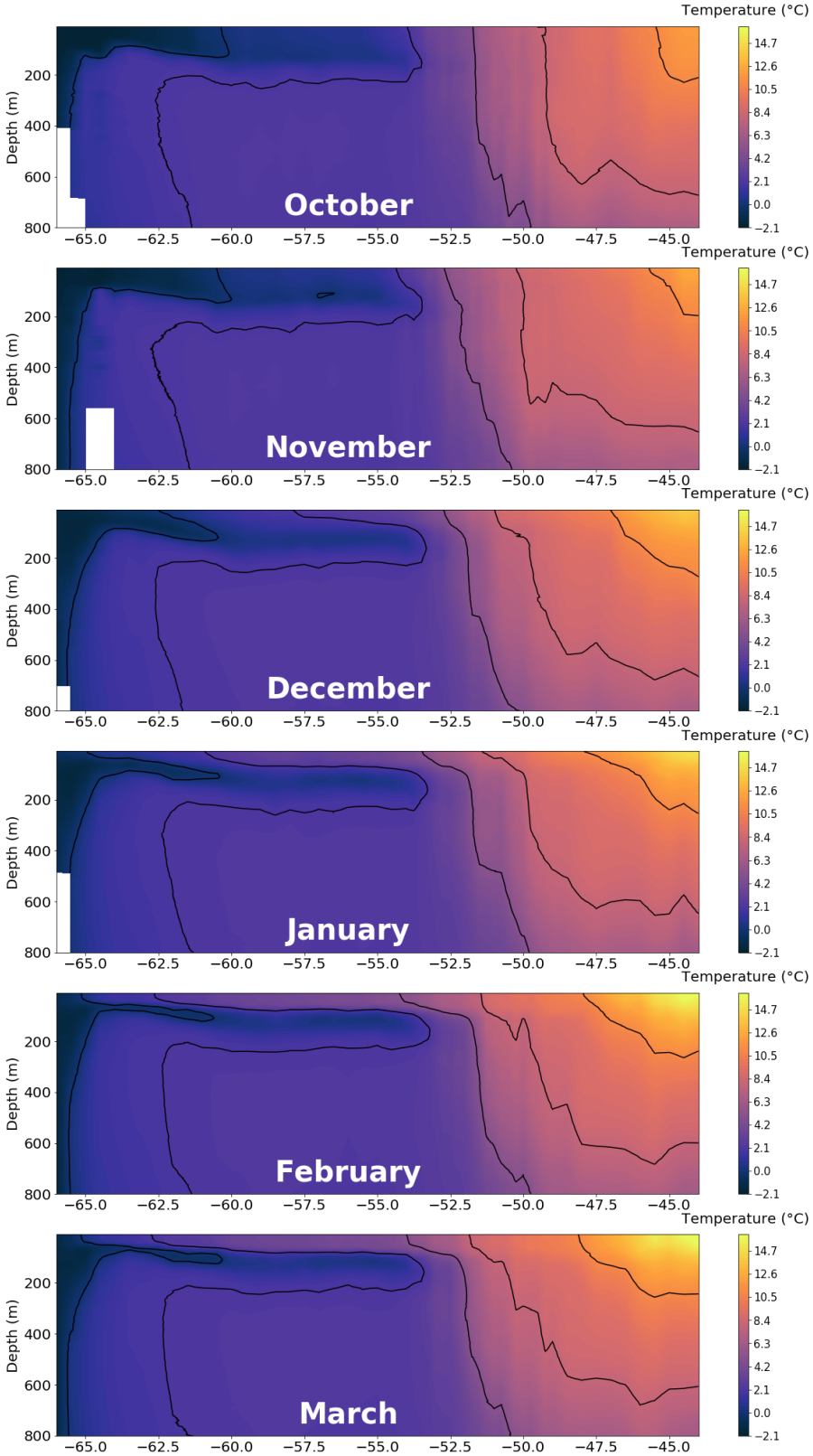
Temperature (°C)
Depth (m)
200
400
600
800
−65.0
−62.5
−60.0
−57.5
−55.0
−52.5
−50.0
−47.5
−45.0
14.7
12.6
10.5
8.4
6.3
4.2
2.1
0.0
−2.1
October
November
December
January
February
March

Supplementary Figure 3: Monthly temperature climatology. October to March monthly mean values based on SURVOSTRAL data from 1993 to 2017. Black contours show the mean isotherms of 0, 2, 5, 8 and 11°C.

Supplementary Note 5: Number of measurements for each grid point

The distribution of the number of measurements per grid box over the 25-years (Supplementary Figure 4) highlights the larger number of observations in the Northern part of the section; seasonal sea-ice is present in the region south of 62°S, particularly in October and November.

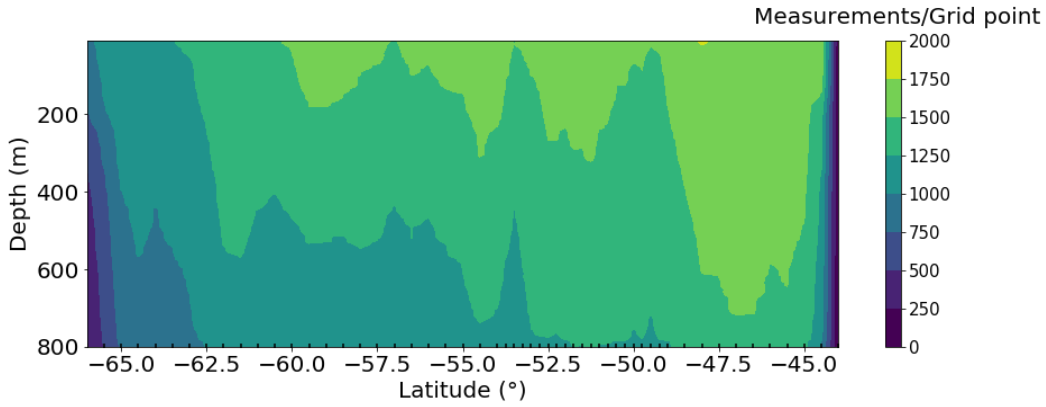

Supplementary Figure 4: Number of measurements per grid point for the 25 years of SURVOSTRAL XBT data. Black dots on the x-axis shows the size of the grid points. The increase of resolution in the polar frontal zone between 49°S and 54°S is compensated by an increase in XBT sampling frequency in this zone.

Supplementary Note 6: Temporal and Spatial repartition of XBT profiles

Supplementary Figure 5 shows the number of XBT profiles used in the analysis over the 25-year period, with valid data reaching at least 200 m (Note our analysis is based on

measurements up to 800m). The number of profiles varies by month (Supplementary Figure 5, left). Profiles are collected every 2h during the ship's route (roughly 35 km separation), doubling to 1h sampling in the polar frontal zone (18 km separation) from 49-54°S.

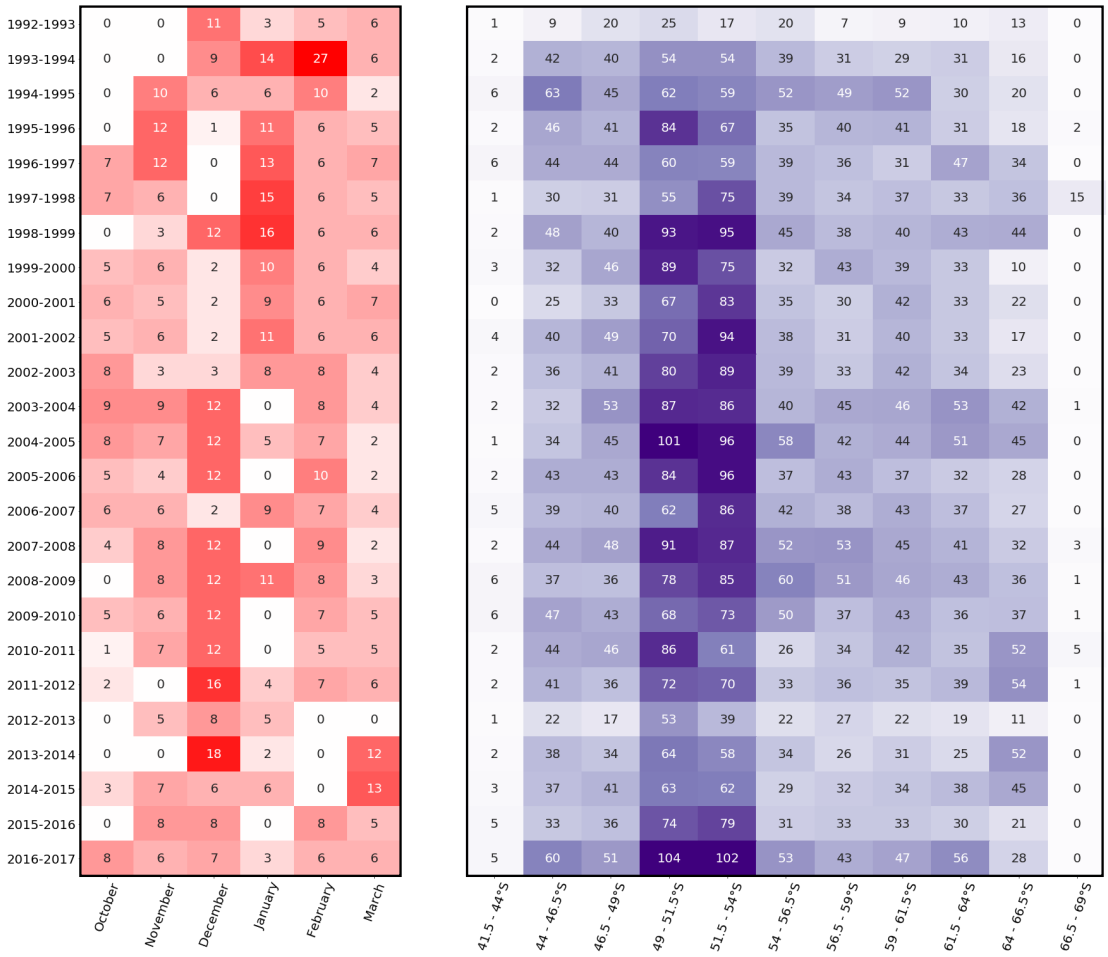

Supplementary Figure 5. Temporal and Spatial repartition of XBT profiles. For each sampling season: a. Number of days with at least one profile sampled within each month. b. Repartition of XBT profiles by latitude band.

Supplementary Note 7: Gridding and measurement error estimation

The measurement error estimation is made by computing the standard deviation (Supplementary Figure 6) of multiple profiles from the same transect occurring within the same latitude-depth box. A standard deviation is computed only when there are at least 3 data points within the same grid point for each transect. This standard deviation is averaged over all transects on the full grid, in order to represent the gridding and measurement error estimation.

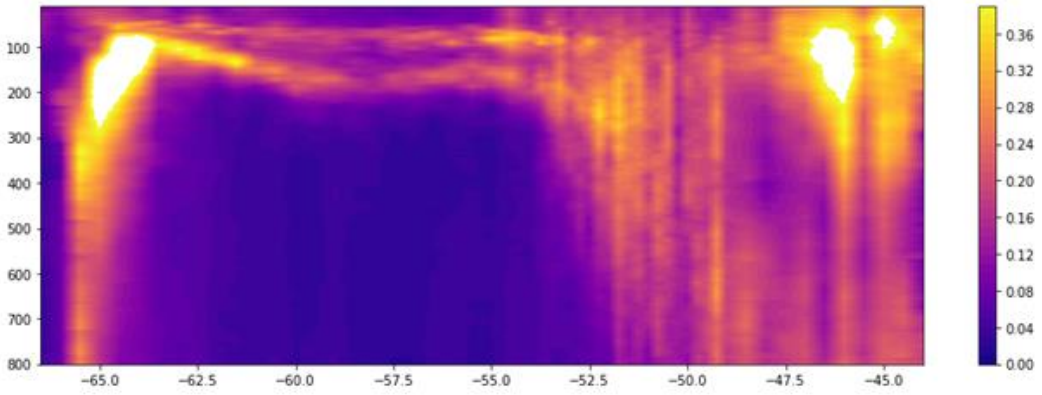

Supplementary Figure 6. Gridding and measurement error estimation. Mean standard deviation of measurements sampled on the same grid point for one transect, based on all transects

Supplementary Note 8: XBT data processing and selection along the SURVOSTRAL line

XBT profiles were processed twice : 1) using the official UNESCO fall-rate processing (Hanawa et al 1995 [55]) available on the IMOS website (http://thredds.aodn.org.au/thredds/catalog/IMOS/SOOP/SOOP-XBT/DELAYED/Line_IX28_Dumont-d-Urville-Hobart/catalog.html.) and 2) with the more recent fall rate and depth correction (Cheng et al 2014 [52]) as recommended by the SOOP XBT panel (http://thredds.aodn.org.au/thredds/catalog/IMOS/SOOP/SOOP-

XBT/PRODUCTS/BiasCorrectedData_ChengEtAl_2014/Line_IX28_Dumont-d-Urville-Hobart/catalog.html). Our trend results over the last 25-years across the Southern Ocean are similar when using either fall-rate correction. This reprocessing allowed us to show the stability and robustness of our results.

XBT profiles with the most recent processing[52] are selected based on their distance to the mean path of the transect. In order to avoid sampling regions with different dynamics, we remove profiles located more than 3° longitude away from the mean path, or samples east of 142°E and south of 65.5°S. Over the 10238 vertical profile sampled, 614 have been discarded due to their location.

SURVOSTRAL campaigns have DOI : 10.18142/172;

3 Conclusion of the chapter

In this chapter, I show that between 1992 and 2017, three distinct regions associated with various water masses stand out as having significant temperature trends when compared to interannual variability.

SAMW have experienced the most intense warming of the meridional section. The temperature change from the surface to 800 meters depth (the depth extent of the XBT measurements) is 0.29 ± 0.09 °C per decade, which is consistent with previous studies (Giglio and Johnson, 2017; Gao et al., 2018). The temperature change was found to be 2.40 times higher than the magnitude of interannual variability, showing the significance of this long-term trend.

During the same period,a surface cooling is observed in the southernmost part of the meridional section, evaluated at -0.07 ± 0.04 °C per decade, also consistent with previous studies (Schmidtko et al., 2014; Haumann et al., 2020; Rye et al., 2020). The amplitude of the observed change over 25 years is similar to the amplitude of typical interannual variability. This surface cooling reaches 200m depth and was found to be even higher for the coolest water masses, reaching -0.09 ± 0.05 °C per decade, and 1.5 times the magnitude of interannual variability.

The upper layer of the CDW experienced a smaller but consistent warming, with a 0.04 ± 0.01 °C warming trend from 200 to 450m. This relatively slight warming is actually drastic when compared to typical interannual variability (3.79 larger). By tracking the CDW temperature maximum over the 25 years, we also found it to be shallowing with a trend of 38.5 ± 9.4 meters per decade, an amplitude 3 to 10 times higher than previously found in other studies (Schmidtko et al., 2014).

One important challenge faced in producing this study was to properly remove the effects of the seasonal cycle of the hydrographic structure of the upper layer. Getting rid of the seasonal cycle of the temperature structure was made possible thanks to the high number of profiles collected each summer month between 1992 and 2017. From all these profiles, a daily summer climatology over the 25 years was constructed and removed from each individual profile to obtain anomalies from this climatology. The supplementary material of the paper presented in the preceding section allows appreciating the irregularity of the measurements between years (Figures S2, S5a-b), between locations in the transect (Figures S2, S4, S5b).

The results presented in this chapter demonstrate that the Southern Ocean system is currently changing significantly, with an amplitude overpassing typical interannual variability. These changes are due to various mechanisms depending on regions and depths. The dataset used in this study is not sufficient to dig into the details of each process. In the subpolar sector, the effects of freshwater fluxes and their changes on how they drive subpolar overturning circulation, upper ocean stratification, and how they can impact temperature change have been put forward in recent analysis (Schmidtko et al., 2014; Haumann et al., 2020; Rye et al., 2020; Sallée et al., 2021; Pellichero et al., 2017b). In the northern region, the effect of winds, increasing heat fluxes, and change in horizontal circulation have been discussed over the yearsSwart et al. (2018); Gao et al. (2018); Gille (2008). In comparison, much less is known about the impact of the subpolar ocean horizontal circulation on temperature change ; similarly, the lack of understanding of the subpolar ocean horizontal circulation prevent us to discuss which regions

of the Southern Ocean continental shelf might be impacted by the large subsurface warming of CDW observed here. This motivates the remainder of my thesis, where I strive to improve our understanding of the horizontal circulation of the subpolar Southern Ocean from satellite altimetry.

CHAPITRE

II

Southern Ocean Sea Level Anomaly in the Sea Ice Covered Sector From Multimission Satellite Observations

Sommaire

1 Preamble

In the previous chapter, I used in-situ measurements to document the temperature changes in the Southern Ocean. I then discussed how a satellite altimetry-derived dataset may allow us a better understanding of the context of these changes and the mechanisms driving them. Here, I exploit the opportunity of the recent improvements in the processing of satellite altimetry in the ice-covered regions (Quartly et al., 2019) and complete them by using the data merging and mapping techniques intensively used in the open ocean for the operational ocean topography datasets (Taburet et al., 2019).

To date, there are only two gridded sea surface topography products in the ice-covered oceans (Armitage et al., 2018; Dotto et al., 2018). These datasets are based on Cryosat-2 along-track measurements and are both mapped the same way on monthly grids. The two products are therefore very similar. Despite their relatively low spatial and temporal resolution they allowed bringing new insights into the ice-covered Southern Ocean variability and dynamics. However, we believe that these products can be improved. Since their publication, much progress has been made in the processing of radar altimeter measurements in the ice-covered oceans (Quartly et al., 2019). Also, more satellites sample the Southern Ocean up to the coast of Antarctica, and global SLA products such as DUACS (Taburet et al., 2019) demonstrate the strength of merging along-track measurements from multiple altimeters into a unique high-resolution gridded dataset. Using existing state-of-the-art processing techniques, along with including other satellites in the computation may allow a dramatic increase of the capacities of the datasets. I took this challenge as part of my thesis, with the goal to improve the existing SLA datasets of the subpolar Southern Ocean. My main motivation here is to be able to observe more accurately the large-scale processes governing the Southern Ocean variability, including its ice-covered parts, and to allow the observation of smaller-scale processes to determine their role in the Southern Ocean system.

To describe the dataset that has been developed in the context of this thesis, I first present the technology of satellite altimetry, and the details of the processing steps and corrections needed to compute SLA from the waveform obtained at each measurement point. Satellite altimetry is a well-proven but complex technique allowing the retrieval of the ocean surface topography. The distance between the sea surface and the satellite is computed using the two time-travel duration of the radar wave, emitted from the satellite to the sea surface, and scattered back to the satellite. This time travel is then corrected from instrumental, environmental, and geophysical effects. The sea surface height is then computed by subtracting the distance between the sea surface and the satellite to its orbit.

I then present the specificities of this technique when applied in sea ice regions, for the recovery of the ocean topography in the leads. Measurements obtained in the leads must first be identified. Echoes retrieved from the leads are very distinct from the ones retrieved on other oceanic surfaces. These measurements are obtained in sea ice regions, and the sea ice echoes must be discarded for the computation of ocean surface topography. This identification is called the waveform classification. The distinction between the open ocean and leads waveforms

also induces issues with the retracking step, that is the step of deducing from the waveform the two time-travel of the radar wave between the satellite and the sea surface. Indeed, specific retracking methods have to be used for the leads.

The next important step is the mapping of the along-track measurements. I introduce the mapping process and how it was adapted from the open ocean product (Taburet et al., 2019) to this Southern Ocean regional dataset.

Lastly, based on the previously presented methods and considering the specificities of high latitude processings, I present the Southern Ocean Sea Level Anomaly product developed in the context of this thesis, its validation, and error estimation.

2 Radar Altimetry in the ice-covered Southern Ocean

2.1) Radar Altimetry Principle

In the general introduction, I presented the principle of the satellite altimetry technique and its evolution over time. Here, I introduce the technical aspects of the satellite altimetry technique for the retrieval of ocean topography. This introduction is more an overview of the techniques involved in the satellite altimetry processing, rather than a fine and exhaustive description of the system.

Satellite altimetry is a technique able to measure the sea surface topography, from radar waves emitted by a satellite. The satellite emits between 20 to 40 radar waves per second at the nadir along its track. The wave propagates in the atmosphere and is backscattered toward the satellite at the sea surface. The time travel of the radar wave is then used to compute the distance between the satellite and the sea surface. The orbit of the satellite being known thanks to the Precise Orbit Determination (POD) system, by correcting the bias induced by the atmosphere and the sea state, it is possible to compute the Sea Surface Height (SSH) from the ellipsoid.

2.2) Along-Track processing

Radar measurement principle

Radar measurement consists of the emission of a radar pulse toward the sea surface and the reception of the backscattered signal. These pulses are emitted at the Pulse Repetition Frequency (PRF) frequency at the nadir of the satellite (18kHz for Ku band satellites, 36kHz for Ka band satellites). The returned echo consists of the time evolution of the received power of the backscattered signal (Stammer and Cazenave, 2018), called "waveform". They are averaged over frequencies between 20 and 40Hz. These waveforms are used to compute the epoch (time delay of the return of the echo in the recieving window) and therefore to deduce the range (distance between the altimeter and the sea surface). But various geophysical parameters can also be extracted from the waveforms, such as the wind amplitude (chelton 1985, monaldo) or the Significant Wave Height (SWH) (monaldo). The extraction of information from the waveform is called retracking. Open ocean echoes, usually called “Brownian echoes”, are represented in Figure II.1 (yellow pannels Stammer and Cazenave, 2018). The emitted signal has a spherical shape toward the sea surface. While no signal reaches the sea surface, the backscattered amplitude is zero. Then when the tip of the sphere meets the sea surface, a small part of the signal is backscattered, depending on the significant wave height (Figure II.1b). Then, from Figure II.1b to Figure II.1c, there is a step of increasing amplitude with time. This part of the waveform is called the leading edge of the echo. The amplitude then reaches its maximum as a bigger part of the signal reaches the sea surface at the same time. It then decreases according to the shape of the antenna gain and the wind amplitude (Figure II.1d). This decreasing part of the echo is called the trailing edge.

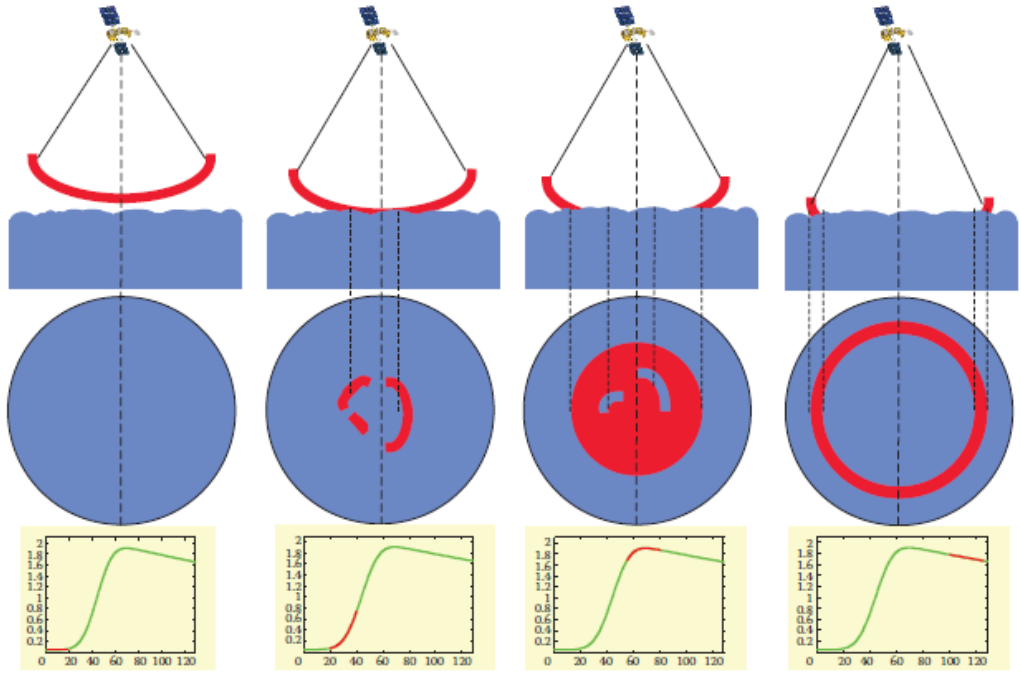

FIGURE II.1: From Stammer and Cazenave (2018) : Altimeter echoes : This figure depicts the time evolution of radar altimeter signal reflection on the sea surface. The upper panel provides a side view, while the middle panel provides a top view of the phenomenon. The lower panel provides the amplitude of the backscattered received signal as a function of time (referred to as waveform). The red part of the waveform curve corresponds to the echo reflection depicted in the upper panels. (From http ://www.altimetry.info.)

The computation of the range, is derived from the epoch and relies on the retracking technique. This retracker fits a waveform model to each echo. There are a lot of different retracking algorithms, estimating various parameters and for multiple purposes. For a Brownian echo, most of the retrackers estimate between 3 and 5 parameters which can be time, significant wave height, power, slope of the trailing edge of the waveform, skewness or mean square slope (Stammer and Cazenave, 2018).

Geophysical corrections

Once the theoretical range is computed, several corrections must be applied. These corrections consist of atmospheric and sea state corrections.

The atmospherical corrections allow considering the effects of the atmosphere on the propagation of the radar wave toward and from the sea surface. They include wet and dry tropospheric corrections and ionospheric correction.

The wet tropospheric correction lies for the atmospheric humidity, mostly contained in the troposphere, that strongly affects the signal emitted from the altimeter. The error induced by this humidity on open ocean signals is evaluated thanks to a radiometer, which is a dedicated instrument onboard of the satellite (Desportes et al., 2006). This multifrequency microwave ra-

diometer measures the tropospheric water vapor content simultaneously with altimetric measurements (Ubelmann et al., 2014). Over the ocean, the wet tropospheric correction varies from a few millimeters at high latitudes to up to 40 cm at the Intertropical Convergence Zone (ITCZ).

The dry tropospheric correction represents the correction due to the dry gases in the troposphere. This correction is the largest applied among all the geophysical corrections, with a mean value of about 2.3 m, but with low temporal variations (Black and Eisner, 1984). This correction is usually retrieved from ERA European Center for Medium-range Weather Forecast (ECMWF) re-analysis.

The last atmospheric component of the geophysical corrections is the ionospheric correction. Indeed, the ionosphere induces dispersion of altimetric signals due to the presence of free electrons which bias the signal (Stammer and Cazenave, 2018). This correction values can reach up to 4cm (Callahan, 1984). As the ionosphere is directly affected by solar radiation, the bias varies in time with the solar cycle.

Ocean corrections must also be applied to the signal, and are grouped under the name of Sea State Bias (SSB). They consist of an electromagnetic bias, a skewness bias, and an instrument tracker bias, and a bias induced by the backscattering difference between troughs and crests of ocean waves. While it was originally corrected using a percentage of the Significant Wave Height (SWH), recent corrections have been computed with a model, estimating the bias from wind speed, radar cross-section, and SWH (Cheng et al., 2019).

Orbit Determination

Once the range of the satellite is computed and corrected, it must be substracted to the orbit of the satellite to obtain the sea surface height over the Earth ellipsoid (Figure .10. The orbit is determined by combining orbit modelling to direct observations.

Direct observations are retrieved through Doppler Orbitography and Radio-positioning Integrated by Satellite (DORIS) and Global Navigation Satellite System (GNSS) systems. DORIS is an uplink Doppler radio system, consisting in the emission of radio-frequencies signals from ground-based orbit-determination beacons to on-board receivers (Auriol and Tourain, 2010). The phase of the signal received onboard by the DORIS receiver allows a high precision determination of the altitude of the satellite, with only a few millimeters of error (Stammer and Cazenave, 2018). About 50 transmitters are distributed on the whole surface of the globe, allowing continuous monitoring of the satellite's orbit. GNSS systems also consist in phase measurements, but from GNSS satellites, also used for positioning of ground mobiles. Both techniques require the estimation of unknown parameters, such as clock biases or atmospheric propagation parameters Stammer and Cazenave (2018).

However, direct observations are not sufficient and need a first estimation to reach sufficient accuracy. This first estimation is obtained through a parametric model, combining observations and an optimization process of the tracking parameters, such as the orbital characteristics, the satellite position, and velocity, or atmospheric parameters. The latest orbit estimation models (POE-E) have an error of up to 8 mm (Taburet et al., 2019).

The orbit determination has a direct implication on the error budget of the final SSH estimation, as the orbit is one of the two distances needed for the computation of the ocean topography. Therefore, errors in the orbit will be directly translated to the SSH estimation. A precise estimation of the satellite altitude is thus essential.

Reference surface

The Sea Level Anomaly (SLA) is the time-varying component of the sea surface height that is only dependent on the ocean circulation. SLA is computed by removing a Mean Sea Surface (MSS) to the Sea Surface Height (SSH). MSS is therefore the mean sea surface height over the reference ellipsoid. To retrieve the ocean circulation from the sea surface height, the time-varying component, the SLA, must be added to the mean sea surface height over the geoid, the Mean Dynamic Topography (MDT). Added together, the ADT and the MDT are the Absolute Dynamic Topography (ADT), which is the full time-varying sea surface height related to geostrophic circulation of the ocean.

Corrections needed for geostrophic currents computation

Before obtaining the SLA component relative to the circulation of the ocean, one must remove the direct effect of the dynamics of the atmosphere and the tides.

The effect of the dynamics of the atmosphere on the SLA is corrected by two components, representing two distinct mechanisms. First, the effects of the low-frequency dynamics of the atmosphere are corrected. They are related to sea level pressure variations of periods longer than 20 days and are related to the response of the ocean to changing atmospheric pressure. To correct this component, the inverse barometer is computed, which is the direct hydrostatic response of the SLP on the SLA (FU 1995). This effect is evaluated at about a 1 cm decrease of the sea surface for a 1 hPa increase of the atmospheric pressure and is computed directly from European Center for Medium-range Weather Forecast (ECMWF) operational model Gaussian grids. Second, the correction on the high-frequency atmospheric dynamics must be obtained. It consists of a correction that considers high-frequency ocean response to high-frequency atmospheric pressure changes, but also the direct effect of the wind on the sea surface. This correction is evaluated by dedicated models (MOG2D ; Carrère and Lyard, 2003).

Several types of tide influence the topography of the ocean, and that must be corrected for the SLA to account only for the geostrophic circulation. Among them are the ocean tides, the solid earth tide, and the pole tide.

Ocean tides include the classic ocean tide, but also the displacement of the bottom of the ocean due to the loading by the water column associated with ocean tides (Vignudelli et al., 2011). Ocean tides corrections are computed by dedicated tide models (FES2014 ; Lyard et al., 2021), and accounts for the effect of all the diurnal, semi-diurnal and mixed tide waves on the sea surface. Solid Earth tide correction must be removed as well. As the oceanic tide, the solid Earth tide is due to the gravitational forces of the Moon and the Sun, but this time applied to the solid part of the earth instead of the hydrosphere. The solid Earth tide correction has an amplitude of up to 20cm (Vignudelli et al., 2011). Finally, the pole tide effects must also be

removed. The pole tide relates to the variation of the axis of rotation of the Earth from the pole, as changes in the centrifugal forces induced by this variation produce a signal in the sea surface height (Desai et al., 2015). The amplitude of this error is about 20 millimeters.

2.3) High latitude processing

All the previously presented processing steps allow the computation of the along-track sea level anomaly from a waveform retrieved on an open ocean surface. However, using the satellite altimetry technique in a high latitude environment induces several specificities. The presence of sea ice on the top of the ocean surface forces the use of dedicated processing techniques to retrieve a representative sea surface height signal while mitigating the errors (Quartly et al., 2019).

Waveform Classification

The main dedicated processing for the sea ice regions is the classification of the waveforms. While most of the open ocean echoes have the characteristic open ocean Brown-like waveform, the waveforms retrieved from sea ice environments differ drastically from this classical model. As their surface is much more irregular than the open ocean and the leads, sea ice floes measurements can be identified and discarded from the computation of ocean topography in the ice-covered ocean (Longépé et al., 2019). In the leads, however, the free surface is protected from the winds by the neighboring sea ice. The surface stress being very low, the surface roughness drops compared to an open-ocean configuration. In the leads, the surface is considered quasi-specular, meaning that it reflects directly the incoming wave back to the satellite. The resulting waveform is a powerful peak, with a very sharp trailing edge characteristic of a sea ice lead. These lead measurements must be identified for dedicated processing to compute the sea surface height in the ice-covered regions (Longépé et al., 2019).

From the shape of the returning echo, it is possible to determine the type of surface that was sampled by the altimeter. To construct a sea surface height product covering both open ocean and ice-covered ocean, Brownian and specular echoes must be identified and isolated from the other measurements. This is the principle of the classification step. The classification is realized by a dedicated algorithm.

Retracking

The difference in the waveforms used to differentiate the echoes from the leads and the open ocean actually leads to specific issues for the retracking step of the waveforms (Quartly et al., 2019). As presented in the along-track processing part, open ocean measurements are retracked by fitting a modelled waveform to the retrieved echo. In this case, the retracking used is physical, as it models the waveform and allows the computation of Significant Wave Height (SWH), wind speed, and range. However, the classical open ocean retrackers are not able to model the leads waveforms, as they are too specular to consistently fit the model. As a result, in most of the studies, a specific retracking algorithm is used, called the Threshold First-Maximum

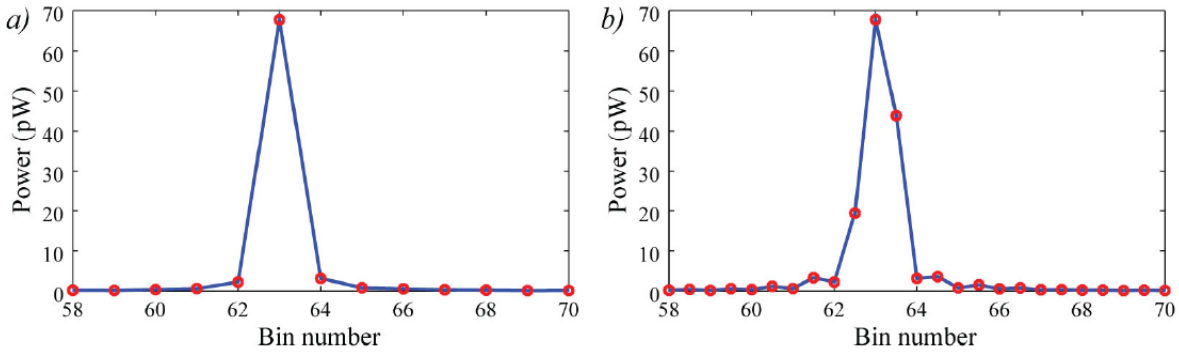

FIGURE II.2: From Quartly et al. (2019) : The effect of zero-padding upon the rendition of a CryoSat-2 waveform over a lead within the sea ice : (a) Without zero-padding, the specular waveform is heavily under-sampled (only one range sample within the main peak). (b) With zero-padding (enabling the FFT to produce more frequent samples within the waveform shape), the peak is better represented, showing the asymmetry in the echo. This allows more precise estimation of the timing associated with the 50% or other thresholds, reducing the jitter noise in the determination of the range. (In both cases, the full waveform corresponds to bins 1 to 128, with the panels being focused on showing the details of the specular peak.)

Retracker Algorithm (TFMRA; Peacock and Laxon, 2004). This retracker relies on the empirical result that the retracking point is fixed at a specific threshold on the leading edge of the waveform (usually 50% or 60%). This is the retracker that has been used for sea ice echoes in Armitage et al. (2018); Dotto et al. (2018) products.

However, for SAR altimeters, the leads waveforms are even peakier than LRM altimeters. This sometimes leads to an undersampling of the part of the waveform containing the signal, as it is sampled on too few bins (Figure II.2a Quartly et al., 2019). To overcome this issue, zero-padding processing is used. It allows sampling the waveform on more bins, therefore having a better representation of the waveform and allowing for a more precise determination of the retracking threshold. An example of the application of the zero-padding processing on a waveform is shown in Figure II.2b (Quartly et al., 2019). This pre-processing is necessary when using SAR measurements in the leads. Moreover, other processings such as Hamming windows allow improving the representation of specular waveforms. These processings are not applied on all of the SAR products within the sea ice, it is thus a condition for choosing the along-track waveforms products used for the gridded dataset.

The waveforms from LRM altimeters are less peaky than the SAR ones. It allowed the recent development of physical retrackers able to model the waveforms both in the open ocean and in the leads. One of them has been developed at CLS and is called the "adaptive" retracker (Poisson et al., 2018), and I was able to use it for one of the satellite exploited in my dataset. In the case of a physical retracker, it is possible to use the same algorithm for both surfaces, allowing the retrieval of a continuous SLA in the open ocean and the ice-covered regions. This is a tremendous progress as using two different retrackers for both surfaces leads to offsets between the SLA of the two regions that are extremely difficult to correct accurately. As an example Armitage et al. (2018) corrects the offset between the open ocean, retracked with a classic physical retracker,

and the ice-covered ocean, retracked with a TFMRA retracker, by computing the monthly mean offset at the sea ice edge, in the gridpoints where there are both open ocean and leads echos. This technique has been found to potentially create a spurious seasonal cycle on the SLA products (Prandi, 2020). Having a continuous surface even at least for one altimeter is therefore a strong asset for a newly developed SLA product.

2.4) Optimal Interpolation (OI) and Mapping

Once all the echoes have been properly selected, retracked, and corrected, they are merged into a gridded interpolated SLA product. To convert an along-track SLA (L3) product into a gridded (L4) product, a mapping and interpolation method is needed. In the previously published regional products (Armitage et al., 2018; Dotto et al., 2018), along-track measurements were averaged monthly on 1° grid cells. This is the simplest way to map along-track measurements on a regular grid. However, when mapping measurements from multiple missions into one gridded product, this method does not stand as it does not consider the different properties of the satellites. In the reference product for SLA in the global ocean (DUACS ; Taburet et al., 2019), an optimal interpolation method is used to interpolate and map L3 products of multiple satellites into a unique daily, high-resolution SLA product. I used the same algorithm for developing the regional dataset, but I adapted some parameters to suit high latitude processing. This mapping technique is based on an optimal interpolation derived from Le Traon et al. (1998); Ducet et al. (2000); Le Traon et al. (2003), and is described in Pujol et al. (2016), *Appendix B*. For each estimation point, it considers all the measurements located within the defined correlation scales around the estimation. Then, the best estimate of the Sea surface height is computed through an inversion of the covariance matrix, based on the expected variance of the signal, the error associated with the instrument of each measurement, based on methods from Bretherton et al. (1976); Colin de Verdière (1989). The estimation of one gridpoint is illustrated in Figure II.3. The input parameters, which are the correlation scales, the expected variance of the signal, or the instrumental errors are defined as compromises between the number and quality of measurements, and the physical ocean topography signal.

I had to recompute or adapt all three of them for this regional Sea Level Anomaly dataset. The processes I applied on the along-track waveforms to construct the gridded dataset are detailed in the following data descriptor.

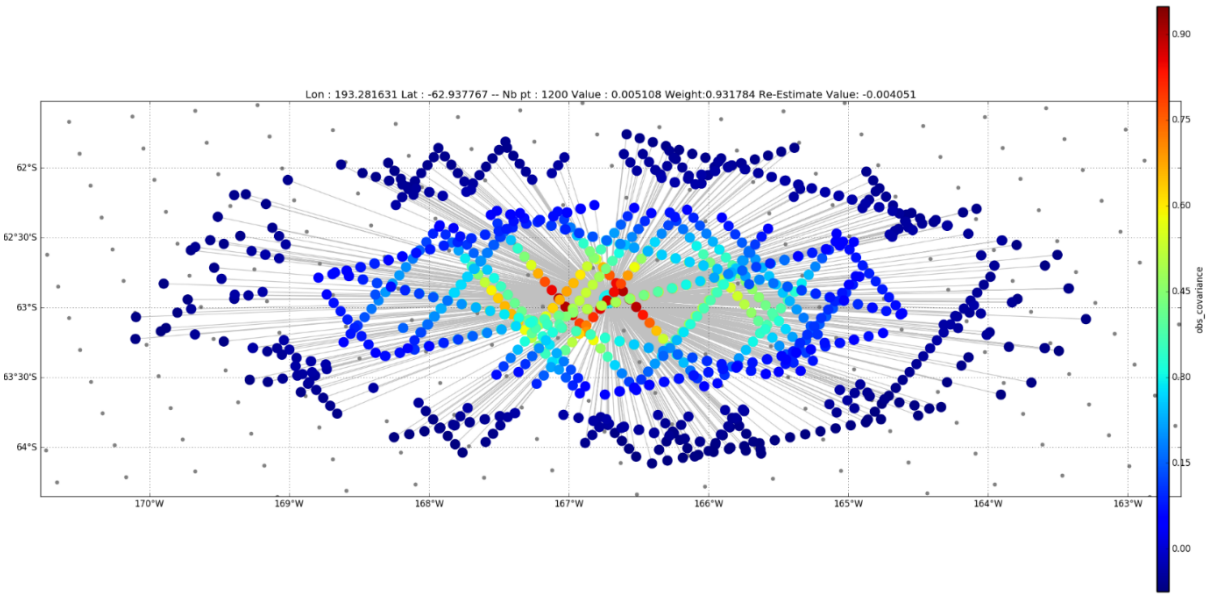

FIGURE II.3: Illustration of the computation of one gridpoint by the Optimal Interpolation process. Colored points are the observation measurements, and the center of the figure is the position of the estimation point. Light grey points are the other points of the grid.

3 Southern Ocean Sea Level Anomaly in the Sea Ice Covered Sector From Multimission Satellite Observations

This section includes a paper submitted as a data descriptor in Scientific Data, which I reformatted here for the purpose of this manuscript. The reference is Auger, M., Prandi, P., Sallée, J.B., Southern Ocean Sea Level Anomaly in the Sea Ice Covered Sector From Multimission Satellite Observations, Submitted at Scientific Data.

Abstract

Despite its central role in the global climate, the Southern Ocean circulation is still one of the least understood ocean circulation systems of the planet. One major constraint to our understanding of this region is the challenge of observing ocean circulation in the seasonally sea ice sector of the Southern Ocean. Here, we present a new Sea Level Anomaly (SLA) product, focusing on the subpolar Southern Ocean and including its sea ice covered parts from 2013 to 2019. Combining observations from multiple satellites, including Cryosat-2, Sentinel-3A, and AltiKa, processed with state-of-the-art algorithms, allows an improvement in spatial and temporal resolution compared with previous products. Validation is made by comparing our estimate with existing SLA products, cross-comparing estimates from individual satellites in the sea ice zones, and comparing the time series of the product with a Bottom Pressure Recorder in the Drake Passage.

3.1) Background & Summary

The Southern Ocean is a central element of the climate system, yet it is very poorly observed, understood, and not well represented in climate models (Meredith et al., 2019). The Southern Ocean is the main anthropogenic heat and carbon sink of the world's oceans (Frölicher et al., 2014; Meredith et al., 2019), and acts as a major hub distributing physical and biogeochemical properties around the globe (Rintoul et al., 2001; Sarmiento et al., 2004). Despite this importance, the Southern Ocean, and particularly its seasonally ice-covered subpolar region, remains poorly sampled, which impedes long-term monitoring of its change and limits progress in its representation in climate models (Newman et al., 2019; Meredith et al., 2019). In particular, very little is known about the drivers of ocean circulation in the subpolar seas and how they are affected by current global climate change (Thompson et al., 2018; Meredith et al., 2019).

In this paper, we revisit the processing of satellite altimeter observations developed over the past decades to produce a new and unprecedented observational dataset of sea-level anomalies (SLA) and geostrophic velocity anomalies in the Southern Ocean subpolar seas from a multi-satellite approach. Since 1992, satellite altimetry has helped to map the global ocean geostrophic circulation through high precision sea level measurements while allowing a better understanding of the Earth's climate variability and response to climate change (Morrow and

Le Traon, 2012). The number of satellites sampling the ocean is now larger than ever, creating new possibilities in terms of combination and sea level mapping resolution. Daily and global multi-mission products such as the Data Unification and Altimeter Combination System (Taburet et al., 2019) (DUACS) reach a horizontal resolution of 100 km at high latitude (Ballarotta et al., 2019). However, these products do not include the ice-covered regions of the global oceans, even though conventional satellite altimetry can help to understand the open ocean parts of the polar oceans (Prandi et al., 2012). Dedicated processing needs to be used over ice-covered areas.

Since the early years of altimetry, many studies have been conducted to understand how to process and obtain valuable ocean observations in sea ice zones. Specular reflectors such as leads or calm open water polynyas were first detected in the altimeter footprint by using an airborne radar altimeter and comparing with large-format aerial photography (Drinkwater et al., 1991). Later, a first ocean / sea ice classification technique was developed using ERS-1 satellite altimeter along with a new threshold retracking algorithm for sea ice, taking into account the fact that conventional models were not able to retrack powerful specular sea ice echoes (Laxon, 1994). The first mean sea surface and sea surface height variability product in the ice-covered Arctic was released using ERS altimeters (Peacock and Laxon, 2004). Using a very similar processing scheme but different satellites, various datasets such as sea ice thickness (Tilling et al., 2018), mean sea level trends (Giles et al., 2012) and sea surface height studies (Bulczak et al., 2015; Kwok and Morison, 2016; Mizobata et al., 2016; Armitage et al., 2016) were released in the Arctic and helped uncover its changes and variability. The first sea surface height variability maps in the subpolar Southern Ocean were limited to its ice-covered parts (Kwok and Morison, 2016). Based on Cryosat-2 observations from 2012 to 2016, the first monthly sea surface height product of the whole Southern Ocean was produced (Armitage et al., 2018; Dotto et al., 2018), allowing to document the seasonal climatology of the subpolar sea surface height, interannual variability and forcings (Garabato et al., 2019). In the present study, we extend this effort by combining observations from multiple satellites, thereby allowing for higher spatial and temporal resolution than previously done. We also leverage recent radar altimetry signal processing advances : a neural network based waveform classification for lead detection and a physical retracker algorithm that alleviates the need for ad-hoc bias correction between the open ocean and sea ice sectors.

3.2) Methods

Data Source

Satellite Altimeters

We use observations from three satellite altimeters : Cryosat-2, Sentinel-3A, and SARAL/AltiKa, which we present below in turn (see also Table II.1).

Cryosat-2 is an ESA mission, which was launched in April 2010. Its SIRAL instrument is a Ku-band (i.e. frequency range from 13 to 17 GHz) radar altimeter working in three different modes : Low Resolution Mode (LRM) over most of the ocean, SARM (Synthetic Aperture Radar Mode) on the sea ice, and SARInM (Synthetic Aperture Interferometric Mode) on the ice-sheets margins

Table II.1: Altimeters characteristics

Altimeter	*Launch Date*	*Mode*	*Sampling Frequency*	*Inclination*
SARAL/AltiKa	2013/02	LRM	40Hz	99
Cryosat-2 (sea ice)	2010/04	SAR	20Hz	92
Sentinel - 3A	2016/02	SAR	20Hz	99

and temperate land-ice (Wingham et al., 2006). Only the ESA Cryosat-2 ICE SAR Baseline-C L1b dataset was used for this study. This dataset includes the sea ice zones within Cryosat-2 SARM mask. SARM allows a better along-track resolution via the use of the Delay Doppler pocessing, reaching about 400 m of effective resolution compared to the 8 km resolution of conventional altimeters (Scagliola et al., 2013).

Sentinel-3A carries the dual-frequency Synthetic Aperture Radar Altimeter (SRAL) instrument, which was launched in 2016 (Donlon et al., 2012). Sentinel 3A CNES Processing Protocol (S3PP) data are used as they include the Zero-Padding and Hamming processings, which are necessary for SAR data in sea ice zones (Quartly et al., 2019).

SARAL/AltiKa is a CNES-ISRO (Centre National d'Etudes Spatiales, Indian Space Research Organisation) satellite, which was launched in February 2013. It carries a conventional (pulse limited) Ka-band (i.e. 35.75 GHz) radar altimeter, which allows a smaller footprint than a Ku-band radar (4 km versus 15 km for an identical orbit) and a higher sampling frequency (40 Hz versus 20 Hz). The primary objective of this high-resolution ocean topography satellite is the observation of ocean mesoscale circulation (Verron et al., 2015).

Data Processing

Combining multiple missions into a single product requires care to adequately take into account differences between instruments. In our study, we must take into account the difference between AltiKa pulse limited altimeter, and Cryosat-2 and Sentinel-3 SAR altimeters. Low-resolution mode altimeters are historically considered as the conventional instruments. Their resolution is limited by the length and width of the pulse. SAR altimeters allow a better along-track resolution due to the multi-look of the target along the path of the satellite (Quartly et al., 2019). The resulting waveforms are narrower and therefore dedicated processing is required. We present below the processing that was organised in five main steps : (i) classification, (ii) retracking, (iii) geophysical corrections, (iv) bias correction, and (v) mapping.

Classification

The SLA field is built using open ocean and lead echoes. Data points located on the continent, continental ice, or sea ice are discarded. For that we use a neural network waveform classification algorithm (Poisson et al., 2018) validated using SAR images (Longépé et al., 2019). Each echo is affiliated to one of 12 classes representing various waveform shapes and surface types. This classification is complemented with the traditional multiple criteria approach, considering backscattered power and pulse peakiness (Peacock and Laxon, 2004; Bulczak et al., 2015). Open ocean and leads data are selected and processed separately. Radar returns are very dif-

	SARAL/AltiKa	Cryosat-2	Sentinel-3A
Orbit		POE-E (Ollivier et al.)	
Ocean Tide		FES14 (Carrere et al., 2015)	
Polar Tide	From Desai et al. (2015)	From C2 Product	From Desai et al. (2015)
Earth Tide		Elastic response to tidal potential (Cartwright and Tayler, 1971)	
Dry Tropospheric Correction		Model from ECMWF gaussian grids	
Wet Tropospheric Correction		Model from ECMWF gaussian grids	
Ionospheric Correction		GIM (Iijima et al., 1999)	
Sea State Bias		Non-Parametric (Tran et al., 2012)	
Dynamic Atmospheric Correction		MOG2D high frequencies (open ocean) and inverse barometer forced with atmospheric ECMWF pressure and wind field (Carrère and Lyard, 2003)	
Mean Sea Suface		CNESCLS15 (Pujol et al., 2018)	

TABLE II.2: Geophysical Corrections applied to each altimeters

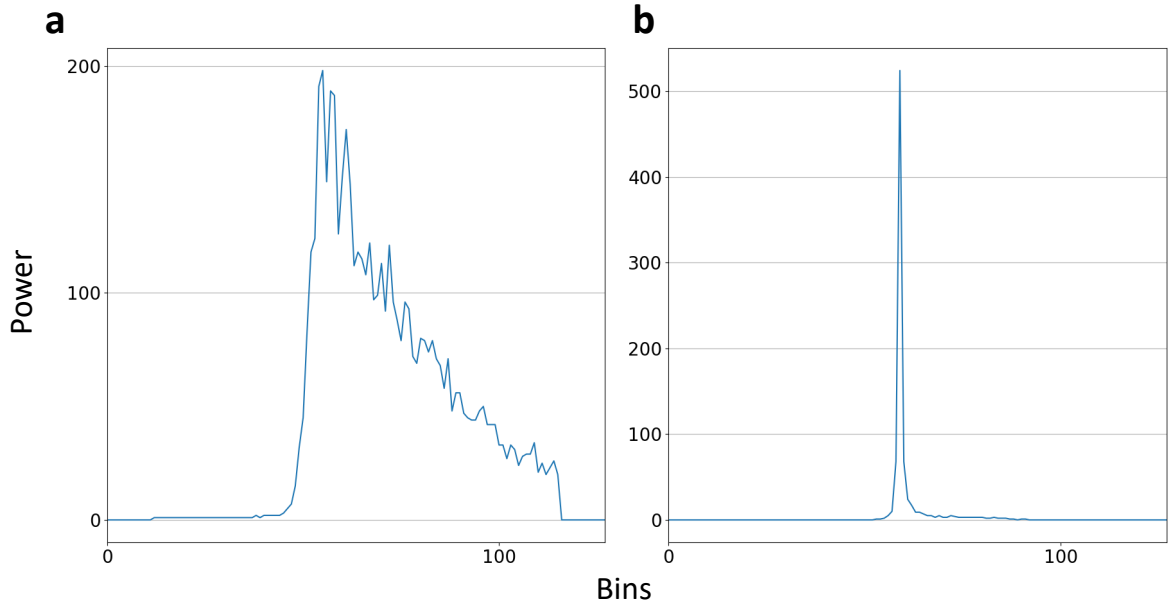

FIGURE II.4: Examples of waveforms from AltiKa altimeter (a) Brownian echo from open ocean. (b) Peaky (specular) echo from a lead.

ferent in terms of specularity and backscattering depending on the surface type and roughness. In the open ocean, the wind on the free surface creates a high surface roughness, leading to the reception of a Brownian type of waveform (Quartly et al., 2019) (Figure II.4a). In the sea ice areas, specular echoes (Figure II.4b) are mostly representative of reflection from the leads, their free surface being protected from the wind by the neighboring floes (Peacock and Laxon, 2004). Thus, the waveform is peakier and more powerful than in the open ocean. We do not investigate for differences between melt ponds and leads in the classification, as they are mostly specific to Arctic sea ice surface melt in summer, and less of an issue in the Antarctic (Maksym, 2016).

Retracking

Waveforms represent the power backscattered from multiple facets over the surface in the altimeter footprint, which are located at different ranges from the altimeter. The retracking process allows the retrieval of the geophysical parameters from these waveforms (Quartly et al., 2019). Retrackers can be either physical or empirical. Physical retrackers, such as SAMOSA SAR for Sentinel-3A (Dinardo et al., 2015), fit an analytical model to the waveform to estimate quantities such as epoch, Significant Wave Height (SWH), and radar backscatter. Physical retrackers are commonly used in the open ocean but most of them are not able to retrack specular waveforms from sea ice. Sea ice echoes are commonly retracked using empirical retrackers such as the TFMRA (Helm et al., 2014) (Threshold First Maximum Retracker Algorithm). In this case, geophysical parameters are estimated by empirical criteria (Laxon, 1994).

Commonly-used physical retrackers are not able to process open water or specular waveforms in the same way (Quartly et al., 2019). In previous studies combining sea ice and open ocean sea-level observations (Dotto et al., 2018; Armitage et al., 2018), Cryosat-2 L1b data were processed using a physical retracker in the open ocean and an empirical (TFMRA) retracker over sea ice, and the bias between the two retrackers was corrected empirically. In these studies, the bias between both zones was corrected by computing SLA differences along the sea ice margins, on grid points where it is possible to find both peaky and Brownian waveforms for each month, or at the transition from open ocean to sea ice along a satellite track. Such bias estimates are based on a limited number of measurements and are therefore highly uncertain. They can also create artifacts in the resulting sea-level anomaly product (Prandi, 2020) that are difficult to distinguish from genuine ocean variability. To try to alleviate this bias, here, we use a new retracker that has been developed for Pulse Limited altimeters, by modifying the conventional physical retracker for the Brownian echoes, making it flexible enough to retrack specular waveforms from the leads (Poisson et al., 2018). This unique 'adaptive' retracking for both open ocean and sea ice echoes was made possible by considering the variation of backscattering power with incidence angle, allowing a processing continuity between the two surfaces for the same altimeter.

The new retracker applies to open ocean and sea ice echoes consistently, allowing to retrieve consistent sea level anomaly maps without empirical bias correction at the sea ice edge, but it is currently only available for AltiKa. For Cryosat-2 and Sentinel-3A in the sea ice zones, we process observations with the TFMRA retracker, but we reference Cryosat-2 and Sentinel-3A to the AltiKa observations (see section "bias correction" below).

Another advantage of using a physical retracker in the leads is that the algorithm models the full waveform, allowing the consideration of residual winds for the retracking. In comparison, the TFMRA algorithm works with the assumption of zero wind in the leads, potentially leaving part of the signal uncorrected.

Geophysical Corrections.

Geophysical corrections are listed in Table II.2. Satellite orbit estimation is computed using POE-E algorithm (Ollivier et al.). Once the range is computed, geophysical corrections are applied to remove the tidal and atmospherical components of the range and to compute the sea surface height. The same corrections are used for each mission when possible for homogeneity.

As in previous studies (Armitage et al., 2018), we do not apply the high frequency dynamic atmospheric correction in the sea ice zone under the assumption that the impact of the wind on the free surface in the leads is limited.

Ocean tide is corrected using FES2014 model (Carrere et al., 2015). Ocean tide errors are estimated by computing the standard deviation of the difference between one year of FES2014 and GOT4V10 (Ray, 2013) tide signal on a 1° grid covering the whole Southern Ocean. Errors obtained are of the order of 1 cm in the open ocean, 2 cm in the seasonally ice-covered ocean, and about 8 cm in the permanently ice-covered Southern Ocean. This error is partially corrected using the long-wavelengths correction (see section "Mapping", below). The Global Ionosphere Maps (GIM) ionospheric correction is applied (Iijima et al., 1999), with a residual signal that can reach 5 mm (Pujol et al., 2016). Wet and dry tropospheric corrections, along with MOG2D high-frequency (Carrère and Lyard, 2003) and inverse barometer low frequency dynamic atmospheric corrections are taken from ECMWF (European Centre for Medium-Range Weather Forecasts) operational model Gaussian grids (https ://www.ecmwf.int/en/forecasts/dataset/operational-archive).

An objective analysis (OA) mapping method is used to convert along-track measurements (Level 2) into a gridded product (Level 4). The OA method requires that time-mean is removed from the data to be mapped (Bretherton et al., 1976). Here, the time-mean that is removed from the along-track observations before mapping is the Mean Sea Surface (MSS) CNESCLS15, which is based on open ocean measurements. Seasonally ice-covered regions of the MSS represent therefore a mean state of the ice-free time of the year, and permanently ice-covered regions are extrapolated (Pujol et al., 2018). As an alternative method which would not use the MSS with potential errors in sea ice covered region, one could instead reference the observations to the geoid, and then grid them, but this alternative method would downgrade the final resolution product, because the geoid is not known at short scales (typically less than 100 km ; Stammer and Cazenave, 2018).

Editing is performed once the fully corrected SLA is estimated. It uses empirical thresholds based on sea ice concentration, peakiness and backscatter coefficient of the echoes to discard possible errors. In the open ocean, the remaining outliers are removed using an iterative editing method. This method consists in applying a 124-points low-pass Lanczos filter on the along-track data, and removing outliers identified as each measurement such as $|SLA - SLA_{filtered}| > 3 * std(SLA - SLA_{filtered})$. This editing step is conducted multiple times until less than 0.1% of the measurements are edited. The iterative editing step is not performed in the sea ice regions, as the sampling is too irregular for applying such along-track filters.

Bias Correction

There are evidences that correcting a monthly bias between retrackers at the sea ice margins as in previously available SLA products (Armitage et al., 2018; Dotto et al., 2018), does not properly correct for the retracking bias in the entire sea ice zone (Prandi, 2020). AltiKa 'adaptive' retracking allows a continuous and consistent SLA computation in the open ocean and under sea ice, without the need of a bias correction. We therefore use AltiKa as our reference mission to properly correct bias between open ocean and sea ice sectors of other missions. Monthly SLA maps at a horizontal resolution of 1x1 degree are therefore constructed with AltiKa observation

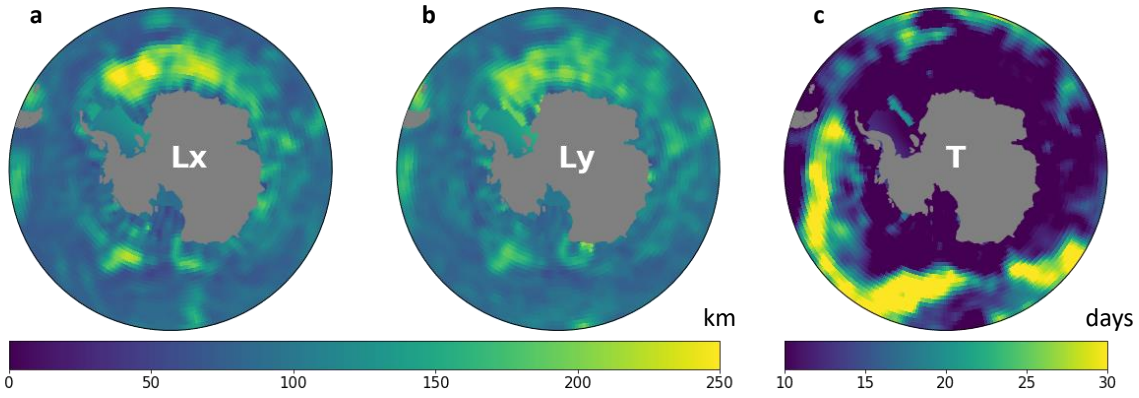

Figure II.5: Correlation scales of Sea Level Anomaly computed on GLORYS12 model outputs. (a) Zonal correlation scales. (b) Meridional correlation scales. (c) Temporal correlation scales.

only, as well as maps computed independently for Cryosat-2 lead observations, Sentinel-3A lead observations, and Sentinel-3A open ocean observations. Median biases between the AltiKa map and every other map are computed and used to correct each mission and surface each month. This allows us to estimate inter-mission biases which are representative of all the data coverage of the mission and retracker, and not only at the sea ice margins.

Mapping

The combination of all along-track observations from each mission into a gridded dataset is done by adapting the latest DUACS-DT2018 mapping procedure (Taburet et al., 2019) to our region of interest. It is based on an optimal interpolation (OI) (Le Traon et al., 1998; Le Traon and Ogor, 1998; Ducet et al., 2000; Le Traon et al., 2003). This OI method uses an a priori statistical knowledge on the covariance functions of the sea level anomalies and the data noise (Le Traon et al., 1998). A selection of observations within a space-time subdomain around a gridpoint and a date of interest is used for the interpolation. We therefore need to define a subdomain around each gridpoint, the expected variance of sea-level, and data noise.

A subdomain is computed for every point of the grid, and its size depends on the correlation scales of the sea level anomaly at that given gridpoint. Only the input files are modified from the DUACS-DT2018 (Taburet et al., 2019) mapping procedure. The correlation scales are computed from 2016 daily outputs of a global ocean model at 1/12° resolution, which assimilates observations (GLORYS12 (Brachet et al., 2004) ; Figure II.5). Minimal temporal correlation scale has been set to 10 days, and the largest values reach 35 days in the most stable meanders of the ACC. Spatial correlation scales range from 150 to 300 km.

The expected variance of the signal is investigated from the DUACS-DT2018 variance. We find however that in our region of interest, south of the ACC, DUACS-DT2018 has very low variance (Figure II.6a), much lower than SLA variance from Armitage et al. (2018) SLA product. Therefore, we here chose to compute the expected variance from our own observations rather than using DUACS-DT2018. We use a recursive method working on one arbitrary chosen year from March 2018 to March 2019. The recursive method starts by producing SLA maps for the given year, by using a large expected variance. We then compute the variance from this series

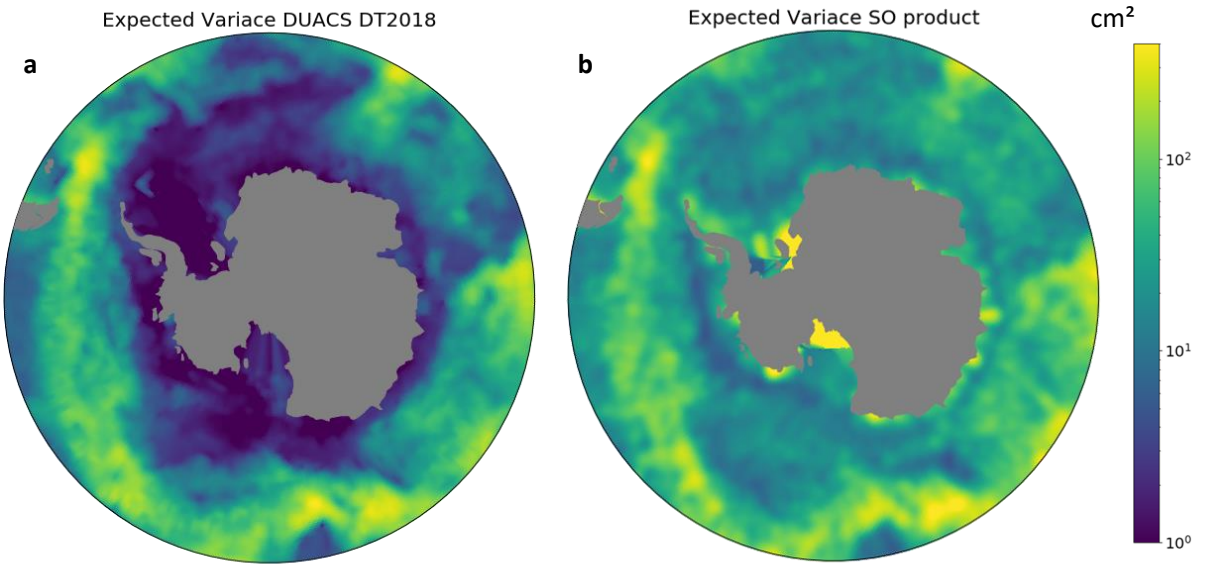

FIGURE II.6: Expected variance input for the Optimal Interpolation method, (a) for DUACS-DT2018 Taburet et al. (2019) product, (b) recomputed for the Southern Ocean regional product.

of maps and recompute a series of maps, but now using the revised variance estimate. And we continue to repeat the procedure until the variance converges toward a stable map. This process converges at the fourth iteration, with a reduction of less than 3% of the variance between the last two iterations. This newly produced variance has the same order of amplitude as the one in DUACS DT2018 in the open ocean, but without the large drop in variance in seasonally ice-covered areas that was present in DUACS DT2018 (see Figure II.6b).

The expected noise is computed by adding MSS CNES-CLS15 error (Pujol et al., 2018) to the instrumental errors (same as applied in DUACS) with a factor that depends on the measurement frequency : the noise from data acquired at a frequency freq is $\sqrt{freq}$ times higher than when acquired at 1Hz. Thus, as the SARAL instrument from the AltiKa mission is sampling at 40Hz, the noise applied to this mission for the mapping will be $\sqrt{2}$ higher than Cryosat-2 and Sentinel-3A altimeters sampling at 20Hz.

We apply a long-wavelength error correction during the mapping to remove along-track correlated signals (Le Traon and Ogor, 1998; Le Traon et al., 1998). Such signals can arise from residual orbit, tide, or dynamic atmospheric correction errors and produce 'stripes' on SLA maps when not accounted for.

Finally, once the product is corrected, we remove the temporal mean of the SLA for a better concordance and comparison with previously published products. Our SLA product represents therefore anomalies from the 2013-2019 mean sea level.

3.3) Data Records

The Southern Ocean SLA and geostrophic currents product is distributed as a single NetCDF file *dt_antarctic_multimission_sea_level_uv_20130401_20190731.nc*. It contains daily Sea Level Anomalies, associated geostrophic currents anomalies, and mapping formal error from April 2013 to July 2019. Individual fields are described in Table III.1. All fields are mapped daily on a 25km EASE2 grid (Brodzik et al., 2014) south of 50°S. Daily grids are dated using the number of days since 1950/01/01.

Field	Description
longitude	Longitude (°)
latitude	Latitude (°)
time	Days since 1950/01/01
sla	Sea Level Anomaly (m)
U	Zonal Geostrophic Current Anomaly (m/s)
V	Meridional Geostrophic Current Anomaly (m/s)
formal_err	Formal Error (m)

Table II.3: Fields of the Sea Level Anomaly product *dt_antarctic_multimission_sea_level_uv_20130401_20190731*

Technical Validation & Orbit Pattern Mitigation

Validation

Validation is performed by comparing the mapping outputs with other data sources. Pearson correlation is used to compare time series. Significance is evaluated using the local temporal correlation scale (Figure II.5) as the interval between two independent measurements. Correlation significance is assessed at the 99% confidence level.

Concordance with DUACS DT2018 in the open ocean

The first validation of our new product is obtained for the open ocean region, where we compare our results to the daily DUACS DT2018 product (Taburet et al., 2019), which has been extensively used and validated in various regions of the global open ocean. Between 2014 and 2018, 85% of total ice-free grid points (grid points that never reach a 1% SIC within the 4 years) have a significant correlation with the DUACS product greater than 0.80. The remaining discrepancies can come from differences in the mapping parameters as well as in the sampling, as the number of satellites used in each product is different.

In-situ validation

Validation in the sea ice zones is limited by the poor number of in situ time series relevant for sea-level anomaly validation in the Southern Ocean. For instance, tide gauges are very sparse along the Antarctic coast, and their sampling period is often not overlapping with our time series. Most of the Permanent Service for Mean Sea Level (PSMSL) dataset ends before 2013 (for instance at Casey or Cape Roberts tide gauge). For the few stations where there is a time overlap with our product, their coastal and landlocked locations (for instance, Scott Base, Rothera, Argentine islands) make comparisons extremely difficult with satellite altimetry. There would

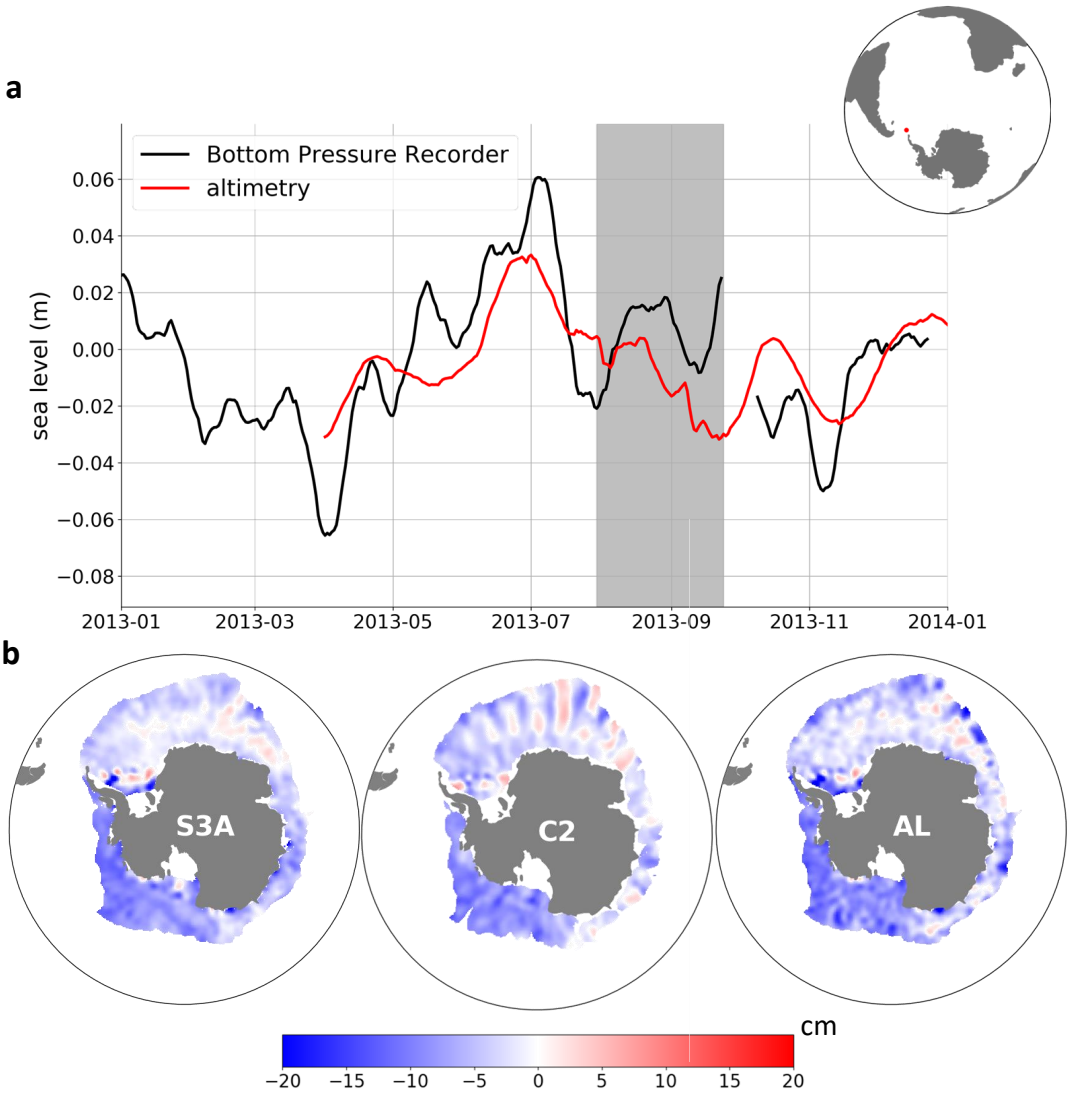

FIGURE II.7: (a) Sea Level Anomaly (SLA) validation in the drake Passage. Black line is sea surface height from the Drake Passage Bottom Pressure Recorder, red line is the SLA from altimetry. Red dot on the map is the location of the Bottom Pressure Recorder (b) Sea Level Anomaly snapshots mapped from the three altimeters in the sea ice zone. Each SLA snapshot is mapped independently from each altimeter.

be a strong need for coastal tide gauges in regions more representative of the open ocean (i.e. less landlocked) around Antarctica, corrected for tides and atmospheric pressure, in order to robustly validate future subpolar Southern Ocean products. Here, we nevertheless attempt to validate using a bottom pressure recorder (BPR) time-series in the open ocean, and second by comparing sea-level anomaly maps produced independently by single altimeters.

Bottom pressure observation obtained at 60.8°S, -54.7°E (https ://www.psmsl.org/data/bottom_pressure/locations/1608.php) is converted in sea level anomaly and filtered with a 15-day running mean. This bottom pressure recorder covers 2012 to the end of 2013, so comparison with our product is only possible from March 2013 to December 2013. BPR time series is compared with ~300 km filtered SLA product at the same grid point. Both time series are shown in Figure II.7a. The agreement between the two time

series is good both during the ice-free and ice-covered seasons, with an overall significant correlation r = 0.61 over 232 days. We note however that some variations differ within a month, and might depend on the altimetry sampling frequency at the location of the bottom pressure recorder. In particular, the correlation improves when averaging multiple grid points around the BPR, reaching 0.81 when averaging over a radius of 150 km around the BPR. In summary, the agreement with the bottom pressure recorder is good, but a longer and less sparse bottom pressure observation would be needed for a more extensive and statistically robust validation.

Consistency between altimeters in the sea ice regions

One alternative validation for our product is performed by comparing maps produced by the different individual altimeters. Although AltiKa serves as a reference, since the other satellite records are corrected using monthly median offsets, the spatial patterns within the sea ice zone indicate local daily differences. It is also a way to evaluate the error induced by sampling differences and disparities within the various altimeter properties. All daily maps are filtered with a ~150 km Gaussian filter to filter out mesoscales which would be sampled differently by altimeter depending on their exact path and time of observation.

Concordance between the maps derived from each altimeter is estimated daily with the standard deviation of the height bias between the maps. From July 2016 to June 2018, the standard deviation ranges from 3 to 6 cm, with a median standard deviation of 4 cm for all altimeters, and a slightly better agreement (lower standard deviation) between C2 and S3A. A snapshot of SLA maps in the sea ice zones from each altimeter is shown Figure II.7b.

Error estimation from independent along-track measurements

To evaluate the precision of the product in a 2-altimeter configuration, we compare the mapped product from AltiKa and Cryosat-2 from July 2016 to July 2018 with the along-track SLA from Sentinel-3. The median zonal and meridional correlation scale south of 50°S is 107 km (Figure II.5a,b). Therefore, Sentinel-3 along-track data is filtered with a ~107 km running mean filter. Error is defined as $|SLA_{along\_track\_S3A} - SLA_{C2\_AL}|$. The root mean square error (RMSE) is computed each month on a 1x1° grid. Figure II.8 shows the RMSE averaged over July, August, and September (JAS) from 2016 to 2017. RMSE values are different within various regions of the Southern Ocean. In the open ocean, the RMSE ranges from 4 to 10 cm in the most energetic jets of the ACC. In the sea ice zones, the RMSE is higher in the permanently ice-coverered regions of the Subpolar southern Ocean, reaching 10 cm regionally. In the seasonally ice-covered southern ocean, the standard deviation of the error ranges from 3 to 5 cm. Over 2 years, the median value of the RMSE in the permanently ice-covered Southern Ocean is 5.8 cm. In the seasonally ice-covered Southern Ocean and in the open ocean, the median RMSE are respectively 3.7 and 4.0 cm.

Cryosat-2 induced pattern mitigation

Several SLA products for the subpolar Southern Ocean have been previously developed (Armitage et al., 2018; Dotto et al., 2018). The observation-based product presented in this paper introduces several processing differences, among them a physical retracker for lead echoes, a long-wavelength error correction, and the multimission combination. Consequently, differences between our product and previous product are expected. The most notable difference

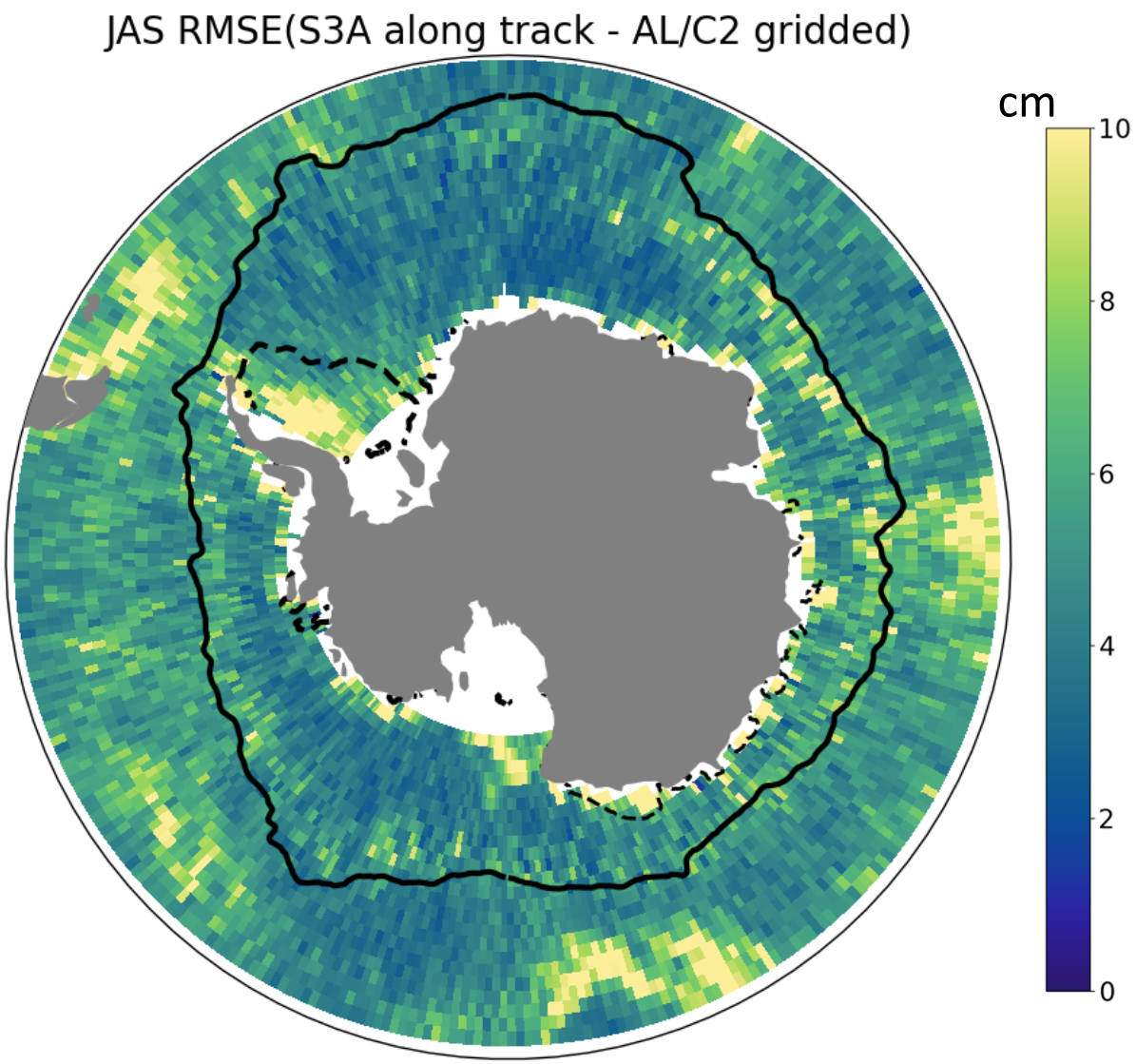

FIGURE II.8: Standard deviation of the error between along track S3A (filtered with a 107-km running mean) and interpolated product constructed only with AltiKa and Cryosat-2. This standard deviation was computed on the July-August-September months of 2016 and 2017. Black solid line is the mean 3% sea ice concentration contour for the July-August-September months of 2016 and 2017. Dotted line is the 3% contour of the minimum sea ice concentration over the years 2013-2019.

when comparing monthly maps between our product and Armitage et al.'s product(Armitage et al., 2018; Dotto et al., 2018) is that our product significantly reduces unphysical meridional stripes in SLA anomalies (Figure II.9). Previous products were based solely on Cryosat-2 observations, which orbit does not allow for an optimal temporal sampling over the ocean : neighboring regions are sampled with a time step of one month. Such a relatively long gap in time between the sampling of two neighboring regions, combined with the fact that SLA variability

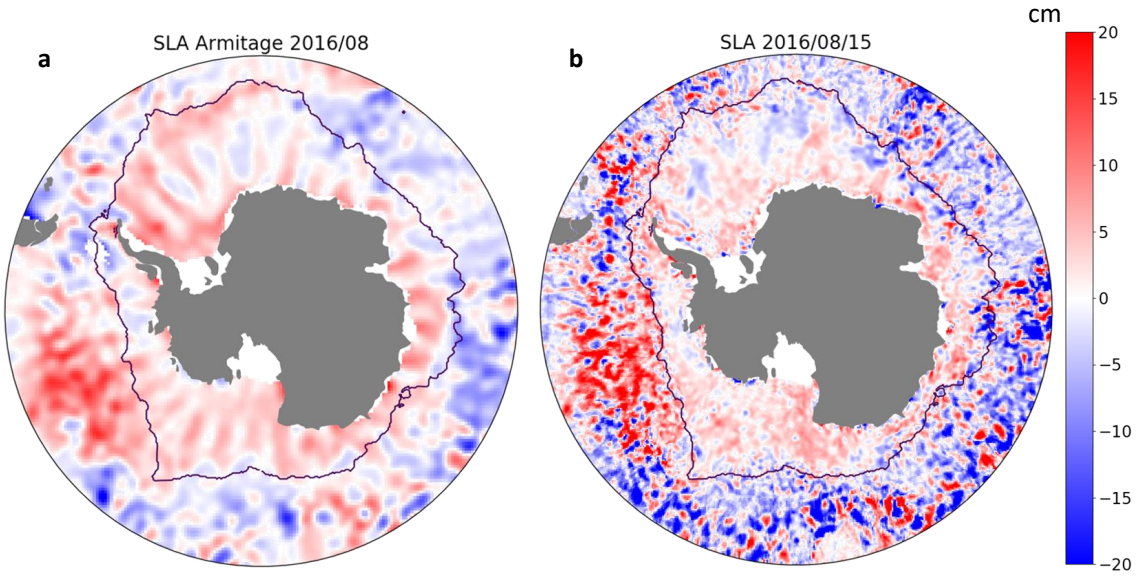

Figure II.9: a. Snapshot of Armitage SLA on 2016/09, showing a meridional pattern due to the orbit of Cryosat-2. b. Snapshot of the Southern Ocean SLA product on 2016/09/15, showing a mitigation of this signal from the use of multiple altimeters.

is large over one month, leads to such stripes when the product is interpolated and gridded (Figure II.9a). Our methodology that combines Cryosat-2 observations with observations from other satellites allows a strong mitigation of such source of error (Figure II.9b).

3.4) Usage Notes

Dataset is publicly available on SEANOE (Auger et al., 2021b) with the doi : 10.17882/81032.

4 Conclusion of the chapter

In this chapter, I presented a newly developed Southern Ocean Sea Level Anomaly product. We worked specifically to improve the spatial and temporal resolution of the dataset, as well as to improve the multiple processing steps compared to already existing products in the subpolar Southern Ocean.

SLA was gridded as monthly maps from Cryosat-2 observations in Armitage et al. (2018) and Dotto et al. (2018). Here, up to three satellites are used at the same time to increase the spatial and temporal resolution. This results in a daily product on a 25 km grid, allowing to observe smaller scale variability than what was possible before. Along-track measurements are mapped using the DUACS DT-2018 Optimal Interpolation (OI) method (Taburet et al., 2019), adapted for the specificities of the region.

Others improvements on the processing steps of the along-track measurements were made. In Armitage et al. (2018) and Dotto et al. (2018), the selection of lead measurements in the sea ice regions was done using empirical criteria. Their retracking steps are done entirely independently between the open ocean and the leads, or between SAR and LRM regions. In the sea ice region, an empirical retracking was used based on a threshold on the leading edge of the waveform. This led to bias that need to be empirically corrected between the different altimeter modes and surfaces types, with the risk of creating spurious seasonal cycle signal corresponding to bias when the sea ice cover advance or retreat. Here, a neural network classification of the echoes is used, selecting objectively the waveforms retrieved from the leads (Poisson et al., 2018). I also use the same retracker for leads and open ocean for AltiKa, allowing to construct a continuous reference surface and limiting the ad-hoc corrections of the bias between surfaces and altimeter types.

The validation of the dataset is difficult, as the number of *in-situ* measurements in the Southern Ocean, and particularly in its ice-covered parts, are extremely limited. I estimate the errors of the product in a 2-altimeters configuration by computing the standard error from along-track independent Sentinel-3A measurements. Three zones stand out with different error behaviour. In the open ocean, the error is small, except in the regions with the higher dynamics, as the amplitude of the signal is stronger. The error is slightly higher in the seasonally ice-covered sector, and more homogeneous within the region. Lastly, the error is highest in the permanently ice-covered regions, probably due to high errors in the Mean Sea Surface (MSS) product used to correct the along with track measurements. This error estimation has however limitations, as the along-track Sentinel-3A data may itself contain errors, potentially increasing the resulting error estimates.

There are several ways this product may be improved in the future. First, the use of physical retrackers for all the satellites will reduce even more the need of correcting bias between the ocean and sea ice regions, which can be a large source of errors (Prandi, 2020). Second, adding the other satellite altimeters available will also be a strong asset for improving resolution and accuracy. Jason 3, Sentinel-3B, or HY-2A and B are available now but have not been added to the product yet. Other satellites will also allow having a longer time series. Adding Envisat will dramatically improve the possibilities for exploitation of the product as it will span from 2002 to 2019.

Future satellites altimeters represent opportunities to keep track of the ice-covered ocean topography. Among them, Sentinel-3C and D, the rest of the HY-2 constellation, and CRISTAL. The latter mission will be launched in 2027, will occupy the same orbit as Cryosat-2, and will carry a dual-frequency altimeter. While the main objective of this dual-frequency is to measure both the ice thickness and the ice depth, it will be interesting to directly compare the effect of the emission band on the ocean topography signal. Moreover, other missions with potential benefit for the polar observation of the sea surface topography have been launched or are planned in the close future. First, the NASA ICESAT-2 satellite has been launched in September 2018, and carries a Lidar instrument onboard allowing to retrieve the topography of the ice and the ocean

with an unprecedented resolution. Second, the SWOT satellite that will be launched in 2022, uses an interferometric altimeter, which will have an interesting application for observing the sea surface in the leads (Morrow et al., 2019).

In the context of this thesis, this dataset will open the door for understanding better the variability of the Southern Ocean in regions that still lack observations, such as its seasonally ice-covered part. We expect that this dataset will bring important insights that may simultaneously improve understanding the mean state, the daily to interannual variability as a prerequisite before future investigations of long-term changes.

CHAPITRE

III

Southern Ocean Seasonal Variability in the Sea Ice-Covered Sector From Multi-mission Satellite Observations of Sea Level Anomaly

Sommaire

1 Preamble

In **Chapter II**, I introduced the new ocean topography product that I developed, which includes both the ice-free and ice-covered Southern Ocean. In the present chapter, I leverage this new tool to analyze the mechanisms driving the mean and seasonal cycle of the Southern Ocean horizontal geostrophic circulation. I focus on the analysis of the subpolar sector of the Southern Ocean, south of the ACC, as that is the sector where the new observation-based product brings the largest advances.

The main features of the subpolar Southern Ocean circulation are two large gyres, the Weddell Gyre and the Ross Gyre, as well as the Antarctic Slope Current (ASC). These systems of currents transport large volumes of water eastward at the northern extent of the gyres, and westward along the Antarctic continental slope. They also have an important role in the meridional heat transport, acting as a series of dynamic barriers preventing southward heat intrusions close to the Antarctic coast (Thompson et al., 2018). Despite the importance of these large scales features, their extent and seasonal variability remain poorly described at large scale.

Major obstacles remain today in the understanding of the Southern Ocean and its changes due to the poor observation coverage of the winter subpolar sector (e.g. Newman et al., 2019; Vernet et al., 2019). In this chapter, I aim to shed light on the seasonal cycle of its horizontal circulation and how it is shaped by physical drivers, like winds, sea ice, and buoyancy forcings (Thompson et al., 2018). I rely on past studies that have paved the way in this direction, either from satellite altimetry (Armitage et al., 2018; Dotto et al., 2018; Garabato et al., 2019) or from mooring observations (Núñez-Riboni and Fahrbach, 2009; Chavanne et al., 2010), and propose to go further using the higher resolution SLA product presented in **Chapter II**, along with a method based on an Empirical Orthogonal Function (EOF) decomposition restricted to the subpolar region. The mode decomposition highlights very distinct mechanisms driving various dynamics in the region, and allow to identify a suite of potential key drivers of the seasonal variability.

2 Southern Ocean Seasonal Variability in the Sea Ice-Covered Sector From Multi-mission Satellite Observations of Sea Level Anomaly

This section includes a paper and its supplementary material submitted in Journal of Geophysical Research : Oceans, which I reformatted here for the purpose of this manuscript. The reference is Auger, M., Sallée, J.B., Prandi, P., and Naveira Garabato, A. C., Southern Ocean Seasonal Variability in the Sea Ice-Covered Sector From Multi-mission Satellite Observations of Sea Level Anomaly. Submitted at Journal of Geophysical Research : Oceans

Abstract

A novel multi-satellite product is used to shed light on the sea surface height seasonal cycle and associated geostrophic circulation in the subpolar Southern Ocean. We find three main modes of variability governing the SLA seasonal cycle, all of them primarily governed by wind forcing. The main mode of seasonal variability is associated with the seasonality of the main subpolar gyres governed by large-scale wind stress curl, qualitatively consistent with Sverdrup dynamics. The second seasonal mode is related to the Antarctic Slope Current (ASC), governed by the coastal easterlies, with a rapid circumpolar propagation of anomalous sea-level along the continental slope that is dynamically consistent with the so-called Southern Mode. The first two modes induce an acceleration of the gyre and the ASC in winter. The third seasonal mode appears to be driven by sea ice-modulated surface stress, and induces an offshore extension of the ASC from autumn to winter.

Plain Language Summary

The Southern Ocean circulation has a strong impact on the global climate. Yet, it is very poorly known due to the large sea ice cover, especially in winter. Here, we benefit from new satellite measurements, enabling us to measure ocean circulation in both the ice-covered and open regions of the Southern Ocean. These measurements are used to describe the seasonal cycle of the ocean circulation in the subpolar Southern Ocean, south of the Antarctic Circumpolar Current. Three processes are identified as being the main drivers of the seasonal variation of the circulation : the large scale wind variations over the whole subpolar Southern Ocean, the seasonal changes in the amplitude of the coastal winds around Antarctica, and the seasonal cycle of the sea ice, modifying locally the wind influence on the ocean surface. This study identifies the effect of these three drivers on the seasonal cycle of the subpolar Southern Ocean circulation, by highlighting their distinct seasonal variations and the regions where they are dominant.

2.1) Introduction

The Southern Ocean plays a central climatic role, and has provided a major service for humankind in recent decades by absorbing up to 75% of all the heat and 40% of all the carbon taken up by the world ocean, thus contributing to regulating global climate change (Frölicher et al., 2015; Sallée, 2018; Meredith et al., 2019). This key climatic role results from the tridimensional Southern Ocean overturning circulation and associated water-mass transformations, which ventilate the deep ocean and lead to the establishment of a global ocean circulation connecting all ocean basins (Talley, 2013; Naveira Garabato et al., 2014).

The horizontal circulation of the Southern Ocean is organized around two prominent features : an eastward-flowing Antarctic Circumpolar Current (ACC) in the latitude band around 40-50°S, and a westward-flowing Antarctic Slope Current (ASC) over the Antarctic continental slope. In between these circumpolar current systems, the subpolar Southern Ocean is spanned by large-scale regional gyres in the Weddell and Ross Seas. These subpolar gyres host key water-mass transformations that fuel the global overturning circulation (Abernathey et al., 2016; Pellichero et al., 2017a), and form the main gateway for the exchange of water masses between the global ocean and the Antarctic margins. In particular, the subpolar gyres mediate the equatorward export of the global ocean's densest water masses, formed in the Antarctic margins (Orsi et al., 1999), as well as the deep oceanic heat transport that regulates the melting of Antarctic ice shelves (Thompson et al., 2018). Despite this important role in global ocean circulation and climate, our knowledge of the circulation of the subpolar Southern Ocean remains sparse and incomplete, in part due to major observational constraints (Newman et al., 2019).

We know today that the subpolar Southern Ocean experiences a strong seasonality (Vernet et al., 2019), as suggested by a number of recent studies based on different lines of evidence. Using two moorings deployed from 1996 to 2006 in the Fimbul ice shelf region, Núñez-Riboni and Fahrbach (2009) documented the ASC's seasonal cycle and its associated forcing, and proposed a decomposition of the cycle into barotropic and baroclinic components. The ASC was found to be most intense at the end of the austral autumn, and weakest in the austral summer. Using six years of monthly maps of the geostrophic circulation constructed from Cryosat-2 altimetric observations in sea ice leads, Armitage et al. (2018) reached the same conclusion, but with a much wider view on the circumpolar footprint of the seasonal signal. From a similar dataset, Dotto et al. (2018) presented a semi-annual intensification of the Ross Gyre in April-May and in November, while Garabato et al. (2019) showed the seasonal cycle of the geostrophic circulation over the entire subpolar Southern Ocean and linked such variations to surface winds modulated by sea ice.

In all these observational studies, wind forcing was found to be the main driver of the seasonal cycle of the ASC and subpolar gyre circulation, consistent with an analysis of numerical models (Mathiot et al., 2011). For the ASC, local wind stress was found to be the dominant forcing of the seasonal cycle, from both moorings (Núñez-Riboni and Fahrbach, 2009) and remote sensing observations (Armitage et al., 2018). However, while Armitage et al. (2018) highlighted the contribution of large-scale wind-stress curl for both Weddell and Ross gyre variability, Dotto

et al. (2018) and Garabato et al. (2019) additionally emphasised the importance of taking into account the role of sea ice in modulating the wind-stress curl, to understand how changes in the subpolar Southern Ocean circulation are driven.

In this study, we complement and expand preceding descriptions of the seasonal variability of the subpolar Southern Ocean circulation by using a novel satellite altimetry product including measurements in the ice-covered regions. We use the product described in Auger et al. [submitted], which is a new multi-mission Sea Level Anomaly (SLA) dataset over the Southern Ocean spanning from 2013 to 2019. This product exploits recent advances in radar altimetry processing to improve measurement selection and correction. Compared to similar previous products (Armitage et al., 2018; Dotto et al., 2018), the data set used here processes observations from three satellites instead of only one, enabling higher spatial and temporal resolutions than before ; and benefits from a novel neural network bias correction that alleviates the need for ad hoc bias correction between the open-ocean and sea ice sectors, which can introduce spurious seasonal cycle (Auger et al., submitted). Here we analyse this 7-year high-resolution SLA product to address the remaining gaps in our knowledge of the seasonal cycle of the subpolar Southern Ocean. Our aim is to unravel the multiple responses of the subpolar Southern Ocean to atmospheric forcing at seasonal time scales. In particular, our product allows us to separate the governing dynamics on and off the continental shelf (which can arguably be subject to different dynamical regimes), as well as to explore the effects of coastal winds, large-scale Sverdrup gyral circulations and sea ice, and the distinct seasonal variabilities of the on- and off-shelf sectors.

To achieve this, we apply a method based on Empirical Orthogonal Functions (EOF) decomposition only in the subpolar region, allowing to go further into the previous analyses of the SLA seasonal cycle. This mode decomposition highlights very distinct mechanisms driving different dynamics in the region, and allow to identify regional disparities in the geostrophic circulation links with the forcings.

2.2) Data and Methods

Southern Ocean SLA product

The regional SLA product used in this paper is presented in Auger et al. [submitted]. It is availale on SEANOE (Auger et al., 2021b) with the doi : 10.17882/81032. It consists of 7 years of daily SLA grids and associated geostrophic current anomalies between 2013 and 2019 on a 25 km EASE2 grid (Brodzik et al., 2014). It results from the processing and mapping of observations from three satellites : AltiKa and Sentinel-3A in the open and ice-covered oceans, and Cryosat-2 in the ice-covered regions. As described in Auger et al. [submitted], the new product allow to retrieve SLA at an increased resolution both in the open and the sea ice-covered oceans, and exhibits a better delineation between on/off continental shelf regimes, and fewer meridional stripes, arguably as a result of a denser recovery of observations reducing non-physical features linked to the satellite orbit. In addition, the methodological advance reduces the risk of introducing an artificial seasonal signal phased with the sea ice seasonal that can be difficult to

distinguish from physical sea-level variability (Auger et al., submitted ; (Prandi, 2020)). The median Root Mean Square Error (RMSE) is 5.9 cm in the permanently ice-covered regions, 3.7 cm in the seasonally ice-covered ocean, and 4.0 cm in the more dynamic open ocean.

Mean Dynamic Topography

Mean geostrophic currents can be computed from the Mean Dynamic Topography (MDT), representing the mean sea surface height above the geoid. There are only a few existing MDT products. Most of the global high-resolution products do not include observations from leads, so MDTs are seasonally biased in all regions affected by sea ice cover. Therefore, to estimate the mean geostrophic currents, we choose to use Armitage et al. (2018) MDT, which has a low resolution compared to conventional open-ocean MDT products, but does contain six years of Cryosat-2 observations in sea ice leads (Figure III.1a).

We use this MDT field to define the subpolar region that we will investigate in this study, as the ocean sector south of the MDT contour -180 cm. This MDT contour is chosen as the best compromise to include the largest region possible while discarding the ACC from our analysis (Figure III.1a).

Ocean surface stress

We investigate the effect of the momentum flux at the sea surface on the subpolar Southern Ocean SLA and dynamics. The main source of large-scale momentum flux at the ocean surface is wind stress, which we estimate from ECMWF (European Centre for Medium-Range Weather Forecasts) ERA5 monthly mean output (DOI : 10.24381/cds.f17050d7). When the ocean is partially covered by sea ice, wind stress is not entirely transferred to the ocean surface, but the ocean also receives momentum through sea ice stress (Tsamados et al., 2014; Martin et al., 2016).

There remain many uncertainties on the quantification of ocean surface stress in sea ice sectors. In this paper, we use two approaches : first we consider the wind stress, $\vec{\tau}_{ao}$, as if it was entirely transferred to the ocean surface without interference from sea ice ; and second we use an approximation of the ocean surface stress, $\vec{\tau}_{ocn}$, modulated by the presence of sea ice, which we derive from Tsamados et al. (2014) and Martin et al. (2016). Therefore, $\vec{\tau}_{ocn}$ takes into account the sea ice concentration A_i and its velocity $\vec{u}_i$ in modulating the surface stress :

$$\vec{\tau}_{ocn} = (1 - A_i)\vec{\tau}_{ao} + A_i\vec{\tau}_{iw} \tag{2.1}$$

with :

$$\vec{\tau}_{ao} = \rho_a C_{dao} |\vec{u}_a - \vec{u}_w| (\vec{u}_a - \vec{u}_w) \tag{2.2}$$

and :

$$\vec{\tau}_{iw} = \rho_w C_{dw} |\vec{u}_i - \vec{u}_w| (\vec{u}_i - \vec{u}_w) \tag{2.3}$$

The wind stress $\vec{\tau}_{ao}$ depends on the air density, ρ_a, the air-ocean drag coefficient, C_{dw}, and the wind and current velocities, respectively $\vec{u}_a$ and $\vec{u}_w$.

The sea ice concentration, A_i, is obtained through NCEI (National Centers for Environmental Information ; DOI : 10.7265/N59P2ZTG), as well as the sea ice velocity, $\vec{u}_i$ (DOI : 10.5067/O57VAIT2AYYY). Ocean current velocity $\vec{u}_w$ is assumed to be the geostrophic velocity, and is constructed from the MDT to derive the mean velocity, to which we add an anomaly from the Auger et al. [submitted] product. We use a constant ocean density of $\rho_w = 1,028 kg.m^{-3}$. For the ocean-ice drag coefficient, C_{dw}, we tested two different parameterizations. First we used a constant ice drag coefficient $C_{dw} = 5.5010^{-3}$ (Garabato et al., 2019). Second, we used a variable sea ice drag, that decomposes into three terms, as in Martin et al. (2016) :

$$C_{dw} = C_{dw_{skin}} + C_{dw_{ridge}} + C_{dw_{floe}} \tag{2.4}$$

where the three terms on the right-hand side are respectively skin, ridge and floe drag coefficients taken from Martin et al. (2016), Tsamados et al. (2014) and Lüpkes and Birnbaum (2005). Non-constant C_{dw} allows us to consider the seasonal changes of sea ice properties, and how they alter the stress applied from the sea ice to the ocean surface. Both constant and variable sea ice drag coefficients show very similar results, so in the remainder of the study, we only present ocean stress computed from the constant drag coefficient parameterization.

Statistical tools

Correlation significance

We use Pearson's correlation to estimate the degree of similarity between time series. Both correlation and significance are computed based on a degree of freedom evaluated from the local temporal correlation scale presented in Auger et al. [submitted], which is assumed to correspond to the time interval between two independent measurements (approximately 15 days in the subpolar Southern Ocean). Correlation significance is assessed at the 99% confidence level.

Robustness of the EOF modes

The tridimensional (time series of maps) SLA signal is decomposed into Empirical Orthogonal Functions (EOFs). This entails the decomposition of the signal into several orthogonal basis functions, sorted in terms of explained variability of the signal. This decomposition allows here to extract the main modes of variability explaining the largest percentage of variance, to then investigate each mode's forcing. We investigated the robustness of the EOF decomposition to two main sources of uncertainty : the error of the SLA product ; and the choice of years analysed in the decomposition. We present these sensitivity tests below.

Impacts of SLA product errors

The multi-mission product used in this paper comes with an estimate of the formal error from the optimal interpolation (Auger et al., submitted). It ranges from 1 to 4 cm in the subpolar Southern Ocean, and peaks at 7 cm locally in some areas of the continental shelf. To investigate the potential effect of this error on the EOF decomposition, we masked the SLA product where the formal error average was greater than 3 cm, and recomputed the EOF decomposition. The first four EOF modes, which this paper focuses on, were unaffected, with an identical value of explained variance, and associated spatial patterns and principal components (i.e. time series).

A specific region identified as potentially high-error is the permanently ice-covered area (i.e. where sea ice does not melt in summer) of the subpolar Southern Ocean, with an error ranging from 4 to 10 cm in a 2-altimeter configuration (Auger et al., submitted). As with the formal error, we computed the SLA modes while masking the permanently ice-covered region, and found that the first four EOF modes were unaffected, with the same variability explained. EOFs are also unaffected when masking both large formal error regions and permanently ice-covered parts of the subpolar Southern Ocean at the same time. We conclude from this analysis that the EOF mode decomposition presented in this paper is robust to consideration of areas with the largest SLA error.

Robustness to the choice of years included in the EOF decomposition

One of the simple methods listed by Navara et al. 2010 to evaluate the robustness of the modes is to apply the decomposition to subsamples of the time series. We here split the time series in two parts, and recompute the EOF analysis for each of the subsets. From April 2013 to May 2016, and from June 2016 to September 2019, the first two EOF modes recovered in each case are identical to the first two EOF modes computed with the full time series (same spatial patterns and principal components). The third mode computed from the two subsets represents, however, the fourth EOF mode computed with the full time series, with a temporal correlation of r=0.78 for the first subset (2013-2016) and r=0.79 for the second subset (2016-2019). This is explained by the fact that in the analysis of the full time series, the third mode primarily captures interannual variability peaking in 2016. This mode is therefore much less influential when the full time series is split in two shorter subsets. The seasonal cycle is associated with the first, second, and fourth modes of the EOF decomposition when computed over the full time series, which correspond to the first, second and third modes of the EOF decomposition computed from the two subsets. We conclude from this analysis that the EOF mode decomposition of the seasonal cycle is robust to the choice of years analysed.

2.3) Results

Large-scale SLA variability is investigated by filtering the 2013-2019 daily sea-level product with a 300 km radius Gaussian filter. The error associated to this large-scale SLA product is computed as in Auger et al. [submitted] by comparing a 2-altimeter product filtered at 300 km, with the along-track independent observation from Sentinel-3A data filtered with a 300 km running mean. The error is 5.7 cm in the permanently ice-covered regions, 3.0 cm in seasonally ice-covered areas, and 3.2 cm in the open ocean. The higher errors in the open ocean than in the ice-covered regions stem from the open ocean being more dynamic, and therefore having a wider range of SLA values and higher SLA variability.

We here focus on the signal in the subpolar Southern Ocean, defined as the region south of the -180 cm MDT contour to exclude the ACC from our analysis (See Method ; Figure III.1a). The subpolar Southern Ocean is then split into two sectors : the "off-shelf sector", north of the Antarctic continental shelf, and defined as the region to the north of the 1000 m isobath in the Antarctic continental slope ; and the "Antarctic continental shelf sector", defined as the region south of the 1000 m isobath in the Antarctic continental slope (See Method ; Figure III.1a).

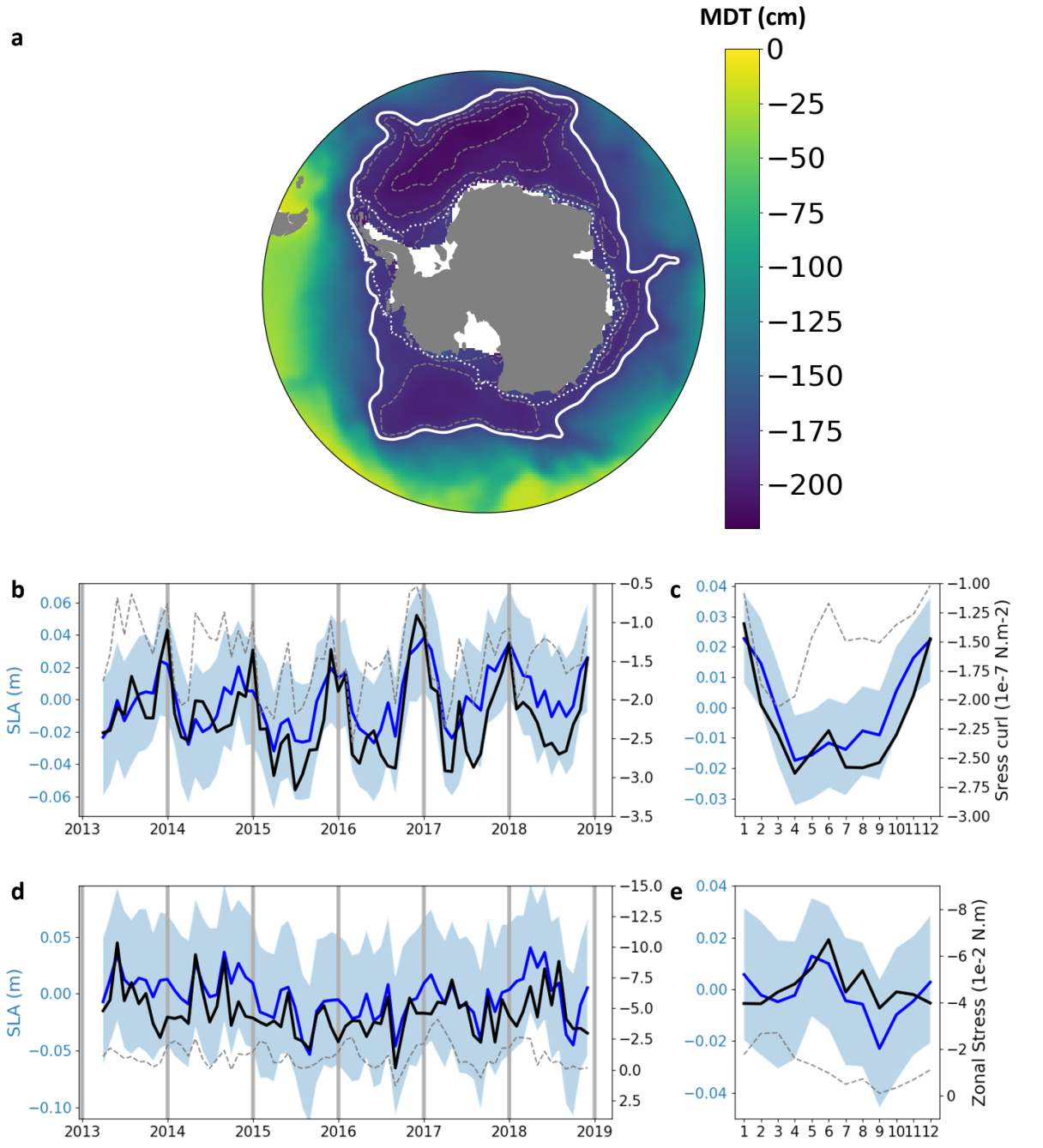

FIGURE III.1: a. Mean Dynamic Topography. The white line is our delimitation of the subpolar Southern Ocean, taken as the northern MDT (Mean Dynamic Topography) contour at -180cm. Black dotted lines are MDT contours of 190, 200 and 210 cm within the subpolar Southern Ocean. The white dotted line is the bathymetry contour at 1000 m and separates on-shelf and off-shelf parts of the subpolar Southern Ocean.b. In blue, time series of integrated off-shelf monthly SLA in the subpolar Southern Ocean. Integrated wind stress curl and ocean stress curl in the same zone are shown in black and dashed grey, respectively. c. Same as a, but averaged over the seasonal cycle. d. In blue, time series of integrated on-shelf monthly SLA in the subpolar Southern Ocean. Integrated zonal wind stress and ocean stress in the same zone are shown in black and dashed grey, respectively. e. Same as c, but averaged over the seasonal cycle. The blue shading shows an upper bound of the error associated with the mean SLA in each sector, derived from the seasonal maps of RMSE between the mapped AltiKa and Cryosat-2 product and independent along-track Sentinel-3A data.

TABLE III.1: Correlation coefficient between integrated SLA off-shelf and on-shelf, and wind forcing integrated in the same zones.

	Wind Stress Curl	***Ocean Stress Curl***	***Zonal Wind Stress***	***Zonal Ocean Stress***
SLA Offshelf	**0.77**	0.50	-0.58	-0.62
SLA Onshelf	0.67	0.18	**-0.70**	-0.44

Subpolar SLA time series and associated forcing

The SLA time series averaged over the subpolar off-shelf sector shows a strong seasonal cycle, with SLA reaching a maximum in December-January and a minimum from April to October (Figure III.1b,c). The amplitude of the seasonal cycle is ~4 cm. Interannual variability superimposes on top of this seasonal cycle, with higher summer maxima in 2017-2018 and 2018-2019, associated both with a slightly larger amplitude of the seasonal cycle in 2017-2018, and with an underlying positive SLA trend from 2013 to 2019.

In contrast, the mean SLA averaged over the Antarctic continental shelf sector shows a strikingly different time series and seasonal cycle (Figure III.1d,e). First, the amplitude of the seasonal cycle is much weaker than that of the interannual variability, and an important part of the seasonal cycle is in antiphase with the off-shelf seasonal cycle. The sea level on the continental shelf is maximum in early winter (May-June), and minimum in spring (September). Summer and autumn show weaker variability, with a local sea level maximum in December-January and a minimum in March. The time series also displays large interannual variability, with an amplitude of about 8 cm, more than twice as large as the amplitude of the seasonal cycle.

We now compare those time series and their seasonal cycle to the corresponding ocean surface stress, computed with ($\vec{\tau}_{ocn}$) and without ($\vec{\tau}_{ao}$) the influence of sea ice (respectively referred to as "ocean stress" and "wind stress" ; see Methods). In both sectors, the correlation of SLA variability and wind stress variability is striking (Figure III.1b-e ; Table III.1). In particular, the SLA time series averaged over the off-shelf sector has a correlation of 0.77 (significant at a 99% confidence level) with the corresponding wind stress curl time series averaged over the same region (Figure III.1c ; Table III.1). The SLA time series averaged over the continental shelf sector has an anticorrelation of 0.70 (significant at a 99% confidence level) with the zonal wind stress time series averaged over the same region (Figure III.1c ; Table III.1). In the two sectors, the comparison between the mean SLA time series and the wind forcing shows very strong similarities, both at seasonal and interannual scales (Figure III.1b-c).

Surprisingly, when considering the effect of sea ice on the stress (see Methods), the correlation with the SLA time series dramatically drops (Figure III.1b-c ; Table III.1).

Beyond the statistical correlation, there is a physical link between negative wind stress curl anomalies of the off-shelf sector and the deepening of the sea surface, through vertical Ekman pumping inducing an upwelling anomaly. Similarly, on the continental shelf, westward (i.e. negative) zonal wind stress anomalies are dynamically linked to an increase in SLA, through meridional Ekman transport anomalies.

From these two opposite seasonal cycles peaking in summer and winter, we can expect a very similar seasonal cycle for the SLA gradient over the Antarctic continental slope, which is the frontier between the on-shelf and off-shelf regions. With a winter (summer) SLA maximum (minimum) on the shelf and a minimum (maximum) north of the shelf, we expect the zonal current anomaly at the slope to be westward (eastward). Therefore, we anticipate from these results that the westward ASC and southern branch of the subpolar gyres strengthen in winter and weaken in summer.

Seasonality of geostrophic circulation in the subpolar Southern Ocean

Geostrophic currents are computed from the SLA maps (Pedlosky, 2013) to investigate the seasonality of the current strength. We here focus on the seasonal cycle of the zonal geostrophic current anomaly (Figure III.2). For reference, the mean zonal geostrophic current map in the subpolar Southern Ocean is shown Supplementary Figure III.8.

In summer (DJF), the Weddell Gyre circulation tends to weaken, as its northern branch shows a negative (westward) anomaly, while its southern branch exhibits a positive (eastward) anomaly (Figure III.2a). This southern eastward anomaly actually spans almost the entire circumpolar extent of the continental shelf, indicating a circumpolar-wide summer weakening of the ASC. The winter (JJA) conditions tend to be opposite to the summer anomaly, with a winter intensification of the ASC and Weddell Gyre (Figure III.2c).

The transition from summer to winter anomalies and from winter to summer anomalies at mid-season displays interesting patterns in East Antarctica, with a meridional northward spreading of the anomaly from the continental shelf to the open ocean north of the continental slope (Figure III.2b,d). In fall (MAM), the acceleration of the ASC that continues over winter is only concentrated over the continental shelf, on the poleward edge of the current (Figure III.2b), and it is only in winter that the current accelerates over its entire width. Similarly, in spring (SON), the deceleration of the ASC that continues over summer is only concentrated over the continental shelf (Figure III.2d), and it is only in summer that the current decelerates over its entire width.

Figure III.1b-e shows two different seasonal cycle shapes in sea surface height on the continental shelf and in the off-shelf sectors. However, those two seasonal cycles have extrema in summer and winter. They might be able to represent the summer-winter contrast in the Weddell Gyre and ASC zonal current anomalies, but they do not capture the spring and autumn offshore spreading of anomalies shown in Figure III.2. To gain a deeper understanding of the mechanisms driving the seasonal cycle of geostrophic circulation in the subpolar Southern Ocean, we next apply a decomposition into Empirical Orthogonal Functions (EOFs) modes.

Spatio-temporal modes of variability in the subpolar SLA

The daily subpolar Southern Ocean SLA product is decomposed into spatial modes of variability using an EOF analysis. The first two modes stand out with respectively 30% and 11% of explained variance, while higher-order modes explain less than 6% of the total variance. As a measure of the prominence of the seasonal cycle for each mode, we compute the correlation

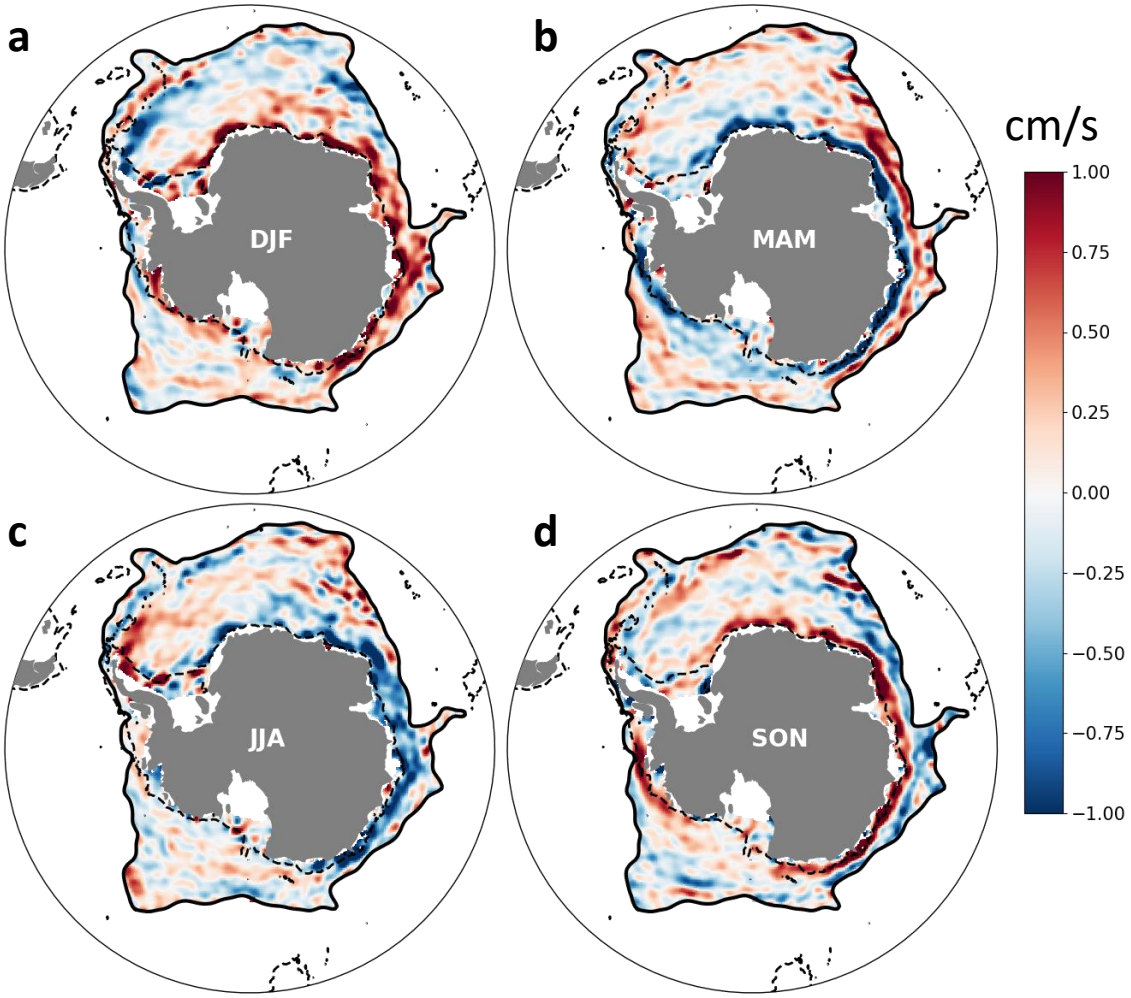

FIGURE III.2: Zonal current anomalies of the subpolar Southern Ocean for each of the four seasons : (a) summer (December, January, February ; DJF) ; (b) fall (March, April, May ; MAM) ; (c) winter (June, July, August ; JJA) ; (d) spring (September, October, November ; SON). The dotted line is the 1000 m isobath ; the black line corresponds to the northern boundary of the subpolar sector as defined in Section 2.2.

TABLE III.2: SLA EOF Modes correlation with their seasonal cycle.

EOF	1	2	3	4	5	6
Correlation with its seasonal cycle	0.78	0.62	0.30	0.72	0.40	0.54
Variance explained	30%	11%	6%	5%	3%	3%

between the time series of each mode and a synthetic time series formed as a repetition of its mean seasonal cycle (Table III.2). The higher the correlation, the more prominent is the seasonal cycle compared to interannual variability for each mode. Modes 1, 2 and 4 stand out as having large seasonal cycle components. To investigate the seasonal cycle of SLA in the subpolar Southern Ocean, we will thus concentrate our analysis on these three modes.

TABLE III.3: Correlation with SLA modes 1 and 2

	Offshelf		***Onshelf***		***Mode 1***		***Mode 2***	
	WSC	**ZWS**	**WSC**	**ZWS**	**WSC**	**ZWS**	**WSC**	**ZWS**
SLA mode 1	-0.78	0.58	-0.02	0.07	0.78	0.66	0.11	0.40
SLA mode 2	0.10	-0.56	-0.67	-0.72	0.20	0.45	0.49	0.66

A gyre mode

The first EOF mode of SLA (SLA_1 ; hereafter X_n refers to the nth mode of variable X) is associated with a prominent seasonal cycle and a spatial pattern characterised by anti-correlation between the off-shelf sector and the continental shelf sector (Figure III.3a). Its principal component and in particular its seasonal cycle (Figures III.3c,d) are reminiscent of the SLA time series averaged over the entire off-shelf sector (Figure III.1b,c). However, the decomposition into modes of variability offers a more detailed on the associated spatial pattern. SLA_1 is associated with a winter SLA drop that is largest at the center of the two main gyre systems in the Ross and Weddell Seas (Figure III.3a), as is particularly evident for the Weddell Gyre. The spatial pattern of SLA_1 stands out as being associated with an intensification of the gyre systems in winter, with an overall eastward intensification of the geostrophic circulation at the northern edge of the subpolar sector, and an eastward intensification on this sector's southern edge over the Antarctic continental slope (Figure III.3b).

This mode of winter gyre intensification is strongly correlated with both the averaged wind stress curl over the off-shelf sector and the principal component of the first EOF mode of wind stress curl (respective correlation coefficients of 0.73 and 0.71, both significant at a 99% confidence level ; Table III.3). Figure III.4 presents the first two EOF modes of the wind stress curl and the zonal wind stress, computed from a 2013-2018 time series over the subpolar Southern Ocean. It is insightful to compare the spatial pattern of the first EOF mode of SLA, SLA_1, with the spatial pattern of the first EOF mode of wind stress curl, WSC_1 (or alternatively the spatial regression of the wind stress curl onto the time series of SLA_1, see Supplementary Figure III.9). Despite the very good correlation between the time series of these two modes, the spatial patterns are distinct. SLA_1, displays a consistent pattern over the entire subpolar Southern Ocean, in contrast to WSC_1, which exhibits a meridional asymmetry. This indicates that SLA variability associated with SLA_1 does not result from a local response to local wind stress curl anomaly. Rather, SLA_1 appears to be associated with a gyre-scale response to a basin-scale anomaly of wind stress curl, as expected from classical conceptualisations of a wind-driven gyre in Sverdrup balance (Pedlosky, 2013).

A slope current mode

The second EOF mode of SLA, SLA_2 (Figure III.5), also shows a strong seasonal cycle, though interannual variability is larger than for SLA_1. This mode displays a strong signal on the Antarctic continental shelf, with a consistent circumpolar-wide rise of sea level over the continental shelf from May to August, and a more stable sea level from September to April (Figure III.5a,c,d). Both the principal component and associated seasonal cycle of SLA_2 are reminiscent of the ave-

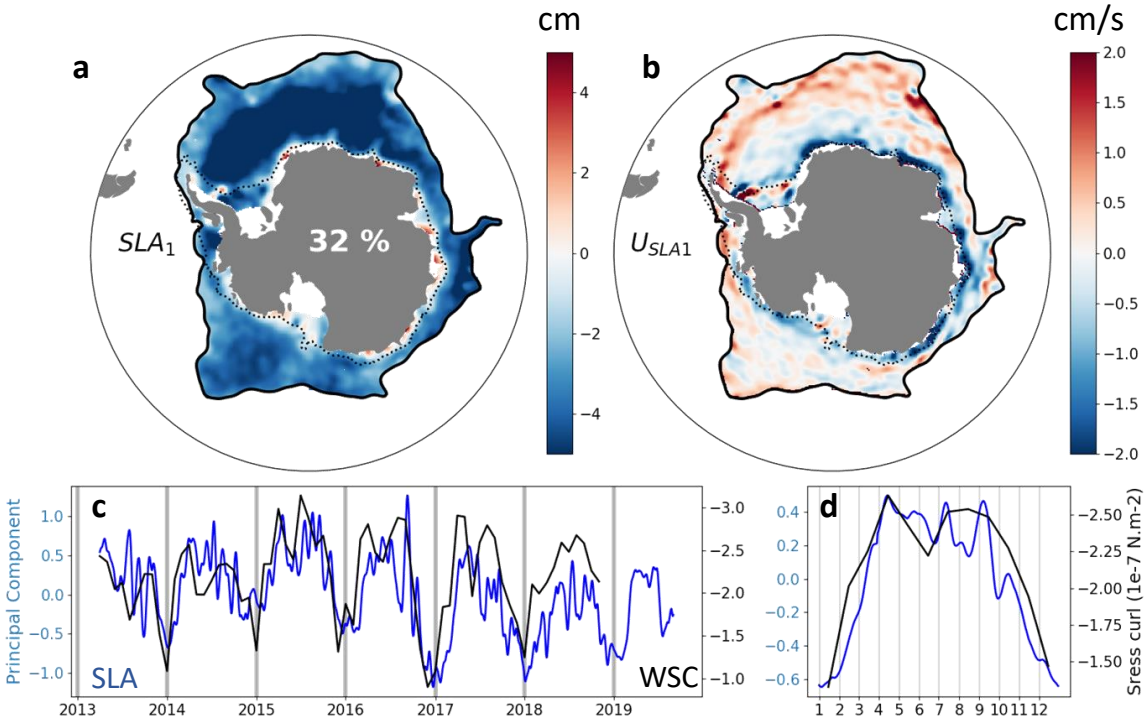

Figure III.3: First Sea Level Anomaly (SLA) EOF mode. (a) First SLA EOF mode spatial pattern. The dotted line is the 1000 m isobath; the black line corresponds to the northern boundary of the subpolar sector as defined in Section 2.2. Percentage is the part of total SLA variance explained by this mode. (b) Zonal geostrophic current anomaly associated with SLA mode 1. (c) SLA Mode 1 principal component (blue), and integrated wind stress curl in off-shelf subpolar Southern ocean (black). (d) Same as (c), but for seasonal cycle.

raged SLA time series over the continental shelf (Figure III.1d,e). The spatial pattern of SLA_2 is associated with a marked circumpolar intensification of the westward-flowing ASC in winter, represented by the strong eastward zonal current anomaly at the slope in Figure III.5b.

The time series of SLA_2 is highly correlated with both the time series of zonal wind stress averaged over the entire Antarctic continental shelf region and the time series of the second EOF mode of zonal wind stress (respective correlation coefficients of 0.74 and 0.64, both significant at a 99% confidence level; TableIII.3). Both the spatial pattern of the second EOF mode of zonal wind stress (ZWS_2) and the regression of the zonal wind stress onto the time series of SLA_2 show that the zonal wind stress pattern associated with SLA_2 is a pronounced winter intensification of the easterlies over the Antarctic continental slope (Figure III.4d; Supplementary Figure III.9). However, the spatial pattern of the wind stress (Figure III.4d) has a much greater degree of circumpolar asymmetry than the marked circumpolar response of SLA_2 (Figure III.5a). In particular, the winter intensification of the easterlies appears confined to the East Antarctic region, while SLA_2 is associated with a winter circumpolar rise over the continental shelf. Similar to SLA_1, this mismatch of the spatial pattern concomitant with a very good correlation of the time series suggests that SLA variance associated with SLA_2 does not result from a local response to local wind stress anomaly. Instead, SLA_2 describes a circumpolar continental shelf

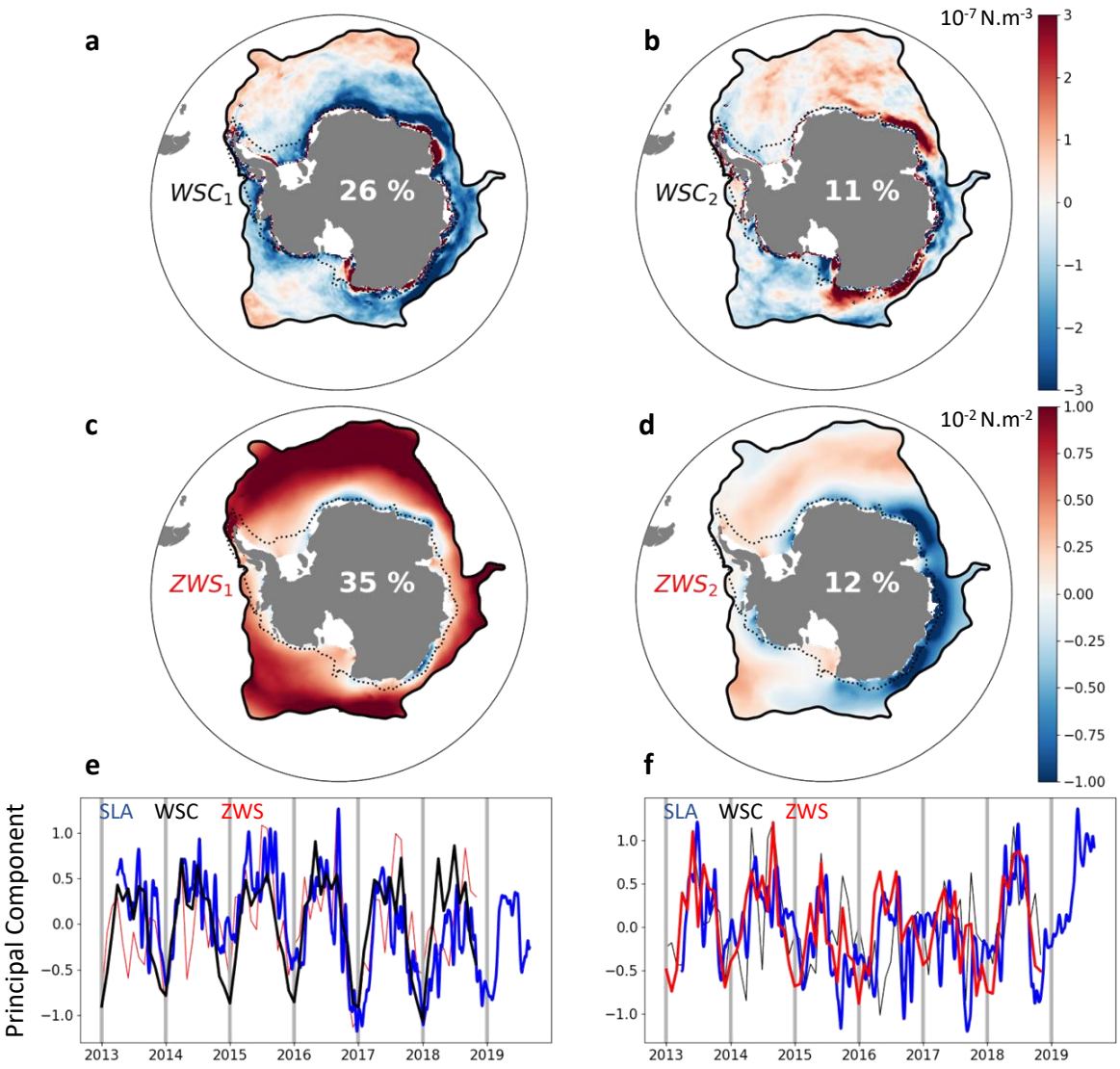

FIGURE III.4: Wind Stress Curl (WSC) and Zonal Wind Stress (ZWS) EOF modes 1 and 2. a,b. Wind stress curl (WSC) EOF modes 1 and 2 spatial patterns. c,d. Zonal wind stress (ZWS) EOF modes 1 and 2 spatial patterns. Percentage is the part of total variable variance explained by this mode. The dotted line on panels a-d is the 1000 m isobath; the black line corresponds to the northern boundary of the subpolar sector as defined in Section 2.2. e. Blue, black and red lines are respectively EOF mode 1 principal components of Sea Level Anomaly (SLA), WSC and ZWS. f. Blue, black and red lines are respectively EOF mode 2 principal components of SLA, WSC and ZWS.

mode, related to remote wind stress perturbations over the continental shelf, consistent with a rapid circumpolar propagation of SLA features via the so-called "Southern Mode", described from observations and numerical models (Aoki, 2002; Hughes et al., 1999, 2003).

Therefore, while the first mode could be described as a subpolar gyre mode, the second can be described as an ASC mode. Although the spatial patterns of the two first EOF modes of SLA are different, the two modes consistently describe a winter intensification of the subpolar ocean circulation in winter (Figure III.2a-d). However, none of these two modes capture the

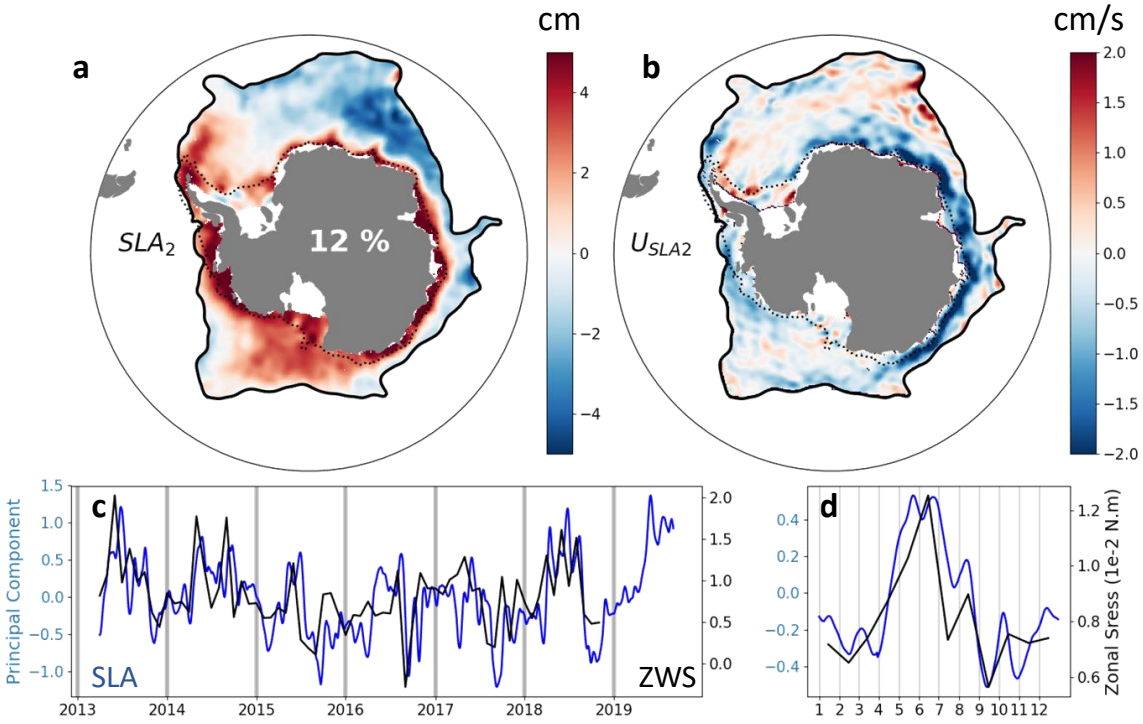

FIGURE III.5: Second Sea Level Anomaly (SLA) EOF mode. (a) Second SLA EOF mode spatial pattern. The dotted line is the 1000 m isobath ; the black line corresponds to the northern boundary of the subpolar sector as defined in Section 2.2. Percentage is the part of total SLA variance explained by this mode. (b) Zonal geostrophic current anomaly associated with SLA mode 1. (c) SLA Mode 1 principal component (blue), and integrated zonal wind stress in the on-shelf subpolar Southern Ocean (black). (d) Same as (c), but for seasonal cycle.

mid-season current anomaly described in Figure III.2a-d. In order to better grasp the potential drivers of such mid-season anomalies, we next investigate higher EOF modes of variability. In particular, we focus on the next mode that has a strong imprint of seasonal signal, the fourth EOF mode of SLA, SLA_4 (See Table III.2). The third SLA mode is not discussed here, as it shows no strong seasonal cycle but only interannual variability (see Supplementary Figure III.10).

Unphased mode - Modulation by sea ice

SLA_4 shows a large seasonal cycle that is not phased with the seasonal cycles of SLA_1 and SLA_2 (Figure III.6). While SLA_1 and SLA_2 are associated with an acceleration of the large-scale current systems in winter months, SLA_4 is instead linked to a circumpolar westward intensification of currents over the continental shelf at the end of summer and before winter, between February and May, which then slows down with a maximum deceleration at the beginning of winter (Figure III.6b,d). This continental shelf signal is accompanied by an opposite anomaly of the geostrophic circulation to the north of the continental slope. Thus, SLA_4 explains the mid-season anomalies that stand out in Figure III.2. Having isolated this signal as an EOF mode, we can now discuss its potential drivers.

SLA_4 is very consistent with the main mode of variability of sea ice concentration (Figure III.7a,c,d), both in terms of the time series (correlated at 0.74, significant at the 99% confidence level) and of the spatial pattern (Figures III.7a, III.6a). This striking relationship suggests that sea ice might have a role in shaping SLA_4. Sea ice can have a thermodynamical effect through steric expansion, but this would have the opposite impact to the one observed, as winter brine rejection contracts the upper-ocean water column. Alternatively, sea ice can have a mechanical effect by modulating momentum transfer at the sea surface. Interestingly, the first EOF mode of the ocean stress curl (see Methods) is well correlated with SLA_4 both in terms of the time series (r = 0.72, significant at a 99% confidence level) and the spatial pattern (Figures III.7b, III.6a). In autumn, the sea ice cover is small, and along-slope easterlies induce on-shelf Ekman transport. The divergence between easterlies and westerlies induces negative SLA anomalies just north of the slope. In winter, sea ice extent expands to hundreds of kilometers north of the slope. This tends to reduce the wind stress that reaches the ocean surface between the slope and the sea ice edge. Winter-spring intensified westerlies are still strong north of the ice edge (See ZWS_2, Figure III.4d), inducing southward Ekman transport and convergence between the slope and the sea ice edge, while divergence is displaced northward. This combination of wind and sea ice seasonal cycles results into a zonally banded structure of SLA seasonal variations, leading to two strong SLA gradients at the slope and the sea ice edge and thereby creating two jets with opposite directions (Figure III.6b).

Overall, this mode leads to a northward spreading of ASC acceleration (deceleration) from summer (winter) to winter (summer). This northward spreading of the acceleration is consistent with the mooring observations of (Núñez-Riboni and Fahrbach, 2009) at longitude 0°, which revealed an off-shelf westward maximum in June, one month after the strongest westward maximum was reached earlier over the slope.

2.4) Conclusion and Discussion

A novel satellite-based SLA product fitted to recover SLA in sea ice-covered regions is used to investigate the seasonal cycle of subpolar Southern Ocean geostrophic currents. The seasonal cycle of SLA in the subpolar Southern Ocean is primarily explained by three main modes of variability. The first mode corresponds to a winter acceleration of the Weddell and Ross gyres, consistent with large-scale variability of wind stress curl, through Sverdrup dynamics. The second mode is associated with a winter intensification of the ASC, forced by easterly wind variability on the continental shelf, with a circumpolarly propagating signal consistent with the so-called Southern Mode (Hughes et al., 2003). The third mode is a mid-season northward progression of the ASC acceleration/deceleration that is consistent with a local response to surface stress modulated by the combination of sea ice and wind stress seasonal cycles.

Our results are in line with those of Armitage et al. (2018), who linked the integrated wind stress curl with the geostrophic ocean circulation in the Ross and Weddell gyres. We however propose that in addition to the wind stress at large scales, which drives the two main modes of seasonal ocean circulation variability, a complete description of the seasonal cycle requires consideration of the local effects of sea ice modulating the stress received by the ocean. This is consistent with Garabato et al. (2019), who highlighted the important role of sea ice in modula-

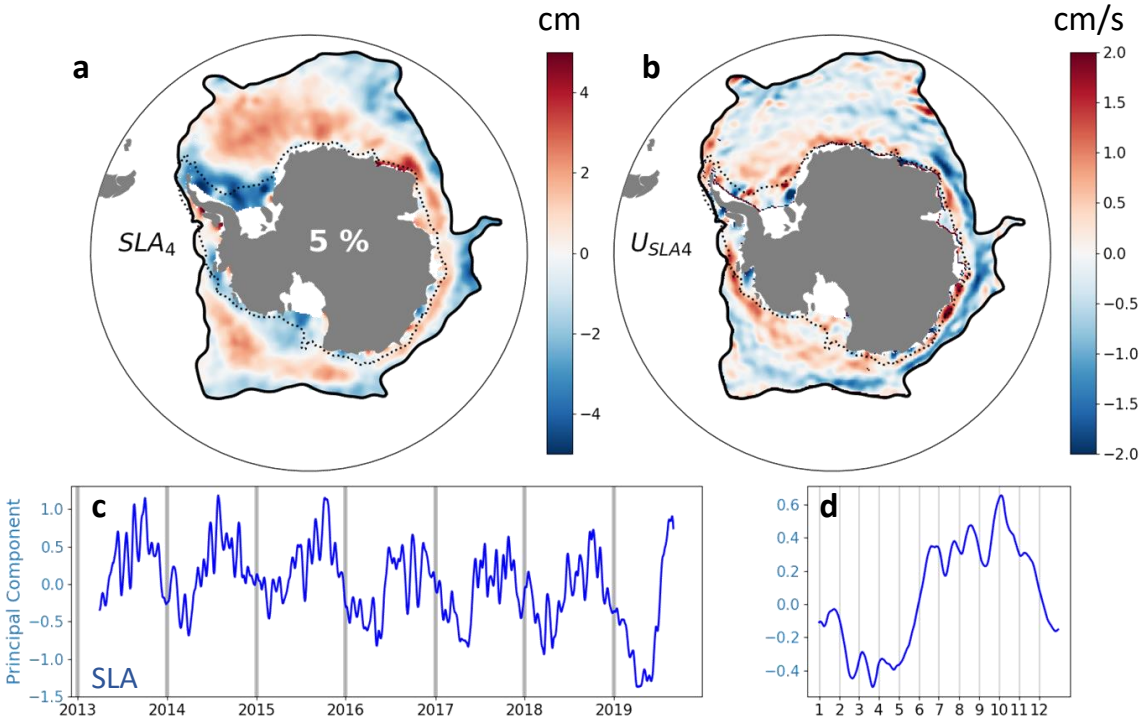

Figure III.6: Fourth Sea Level Anomaly (SLA) EOF mode. (a) Fourth SLA EOF mode spatial pattern. The dotted line is the 1000 m isobath ; the black line corresponds to the northern boundary of the subpolar sector as defined in Section 2.2. Percentage is the part of total SLA variance explained by this mode. (b) Zonal geostrophic current anomaly associated with SLA mode 1. (c) SLA Mode 1 principal component. (d) Same as (c), but for seasonal cycle.

ting the momentum stress received by the ocean. In addition, our results allow us to delineate on-shelf and off-shelf dynamics, and to highlight their distinct seasonal cycles, owing to the use of a multi-satellite product to recover SLA variability at higher spatio-temporal resolution than previously achievable.

Using moorings, Núñez-Riboni and Fahrbach (2009) described a delay of several months between on-shelf and off-shelf ASC maxima. Over the 9 years they analysed, they found that the ASC's barotropic component reaches a maximum in April on the continental shelf, while the ASC maximum was only reached two months later directly to the north of the continental slope. This was explained by the northward displacement of the ice edge in winter seasonally moving the maximum of momentum transfer. Our ice-related mode and zonal current climatology (Figures III.2 and III.6) are consistent with this result, and provide an overarching vision of this process all around Antarctica. In East Antarctica and in the Admundsen-Bellingshausen seas, where the seasonal variation of sea ice extent is weak, the ASC's response to sea ice modulation of the surface stress is stronger, as the sea ice edge moves northward but stays in regions of strong westerlies. The impact on the ASC is lower in the Weddell and Ross Gyres as the sea ice expands northward, for the sea ice edge is displaced too far from the slope to have a strong impact on the ASC.

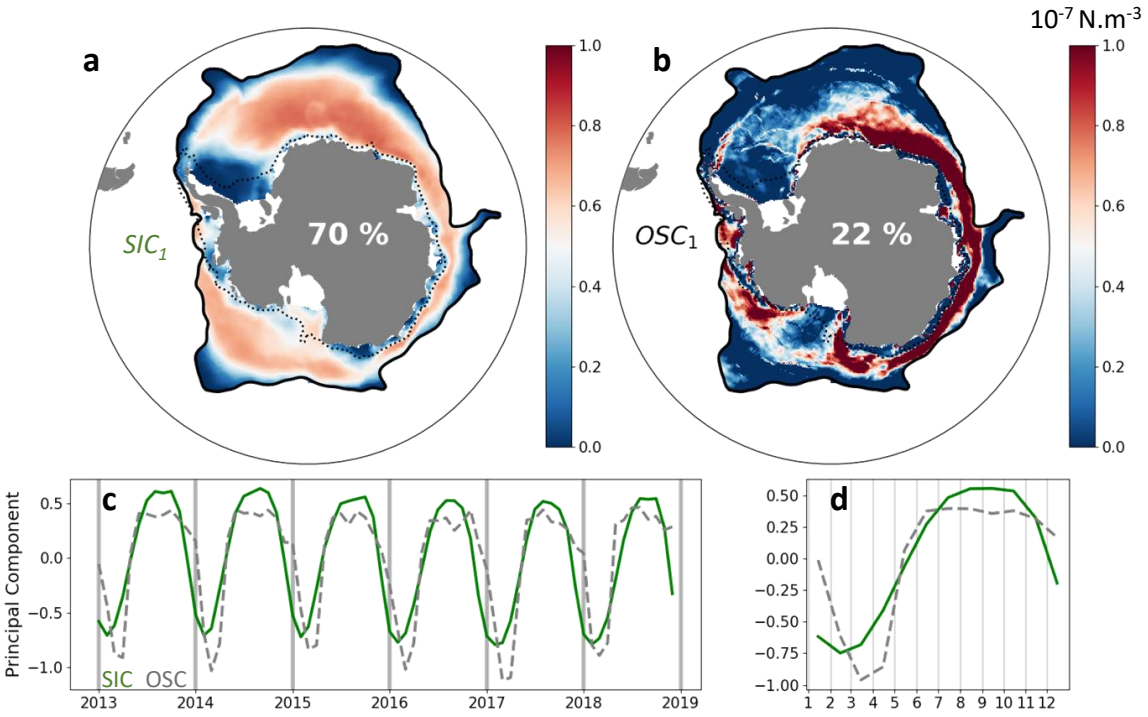

FIGURE III.7: Sea Ice concentration (SIC) and Ocean Stress curl (OSC) first EOF modes. a. SIC EOF mode 1 spatial pattern. Colorbar boundaries are not centered on 0 for a better comparison with Fig. 8. The dotted line is the 1000 m isobath ; the black line corresponds to the northern boundary of the subpolar sector as defined in Section 2.2. b.OSC EOF mode 1 spatial pattern. c. In green, SIC mode 1 principal component. In dashed green, OSC mode 1 principal component. d. Seasonal cycles of both principal components.

Flexas et al. (2015); Stewart et al. (2019) discussed the important effect of the tides and eddies in maintaining the Antarctic Slope Front and forcing the ASC. These processes were not considered in this study, as SLA was filtered prior to analysis and large scale seasonal variations of the circulation were consistent with atmospheric-driven processes. However, Auger et al. [submitted] high resolution product may have the potential for observing some mesoscale features in the subpolar Southern ocean, including in its ice-covered parts. This could be a perspective for future research. More generally, future sea surface height products merging even more satellite observations, or new instrument allowing to observe sea surface topography at higher resolution (e.g. the NASA/CNES mission SWOT (Biancamaria et al., 2016)), provide promising avenues to investigate smaller scale processes in sea ice regions.

Our results allow us to identify the forcing of the main features of the subpolar Southern Ocean current system. While the gyres appear really tied to large-scale wind stress curl, the slope current responds more to the coastal easterlies. In a context of changing climate, Southern Hemisphere westerlies are projected to intensify (except for aggressive mitigation scenarios), but no clear trends are projected for coastal easterlies (Bracegirdle et al., 2020; Goyal et al.). We can therefore anticipate that while Southern Ocean subpolar gyres are being and will continue to be spun-up in response to increasing westerlies, the Antarctic Slope Current is and will be

much less sensitive to such change. However, as sea ice changes regionally or circumpolarly, the mid-season transitions of the Antarctic Slope Current seasonal cycle are likely to be affected by local surface stress modulation.

Supplementary Material of the paper : *Southern Ocean Seasonal Variability in the Sea Ice-Covered Sector From Multi-mission Satellite Observations of Sea Level Anomaly* by Auger et al.

The supplementary information presented here provides more insights out the results described in the main paper. The mean zonal geostrophic current over the subpolar Southern Ocean serves as a reference to understand the anomalies zonal current presented in the main paper. Wind Stress Curl and Zonal Wind Stress regressions on Sea Level Anomaly modes 1 and 2 support our results on sea level anomaly forcings, while the SLA third mode of variability is displayed to convice the reader that this mode was out of the scope for a description of the seasonal variability.

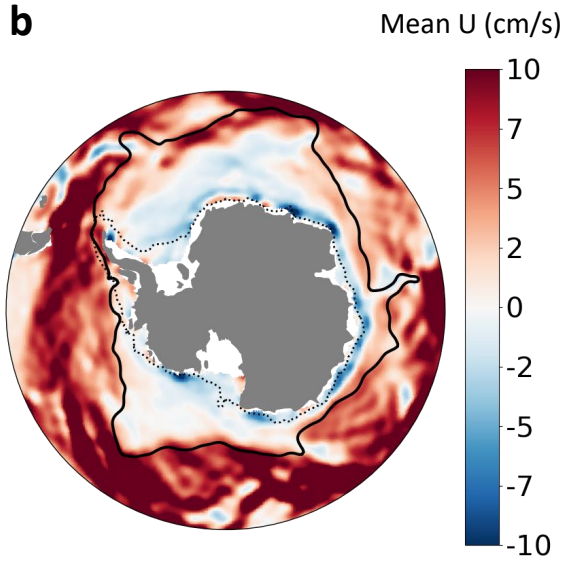

Figure III.8: Mean zonal geostrophic currents computed from Figure 1a MDT. The black line is the MDT contour at -180cm.

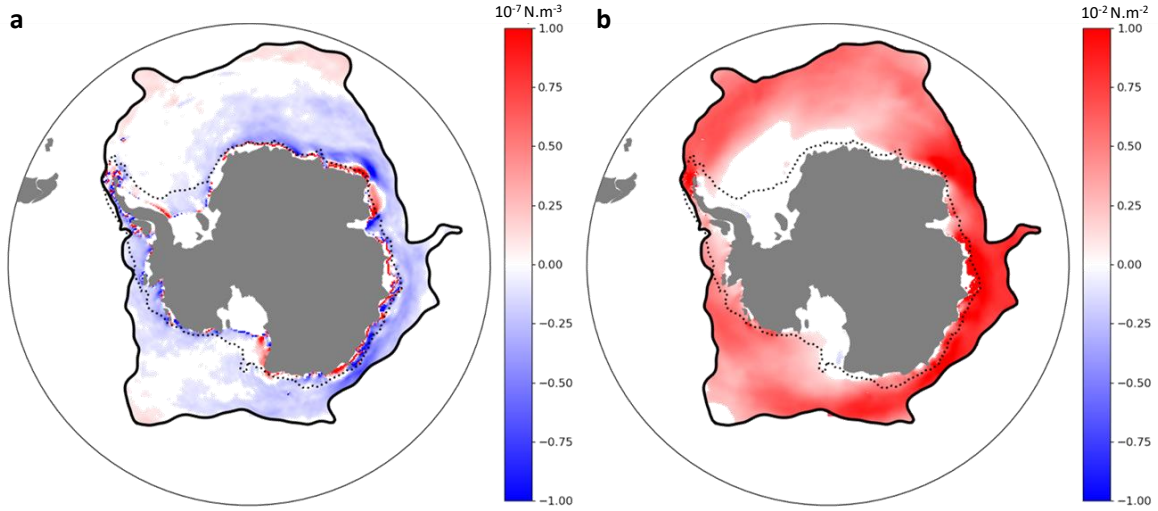

FIGURE III.9: a. WSC Regression on SLA EOF mode 1. b. ZWS regression on SLA EOF mode 2. The dotted line is the 1000 m isobath ; the black line corresponds to the northern boundary of the subpolar sector as defined in Section 2.2.

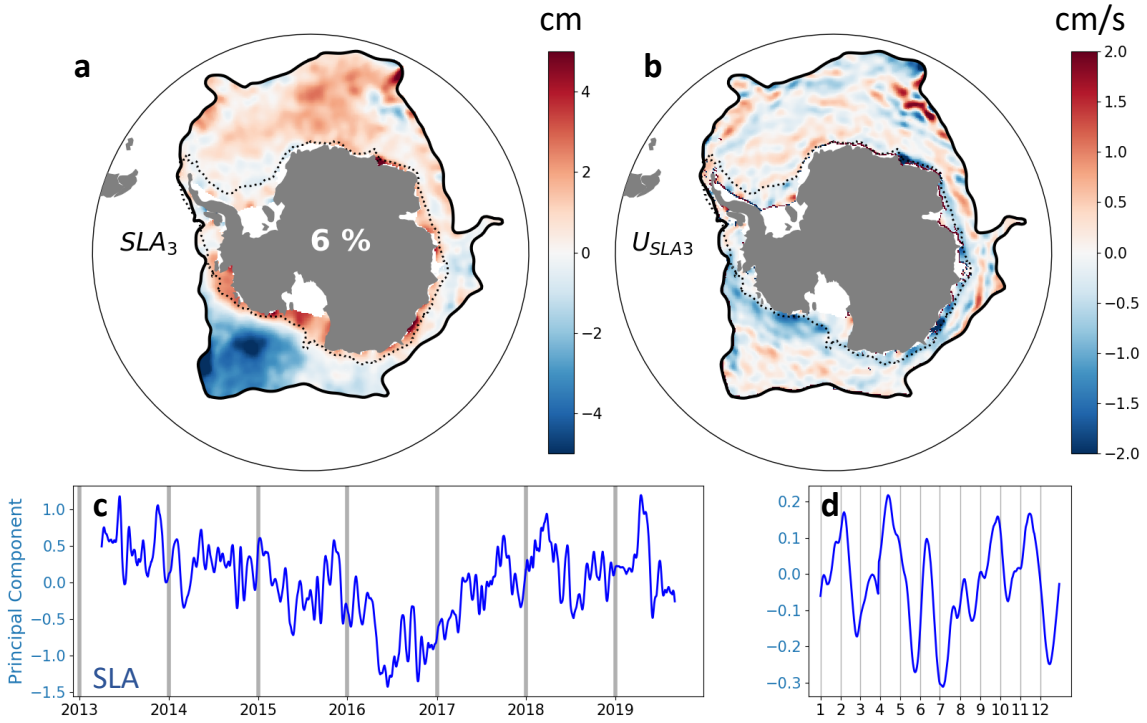

FIGURE III.10: Third Sea Level Anomaly (SLA) EOF mode. (a) Third SLA EOF mode spatial pattern. The dotted line is the 1000 m isobath ; the black line corresponds to the northern boundary of the subpolar sector as defined in Section 2.2. Percentage is the part of total SLA variance explained by this mode. (b) Zonal geostrophic current anomaly associated with SLA mode 1. (c) SLA Mode 1 principal component (blue). (d) Same as (c), but for seasonal cycle.

3 Conclusion of the chapter

In this chapter, I exploited the new SLA product I developed and presented in **Chapter II**. I was able to identify three main modes of variability in the subpolar Southern Ocean topography and associated surface geostrophic circulation. I also aimed at documenting some potential mechanisms driving these main modes of variability.

The mode of variability associated with the largest amount of explained variance of the subpolar ocean signal is a gyre mode. It appears strongly correlated with large-scale wind stress curl, consistently with our physical understanding of the Sverdrup dynamics. The Southern Hemisphere mid-latitude westerlies weaken in Summer and strengthen in Winter, which leads to a winter increase of wind stress curl over most of the subpolar Southern Ocean basin, which integrates into a winter intensification of the subpolar gyres. Interestingly the correlation between the gyre strength and wind stress curl is much greater for the integrated wind stress curl over the entire subpolar basin, than with local wind stress curl at each grid cell, which further points to Sverdrup gyre dynamics.

The second largest mode of variability is a mode where most of the signal is concentrated around the continental shelf break. It describes a winter intensification of the ASC and is strongly correlated with zonal winds integrated over the continental shelf region. Interestingly, this mode is circumpolar, with the entire continental shelf varying consistently, and is more correlated with circumpolarly integrated zonal winds than with local zonal winds at each grid cell. These dynamics are reminiscent of the previously documented *Southern Mode* (Kusahara and Ohshima, 2009; Spence et al., 2017), whereby, a local zonal wind anomaly, creates a local SLA anomaly on the continental shelf, which propagates almost instantly over the entire circumpolar band.

The third largest mode of variability is forced by local winds, with the direct influence of sea ice concentration in modulating the stress at the surface of the ocean. This mode is therefore phased with the sea ice seasonal cycle and follows the positions of the sea ice edge throughout the year. It also induces seasonal changes in the dynamics of the ASC, but with distinct effects on its shelf and offshelf parts. As a result, the seasonal cycle off the shelf is delayed by a few months from the onshelf seasonal cycle.

These three modes show three distinct responses to various atmospheric and sea ice seasonal variations. While all of them are somehow related to the seasonal cycle of the wind, each mechanism is different and drives variability at different locations and phases.

For convenience, I have filtered out the small-scale variations of Sea Level Anomaly in this study. However, important information coming from the mesoscale signal might be lost, along with its variations and interactions with the large-scale seasonal cycle we described here. In the next chapter, I focus specifically on this smaller-scale signal.

CHAPITRE

IV

Southern Ocean ice-covered Eddy properties from satellite altimetry

Sommaire

1 Preamble

In **Chapter III**, I used the dataset presented in **Chapter II** to investigate the seasonal cycle of the circulation of the subpolar Southern Ocean, including its ice-covered parts. Those results come from a spatially filtered version of the Sea Level Anomaly (SLA) dataset, which allows focusing on the large-scale processes and circulation changes at the seasonal scale. However, the filtering erases much of the smaller scale variability, whereas one important assets of this dataset is its resolution. Here, I dig into the smaller scale signal of the dataset to investigate what can be learned (if anything) from this product on the properties of mesoscale eddies in the ice-covered Southern Ocean.

One of the most energetic scales for the variability of the ocean circulation is the mesoscale variability (Morrow and Le Traon, 2012). In the general introduction, I presented the essential role of the mesoscale eddies in the global climate, and particularly in the Southern Ocean system. I also presented some hints of the knowledge of the sub-ice eddies generation, properties and behaviour. As it has been documented by observation in the Arctic (Timmermans et al., 2008; Zhao et al., 2014, 2016) and modeled in the Antarctic (Cohanim et al., 2021), most of the eddy activity in the sub-ice regions is concentrated in the halocline layer. These eddies are mostly anticyclonic (Timmermans et al., 2008; Zhao et al., 2014, 2016; Cohanim et al., 2021), and survive in the halocline as they are shielded from the sea ice-induced dissipation by the strong stratification (Meneghello et al., 2020). However, very little is known about the surface eddies in the sea ice regions. In the Arctic, Eddy Kinetic Energy (EKE) observation shows that sea ice is responsible for a strong dissipation of the eddies in the first 50 meters of the water column, while preventing the formation of new ones (Meneghello et al., 2020). The same study however emphasizes the need for better surface measurements, as the Ice Tethered Profilers used in the ice-covered regions are limited to depths larger than 7 meters, while the surface layer may be the preferred region for an intense eddy activity.

Here, I use the dataset developed in the context of this study to explore if some information on surface mesoscale eddies in the ice-covered oceans can be extracted, as a first observation-based attempt to document mesoscale eddies in the ice-covered subpolar Southern Ocean. To do that, I use an eddy detection and tracking method extensively used to document the eddies in ice-free regions (e.g. Chelton et al., 2011; Pegliasco et al., 2015; Mason et al., 2017). The effect of the sea ice and the background circulation on the detected eddies is investigated, and the special case of the Marginal Ice Zone (MIZ) is developed. There are very few to no other observations of eddies in the surface layer of ice-covered oceans to compare our results with. Moreover, I am conscious of the limitations inherent to the dataset and the detection method. That is why I try to evaluate the robustness of the results with a sensitivity study. In the following manuscript, I also assess how these results might be impacted by observational issues. While I am cautious about the outcomes of this study, it may contribute to a better understanding of the eddy activity in the subpolar Southern Ocean, and more broadly to the ice-covered oceans.

2 Southern Ocean ice-covered Eddy properties from satellite altimetry

This section includes a manuscript and its supplementary material currently in preparation for submission in the Journal of Geophysical Research : Ocean. The reference is Auger, M., Sallée, J.B., Prandi, P., Pauthenet, E. Mesoscale eddy properties in the ice-covered Southern Ocean explored from satellite altimetry, In prep.

Abstract

We investigate mesoscale activity and eddy properties in the subpolar, seasonally ice-covered Southern Ocean. Based on a recent regional Sea Level Anomaly (SLA) satellite altimetry dataset, we compute Eddy Kinetic Energy (EKE) of the basin and detect mesoscale eddies in the ice-covered Southern Ocean. The EKE is spatially consistent with the background circulation. It is one order of magnitude higher in the northern sector of the subpolar basin, close to the southern boundary of the Antarctic Circumpolar Current, and on the continental slope, than in the middle of the Weddell and Ross gyres. We apply an eddy detection methodology, which detects around 600 eddies per day. While they are on average distributed evenly in the subpolar Southern Ocean, their amplitude follows the spatial pattern of EKE. On top of the importance of large currents (Antarctic Circumpolar Current, or Antarctic Slope Current), sea ice concentration appears as a important drivers of eddy properties. Eddies have very low amplitude and density in the pack ice, even lower when it is in the middle of the gyres, where no background circulation favors eddies or instabilities. In contrast, the northern part of the Marginal Ice Zone (n-MIZ) is very favorable for mesoscale eddies, particularly cyclonic. There, mesoscale eddies are stronger and their density is higher than in any other region of the ice-covered or ice-free subpolar Southern Ocean. This may be a response to the meltwater front at the sea ice edge or local upwelling generated from interactions between the wind and the sea ice. These cyclonic eddies may be the surface signature for the generation of the long-living halocline anticyclonic eddies reported in previous studies. We are conscious that we cannot resolve or detect all the mesoscale eddies of the Southern Ocean due to the very small Rossby radius, especially at high latitude. Yet, we believe our results contribute to understanding the interactions between mesoscale eddies, sea ice, and the background circulation in the subpolar region.

2.1) Introduction

As a turbulent system, the oceanic circulation is dominated by mesoscale instabilities : in the global oceans, the eddies are ten times more energetic than the mean currents (Morrow and Le Traon, 2012). Mesoscale eddies are oceanic features forming water vortices, with spatial scales ranging from tens to hundreds of km, and lifetime from several days to a few months (Chelton et al., 2011). These structures are essential for ocean dynamics, as they can induce

mass and tracer transport through the so-called 'bolus' velocity and also by trapping water in their core (McWilliams, 1985; Chelton et al., 2011; Morrow and Le Traon, 2012). They also increase diffusion of tracers through their stirring of the ocean (Garrett, 1983; Gent et al., 1995), and convert potential energy into kinetic energy, while transferring this energy into various scales (Visbeck et al., 1997; Stammer, 1998).

Eddies are detectable from surface topography maps derived from satellite altimetry. From the 2000s, high-resolution SSH products (Ducet et al., 2000) allowed showing the ubiquity of mesoscale eddies in the global oceans. Chelton (2013) described eddy characteristics in the global ocean, by applying eddy detection and tracking algorithms to a high-resolution Sea Surface Height dataset. Most of the eddies they observed were found to be nonlinear, with their rotation speed being larger than their translation speed (Chelton et al., 2011). The scale of eddies is intimately linked to the first baroclinic Rossby radius of Deformation (Chelton et al., 1998), which varies from larger scales ($\simeq 250km$) at the equator to smaller scales ($\simeq 10km$) at high latitudes (Chelton, 2013). While both cyclonic and anticyclonic eddies were found to mainly propagate toward the west, there is a slight tendency for cyclones (anticyclones) to propagate poleward (equatorward) on top of their westward propagation (Chelton et al., 2007). Chelton (2013) also mapped the mean radius, translation, and rotation speed of the eddies allowing a better representation of the mesoscale eddies and their disparities between the various oceanic basins of the globe.

Ocean eddies are particularly important in the Southern Ocean circulation, being the dominant mechanisms for meridional heat transport across the Antarctic Circumpolar Current (ACC) (Jayne and Marotzke, 2002), central for setting the ACC momentum balance (Gille, 1997; Rintoul et al., 2001; Ivchenko et al., 2008), and key for the Southern Ocean meridional overturning circulation (Speer et al., 2000; Marshall, 2003; Marshall and Radko, 2003; Ivchenko et al., 2008). In the context of a changing climate, Southern Ocean eddies are thought to be important in shaping the response of the ACC and the response of the overturning circulation to change in westerly winds (Farneti et al., 2010; Dufour et al., 2012; Patara et al., 2016; Gent, 2016; Rintoul, 2018).

In contrast to the ACC region, Southern Ocean eddies in the subpolar region (south of the ACC) are poorly known due to observational constraints in the presence of sea ice. However, they are also there thought to be an essential component of the circulation and transport of water masses. For instance, Thompson et al. (2014) found a fingerprint of eddy transport across the slope of the Antarctic continental shelf and suggested an important eddy contribution to the Antarctic overturning circulation through cross-shelf transport of the warm intermediate layers. Later, (Stewart and Thompson, 2015) confirmed from an eddy-resolving model of the Antarctic Slope Front (ASF), that eddies were indeed a potentially efficient mechanism for the shoreward transport of relatively warm Circumpolar Deep Water (CDW) along density surfaces. This onshore transport is enhanced by bathymetry features such as coastal trough in the continental shelf of the Bellingshausen sector (Nakayama et al., 2014), or at bottom water formation sites (Stewart and Thompson, 2015). Eddy stirring was also proposed as one potentially impor-

tant process transferring heat toward the shelf (Stewart et al., 2018). Finally, eddies were also found to have a potentially large influence on the intensity of the zonal Antarctic Slope Current (Stewart et al., 2019).

In spite of such potentially important role of eddies in the subpolar region of the Southern Ocean, mesoscale activity remains largely unknown in this region from large scale observations (Vernet et al., 2019). This hinders our advance in understanding their role in polar climates as well as their interactions with sea ice. Signature of mesoscale eddies in sea ice regions have been observed from moorings (Meneghello et al., 2020), ice-Tethered profilers (Timmermans et al., 2008; Zhao et al., 2014, 2016) profiling glider sections (Thompson et al., 2014), acoustically tracked profiling floats (Vignes et al. [submitted]), or satellite-based Synthetic Aperture Radar (SAR) images (Kozlov et al., 2019). However, none of such methods provide wide spatio-temporal coverage allowing to robustly describe eddy characteristics, a prerequisite towards investigating their influence on large-scale circulation. In the Arctic basin, (Meneghello et al., 2020) combined observations and high-resolution modeling to establish the seasonality of mesoscale activity as a function of depth and sea ice cover. Surface eddies were found to be highly damped by sea ice, while eddies in the halocline had a constant activity throughout the year. (Zhao et al., 2014, 2016) found that these halocline eddies were predominantly cold-core anticyclonic eddies, and were found in higher concentrations close to the topographic margins and boundaries of the Beaufort gyre. In the subpolar Southern Ocean, large-scale description of mesoscale eddies and their interaction with sea ice are still entirely lacking.

In this paper, we investigate mesoscale eddy properties by leveraging on a new satellite altimeter product (Auger et al., 2021a). One important challenge in doing so is the decreasing Rossby Radius at high latitude, or the order of 10-20 km in the subpolar gyres, and reaching only a few kilometers on the continental shelf. In this context, and with the existing gridded products which today have grid resolution of 25 kilometers at most (Auger et al., 2021a), it is clear that an exhaustive description of eddy activity remains out of reach. In this paper, we use such products that do sample eddies, even if arguably aliased in some regions, to propose a first description of eddy hotspots and characteristics in the subpolar sector of the Southern Ocean. For doing so, we apply an eddy detection and tracking method, which we describe in Section 2, and investigate eddy characteristics and how they relate to sea ice cover and the dynamical regime of the subpolar region in section 3. We first describe the spatial variability of the EKE from the daily Sea Level Anomaly (SLA). We then evaluate the impact of the sea ice concentration and ocean depth (as a proxy for shelf, slope, and abyssal plains) on the presence and strength of the detected eddies. Lastly, we focus on the Marginal Ice Zone which stands out as a particular region with enhanced eddy activity. We discuss the implication and limitations of our approach in Section 4.

2.2) Data and Methods

Datasets

SLA product

The regional SLA product used in this paper is presented in Auger et al. (2021a). It is available on SEANOE with the doi : 10.17882/81032 (Auger et al., 2021b). It consists of seven years of daily SLA grids and associated geostrophic current anomalies between 2013 and 2019 on a 25 km EASE2 grid (Brodzik et al., 2014). The product is based on the processing and mapping of observations from three satellites : AltiKa and Sentinel-3A in the open and ice-covered oceans, and Cryosat-2 in the ice-covered regions. Dataset validation and error estimation have been estimated in Auger et al. (2021a).

Other datasets

The Mean Dynamic Topography (MDT) represents the mean surface of the ocean relative to the geoid. To compute the Absolute Dynamic Topography (ADT) needed for the tracking of the eddies, the time-mean MDT from Armitage et al. (2018), with the daily evolving SLA from Auger et al. (2021a).

We also use satellite-based sea ice observations : Sea Ice Concentration (Peng et al., 2013; Meier, 2017) and Sea Ice Drift velocity from the National Centers for Environmental Information (Tschudi and CO, 2016).

The bathymetry is computed from the GEBCO_2014 dataset (Weatherall et al., 2015).

Methods

Eddy detection and tracking

Eddy detection and tracking methods are derived from Mason et al. (2014). The method is based on the analysis of ADT in which small-scale closed contours are sought for. The first step is to remove the large-scale pattern by applying a 600 km high pass Gaussian filter to this ADT. A high-pass filter with a cutoff of several hundreds of kilometers is needed to remove the large scale signal from the dataset (Mason et al., 2014; Pegliasco et al., 2021). The spatial scale of 600 km is arbitrarily chosen here but is not sensitive for our results as far as it is chosen large enough to make sure the filters do not remove mesoscale features. Then, eddies are identified by searching for closed contours. Once a closed contour is found, several tests are performed, as described below, to ensure it does correspond to a mesoscale eddy.

The series of tests applied to detect eddies from the ensemble of SLA closed contours are listed in (Mason et al., 2014), but are presented here for the convenience of the reader. First, the contour circularity is checked by computing the ratio between the surface of the identified eddy and the surface of its circular approximation, which must be lesser than 70%. Then, an eddy must contain at least 8 pixels in the grid and have an amplitude greater than 1 centimeter. It must also contain only SLA pixels with values lower than the closed contour for a cyclone, and higher for an anticyclone, while containing only one local maximum or minimum of SLA. When a closed contour passes all these tests, it is considered an eddy. It is then possible to compute its properties such as its rotation speed, radius, center, and amplitude.

The tracking process consists in drawing ellipses of 150 km radius around eddies and determining the candidates, that are eddies detected the day after, that fall into this ellipse (Chelton et al., 2011). When there are multiple candidates, the couple is determined by minimizing S : a dimensionless parameter computed from the distance, radius differences, and amplitude differences between the eddies and their candidates. As in (Mason et al., 2014), S is defined for each

eddy at the date k and candidates $k+1$ as :

$$S_{k,k+1} = \sqrt{(\frac{\Delta d}{d_0})^2 + (\frac{\Delta a}{a_0})^2 + (\frac{\Delta A}{A_0})^2}, \tag{2.1}$$

where Δd is the distance between the eddy at the date k and the candidate at the date k+1, Δa and ΔA are respectively the difference of area and amplitude between the eddy and the candidate.

In this study, we only consider eddies that have been tracked for 10 days or more. This allows removing more than 30 000 identifications over the seven years in the subpolar Southern Ocean, to remove potential noises, and to concentrate on eddies that may have a stronger influence on the subpolar Southern Ocean water masses and circulation.

Computation of the Eddy Kinetic Energy

The Eddy Kinetic Energy over the Southern Ocean south of 50°S is computed from Auger et al. (2021a) sea level anomaly and geostrophic current anomalies product. We used the formula

$$EKE = \frac{1}{2}(u'^2 + v'^2), \tag{2.2}$$

with u' and v' respectively the anomalies of zonal and geostrophic current from the dataset.

Definition of sea ice regions

The sea ice cover can be decomposed in various sectors corresponding to different ranges of sea ice concentrations. At high concentration, typically above 70%, the drifting sea ice cover is referred to as pack ice ; at lower concentration but above 10%, it is commonly referred as Marginal Ice Zone (MIZ), which itself can be decomposed in a southern part of MIZ called 'open ice' for concentration between 40%-70%, and a northern part of MIZ called 'very open ice' for concentration between 10%-40%. In the present paper, we adopt these terms and definitions in agreement with the World Meteorological Organization sea ice nomenclature (Ice, 2009). Thereafter we refer to the 10-40% sea-concentration sector as n-MIZ and the 40-70% sea-concentration sector as s-MIZ.

Sensitivity of our results

As stated in Auger et al. (2021c), the root mean square error between the two-satellites merged product and a third satellite along-track signal is around 3.7 centimeters. We attempted to test how our results could be sensitive to weak eddies, and in particular to the presence of eddies of amplitude of less than 3.7 cm. As such, we repeated the analysis presented in this paper but removed entirely all eddies that have an amplitude less than 3.7 cm. The sensitivity analysis is shown in Supplementary Figures IV.8, IV.9, IV.10. All figures and relationships between sea ice and eddies discussed in this paper remain robust. In order to keep a maximum of eddies in our statistical description of mesoscale eddies, we chose to keep all detected eddies in the remainder of this paper.

Influence of the resolution of the altimetry product

Diagnostics derived from eddy identification and tracking may be sensitive to the density of observation, and so the position of the tracks of the satellites before the mapping of the dataset (Amores et al., 2018). To assess the sensitivity of the effect of the density of the along-track

observation on our results, we repeated the main diagnostics of this paper but with a dataset mapped from subsampled along-track observations. This sensitivity test is shown in Supplementary Figures IV.8, IV.9, IV.10 as well. The main conclusions presented in this paper remain the same with the original and subsampled dataset.

2.3) Results

Eddy Kinetic Energy (EKE) south of 50°S is computed from the SLA product and shown in Figure IV.1. Regions permanently ice-covered are hidden as they are the regions with the highest product errors (Auger et al., 2021a). The thick black line in Figure IV.1 corresponds to the Mean Dynamic Topography contour -180 cm, and is used thereafter as the northern extent of the region we refer to as the subpolar Southern Ocean in this paper (Auger et al., 2021c). North of this subpolar region the signature of the ACC is visible with EKE values reaching more than 500 $cm^2.s^{-2}$ in hotspots downstream of the major topographic features, consistent with previous studies (Zhang et al., 2021, e.g.). In contrast, the subpolar ocean is much quieter. Three distinct regions stand out in the subpolar region. First, the northern boundary of the subpolar region shows relatively large values of EKE, around 100 $cm^2.s^{-2}$, which appears as being a fingerprint of the southern boundary of the ACC. Second, the regions inside the two main subpolar gyres are associated with very low values of EKE of the order of 10 $cm^2.s^{-2}$. Third, the continental shelf and slope show relatively elevated EKE, but with important disparities depending on sectors around Antarctica. In general, EKE on the continental slope and shelf reaches around several 10s to 100 $cm^2.s^{-2}$, but reaches several 100s $cm^2.s^{-2}$ in specific regions such as the Western Amundsen sea, and East Antarctica. Consistently, these two regions have been identified as hosting the most intense ASC (Auger et al., 2021c). The West Antarctic Peninsula and Bellingshausen sea stand out as a region in which peak EKE values are not found on the continental shelf break (black dashed line) but closer to the Antarctic continent (Figure IV.1), consistent with the absence of an Antarctic Slope Current (ASC) is this region (Moffat and Meredith, 2018), and instead the presence of an active Antarctic Coastal Current (Schubert et al., 2021; Schulze Chretien et al., 2021).

We now investigate how this spatial structure in EKE estimate compares to estimates of eddy presence and characteristics. We first investigate overall eddy characteristics in the subpolar Southern Ocean, then investigate the role of sea ice in modulating eddy occurrence and characteristics, and finally investigate the difference of eddy characteristics in distinct dynamical regimes of the subpolar region.

Eddy detection in the subpolar Southern Ocean

More than 1,4 million eddy occurrences are found in the detection analysis applied on the seven years of daily observations. Figure IV.2a. shows the frequency of eddy occurrence in the subpolar Southern Ocean. The frequency is about 0.2 (meaning that the pixel is detected in an eddy for 20% of the full period of observation) in most of the subpolar Southern Ocean. Surprisingly, the regional pattern of eddy frequency is different from the pattern of EKE. For instance, there is a clear drop in frequency in the gyres and increase on the continental shelf

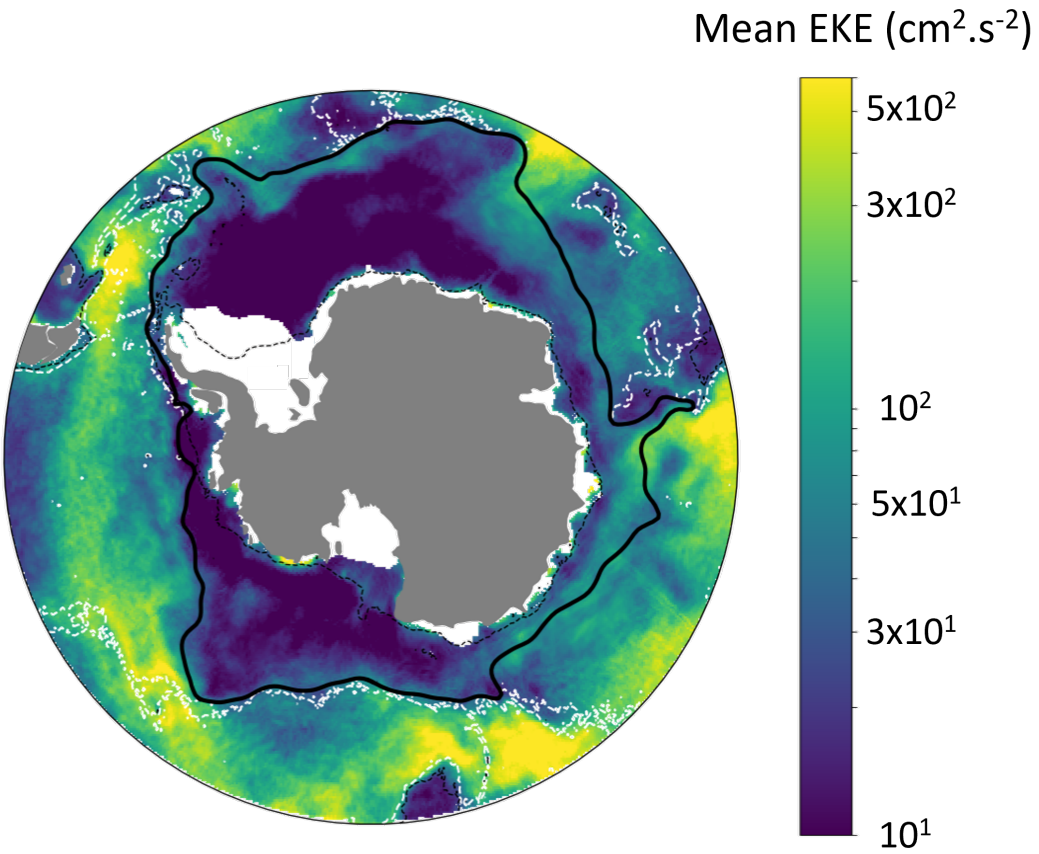

FIGURE IV.1: Eddy Kinetic Energy in the Southern Ocean. Eddy Kinetic Energy was computed as $\frac{1}{2}(u'^2 + v'^2)$, with u' and v' respectively the anomalies of zonal and geostrophic current derived from Auger et al. (2021c). White dashed lines are the -3000m isobath north of the subpolar Southern Ocean. The black dashed line is the -1000m isobath. The bold black line is the limit of the subpolar Southern Ocean as defined in this study.

break. While this might be surprising, it is an encouraging indication that EKE patterns are not shaped by the ability of the altimeter product to sample or miss eddies in the subpolar regions. Rather, it is clear that EKE is shaped by the intensity of the detected eddy (Figure IV.2b).

While the frequency of eddies detected is relatively homogeneous over the subpolar region (Figure IV.2a), the detected eddies have much weaker amplitudes in the subpolar gyres, compared to the northern or southern boundaries of the subpolar domain (Figure IV.2b). The mean amplitude is computed as the mean height of the crest or the bump in ADT associated with each eddy. The amplitude range from 5-10 cm in most energetics sector of the subpolar region,

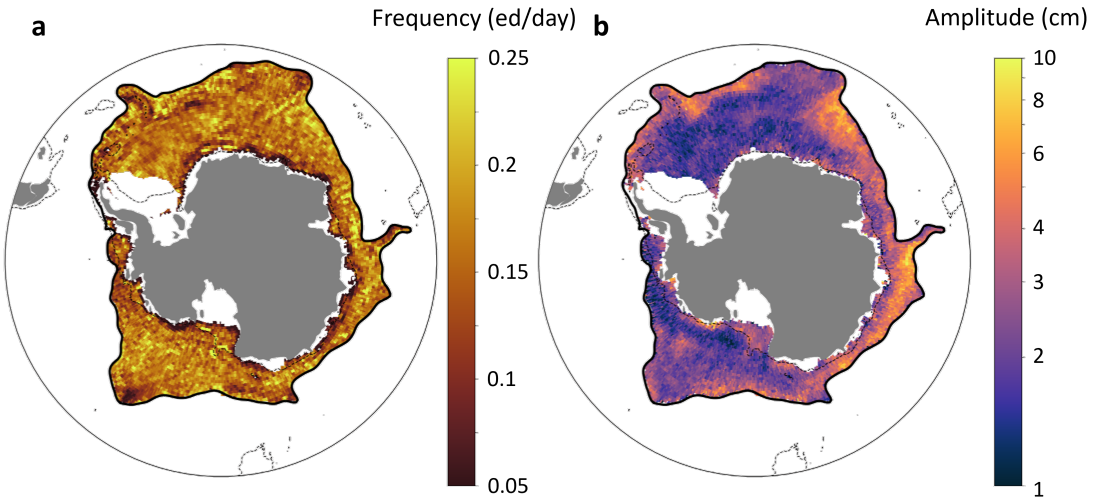

FIGURE IV.2: (a) Eddy frequency per pixel in the subpolar Southern Ocean. (b) Mean eddy amplitude per 0.5° pixel in the subpolar southern ocean. Black dashed line is the -1000m isobath. Bold black line is the limit of the subpolar Southern Ocean as defined in this study.

to 1-2 cm in the less energetic regions in the middle of the subpolar gyres. Overall, the spatial patterns of EKE (Figure IV.1) and of the mean amplitude of the detected eddies (Figure IV.2b) are very similar. This means that the spatial pattern of EKE is not driven by the frequency of eddy occurrence, but more by the strength of these eddies. It appears clear that while the probability of detecting an eddy is relatively homogeneous over the subpolar ocean domain, the amplitude and the energy associated with these eddies are strongly dependent on the local dynamical regime : southern ACC region, subpolar gyre, continental shelf break. We next investigate if, on top of the dynamical regime, the seasonal presence or absence of overlying sea ice cover impacts eddy frequency and characteristics.

Impact of the sea ice on eddy frequency and amplitude

The area of the ice-free and ice-covered sectors of the subpolar ocean (which are by construction anti-correlated) undergo a very large seasonal cycle (Figure IV.3a,b). The number of eddies detected in each of these sectors follows closely the seasonal evolution of the area of each sector (black lines in Figure IV.3c,d), so that the density of the eddies per unit area is relatively constant seasonally (black lines in Figure IV.3e,f). The eddy density reaches a minimum at the time of the year when the corresponding surface is minimum in both sectors. We note that there are slightly more eddies per unit area in the ice-free regions (3.8 ± 0.2 eddies per 100,000 km^2) than in the ice-covered region (3.2 ± 0.3 eddies per 100,000 km^2), which might be an indication that sea ice dampens the presence of eddies. For both ice-free and ice-covered sectors, more cyclones (blue lines) are detected than anticyclones (red lines). This difference in

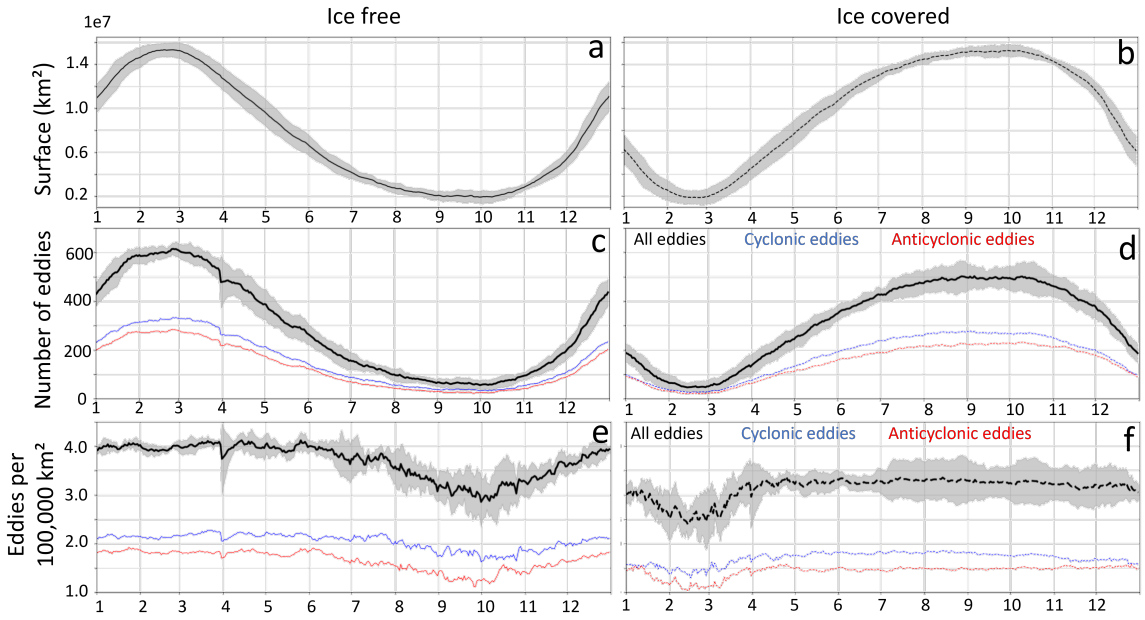

FIGURE IV.3: (a)(b) Surfaces, (c)(d) number of daily eddies detected, and (e)(f) density the eddies in the respectively ice-free and ice-covered region. The density is computed as the number of eddies per 100 000km². Plain lines are for the ice-free regions, dashed lines are for the ice-covered regions. Black lines in (c)(d)(e)(f) are the number and density of all the eddies, while the blue and red curves are respectively the number and density of cyclones and anticyclones.

the number of cyclones/anticyclones is consistent throughout the year. Interestingly, the dominance of cyclones over anticyclones is consistent with what was described in global ocean analysis (e.g. Chelton, 2013).

Figure IV.4 brings more details to the relation between the density of the eddies and the sea ice cover. By computing the number of eddies and calculating the surface of the corresponding region in 10% bins of sea ice concentration, we computed the relationship between the density of eddies and the sea ice concentration (Figure IV.4a). For the Anticyclones, the density of eddies is rather constant around 1.6 anticyclonic eddies per 100,000 km^2. In contrast, the density of cyclonic eddies seems to be much more impacted by the overlying sea ice concentration than the density of anticyclonic eddies. In the n-MIZ 10 and 40% of SIC values, the density of cyclonic eddies reaches values up to 2.6 cyclones per 100,000 km^2, which is higher than the density of cyclones in the ice-free ocean (about 2.1 cyclones per 100,000 km^2 Figure IV.3e). Thus, the n-MIZ seems to be a favorable region for cyclonic eddies. The density lowers in higher SIC, reaching about 1.6 cyclones per 100,000 km^2 between 60 and 90% of sea ice concentration and is minimum for sea ice concentration of 90-100% with a density of about 1.4 eddies per 100,000 km^2.

The variation in the density of eddies as a function of sea ice concentration (fewer eddies with more sea ice) could be an indication that valid sea-level observations in higher sea ice concentrations are scarcer which could affect our ability to observe eddies. However, if it was indeed our methodology that was sensitive to the presence of sea ice, it would affect indepen-

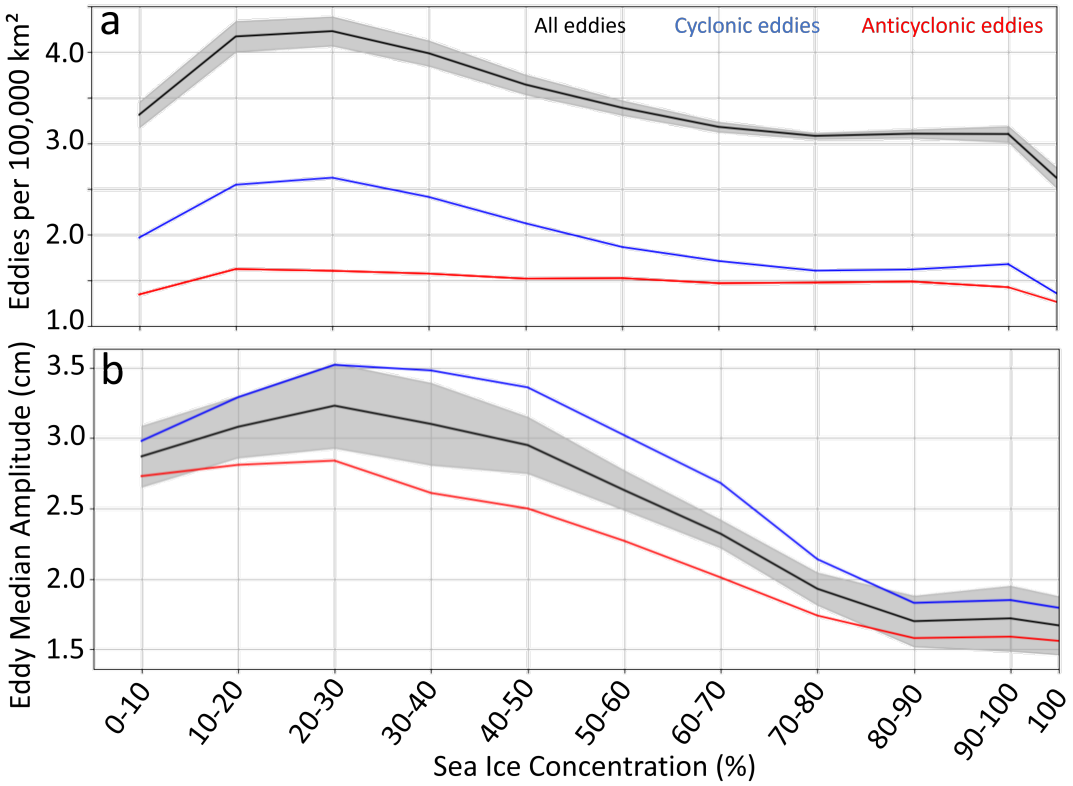

FIGURE IV.4: Density and amplitude of the detected eddies as a function of Sea Ice Concentration (SIC). (a) Density of all the eddies (black), cyclonic eddies (blue), and anticyclonic eddies (red) as a function of the sea ice cover. The density is computed as the number of eddies per 100 000km² within each SIC bin. The shaded interval around the density of all the eddies is the standard deviation of this distribution computed for each year of the analysis (2013-2018). (b) Median amplitude of all the eddies (black), cyclonic eddies (blue), and anticyclonic eddies (red) as a function of the sea ice cover. The shaded interval around the median amplitude of all the eddies is the standard deviation of this distribution computed for each year of the analysis (2013-2018).

dently observations of cyclones and anticyclones. The robust difference observed here between cyclones and anticyclones is an indication of the robustness of our result that the concentration of sea ice does have an impact on the presence of eddies.

Similar to eddy density, the amplitude of eddies varies with sea ice concentrations (Figure IV.4b). The shape of the relationship is however slightly different. Eddy amplitude maximize in regions of lower sea ice concentration, with amplitude around 3 cm, and minimize in the regions of higher sea ice concentration, with amplitude around 2 cm. This general tendency is observed for both cyclones and anticyclones, but we find that cyclones are on average 40-70% larger than anticyclones with a maximum difference in absolute amplitude reaching 1 cm in the n-MIZ. We saw in Figure IV.2b that the amplitude of eddies also strongly varies regionally depending on the local dynamical regime : southern ACC region, gyres, and continental shelf break. We next attempt to investigate how the effect of sea ice on eddy amplitude differs in the subpolar gyres and at the continental shelf break.

Figure IV.5b shows the amplitude of eddies binned as a function of overlying sea ice concentration bins and underlying bathymetry contours. The associated bathymetry of the subpolar Southern Ocean is shown IV.5a. Subpolar gyres are typically associated with abyssal plains deeper than 3000-4000 m, while the continental shelf break is typically associated with bathymetry contours of 500-2000 m. It is striking that the overall behavior of larger eddy amplitude in lower sea ice concentration holds for all bathymetry contours. However, there is also a clear a distinct shape to the reduction of amplitude with a sea ice concentration in these two sectors : sea ice concentration dampen eddy amplitude more efficiently in abyssal plains compared to the shelf break (Figure IV.5b). This is illustrated by the ratio between the median eddy amplitudes in the n-MIZ and the pack ice (Figure IV.5b). This ratio is the strongest in the low bathymetry regions, where the amplitude of the eddies in the n-MIZ is twice as high as in the pack ice. This ratio then decreases with the depth of the water column, reaching 1.2 at the shelf. This is consistent with the presence of the energetic ASC over most of the continental shelf break that might counterbalance eddy dampening by sea ice due to a sustained input of energy from the ASC. We also note that over bathymetry contours corresponding to the continental shelf break, the decrease in eddy amplitude with sea ice concentration stops around 80%, and increase again for larger sea ice concentration bins. This might result from seasonal variability of the ASC strengths, which substantially increases in winter (Armitage et al., 2018; Auger et al., 2021a) when sea ice concentration is at its maximum.

Eddies in the northern Marginal Ice Zone

Most of the diagnostics presented above about the relationship between the sea ice and the presence and amplitude of eddies point to the n-MIZ as a particular region. The n-MIZ stands out as a region associated with larger eddy density, larger eddy amplitude, and a clear dominance of cyclones over anticyclones. In this section, we investigate some possible reasons for this behaviour in the n-MIZ.

Both Arctic and Antarctic MIZ have been identified as hotspots for eddy-like features in past studies (Lu et al., 2015; Manucharyan and Thompson, 2017). Both mechanical and thermodynamical effects have been put forward as potential explanations. In the following, we investigate, in turn, if mechanical or thermodynamical forcing would be qualitatively consistent with our results.

The n-MIZ is a region favorable for large Ekman pumping due to large gradients in mechanical stress : the presence of sea ice dampens the transfer of momentum from the winds, creating a large stress curl in the n-MIZ region. In consequence, the n-MIZ is associated with intense upwelling or downwelling, which may create an n-MIZ jet favorable for instabilities (Häkkinen, 1986). In the Southern Hemisphere, the strong mid-latitude westerlies are very efficient at creating in complicity with sea ice a large upwelling at the ice edge and in the n-MIZ (Figure IV.6a ; upwelling corresponds to negative ocean stress curl). These Ekman-driven upwellings have been described to have the potential to locally increase eddy activity due to both lateral buoyancy gradients and the creation of a local jet following the sea ice edge (Häkkinen, 1986). The easterlies interacting with this local jet may trigger an eddy response as well, as these type of conditions enhance the formation of intra-pycnocline eddies (Thomas, 2008; Lu et al.,

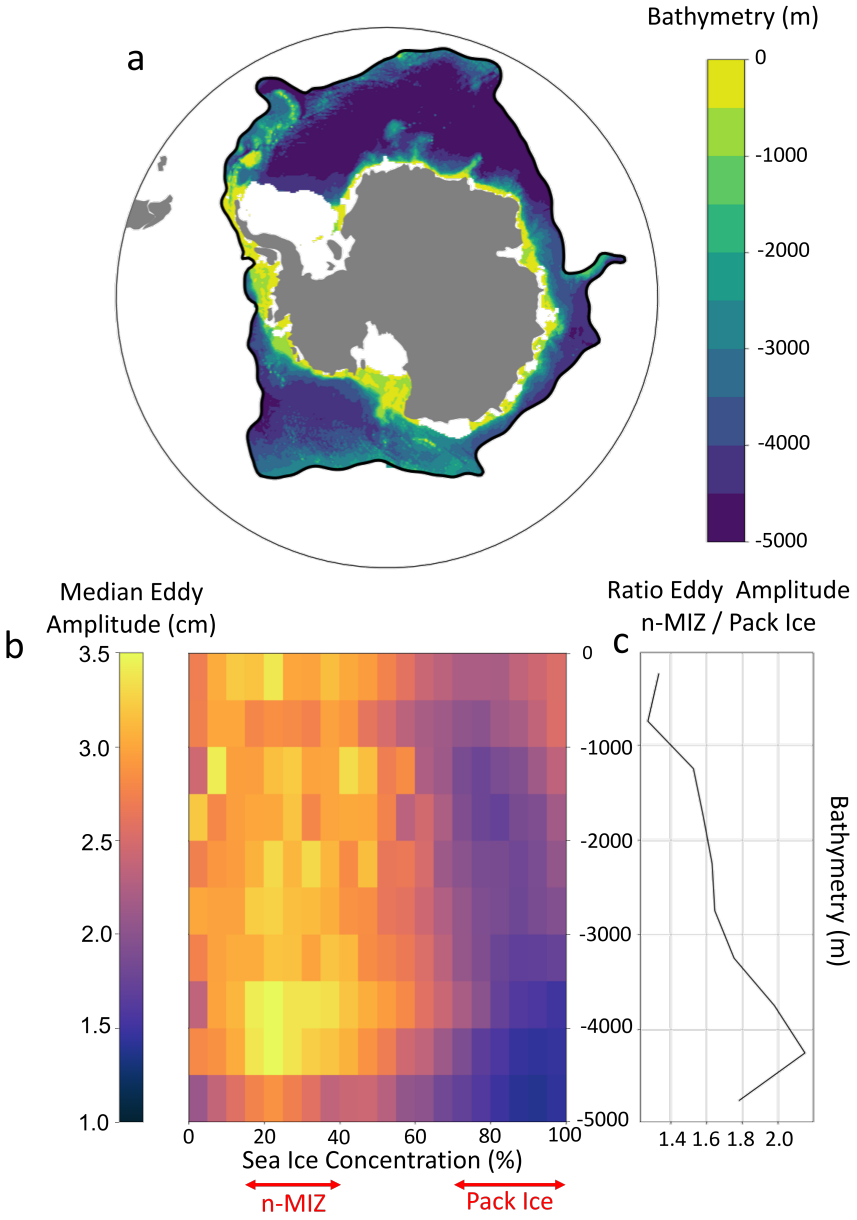

FIGURE IV.5: (a) Bathymetry of the subpolar Southern Ocean. (b) Median amplitude of the eddies tracked in the subpolar Southern Ocean as a function of the local bathymetry and the Sea Ice Concentration. Red lines delimitate the frontiers of the northern MIZ (n-MIZ) and the Pack Ice. (c) Ratio between the median amplitude of the n-MIZ and the median amplitude of the pack ice values as a function of bathymetry.

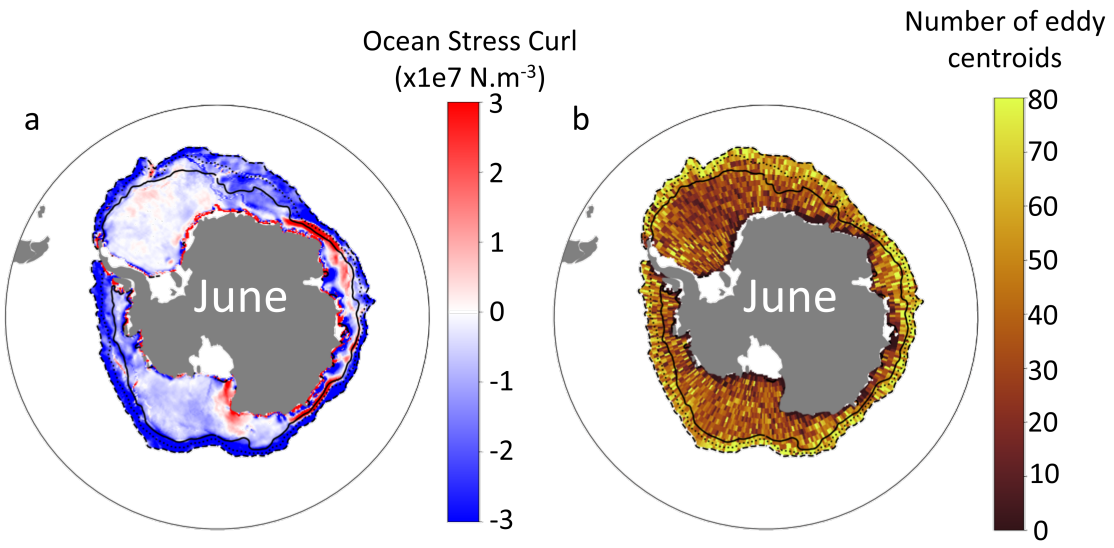

FIGURE IV.6: (a) Mean Ocean Stress Curl in June in the Southern Ocean, between 2013 and 2019. (b) Number of eddies detected in 1° pixel in the sea ice zone in June. The black dashed, dotted and plain lines are respectively the contours of 10%, 40% and 70% of Sea Ice Concentration.

2015). This is consistent with our observation of a collocated increase in eddy density (Figure IV.6b). On the specific months (June) displayed in Figure IV.6b, it is striking that we detect more eddies in the northern part of the MIZ (Figure IV.6b), consistent with the location of the largest Ekman-driven upwelling (Figure IV.6b).

On top of mechanical impact, the n-MIZ is also prone to thermodynamical instabilities at the sea ice edge meltwater front (Lu et al., 2015; Manucharyan and Thompson, 2017). Sea ice in the n-MIZ provides an important source of freshwater, which when melting, generates a large meridional buoyancy gradient that would enhance instabilities (Lu et al., 2015). Consistent, the largest eddy density of the n-MIZ is found during the melting season (Figure IV.7). Sea ice melting is associated with any pixels in which sea ice concentration has locally decreased in the preceding 30 days. The largest eddy density and the largest difference between cyclonic and anticyclonic eddy densities are found in pixels where the sea ice concentration reduced by 0-30% in one month. We note however that our proxy for the melting season has important limitations, as in particular, it assumes that local decrease in sea ice concentration is associated with a melting event, while it could be due to sea ice advection. Analysis of colocated temperature-salinity profile might be needed in the future to better grasp the main fording associated with cyclones in the MIZ.

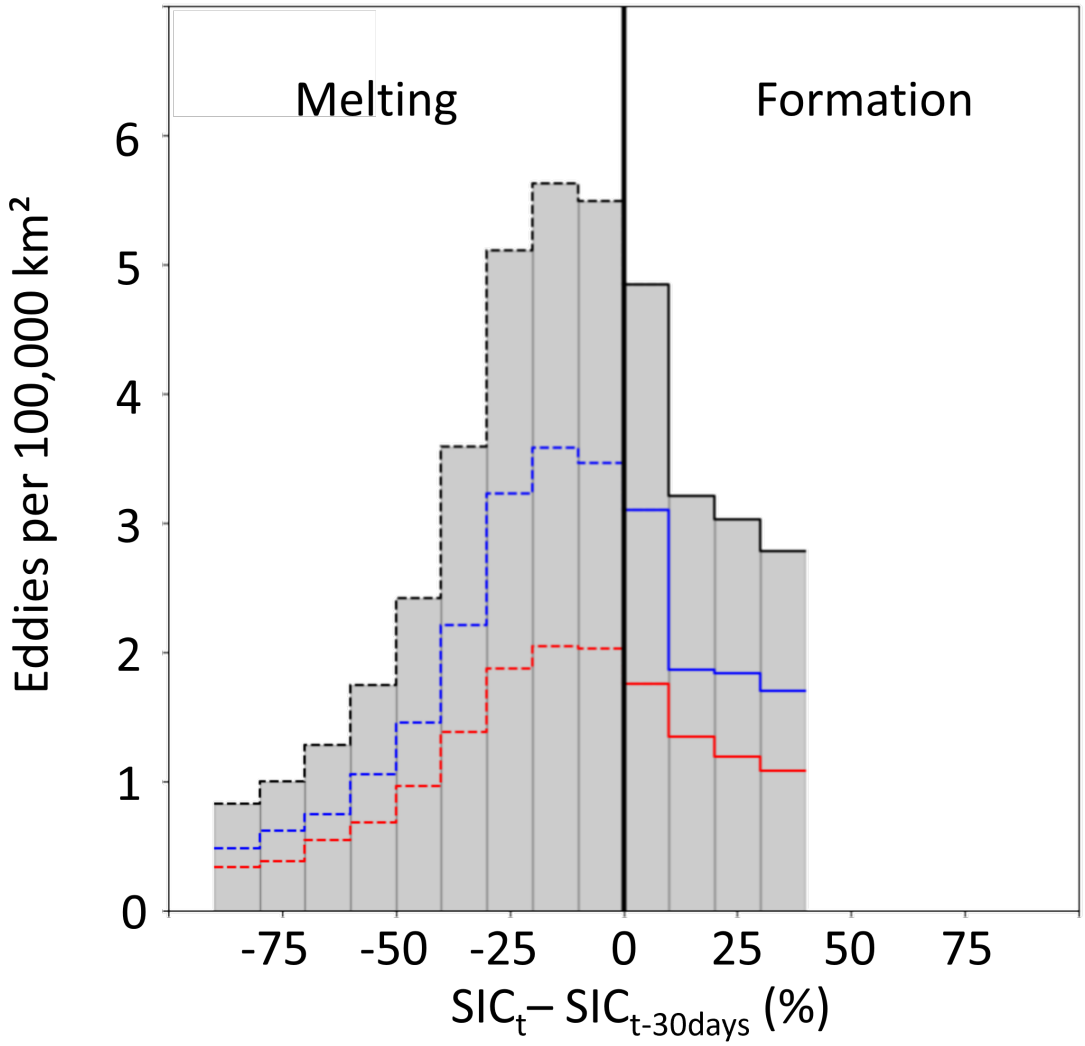

FIGURE IV.7: Presence of eddies within the northern Marginal Ice Zone (n-MIZ). Mean eddy density over the full observation period as a function of the temporal gradient of SIC. Here, this gradient is defined as $\delta_t SIC = SIC_t - SIC_{t-30days}$. Blue, red and black curves are respectively the density of cyclones, anticyclones, and all eddies. Dashed (plain) lines are the density of eddies in the melting (formation) season.

2.4) Conclusion and Discussion

We used a new satellite altimetry product covering both the ice-free and ice-covered Southern Ocean to investigate eddy activity in the subpolar sector of the Southern Ocean. To this end, we document the EKE, the number of eddies per unit area, and the eddy amplitude. We are particularly interested in documenting the influence of the presence of a sea ice cover on these quantities. The EKE shows a spatial distribution consistent with the location of the main circulation system of the Southern Ocean. High EKE hotspots are found in the ACC downstream of the major topographic features, and more generally follow the path of the ACC and ASC. We

show that these regions are associated with larger amplitude closed-core eddies. We find that with higher sea ice concentration the number of eddies observed per unit area as well as their amplitude decreases. While these results might reflect a methodological bias, by which the presence of sea ice decreases the valid observations points in a pixel and therefore our ability to observe eddies, we believe that it is a robust result. Indeed, if it was resulting from a methodological bias, both cyclones and anticyclones would be affected in the same way. In contrast, we find that the sea ice cover mostly affects cyclones, with the northern MIZ being a hotspot of strong cyclonic eddies. There, both freshwater fluxes from sea ice melting and sea ice edge-driven upwelling may contribute to enhance eddy activity.

While we believe that our results shed unprecedented light on under-ice eddies in the Southern Ocean, they are also associated with important remaining limitations. First and foremost, the satellite altimetry product we used (Auger et al., 2021a), while being at the highest resolution altimetry product we are aware of in this region, is gridded at a 25 km resolution, i.e. larger than the Rossby radius in most of the subpolar sector. The grid is actually much coarser than the density of observation coverage, which is, in the worst cases in the high concentration of sea ice, around 10 observations per grid cell. We also note that there are no strong disparities in the number of observations despite varying sea ice concentration, potentially due to the tightened satellite tracks when going southward compensating for fewer leads available. Many small-scale eddies must be missed or smoothed out in our altimetry product. Future altimetry missions will certainly fill an important gap in this direction in the future. While it is very difficult to assess the impact of such limitation on our results, we did test the robustness of our results to a coarsened observation-based product. Namely, we repeated the same analysis, but from an altimetry dataset produced with subsampled along-track observations before we mapped it. Only weak sensitivity to both amplitude or density of detected eddies was found (Supplementary Material Figures S1, S2, and S3).

The methodology for detecting and tracking eddies based on satellite-derived sea surface topography has also limitations. For instance, the noise in the ocean topography dataset may create spurious small eddies. We tested the sensitivity of our result to this limitation by removing from our analysis all eddies with amplitude smaller than an upper bound of the evaluated error of the product. This analysis can be found in Supplementary Material S1, S2 and S3, and shows that our results are robust to this test.

Our results are hardly comparable to other studies observing the eddies in the sea ice regions, as the observation methods and the nature of observations are radically different. Most of the eddies previously observed in the sea ice region have been observed in the halocline, between 50 and 250 meters depths, from in-situ measurements (Timmermans et al., 2008; Zhao et al., 2014, 2016; Meneghello et al., 2020). Those eddies are mostly anticyclonic (Zhao et al., 2014, 2016), and do not seem to be impacted by the overlying sea ice as they may have lifetimes lasting more than 6 months (Timmermans et al., 2008). Here, we observe a dominance of cyclonic eddies over cyclonic eddies in both the ice-free and ice-covered subpolar Southern Ocean. Except close to the main features of the background circulation, eddies seem to be sensitive to the presence of sea ice. This is consistent with the winter dampening of surface eddy kinetic energy that was discussed in (Meneghello et al., 2020). Our results show that the northern

part of the MIZ is a region very favorable for eddies, particularly cyclonic. Multiple studies already demonstrated the MIZ to be a region with an intense eddy activity, due to its meltwater front (Lu et al., 2015; Manucharyan and Thompson, 2017) or the local wind-driven upwellings or downwelling at the ice edge (Häkkinen, 1986) and subsequent jet (Thomas, 2008). But the dominance of cyclonic eddies in this study may in fact reflect the structure of the response of eddies in the MIZ. Taking inspiration from the fronts at Arctic sea ice edges, (Manucharyan and Timmermans, 2013) demonstrated that eddies generated at surface fronts are often formed as dipoles, with surface cyclones and weaker subsurface anticyclones. Those anticyclones then travel in the halocline of the sub-ice regions far from their formation regions (Timmermans et al., 2008; Manucharyan and Timmermans, 2013) where they have been observed by multiple studies (Timmermans et al., 2008; Zhang et al., 2014; Zhao et al., 2016). Consequently, the observed dominance of cyclones in the n-MIZ may be the surface signature of the generation of halocline anticyclones. In any case, they demonstrate the intense eddy generation occurring at the ice edge.

Supplementary Material of the paper : *Southern Ocean ice-covered Eddy properties from satellite altimetry* by Auger et al.

The supplementary information presented here provides more insights into the results described in the main paper. We are conscious that there are many unknowns on the capacities of the observation dataset for the observation of mesoscale eddies under sea ice, even more considering the small Rossby radius of the region (Chelton et al., 2011). This supporting information provides more insights into the robustness of the results presented here and into the spatial scales resolved by the dataset.

2.5) Sensitivity study

As stated in the paper, we have been concerned by both the effects of the possible artifacts of the dataset and the along track resolution of the source data. We decided to tackle these issues by reproducing some of the diagnostics of the paper, either by selecting only the eddies with an amplitude larger than the error estimated in the seasonally ice-covered regions or by subsampling the along-track measurements upstream of the mapping of the Sea Level Anomaly dataset and the eddy detection process. We therefore define two experimental cases :

— The "All" case is the original case. We kept all the eddies and all the along-track measurements before the mapping.

— The "Amp" case. In this case, we remove all the eddies with amplitudes lower than the mean error of the ice-covered regions (Auger et al., 2021c, i.e. 3.7cm).

— The "Samp" case. In this case, the along-track measurements have been subsampled before the mapping of the product presented in Auger et al. (2021a). We sampled the AltiKa and Sentinel-3A to reach 1 Hz measurements in the ice-free ocean. In the ice-covered measurements, we only kept 1 valid point out of 3 for Sentinel-3A and Crysosat-2, and 1 out of 6 for AltiKa, as it is emitting twice more measurements compared to the for-

mers. These values were chosen arbitrarily to find a compromise between downgrading the dataset and not flattening all the signal. Other sampling frequencies were not tested as the computation of a new dataset requires lots of time and computing power. After this subsampling, we constructed the dataset the same way as its unsampled, original version. We then applied the detection and tracking method.

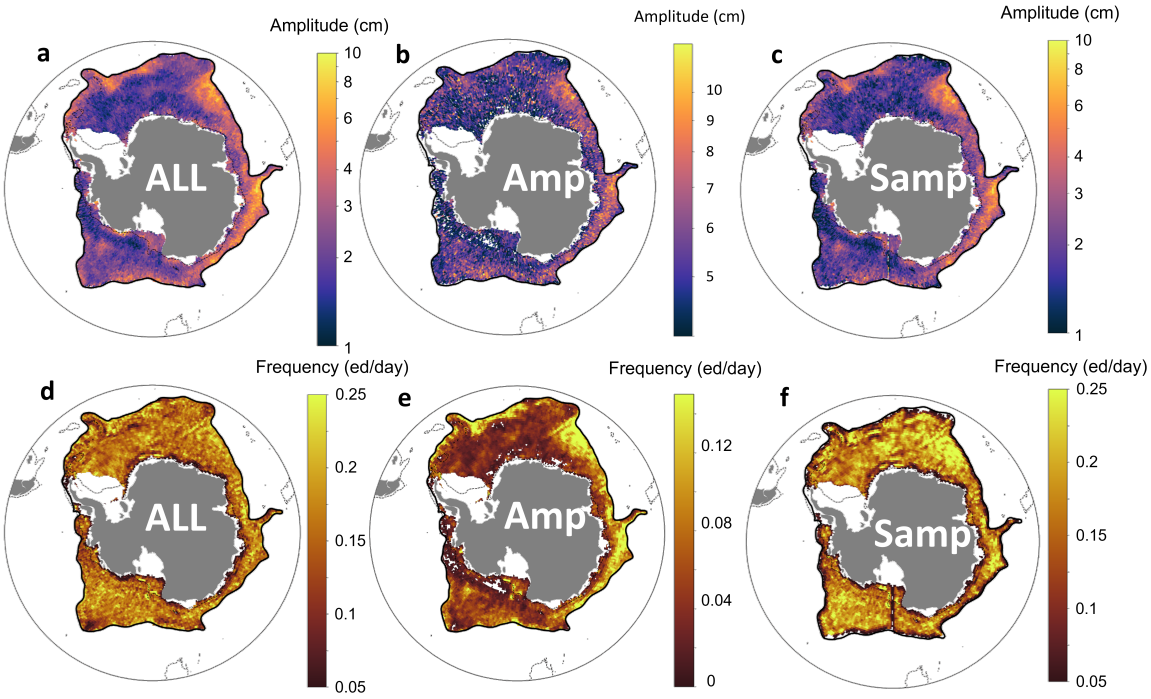

FIGURE IV.8: Sensitivity study of the maps of mean amplitudes and frequency. The first line (a-c) shows the map of the mean amplitude of the tracked eddy for each sensitivity study. The second line (d-f) shows the map of the frequency of the days the pixels are located into an eddy. The first row (a,d) is the case presented in this study containing all the eddies (ALL case). The second row (b,e) is the case for which only the eddies with an amplitude larger than 3.7 centimeters are included in the calculation (Amp case). The last row (c,f) is the case for which the along-track data was subsampled before the mapping of the Sea Level Anomaly product (Samp). The black dashed line is the -1000m isobath. The bold black line is the limit of the subpolar Southern Ocean as defined in this study.

Supplementary Figure IV.8 shows the maps of the mean eddy amplitudes and frequencies. The spatial pattern of eddy amplitude is rather consistent between all the cases. The amplitudes are distributed the same way for all the cases (Supplementary Figure IV.8a-c), but with unsurprisingly stronger amplitudes in the Amp case. The amplitude in the Samp case is a little lower than in the All case, showing a slight flattening effect of having fewer measurements. One point of the paper is the uniform distribution of the eddies in the subpolar basin. Supplementary Figure IV.8d-e shows how this changes between the various cases. The eddy frequency in the Amp case is twice as small as the All case. This shows that a large part of the eddies detected has an amplitude lower than the estimated error of the dataset. In the Amp case, the density is

less uniform as there are stronger eddies in the northern extent of the subpolar region, where the mesoscale activity is enhanced by the neighboring ACC. In the Samp case, the frequency is uniform and higher than in the All case. Amores et al. (2018) pointed that lower resolution along-track measurements upstream of the mapping of ocean topography may induce larger eddies, as the interpolation would spread the signal further. In this study, we decided to not focus on the radius as it is one of the eddy properties the most impacted by varying resolution of the input dataset. In this case, the higher frequency may be explained by larger eddies covering more pixels, thus increasing the chances for a gridpoint to be contained into an eddy.

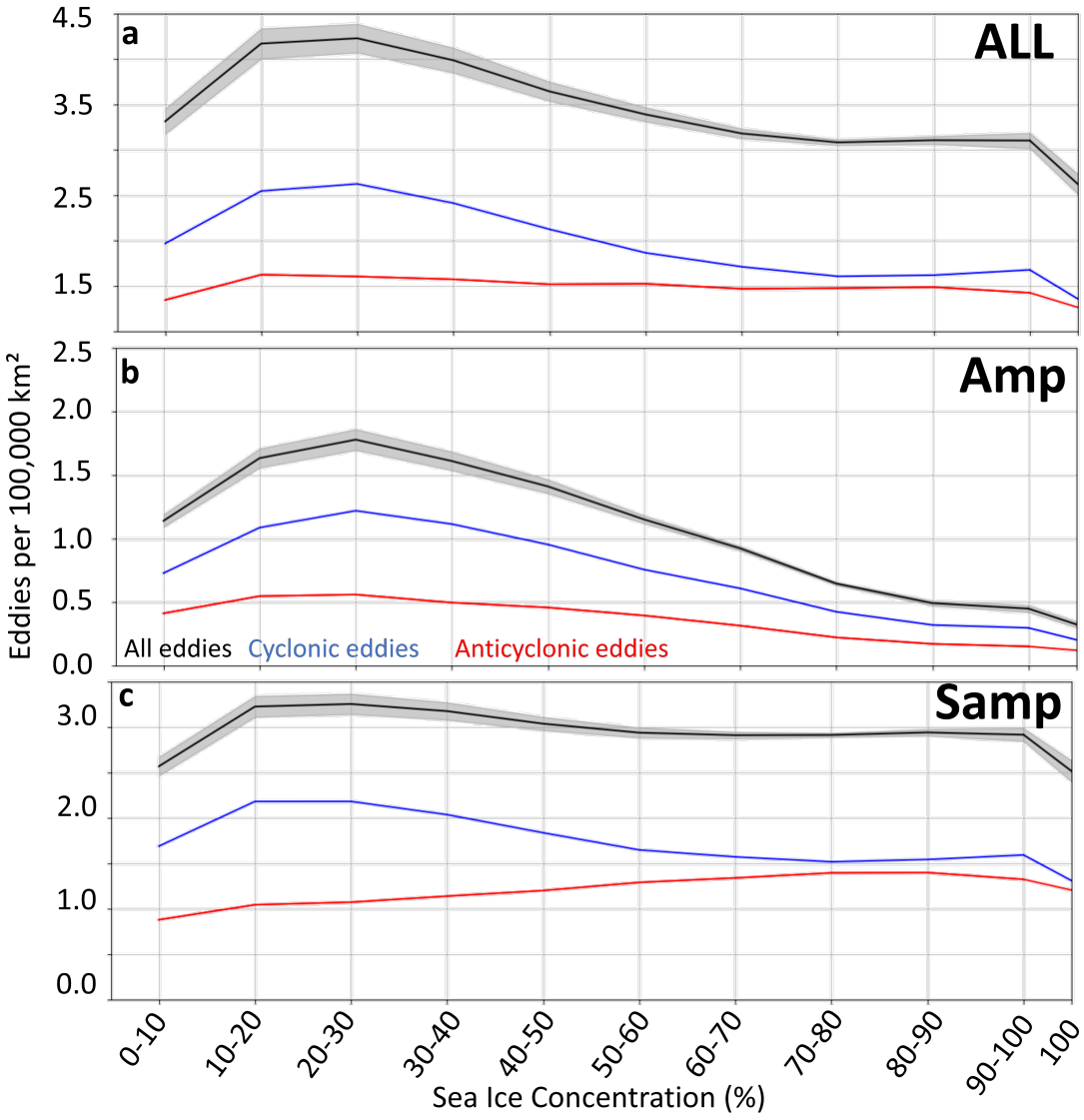

FIGURE IV.9: Sensitivity study of the density of the eddies as a function of the Sea Ice Concentration (SIC). The black curve is the density of all the eddies, the blue one is the density of the cyclonic eddies and the red one is the density of the anticyclonic eddies (red) as a function of the sea ice cover. (a) is the case presented in this study containing all the eddies (ALL case). Panel (b) is the case for which only the eddies with an amplitude larger than 3.7 centimeters are included in the calculation (Amp case). Panel(c) is the case for which the along-track data was subsampled before the mapping of the Sea Level Anomaly product (Samp).

Supplementary Figure IV.9 shows the sensitivity of the density of the eddies as a function of sea ice concentration. The distributions of the three cases are similar and show higher densities in the northern-MIZ, but with lower densities for both experimental cases. In the Amp case, the dominance of cyclones over and anticyclonic eddies is even larger than the ALL case, with cyclones density reaching twice the one of anticyclones in SIC between 20 and 30%. Interestingly,

the overall dominance of the eddy density in the n-MIZ is smaller in the Samp case, as the diminishing number of cyclones is compensated by a growing number of anticyclones. We do not have explanations for this growing density of cyclones with SIC when subsampling the dataset.

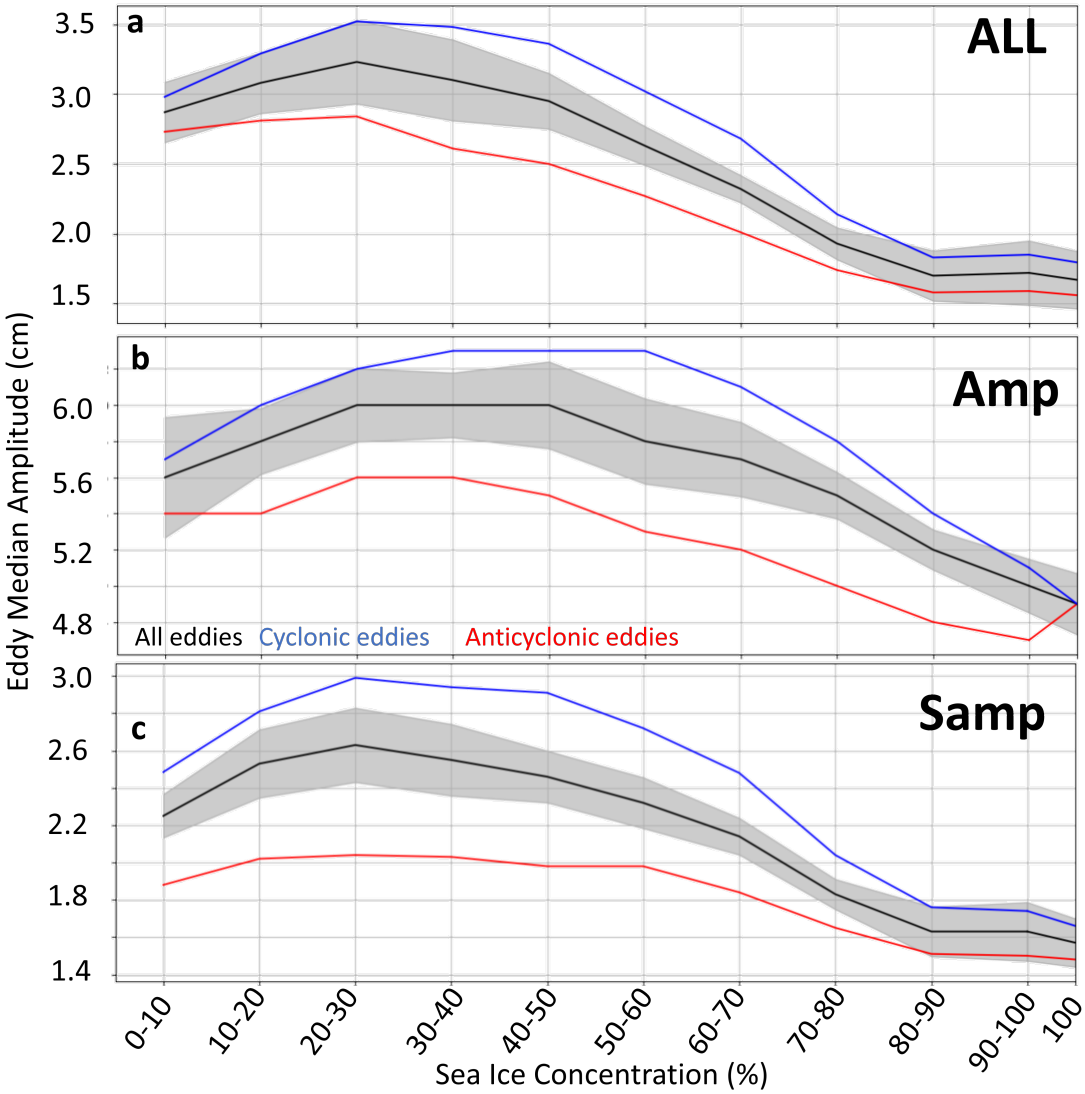

FIGURE IV.10: Sensitivity study of the amplitude of the eddies as a function of the Sea Ice Concentration (SIC). The black curve is the median amplitude of all the eddies, the blue one is the median amplitude of the cyclonic eddies and the red one is the median amplitude of the anticyclonic eddies (red) as a function of the sea ice cover. (a) is the case presented in this study containing all the eddies (ALL case). Panel (b) is the case for which only the eddies with an amplitude larger than 3.7 centimeters are included in the calculation (Amp case). Panel (c) is the case for which the along-track data was subsampled before the mapping of the Sea Level Anomaly product (Samp).

Supllementary Figure IV.10 shows the distribution of the median density of the eddies as a function of sea ice concentration for all the cases. Once again the distribution is similar, with larger eddies in the MIZ than in the pack ice. However, when selecting only the strongest eddies (Amp), the maximum density is found in both the southern and northern MIZ, between 20 and

50 % of SIC, and cyclonic eddies at their maximum amplitude even up to 60% of SIC. This does not change the conclusions of our study. Figures S1, S2, and S3 show that our results are robust to the impact of the small eddies and to the resolution of the measurements used.

3 Conclusion of the chapter

In this chapter, I investigated the presence and properties of the mesoscale eddies in the subpolar Southern Ocean. To undertake this, I used the Sea Level Anomaly (SLA) dataset presented in **Chapter II** and used an eddy detection and tracking method derived from Mason et al. (2014).

The sea ice unsurprisingly dictates the presence and strength of the eddies, along with the background circulation.

In the pack ice, the density of eddies and their amplitude is lower than anywhere else in the subpolar Southern Ocean. There, surface friction with the surface might dissipate the existing eddies and prevent their generation (Meneghello et al., 2020). This is more true in the middle of the gyres than in the large-scale features of the background circulation, such as the ACC or the ASC. There, the energetic currents might compensate in generating stronger eddies that are not directly dissipated by the sea ice.

The Marginal Ice Zone (MIZ) shows the highest density of detected mesoscale eddies and hosts the strongest eddies of the ice-covered regions. The largest part of these MIZ eddies is detected in its northern part, defined here with Sea Ice Concentration values between 10 and 40%. These eddies are mostly cyclonic and do not seem to propagate in other regions. In the middle of the gyres, their amplitude can reach as high as twice the amplitude of the eddies detected in the same region in pack ice conditions. The generation of these northern-MIZ eddies is consistent with an intense wind and sea ice-induced upwelling at the sea ice edge (Häkkinen, 1986; Lu et al., 2015). It is also consistent with the ice edge associated meltwater front, which may enhance instabilities due to strong meridional gradients of salinity (Lu et al., 2015; Manucharyan and Thompson, 2017). While the lack of joined observation prevents us from drawing definitive conclusions, these cyclonic eddies may be the surface signature of the halocline anticyclonic eddies presented in previous studies (Timmermans et al., 2008; Zhao et al., 2014, 2016). Dedicated modelling studies may be one of the best ways to document these processes. It would indeed therefore be interesting to observe the signature of the MIZ dipoles modeled in Manucharyan and Timmermans (2013) on the ocean topography.

While my results seem to be robust, documenting the signal close to its maximal capacity may enhance the errors. The lack of independent datasets for cross-comparison forces us to develop our analysis with careful consideration for the limitations of the SLA product developed in the context of this thesis. Future improvements in in-situ and remote sensing observation will allow documenting further the interaction between the sea ice and the mesoscale eddies in the Southern Ocean. Until then, the outcomes presented here must be taken with caution.

CHAPITRE

V General Discussion

Sommaire

My thesis focuses on the study of the variability and changes of the subpolar Southern Ocean circulation and hydrography. In particular, I aimed at strengthening the observation of the changes affecting the Southern Ocean and exploring the variability of the large-scale and mesoscale circulation. Over the course of my Ph.D., I chose to focus on three distinct spatio-temporal scales : long-term multi-decadal and basin-scale change ; seasonal, and mesoscale variabilities, and try to connect the circulation systems to winds, buoyancy forcings, and sea ice.

In this chapter, I propose a general conclusion structured around the main scientific questions that motivate my thesis, which I listed in my introduction ; I then address the limitations and caveats of the studies I developed ; I next discuss some implications of my results ; I finish by providing perspectives for future work.

1 Conclusion and Discussion

As discussed in the Introduction, my thesis is motivated and structured around three main questions. In the following, I come back to these questions to attempt a conclusion and discussion of the results of the different chapters.

How have the circulation and hydrography of the Southern Ocean changed over the past several decades and are documented changes a significant departure compared to interannual variability ?

Observational coverage of Southern Ocean hydrography and Southern Ocean circulation remains relatively short compared to other oceanic basins. Yet, important long-term changes have been inferred from observation in many parts and aspects of the Southern Ocean (Meredith et al., 2019). While some of these changes have been attributed to human-induced climate change (especially hydrographic changes in the northern part of the basin ; Swart et al., 2018; Hobbs et al., 2021), several studies have pinpointed the potentially important role of decadal variability in Southern Ocean circulation and associated temperature/salinity changes (DeVries and Primeau, 2011; Abrahamsen et al., 2019; Silvano et al., 2020; Zika et al., 2021).

In this context, one of the aims of my thesis was to revamp observation datasets to investigate long-term time series with a fresh eye. In **Chapter I**, I investigated the long-term changes in the upper layer of the Southern Ocean using a 25-year time series of high-resolution temperature transects. This is one of the longest XBT time-series of the Southern Ocean (especially with such a resolution of the seasonal cycle, with up to 6 repeats of the section per year, between October and March), acquired over the years by the LEGOS/IPEV SURVOSTRAL program (and I must say I am particularly happy to be currently in quarantine at Hobart as I write these lines, in preparation for leading the sampling of the next XBT section). The analysis of temperature trends is consistent with past work, but the new aspect I was able to bring is to compare these changes to interannual variability, as well as ensure that the seasonal cycle (sometimes large) is properly removed. I uncover that only three regions have long-term trends with an ampli-

tude that is stronger than the interannual variability. First, the region that is associated with the largest warming of the section, north of the Southern Ocean in the SubAntarctic Modal Water (SAMW) layer. Second, the only region of the section that is cooling, found in the cold near-surface waters close to Antarctica. Third, the southern and upper part of the Circumpolar Deep Water (CDW), directly below the winter mixed layer, that warms relatively slowly but steadily, and actually corresponds to the largest magnitude of warming when compared to interannual variability. A shallowing of the maximum temperature of the CDW has also been found, an order of magnitude larger than what was described in previous studies, with potential impact to consider on nearby continental shelves and ice shelves.

Possible reasons for these long-term changes were discussed based on previous studies, but demonstrations were limited as having only temperature observations available does not allow to dig into circulation or density stratification. This led me to seek ways to better grasp long-term changes of the circulation, especially in the sector seasonally covered by the sea ice. I believe that satellite altimetry is a promising avenue toward this goal. While I tried to pave the way toward investigating long-term circulation change from satellite altimetry in seasonally sea ice-covered regions of the Southern Ocean, the task was too large to fit in the time-scale of my thesis. The first steps toward this goal, which constitutes part of my thesis include : building a robust framework for multi-satellite analysis of altimetry in sea ice-covered regions ; and investigating the long-term mean, seasonal, and shorter timescale variability of the circulation to be able to properly remove from the long-term analysis. Long-term analysis now needs to build on this framework to include more satellites, which involves significant treatment of the dataset to make sure to not include spurious change across the long time series.

What mechanisms drive the variability and changes of Southern Ocean circulation and hydrography ?

At least as important as documenting long-term change, I believe that process-understanding of underlying drivers is key for our comprehension of the Southern Ocean system. As mentioned above, I was not able to precisely attribute long-term temperature changes evidenced in **Chapter I** to specific drivers. Instead, I relied on previous studies to provide hints on the causes of the long-term trends. Investigating drivers of the mesoscale and large scale seasonal variability was however one of the main objectives of **Chapters III** and **IV**.

From the results in **Chapters III** and **IV**, winds appear as one central driver of the Southern Ocean circulation variability at seasonal time-scale and higher frequency. The westerlies drive part of the Southern Ocean circulation variability at both large and smaller spatial scales. At large scale, the mid-latitude westerlies contribute to the wind stress curl over the subpolar basin, impacting the strength of the Weddell and Ross gyres and their winter intensification. The higher-latitude easterlies also have a strong impact on the horizontal subpolar circulation variability at seasonal scale. They modulate wind stress curl over the gyres and trigger circumpolar sea level anomalies, from the propagation of wind-induced kelvin waves at the continental slope, directly impacting the seasonal cycle of the ASC, and higher frequency variability.

The sea ice is unsurprisingly another important driver of the Southern Ocean variability. Its effect may be either mechanical or thermodynamical. The mechanical effect of the sea ice points to its role in damping the local surface stress and momentum transfer from the winds to the ocean surface. Specifically, **Chapters III** and **IV** show that the interaction between the sea ice and the westerlies may create a local upwelling at the sea ice edge, driving enhanced instabilities and cyclonic eddies generation, or a winter spreading of the ASC in East Antarctica. But the sea ice is also associated with intense seasonal freshwater fluxes. At the sea ice edge, fronts formed by local meltwater supply are highly unstable, with the density of cyclonic eddies being 2 to 3 times higher than in the rest of the subpolar Southern Ocean.

Lastly, the large-scale circulation is itself a driver of the mesoscale variability. When focusing on the subpolar Southern Ocean, I find stronger eddies in the boundary of the ACC and the continental shelf and slope region close to the ASC.

How do we expect the Southern Ocean circulation and hydrography to change in the future ?

While this thesis does not tackle future projections, identifying first order processes that drive the circulation can be used to discuss potential future circulation change. A way to do this is investigating how individual processes may change in the future as response to greenhouse gas emissions. While this kind of exercise which develop plausible narrative of future change might be interesting, it is also of course limited, as not all processes have been identified, and some might be associated with complex feedback. Moreover, some processes that happen at specific temporal scales may not transfer to long-term changes. Despite these limitations, I try here to combine the main climate projections of the changes by the end of the century with the results presented here. To do that, I discuss the response of the Southern Ocean system to projected changes of what I identified as the main drivers of the subpolar Southern Ocean circulation and hydrography : namely the winds and the cryosphere.

In both **Chapters III and IV**, zonal winds have been identified as drivers of the variability of the circulation at weekly to seasonal time scales. In the Southern Ocean, the two main components of the zonal winds are the mid-latitude westerlies blowing over the ACC and higher latitude easterlies blowing over the continental shelf break. These two wind components are not projected to change the same way in the 21st century, under increased radiative forcing.

The projection on the westerlies is associated with projections of the Southern Annular Mode (SAM). Under high emission scenarios, the positive trend in the SAM is expected to continue, leading to an even stronger jet and the displacement of the westerlies belt (Lee et al., 2021). This intensification of the westerlies is expected to continue at least until 2100, except strong mitigation scenario (SSP1-2.6) for which the trend stabilizes around 2040 (Bracegirdle et al., 2020). In the context of strengthening westerlies, several mechanisms described in this thesis might occur. The large-scale negative wind stress curl over the subpolar basin might strengthen due to the acceleration of its northern component, driving further upwelling and spinning up the subpolar gyres. The long-term consequences of an intensification of these gyres are not es-

tablished yet, as the gyre systems could either reach a new equilibrium or change linearly or exponentially (Vernet et al., 2019). In any case, an intensification of the gyres is expected to have consequences on all the Southern Ocean system, through changes in its circulation, geochemistry, sea ice, interactions with the atmosphere or water mass formation (Vernet et al., 2019). Another consequence of the enhanced upwelling of the subpolar Southern Ocean may be the increased shallowing of the warm CDW. Indeed, **Chapter I** shows that these warm waters have been shallowing at a strong rate of 39 ± 9 meters per decade in the East Antarctic sector. In that study, I was not able to demonstrate the contribution to a wind stress curl trend on this shallowing trend. However, future intensification of the negative wind stress may increase it, with important consequences on sea ice, warm intrusions on the continental shelf, and stability of the Antarctic ice cap.

These increasing westerlies might as well impact the local wind stress curl anomaly at the sea ice edge. In a projection of strengthened winds, the negative ocean stress curl at the ice edge and over the MIZ would be even stronger, enhanced by the meridional gradient of zonal surface stress. In that case, the winter intensification of the northward spreading of the ASC might be even stronger. This may also enhance the winter generation of cyclonic eddies in the northern MIZ, through an intensified upwelling at the ice edge. Those cyclonic eddies can trap sea ice and advect it northward where it melts (Manucharyan and Thompson, 2017). Therefore, intensified winter upwelling at the ice edge may enhance sea ice melting. As hypothesized in **Chapter IV**, those cyclonic eddies may be the surface signature of the generation of anticyclonic, under ice, halocline eddies. If this is the case, strengthened winds at the ice shelf may generate even more anticyclonic eddies, advecting more physical and biogeochemical properties to the interior of the ice-covered subpolar basin. The projections of both the intensification of the ASC and the enhancement of the eddy generation in the MIZ as a response to strengthened westerlies might be only possible in winter conditions. Indeed they result from the interactions between westerlies and sea ice : in summer, the sea ice may be located too south for these processes to occur.

To my knowledge, there has been no clear observed trend on the position or strength of the easterlies at the Eastern Coast of Antarctica. In the future, while the 21st century changes in the westerlies stand out for the projection of all CMIP6 models, the same models do not show any consistent projected changes for the easterlies (Bracegirdle et al., 2020).

Future changes in sea ice will have important implications on the results presented here. While many uncertainty remain, change in sea ice has been linked to surface cooling and subsurface warming described in **Chapter I**. In addition, the position of the ice edge has been shown to drive strong instabilities in the MIZ when colocalized with the westerlies (**Chapter IV**), while impacting part of the variability of the ASC (**Chapter III**). There are already projections for a larger MIZ in the Arctic (Strong and Rigor, 2013). If this happens in the Southern Ocean, it may generate even more instabilities, with cyclonic eddies enhancing the sea ice melt by northward advection (Manucharyan and Thompson, 2017). However, projections of the future of the Antarctic sea ice in the 21st century remains uncertain. CMIP6 models poorly represent past

changes in sea ice cover (Roach et al., 2020). The poor agreement of these models for future 21st century projections makes us having only low confidence in the future of antarctic sea ice (Fox-Kemper et al., 2021).

While I did not discuss the ice shelves meltwater impacts in my results, they may keep on spreading the surface cooling observed in **Chapter I**, and enhance the surface mixed layer stratification through a freshening of the surface layer. This may lead to less mixing at the interface between the mixed layer and the CDW, and thus to further warming of the upper layer of the CDW (Haumann et al., 2020; Sallée et al., 2021). In fact, the warming and shallowing of the CDW documented in **Chapter I** may feedback in more meltwater from the shelves, causing more stratification, causing warming and shallowing of the CDW (Golledge et al., 2019; Sadai et al., 2020). In some regions, it has also been shown to potentially convert current fresh shelves into warm shelves in the future (Hellmer et al., 2012, 2017; Naughten et al., 2018).

I know the outcomes of the various chapters do not necessarily extend to the longer-term changes. I here discuss what could be the future changes, but with strong assumptions. I think nonetheless that linking the past changes and the shorter-term variability to implications for our understanding of future Southern Ocean system is an interesting exercise.

Further implications of the thesis : carbon cycle

The subpolar part of the Southern Ocean has major importance in basin carbon cycle (Frölicher et al., 2015), as it is where the nutrient and carbon-rich CDW are upwelled and allow large outgassing of natural carbon (Gray et al., 2018), and a spreading of the nutrients, fertilizing the biological production of the global oceans (Sarmiento et al., 2004). The upwelling driven carbon outgassing is locally partly counterbalanced by high-latitude dense water formation and export, and biological pump (Vernet et al., 2019). Recent studies have pointed the role of the horizontal circulation and the biogeochemical processes in the offshore subpolar Southern Ocean (Hoppema et al., 2015; MacGilchrist et al., 2019), previously underestimated compared to the carbon fluxes related to the meridional overturning circulation.

I discussed above that there are good reasons to think that subpolar gyres might intensify in the future as a response to strengthening mid-latitude westerlies. This intensification of the cyclonic gyres may enhance the upwelling of carbon and nutrient-rich waters (Hoppema et al., 2015). An increase in surface nutrients has actually already been described in the Weddell Gyre (Hoppema et al., 2015). While nutrient increases are unlikely to increase CO2 uptake in this region which is already characterized as a high nutrient, low chlorophyll region, the increased carbon upwelling at the surface would increase natural carbon outgassing in the gyres (Le Quéré et al., 2007). Other processes may intervene in the case of the intensification of the cyclonic gyres, such as the enhancement of the biological activity in the northern part of the subpolar Southern Ocean and in the ACC. Indeed, the Weddell gyre and the variability of its circulation is directly related to the productivity of remote ACC regions (Youngs et al., 2015). The southern branch of the gyre transports iron and krill over the shelf and export them to the Scotia sea (Thorpe et al., 2004), allowing biological productivity in the drake passage (Thompson and Youngs, 2013). An intensification of the Weddell gyre may enhance this transport of iron and krill, allowing further biogeochemical productivity and contributing further to the oceanic car-

bon sink. Future changes on the shelf are still unclear, but if CDW intrusion increases, it might increase nutrient supply on the continental shelf with higher nutrient content water-masses reaching closer to the surface, and it might also increase iron supply on the continental shelf, through increase influx of iron-rich ice-shelf meltwater.

Many uncertainties reside in these speculations, and one should not put too much weight on them. They are however useful to understand the important implications that variability and change of the subpolar Southern Ocean system may have on the carbon cycle.

2 Limitations and Caveats

This thesis draws on observations of the physics of the Southern Ocean from multiple means of observation. The various observation techniques used rely on several approximations and uncertainties. The analysis methods and scientific approaches may have limitations as well. Here, I try to enumerate and evaluate the limitations inherent to this thesis. I hope that it may help individuals that consider using similar techniques or methods to have an overview of their possibilities and constraints.

In **Chapter I**, I used a dataset of more than 10,000 eXpandables BathyThermograph profiles sampled over 25 years across the Southern Ocean to investigate long term temperature trends in its upper layer. However, both the construction of the product and the scientific conclusions have several limitations. First, there is an impact of the spatial and temporal sampling variability between each year. This impact is very difficult to evaluate. A few precautions were set up to mitigate the possible errors induced by this kind of heterogeneity. The profiles sampled too far away from the mean path of the vessel were deleted. While the circulation of the Southern Ocean is mainly circumpolar, the goal was to be independent of the zonal variations of the positions of the fronts. To dig deeper into the effects of the fronts and eddies on the trends, I colocated each path of the vessel and the position of meanders and eddies detected from satellite altimetry. Some profiles were indeed found inside eddies or meanders, but removing or keeping them in the calculation did not change the obtained trends. Moreover, the frontal regions are regions with intense interannual variability, often stronger than long-term trends, and were therefore not the focus of my study. To get rid of the temporal sampling variability, and remove potential temperature bias coming from the hydrographic seasonal cycle, I computed a daily seasonal cycle climatology over the sampling season. This climatology was then removed from each profile before computing the trends. There might be however spatial or temporal variability signals that have not been corrected, and that can hardly be evaluated.

Creating a SLA product as part of this thesis (**Chapter II**) was a great opportunity to explore an original dataset and to investigate the Southern Ocean variability in a new and innovative way (**Chapters III** and **IV**). However, the numerous processing steps, the amount of input data, in the sea ice regions make the development very challenging. There are therefore several limitations impacting the product and the subsequent studies that us or will use it.

After several decades of activity, the satellite altimetry technique can be considered a mature technology. However, its application in the ice-covered oceans, while being studied for a long time, is still young in terms of the number of datasets developed in these regions. It means that there is no precise protocol to apply and several approximations or assumptions that may or may not be used.

I list here most of the approximation I used in the development of the satellite altimetry dataset, and explain further the main one. Among the approximations are the use of a model to estimate the correlation scales for the mapping or the use of a reference satellite to correct the offset between various instruments or surfaces. The latter offeset was computed in previous studies at the sea ice edge, by colocating leads and open ocean echoes (Armitage et al., 2018; Dotto et al., 2018). However, considering the processes happening at the sea ice edge as evidenced in **Chapters III and IV**, I have low confidence in this method. Rather, I propose to use AltiKa as the reference mission, as it benefits from a continuous retracker between leads and the open ocean. Nevertheless, while I believe this method is an improvement compared to previous studies, it relies on a comparison between satellites with different instruments and orbits.

This product also draws on several assumptions. Among them, the assumption that it is possible to compute the expected variance for the mapping method recursively, or the assumption that there is 0-wind or waves in the leads. The latter assumption is common in the studies using radar measurements in the leads. However, in low sea ice concentrations, strong winds, or large leads, this may not be true. This assumption is necessary for the commonly used TFMRA retracker, which is a simple threshold retracking algorithm and does not allow the retrieval of winds and waves from the waveform. This is what I used for Sentinel-3 and Cryosat-2 missions. One improvement though is the physical retracker developed for AltiKa, which allows to retrack the signal while computing the effect of residual winds in the leads. This may be used to compute a sea state bias correction and enhance the accuracy in the sea ice regions. In any case for both retrackers, the criteria used for the selection of the echoes in the leads should not allow waveforms too impacted by the wind and waves. For this reason, I do not expect a strong error induced by this approximation in the dataset. In the end, it is extremely hard to evaluate the impact of these approximations on the SLA product due to the small or nonexistent amount of external data available to validate the measurements.

As it is explained in **Chapter II**, most of the tide gauges are in landlocked locations, badly positioned for comparison with satellite altimetry. Moreover, only few tide data is available during the SLA product 2013-2019 time period. Precise error estimate is therefore difficult. I proposed a validation by an independent altimeter, which was conducted for 2 years by comparing Sentinel-3A along track measurements with the gridded SLA product constructed using AltiKa and Cryosat-2. This validation gives an overview of the errors of the product. However, Sentinel-3A measurements may have errors as well. Thus, using data with noise as the validation reference may have enhanced the estimated errors values, therefore decreasing confidence in the applications of these products for signals with an amplitude weaker than the estimated error.

Despite the methodology which I tried to construct as the optimal way to bring answers to my scientific questions, conclusions and results may have been limited by several factors.

In **Chapter I**, the interpretation of the temperature trends was limited due to the lack of simultaneous salinity measurements. In the subpolar Southern Ocean, the density is mostly dictated by freshwater. Changes in the structure of the water column of the Southern Ocean may have a stronger signature in salinity than in temperature. Therefore, I could only make assumptions on the drivers of the temperature trends, instead of discussing density changes and associated with circulation and thermodynamic forcing changes.

One of the main limitations concerning **Chapters II, III**, and **IV** is the length of the time series. The final SLA product published in the context of this Ph.D. thesis spans 2013-2019, starting with the launch of the AltiKa satellite. The simplest way to extend the time series is by adding Envisat to the constellation of satellites used. Envisat was a Low Resolution Mode conventional satellite that measured the topography of the oceans, with a latitudinal extent high enough to entirely cover the Southern Ocean. This satellite was launched in 2002 and stopped its activity in 2012. Integrating Envisat would would have made the dataset monomission for several years, inducing a heterogeneous resolution, but would have allowed long-term and interannual variability analyses. However, and despite months working on this issue, I was not able to integrate Envisat into the final product. The reason for this is that the physical retracker algorithm I was using was found to induce a bias between the open ocean and the leads echoes. This retracker will need further development in the coming years by CLS, which will be too late for the integration of Envisat in this thesis.

Lastly, the spatial and temporal resolution of the product is not defined, as it depends on the position of the leads and the satellite tracks. This limitation has been mitigated for applications in **Chapter II**, as the filtering and seasonal averaging may have reduced the heterogeneity of the resolution. Still, a higher and homogeneous resolution may have allowed evaluating the impact of the tides and eddies on the circulation modes presented in this chapter. For eddy detection tracking in **Chapter III**, this represents an important limitation. Indeed high-latitudes are associated with a low Rossby Radius, implying eddies with spatial scales of the order of 10km (Chelton et al., 1998). The position of the satellite tracks may also impact the results for mesoscale eddies, which is why I conducted a sensitivity analysis on results, which will need further development. This issue may be overcome by a proper evaluation of the effective resolution of the dataset, as in Ballarotta et al. (2019), which I will conduct in the near future before finalising the paper presented in **Chapter IV**.

3 Perspectives

Despite my efforts to not spread myself too thinly, I thought about several prospects I did not have the time or could not set up during those three years working on this Ph.D. thesis. These perspectives relate to both technical and scientific parts of this thesis and are classified per main themes.

In-situ observations. In this thesis, I relied on in-situ observations to evaluate the temperature trends in the Southern Ocean. However, no in-situ measurements were used for the evaluation of large-scale and mesoscale variability. I actually tried to complement the eddy detection and tracking with Temperature and Salinity (T/S) profiles taken from a database merging observation from ships, moorings, Argo, and marine mammals. I also used the T/S climatology from Pauthenet et al. (2021) to transform these profiles into anomalies, colocated them with eddy observations, and tested several statistical approaches (such as a Hierarchic Ascending Classification technique) to evaluate the signature eddies detected from altimetry on the water column (as previous studies in the ice-free ocean : e.g. Pegliasco et al., 2015). While the results were promising, they were not mature enough to be presented among the diagnostics of the ice-covered eddies presented in **Chapter IV**. In the future, with more under-ice observation and more satellites integrated in regional Southern Ocean products, this kind of study will probably lead to important improvements in the ability to infer anomalies in the water column from remote observation. Combining the eddies detected from altimetry with the ones detected in situ like in Zhao et al. (2014, 2016) studies in the Arctic would allow the validation both datasets while allowing them to complement in order to go deeper into the physical analysis.

Satellite Altimetry. In the future, ocean topography datasets tracing back the early years of altimetry will be of great asset to document the long-term changes of the subpolar Southern Ocean. There are some possibilities of adding satellites such as Envisat, ERS-1, and ERS-2. Even if the precision of former satellites is lower, long-term monitoring of the large-scale geostrophic current will allow getting a direct view of the Southern Ocean circulation response to the atmospheric, cryospheric, and global oceanic circulation changes. One of satellite altimetry important asset is to monitor the full region continuously for decades. Another way to improve the dataset is to add more satellites before the interpolation of the along-track measurements. The satellite constellation is now larger than ever, and it is technically possible to implement recently launched altimeters in the multimission product. Satellites such as Jason-3, Sentinel 3-B, or Cristal should be added in the future. This will be great for improving the resolution and the observability of smaller-scale variability. This however represents a very large amount of work in the acquisition, processing, and merging of all the satellites and might not be done before several years. Both expanding the length of the time series and adding satellites for a better resolution have been set as future goals of the CNES (Centre National des Etudes Spatiales) and CLS (Collecte Localisation Satellite), and I might be involved indirectly in such work in the future. In the long run, ice-covered sea level topography products may be integrated into the global operational products, which would be great to have a quasi-instantaneous large-scale view of the Southern Ocean dynamics at any time. It might be also a great asset for oceanographic campaigns in these regions, to spot eddies or interesting circulation features at the time of the expedition.

Long term trends in the Southern Ocean. The results of the Chapter I of this manuscript show long-term temperature trends of several regions of the Southern Ocean, and how they compare to interannual variability. One easy perspective of this work is to continue to sample and monitor the temperature trends from that specific section. The longer the observation last, the easier it will be to extract the long-term changes from the shorter variability. Other perspectives regarding the Southern Ocean long-term trends are related to the satellite observations. As stated in the technical part of this Perspectives section, I would have loved to look at longer trends in the ocean topography and geostrophic circulation, but was unable to do so due to the shortness of the satellite product time series. This would have allowed not only to infer processes that may happen in a changing climate but to observe them directly. Future development of such datasets may lead to this opportunity. In particular, with SURVOSTRAL, and other long-term repeated sections of Southern Ocean, having these datasets covering similar periods than satellite altimetry will be an incredible chance to combine surface and in-depth ocean, hydrography, and dynamics. This would allow observing the interactions between the structure of the ocean and changes in its dynamics, with applications on the monitoring of the Southern Ocean meridional overturning circulation, heat transport at the shelf or within the gyres.

Ice-Ocean interactions. One of the main angle of my PhD is to better understand the role of the cryosphere on the circulation and hydrography of the subpolar Southern Ocean.

There might be processes discussed in this thesis that my of interest to better understand the ocean - sea ice interactions. On the mechanical processes first, about how the sea ice impacts the momentum transfer between the winds and the ocean surface, and also inputs momentum itself when drifting. The way this is implemented in the climate models and when computing that process is rather simple and has been used several times in this thesis as the Ocean Stress Curl (**Chapters III** and **IV**). While a more accurate implementation of that process requires more observation of sea ice shape and properties (Tsamados et al., 2014; Martin et al., 2016), improved observations of ocean circulation response to wind and sea ice mechanical forcing may help uncovering further this process. As for its importance in the circulation processes, better representing the sea ice contribution of momentum input and modulation of the wind-induced surface stress might lead to strong improvements of the climate models. Other further perspectives on the ocean - sea ice interactions would be the to further explore the feedbacks between the sea ice-induced heat and freshwater fluxes and the ocean circulation and hydrography. These processes may be addressed in various ways, such as better understanding the effect of the circulation of large polynyas openings (Campbell et al., 2019) and their feedbacks on ocean circulation (de Lavergne et al., 2014). Following the framework of this thesis, the ocean - sea ice interactions might be explored at the seasonal time scale as well, by exploring for example the north-south asymetry of the salt and freshwater fluxes during melt and formation seasons (Abernathey et al., 2016; Pellichero et al., 2018). This has been studied in specific regions (Hattermann, 2018), but not at the whole subpolar basin scale.

As I focused on the zonal dynamics in **Chapter III**, I may have pursued in looking at the meridional dynamics, and particularly at the cross-shelf transport. The ocean topography dataset might allow looking at both direct advective and eddy-mediated cross-shelf transport. In fact,

the whole regional circulation may have strong impact on the ice shelves, directly impacting their melting rates and the stability of the Antarctic ice cap. I was actually involved in the work of Julius Lauber et al., who used the dataset I developed to show that the remote sea level forcing and wind, along with local wind as well, contributes inflow of warm water below the Fimbulisen ice shelf (paper in prep.). The mechanism is the same as the second mode presented in **Chapter III**, with remote winds forcing the SLA, resulting in an ASC anomaly. This contributes to a weaker ASC in the three last years of the record, bringing warm offshore water closer to the sill, where it may be pushed over the edge of the cavity by local winds. These inflows were directly linked to the melting rate of the ice shelf, impacting the meltwater fluxes as well and the regional ocean circulation and hydrography. I think it would be very interesting to conduct similar studies on other cavities, to further identify the mechanisms bringing heat toward the ice shelves.

More broadly, in the work presented here, I considered the subpolar Southern Ocean the same way all around Antarctica, with only few consideration for regional processes. This methodological choice comes from the wish to start from the large scale and very general processes, to then tighten the focus on smaller and more regional processes. In this thesis, I only had the time to reach the mesoscale processes. But the logical follow up to this would be to look at more regional processes, such as ASC local variations over specific regions and implications on warm water intrusions, or polynya events.

4 General Comments

The Southern Ocean is a fascinating region. Its remoteness from inhabited regions, harsh climatic conditions, and outstanding biodiversity close to Antarctica raise curiosity, and sometimes make people dream. This is the case for me, and as I am writing these lines, I will be in a few days boarding on *l'Astrolabe* to finally meet in real life the ocean I spent more than three years studying. But working on the Southern Ocean was also very exciting for its physics, with complex processes still largely unknown, but having considerable importance on the global climate. I feel grateful for having the opportunity to work on this region of the world, and even more in this context of climate change, as better understanding the system and projecting its changes may help raise awareness about the issue and fight it. I now look forward to witnessing what the climate science community will achieve in the future, and I hope that I will have the opportunity to continue being involved in the progress toward a better knowledge of the Southern Ocean.

Bibliographie

Aagaard, K. and Carmack, E. C. (1989). The role of sea ice and other fresh water in the Arctic circulation. *Journal of Geophysical Research : Oceans*, 94(C10) :14485–14498. _eprint : https ://onlinelibrary.wiley.com/doi/pdf/10.1029/JC094iC10p14485.

Abernathey, R., Marshall, J., and Ferreira, D. (2011). The Dependence of Southern Ocean Meridional Overturning on Wind Stress. *Journal of Physical Oceanography*, 41(12) :2261–2278. Publisher : American Meteorological Society Section : Journal of Physical Oceanography.

Abernathey, R. P., Cerovecki, I., Holland, P. R., Newsom, E., Mazloff, M., and Talley, L. D. (2016). Water-mass transformation by sea ice in the upper branch of the Southern Ocean overturning. *Nature Geoscience*, 9(8) :596–601. Number : 8 Publisher : Nature Publishing Group.

Abrahamsen, E. P., Meijers, A. J. S., Polzin, K. L., Naveira Garabato, A. C., King, B. A., Firing, Y. L., Sallée, J.-B., Sheen, K. L., Gordon, A. L., Huber, B. A., and Meredith, M. P. (2019). Stabilization of dense Antarctic water supply to the Atlantic Ocean overturning circulation. *Nature Climate Change*, 9(10) :742–746. Bandiera_abtest : a Cg_type : Nature Research Journals Number : 10 Primary_atype : Research Publisher : Nature Publishing Group Subject_term : Climate change ;Physical oceanography Subject_term_id : climate-change ;physical-oceanography.

Abram, N. J., Mulvaney, R., Vimeux, F., Phipps, S. J., Turner, J., and England, M. H. (2014). Evolution of the Southern Annular Mode during the past millennium. *Nature Climate Change*, 4(7) :564–569. Bandiera_abtest : a Cg_type : Nature Research Journals Number : 7 Primary_atype : Research Publisher : Nature Publishing Group Subject_term : Atmospheric dynamics ;Palaeoclimate Subject_term_id : atmospheric-dynamics ;palaeoclimate.

Akhoudas, C. (2019). *Un nouveau regard sur la dynamique de l'océan Austral et ses interactions avec la cryosphère révélé par une approche isotopique*. These en préparation, Sorbonne université.

Akhoudas, C. H., Sallée, J.-B., Haumann, F. A., Meredith, M. P., Garabato, A. N., Reverdin, G., Jullion, L., Aloisi, G., Benetti, M., Leng, M. J., and Arrowsmith, C. (2021). Ventilation of the abyss in the Atlantic sector of the Southern Ocean. *Scientific Reports*, 11(1) :6760. Bandiera_abtest : a Cc_license_type : cc_by Cg_type : Nature Research Journals Number : 1 Primary_atype : Research Publisher : Nature Publishing Group Subject_term : Ocean sciences ;Physical oceanography Subject_term_id : ocean-sciences ;physical-oceanography.

Allison, I. (1981). Antarctic ice growth and oceanic heat flux. *Sea level, ice and climatic change. Proc. Canberra symposium, December 1979*, 131.

Allison, L. C., Johnson, H. L., Marshall, D. P., and Munday, D. R. (2010). Where do winds drive the Antarctic Circumpolar Current ? *Geophysical Research Letters*, 37(12). _eprint : https ://onlinelibrary.wiley.com/doi/pdf/10.1029/2010GL043355.

Amores, A., Jordà, G., Arsouze, T., and Sommer, J. L. (2018). Up to What Extent Can We Characterize Ocean Eddies Using Present-Day Gridded Altimetric Products ? *Journal of Geophysical Research : Oceans*, 123(10) :7220–7236. _eprint : https ://agupubs.onlinelibrary.wiley.com/doi/pdf/10.1029/2018JC014140.

Aoki, S. (2002). Coherent sea level response to the Antarctic Oscillation. *Geophysical Research Letters*, 29(20) :11–1–11–4. _eprint : https ://agupubs.onlinelibrary.wiley.com/doi/pdf/10.1029/2002GL015733.

Aoki, S., Bindoff, N. L., and Church, J. A. (2005). Interdecadal water mass changes in the Southern Ocean between 30°E and 160°E. *Geophysical Research Letters*, 32(7). _eprint : https ://agupubs.onlinelibrary.wiley.com/doi/pdf/10.1029/2004GL022220.

Aoki, S., Kitade, Y., Shimada, K., Ohshima, K. I., Tamura, T., Bajish, C. C., Moteki, M., and Rintoul, S. R. (2013). Widespread freshening in the Seasonal Ice Zone near 140°E off the Adélie Land Coast, Antarctica, from 1994 to 2012. *Journal of Geophysical Research : Oceans*, 118(11) :6046–6063. Number : 11.

Armitage, T. W. K., Bacon, S., Ridout, A. L., Thomas, S. F., Aksenov, Y., and Wingham, D. J. (2016). Arctic sea surface height variability and change from satellite radar altimetry and GRACE, 2003–2014. *Journal of Geophysical Research : Oceans*, 121(6) :4303–4322. _eprint : https ://agupubs.onlinelibrary.wiley.com/doi/pdf/10.1002/2015JC011579.

Armitage, T. W. K., Kwok, R., Thompson, A. F., and Cunningham, G. (2018). Dynamic Topography and Sea Level Anomalies of the Southern Ocean : Variability and Teleconnections. *Journal of Geophysical Research : Oceans*, 123(1) :613–630. _eprint : https ://agupubs.onlinelibrary.wiley.com/doi/pdf/10.1002/2017JC013534.

Armour, K. C., Marshall, J., Scott, J. R., Donohoe, A., and Newsom, E. R. (2016). Southern Ocean warming delayed by circumpolar upwelling and equatorward transport. *Nature Geoscience*, 9(7) :549–554. Number : 7 Publisher : Nature Publishing Group.

Assmann, K. M. and Timmermann, R. (2005). Variability of dense water formation in the Ross Sea. *Ocean dynamics*, 55(2) :68–87. Number : 2.

Auger, M., Prandi, P., and Sallee, J.-B. (2021a). Southern Ocean Sea Level Anomaly in the Sea Ice-Covered Sector From Multimission Satellite Observations.

Auger, M., Prandi, P., and Sallée, J.-B. (2021b). Daily Southern Ocean Sea Level Anomaly And Geostrophic Currents from multimission altimetry, 2013-2019. Type : dataset.

Auger, M., Sallee, J.-B., Prandi, P., and Naveira Garabato, A. C. (2021c). Southern Ocean Seasonal Variability in the Sea Ice-Covered Sector From Multimission Satellite Observations of Sea Level Anomaly.

Auriol, A. and Tourain, C. (2010). DORIS system : The new age. *Advances in Space Research*, 46(12) :1484–1496.

Ballarotta, M., Ubelmann, C., Pujol, M.-I., Taburet, G., Fournier, F., Legeais, J.-F., Faugère, Y., Delepoulle, A., Chelton, D., Dibarboure, G., and Picot, N. (2019). On the resolutions of ocean altimetry maps. *Ocean Science*, 15(4) :1091–1109. Publisher : Copernicus GmbH.

Banerjee, A., Fyfe, J. C., Polvani, L. M., Waugh, D., and Chang, K.-L. (2020). A pause in Southern Hemisphere circulation trends due to the Montreal Protocol. *Nature*, 579(7800) :544–548. Bandiera_abtest : a Cg_type : Nature Research Journals Number : 7800 Primary_atype : Research Publisher : Nature Publishing Group Subject_term : Atmospheric dynamics ;Attribution Subject_term_id : atmospheric-dynamics ;attribution.

Barker, L. D. L. and Whitcomb, L. L. (2016). A preliminary survey of underwater robotic vehicle design and navigation for under-ice operations. In *2016 IEEE/RSJ International Conference on Intelligent Robots and Systems (IROS)*, pages 2028–2035. ISSN : 2153-0866.

Biancamaria, S., Lettenmaier, D. P., and Pavelsky, T. M. (2016). The SWOT Mission and Its Capabilities for Land Hydrology. *Surveys in Geophysics*, 37(2) :307–337.

Bintanja, R., van Oldenborgh, G. J., Drijfhout, S. S., Wouters, B., and Katsman, C. A. (2013). Important role for ocean warming and increased ice-shelf melt in Antarctic sea-ice expansion. *Nature Geoscience*, 6(5) :376–379. Number : 5 Publisher : Nature Publishing Group.

Black, H. D. and Eisner, A. (1984). Correcting satellite Doppler data for tropospheric effects. *Journal of Geophysical Research : Atmospheres*, 89(D2) :2616–2626. _eprint : https ://agupubs.onlinelibrary.wiley.com/doi/pdf/10.1029/JD089iD02p02616.

Bonaduce, A., Cipollone, A., Johannessen, J. A., Staneva, J., Raj, R. P., and Aydogdu, A. (2021). Ocean Mesoscale Variability : A Case Study on the Mediterranean Sea From a Re-Analysis Perspective. *Frontiers in Earth Science*, 9 :816.

Bracegirdle, T. J., Krinner, G., Tonelli, M., Haumann, F. A., Naughten, K. A., Rackow, T., Roach, L. A., and Wainer, I. (2020). Twenty first century changes in Antarctic and Southern Ocean surface climate in CMIP6. *Atmospheric Science Letters*, 21(9) :e984. _eprint : https ://rmets.onlinelibrary.wiley.com/doi/pdf/10.1002/asl.984.

Brachet, S., Traon, P. Y. L., and Provost, C. L. (2004). Mesoscale variability from a high-resolution model and from altimeter data in the North Atlantic Ocean. *Journal of Geophysical Research : Oceans*, 109(C12). _eprint : https ://agupubs.onlinelibrary.wiley.com/doi/pdf/10.1029/2004JC002360.

Bretherton, F. P., Davis, R. E., and Fandry, C. B. (1976). A technique for objective analysis and design of oceanographic experiments applied to MODE-73. *Deep Sea Research and Oceanographic Abstracts*, 23(7) :559–582.

Brodzik, M. J., Billingsley, B., Haran, T., Raup, B., and Savoie, M. H. (2014). Correction : Brodzik, M.J., et al. EASE-Grid 2.0 : Incremental but Significant Improvements for Earth-Gridded Data Sets. ISPRS International Journal of Geo-Information 2012, 1, 32–45. *ISPRS International Journal of Geo-Information*, 3(3) :1154–1156. Number : 3 Publisher : Multidisciplinary Digital Publishing Institute.

Bromwich, D. H., Nicolas, J. P., and Monaghan, A. J. (2011). An Assessment of Precipitation Changes over Antarctica and the Southern Ocean since 1989 in Contemporary Global Reanalyses. *Journal of Climate*, 24(16) :4189–4209. Publisher : American Meteorological Society Section : Journal of Climate.

Bronselaer, B., Winton, M., Griffies, S. M., Hurlin, W. J., Rodgers, K. B., Sergienko, O. V., Stouffer, R. J., and Russell, J. L. (2018). Change in future climate due to Antarctic meltwater. *Nature*, 564(7734) :53–58. Bandiera_abtest : a Cg_type : Nature Research Journals Number : 7734 Primary_atype : Research Publisher : Nature Publishing Group Subject_term : Climate and Earth system modelling ;Climate-change impacts ;Physical oceanography ;Projection and prediction Subject_term_id : climate-and-earth-system-modelling ;climate-change-impacts ;physical-oceanography ;projection-and-prediction.

Bulczak, A. I., Bacon, S., Garabato, A. C. N., Ridout, A., Sonnewald, M. J. P., and Laxon, S. W. (2015). Seasonal variability of sea surface height in the coastal waters and deep basins of the Nordic Seas. *Geophysical Research Letters*, 42(1) :113–120. _eprint : https ://agupubs.onlinelibrary.wiley.com/doi/pdf/10.1002/2014GL061796.

Böning, C. W., Dispert, A., Visbeck, M., Rintoul, S. R., and Schwarzkopf, F. U. (2008a). The response of the Antarctic Circumpolar Current to recent climate change. *Nature Geoscience*, 1(12) :864–869. Bandiera_abtest : a Cg_type : Nature Research Journals Number : 12 Primary_atype : Research Publisher : Nature Publishing Group.

Böning, C. W., Dispert, A., Visbeck, M., Rintoul, S. R., and Schwarzkopf, F. U. (2008b). The response of the Antarctic Circumpolar Current to recent climate change. *Nature Geoscience*, 1(12) :864–869. Number : 12.

Callahan, P. S. (1984). Ionospheric Variations Affecting Altimeter Measurements : A Brief Synopsis. *Marine Geodesy*, 8(1-4) :249–263. Publisher : Taylor & Francis _eprint : https ://-doi.org/10.1080/15210608409379505.

Campbell, E. C., Wilson, E. A., Moore, G. W. K., Riser, S. C., Brayton, C. E., Mazloff, M. R., and Talley, L. D. (2019). Antarctic offshore polynyas linked to Southern Hemisphere climate anomalies. *Nature*, 570(7761) :319–325. Bandiera_abtest : a Cg_type : Nature Research Journals Number : 7761 Primary_atype : Research Publisher : Nature Publishing

Group Subject_term : Atmospheric dynamics ;Climate and Earth system modelling ;Cryospheric science ;Physical oceanography Subject_term_id : atmospheric-dynamics ;climate-and-earth-system-modelling ;cryospheric-science ;physical-oceanography.

Carrere, L., Lyard, F., Cancet, M., and Guillot, A. (2015). FES 2014, a new tidal model on the global ocean with enhanced accuracy in shallow seas and in the Arctic region. 17 :5481. Conference Name : EGU General Assembly Conference Abstracts.

Carrère, L. and Lyard, F. (2003). Modeling the barotropic response of the global ocean to atmospheric wind and pressure forcing - comparisons with observations. *Geophysical Research Letters*, 30(6). _eprint : https ://agupubs.onlinelibrary.wiley.com/doi/pdf/10.1029/2002GL016473.

Cartwright, D. E. and Tayler, R. J. (1971). New Computations of the Tide-generating Potential. *Geophysical Journal International*, 23(1) :45–73.

Castagno, P., Capozzi, V., DiTullio, G. R., Falco, P., Fusco, G., Rintoul, S. R., Spezie, G., and Budillon, G. (2019). Rebound of shelf water salinity in the Ross Sea. *Nature Communications*, 10(1) :5441. Bandiera_abtest : a Cc_license_type : cc_by Cg_type : Nature Research Journals Number : 1 Primary_atype : Research Publisher : Nature Publishing Group Subject_term : Ocean sciences ;Physical oceanography Subject_term_id : ocean-sciences ;physical-oceanography.

Chaigneau, A., Morrow, R. A., and Rintoul, S. R. (2004). Seasonal and interannual evolution of the mixed layer in the Antarctic Zone south of Tasmania. *Deep Sea Research Part I : Oceanographic Research Papers*, 51(12) :2047–2072. Number : 12.

Chapman, C. C., Lea, M.-A., Meyer, A., Sallée, J.-B., and Hindell, M. (2020). Defining Southern Ocean fronts and their influence on biological and physical processes in a changing climate. *Nature Climate Change*, 10(3) :209–219. Number : 3 Publisher : Nature Publishing Group.

Chavanne, C. P., Heywood, K. J., Nicholls, K. W., and Fer, I. (2010). Observations of the Antarctic Slope Undercurrent in the southeastern Weddell Sea. *Geophysical Research Letters*, 37(13). _eprint : https ://agupubs.onlinelibrary.wiley.com/doi/pdf/10.1029/2010GL043603.

Chelton, D. B. (2013). Mesoscale eddy effects. *Nature Geoscience*, 6(8) :594–595. Bandiera_abtest : a Cg_type : Nature Research Journals Number : 8 Primary_atype : News & Views Publisher : Nature Publishing Group Subject_term : Atmospheric dynamics ;Physical oceanography Subject_term_id : atmospheric-dynamics ;physical-oceanography.

Chelton, D. B., deSzoeke, R. A., Schlax, M. G., Naggar, K. E., and Siwertz, N. (1998). Geographical Variability of the First Baroclinic Rossby Radius of Deformation. *Journal of Physical Oceanography*, 28(3) :433–460. Publisher : American Meteorological Society Section : Journal of Physical Oceanography.

Chelton, D. B., Schlax, M. G., and Samelson, R. M. (2011). Global observations of nonlinear mesoscale eddies. *Progress in Oceanography*, 91(2) :167–216.

Chelton, D. B., Schlax, M. G., Samelson, R. M., and Szoeke, R. A. d. (2007). Global observations of large oceanic eddies. *Geophysical Research Letters*, 34(15). _eprint : https ://agupubs.onlinelibrary.wiley.com/doi/pdf/10.1029/2007GL030812.

Cheng, Y., Xu, Q., Gao, L., Li, X., Zou, B., and Liu, T. (2019). Sea State Bias Variability in Satellite Altimetry Data. *Remote Sensing*, 11(10) :1176. Number : 10 Publisher : Multidisciplinary Digital Publishing Institute.

Chidichimo, M. P., Donohue, K. A., Watts, D. R., and Tracey, K. L. (2014). Baroclinic Transport Time Series of the Antarctic Circumpolar Current Measured in Drake Passage. *Journal of Physical Oceanography*, 44(7) :1829–1853. Publisher : American Meteorological Society Section : Journal of Physical Oceanography.

Cohanim, K., Zhao, K. X., and Stewart, A. L. (2021). Dynamics of Eddies Generated by Sea Ice Leads. *Journal of Physical Oceanography*, 51(10) :3071–3092. Publisher : American Meteorological Society Section : Journal of Physical Oceanography.

Colin de Verdière, A. (1989). On the interaction of wind and buoyancy driven gyres. *Journal of Marine Research*, 47(3) :595–633.

Comiso, J. C., Meier, W. N., and Gersten, R. (2017). Variability and trends in the Arctic Sea ice cover : Results from different techniques. *Journal of Geophysical Research : Oceans*, 122(8) :6883–6900. _eprint : https ://agupubs.onlinelibrary.wiley.com/doi/pdf/10.1002/2017JC012768.

Cook, A. J., Holland, P. R., Meredith, M. P., Murray, T., Luckman, A., and Vaughan, D. G. (2016). Ocean forcing of glacier retreat in the western Antarctic Peninsula. *Science*, 353(6296) :283–286. Publisher : American Association for the Advancement of Science Section : Report.

Cunningham, S. A., Alderson, S. G., King, B. A., and Brandon, M. A. (2003). Transport and variability of the Antarctic Circumpolar Current in Drake Passage. *Journal of Geophysical Research : Oceans*, 108(C5). _eprint : https ://agupubs.onlinelibrary.wiley.com/doi/pdf/10.1029/2001JC001147.

Darelius, E., Fer, I., and Nicholls, K. W. (2016). Observed vulnerability of Filchner-Ronne Ice Shelf to wind-driven inflow of warm deep water. *Nature Communications*, 7(1) :12300. Bandiera_abtest : a Cc_license_type : cc_by Cg_type : Nature Research Journals Number : 1 Primary_atype : Research Publisher : Nature Publishing Group Subject_term : Cryospheric science ;Physical oceanography Subject_term_id : cryospheric-science ;physical-oceanography.

de Lavergne, C., Palter, J. B., Galbraith, E. D., Bernardello, R., and Marinov, I. (2014). Cessation of deep convection in the open Southern Ocean under anthropogenic climate change. *Nature Climate Change*, 4(4) :278–282. Number : 4.

Deacon, G. E. R. (1979). The Weddell gyre. *Deep Sea Research Part A. Oceanographic Research Papers*, 26(9) :981–995.

Desai, S., Wahr, J., and Beckley, B. (2015). Revisiting the pole tide for and from satellite altimetry. *Journal of Geodesy*, 89(12) :1233–1243.

Desbruyères, D. G., Purkey, S. G., McDonagh, E. L., Johnson, G. C., and King, B. A. (2016). Deep and abyssal ocean warming from 35 years of repeat hydrography. *Geophysical Research Letters*, 43(19) :10,356–10,365. _eprint : https ://onlinelibrary.wiley.com/doi/pdf/10.1002/2016GL070413.

Desportes, C., Obligis, E., and Eymard, L. (2006). On Wet Tropospheric Correction for Altimetry in Coastal Regions. In *2006 IEEE MicroRad*, pages 228–234.

DeVries, T. and Primeau, F. (2011). Dynamically and Observationally Constrained Estimates of Water-Mass Distributions and Ages in the Global Ocean. *Journal of Physical Oceanography*, 41(12) :2381–2401. Publisher : American Meteorological Society Section : Journal of Physical Oceanography.

Dinardo, S., Lucas, B., and Benveniste, J. (2015). Sentinel-3 STM SAR ocean retracking algorithm and SAMOSA model. In *2015 IEEE International Geoscience and Remote Sensing Symposium (IGARSS)*, pages 5320–5323. ISSN : 2153-7003.

Doddridge, E. W., Marshall, J., Song, H., Campin, J.-M., and Kelley, M. (2021). Southern Ocean Heat Storage, Reemergence, and Winter Sea Ice Decline Induced by Summertime Winds. *Journal of Climate*, 34(4) :1403–1415. Publisher : American Meteorological Society Section : Journal of Climate.

Donlon, C., Berruti, B., Buongiorno, A., Ferreira, M. H., Féménias, P., Frerick, J., Goryl, P., Klein, U., Laur, H., Mavrocordatos, C., Nieke, J., Rebhan, H., Seitz, B., Stroede, J., and Sciarra, R. (2012). The Global Monitoring for Environment and Security (GMES) Sentinel-3 mission. *Remote Sensing of Environment*, 120 :37–57.

Donohue, K. A., Tracey, K. L., Watts, D. R., Chidichimo, M. P., and Chereskin, T. K. (2016). Mean Antarctic Circumpolar Current transport measured in Drake Passage. *Geophysical Research Letters*, 43(22) :11,760–11,767. _eprint : https ://agupubs.onlinelibrary.wiley.com/doi/pdf/10.1002/2016GL070319.

Dotto, T. S., Garabato, A. N., Bacon, S., Tsamados, M., Holland, P. R., Hooley, J., FrajkaWilliams, E., Ridout, A., and Meredith, M. P. (2018). Variability of the Ross Gyre, Southern Ocean : Drivers and Responses Revealed by Satellite Altimetry. *Geophysical Research Letters*, 45(12) :6195–6204. _eprint : https ://agupubs.onlinelibrary.wiley.com/doi/pdf/10.1029/2018GL078607.

Dowdeswell, J. A., Evans, J., Mugford, R., Griffiths, G., McPhail, S., Millard, N., Stevenson, P., Brandon, M. A., Banks, C., Heywood, K. J., Price, M. R., Dodd, P. A., Jenkins, A., Nicholls, K. W., Hayes, D., Abrahamsen, E. P., Tyler, P., Bett, B., Jones, D., Wadhams, P., Wilkinson, J. P., Stansfield, K., and Ackley, S. (2008). Autonomous underwater vehicles (AUVs) and investigations of the ice–ocean interface in Antarctic and Arctic waters. *Journal of Glaciology*, 54(187) :661–672. Publisher : Cambridge University Press.

Drinkwater, M. R., Kwok, R., Winebrenner, D. P., and Rignot, E. (1991). Multifrequency polarimetric synthetic aperture radar observations of sea ice. *Journal of Geophysical Research : Oceans*, 96(C11) :20679–20698. _eprint : https ://agupubs.onlinelibrary.wiley.com/doi/pdf/10.1029/91JC01915.

Drucker, R., Martin, S., and Kwok, R. (2011). Sea ice production and export from coastal polynyas in the Weddell and Ross Seas. *Geophysical Research Letters*, 38(17). _eprint : https ://onlinelibrary.wiley.com/doi/pdf/10.1029/2011GL048668.

Ducet, N., Traon, P. Y. L., and Reverdin, G. (2000). Global high-resolution mapping of ocean circulation from TOPEX/Poseidon and ERS-1 and -2. *Journal of Geophysical Research : Oceans*, 105(C8) :19477–19498. _eprint : https ://agupubs.onlinelibrary.wiley.com/doi/pdf/10.1029/2000JC900063.

Dufour, C. O., Sommer, J. L., Zika, J. D., Gehlen, M., Orr, J. C., Mathiot, P., and Barnier, B. (2012). Standing and Transient Eddies in the Response of the Southern Ocean Meridional Overturning to the Southern Annular Mode. *Journal of Climate*, 25(20) :6958–6974. Publisher : American Meteorological Society Section : Journal of Climate.

Durack, P. J. and Wijffels, S. E. (2010). Fifty-Year Trends in Global Ocean Salinities and Their Relationship to Broad-Scale Warming. *Journal of Climate*, 23(16) :4342–4362. Publisher : American Meteorological Society Section : Journal of Climate.

Durack, P. J., Wijffels, S. E., and Matear, R. J. (2012). Ocean Salinities Reveal Strong Global Water Cycle Intensification During 1950 to 2000. *Science*, 336(6080) :455–458. Publisher : American Association for the Advancement of Science Section : Report.

Eayrs, C., Li, X., Raphael, M. N., and Holland, D. M. (2021). Rapid decline in Antarctic sea ice in recent years hints at future change. *Nature Geoscience*, 14(7) :460–464. Bandiera_abtest : a Cg_type : Nature Research Journals Number : 7 Primary_atype : Reviews Publisher : Nature Publishing Group Subject_term : Atmospheric dynamics ;Climate and Earth system modelling ;Climate-change impacts ;Cryospheric science ;Projection and prediction Subject_term_id : atmospheric-dynamics ;climate-and-earth-system-modelling ;climate-change-impacts ;cryospheric-science ;projection-and-prediction.

Edwards, T. L., Nowicki, S., Marzeion, B., Hock, R., Goelzer, H., Seroussi, H., Jourdain, N. C., Slater, D. A., Turner, F. E., Smith, C. J., McKenna, C. M., Simon, E., Abe-Ouchi, A., Gregory, J. M., Larour, E., Lipscomb, W. H., Payne, A. J., Shepherd, A., Agosta, C., Alexander, P., Albrecht, T., Anderson, B., Asay-Davis, X., Aschwanden, A., Barthel, A., Bliss, A., Calov, R., Chambers, C., Champollion, N., Choi, Y., Cullather, R., Cuzzone, J., Dumas, C., Felikson, D., Fettweis, X., Fujita, K., Galton-Fenzi, B. K., Gladstone, R., Golledge, N. R., Greve, R., Hattermann, T., Hoffman, M. J., Humbert, A., Huss, M., Huybrechts, P., Immerzeel, W., Kleiner, T., Kraaijenbrink, P., Le clec'h, S., Lee, V., Leguy, G. R., Little, C. M., Lowry, D. P., Malles, J.-H., Martin, D. F., Maussion, F., Morlighem, M., O'Neill, J. F., Nias, I., Pattyn, F., Pelle, T., Price, S. F., Quiquet, A., Radić, V., Reese, R., Rounce, D. R., Rückamp, M., Sakai, A., Shafer, C., Schlegel, N.-J., Shannon, S., Smith, R. S., Straneo, F., Sun, S., Tarasov, L., Trusel, L. D., Van Breedam, J., van de Wal, R.,

van den Broeke, M., Winkelmann, R., Zekollari, H., Zhao, C., Zhang, T., and Zwinger, T. (2021). Projected land ice contributions to twenty-first-century sea level rise. *Nature*, 593(7857) :74–82. Bandiera_abtest : a Cg_type : Nature Research Journals Number : 7857 Primary_atype : Research Publisher : Nature Publishing Group Subject_term : Climate and Earth system modelling ;Cryospheric science ;Projection and prediction Subject_term_id : climate-and-earth-system-modelling ;cryospheric-science ;projection-and-prediction.

Eriksen, C., Osse, T., Light, R., Wen, T., Lehman, T., Sabin, P., Ballard, J., and Chiodi, A. (2001). Seaglider : a long-range autonomous underwater vehicle for oceanographic research. *IEEE Journal of Oceanic Engineering*, 26(4) :424–436. Conference Name : IEEE Journal of Oceanic Engineering.

Fahrbach, E., Peterson, R. G., Rohardt, G., Schlosser, P., and Bayer, R. (1994). Suppression of bottom water formation in the southeastern Weddell sea. *Deep Sea Research Part I : Oceanographic Research Papers*, 41(2) :389–411.

Farneti, R., Delworth, T. L., Rosati, A. J., Griffies, S. M., and Zeng, F. (2010). The Role of Mesoscale Eddies in the Rectification of the Southern Ocean Response to Climate Change. *Journal of Physical Oceanography*, 40(7) :1539–1557. Publisher : American Meteorological Society Section : Journal of Physical Oceanography.

Flexas, M. M., Schodlok, M. P., Padman, L., Menemenlis, D., and Orsi, A. H. (2015). Role of tides on the formation of the Antarctic Slope Front at the Weddell-Scotia Confluence. *Journal of Geophysical Research : Oceans*, 120(5) :3658–3680. _eprint : https ://agupubs.onlinelibrary.wiley.com/doi/pdf/10.1002/2014JC010372.

Foppert, A., Rintoul, S. R., and England, M. H. (2019). Along-Slope Variability of Cross-Slope Eddy Transport in East Antarctica. *Geophysical Research Letters*, 46(14) :8224–8233. _eprint : https ://agupubs.onlinelibrary.wiley.com/doi/pdf/10.1029/2019GL082999.

Fox-Kemper, B., Hewitt, H., Xiao, C., Aðalgeirsdóttir, G., Drijfhout, S., Edwards, T., Golledge, N., Hemer, M., Kopp, R., Krinner, G., Mix, A., Notz, D., Nowicki, S., Nurhati, I., Ruiz, L., Sallée, J.-B., Slangen, A., and Yu, Y. (2021). Ocean, cryosphere, and sea level change. In : IPCC AR6 Climate Change 2021 : The Physical Science Basis.

Frölicher, T. L., Sarmiento, J. L., Paynter, D. J., Dunne, J. P., Krasting, J. P., and Winton, M. (2014). Dominance of the Southern Ocean in Anthropogenic Carbon and Heat Uptake in CMIP5 Models. *Journal of Climate*, 28(2) :862–886. Number : 2.

Frölicher, T. L., Sarmiento, J. L., Paynter, D. J., Dunne, J. P., Krasting, J. P., and Winton, M. (2015). Dominance of the Southern Ocean in Anthropogenic Carbon and Heat Uptake in CMIP5 Models. *Journal of Climate*, 28(2) :862–886. Publisher : American Meteorological Society Section : Journal of Climate.

Fu, L.-L., Christensen, E. J., Yamarone, C. A., Lefebvre, M., Ménard, Y., Dorrer, M., and Escudier, P. (1994). TOPEX/POSEIDON mission overview. *Journal of Geophysical Research : Oceans*, 99(C12) :24369–24381. _eprint : https ://agupubs.onlinelibrary.wiley.com/doi/pdf/10.1029/94JC01761.

Fučkar, N. S. and Vallis, G. K. (2007). Interhemispheric influence of surface buoyancy conditions on a circumpolar current. *Geophysical Research Letters*, 34(14). _eprint : https ://onlinelibrary.wiley.com/doi/pdf/10.1029/2007GL030379.

Gao, L., Rintoul, S. R., and Yu, W. (2018). Recent wind-driven change in Subantarctic Mode Water and its impact on ocean heat storage. *Nature Climate Change*, 8(1) :58–63. Number : 1.

Garabato, A. C. N., Dotto, T. S., Hooley, J., Bacon, S., Tsamados, M., Ridout, A., Frajka-Williams, E. E., HerraizBorreguero, L., Holland, P. R., Heorton, H. D. B. S., and Meredith, M. P. (2019). Phased Response of the Subpolar Southern Ocean to Changes in Circumpolar Winds. *Geophysical Research Letters*, 46(11) :6024–6033. _eprint : https ://agupubs.onlinelibrary.wiley.com/doi/pdf/10.1029/2019GL082850.

Garrett, C. (1983). On the initial streakness of a dispersing tracer in two- and three-dimensional turbulence. *Dynamics of Atmospheres and Oceans*, 7(4) :265–277.

Gent, P. R. (2016). Effects of Southern Hemisphere Wind Changes on the Meridional Overturning Circulation in Ocean Models. *Annual Review of Marine Science*, 8(1) :79–94. Publisher : Annual Reviews.

Gent, P. R., Large, W. G., and Bryan, F. O. (2001). What sets the mean transport through Drake Passage ? *Journal of Geophysical Research : Oceans*, 106(C2) :2693–2712. _eprint : https ://onlinelibrary.wiley.com/doi/pdf/10.1029/2000JC900036.

Gent, P. R., Willebrand, J., McDougall, T. J., and McWilliams, J. C. (1995). Parameterizing Eddy-Induced Tracer Transports in Ocean Circulation Models. *Journal of Physical Oceanography*, 25(4) :463–474. Publisher : American Meteorological Society Section : Journal of Physical Oceanography.

Giglio, D. and Johnson, G. C. (2017). Middepth decadal warming and freshening in the South Atlantic. *Journal of Geophysical Research : Oceans*, 122(2) :973–979. Number : 2.

Giles, K. A., Laxon, S. W., Ridout, A. L., Wingham, D. J., and Bacon, S. (2012). Western Arctic Ocean freshwater storage increased by wind-driven spin-up of the Beaufort Gyre. *Nature Geoscience*, 5(3) :194–197. Number : 3 Publisher : Nature Publishing Group.

Gille, S. T. (1997). The Southern Ocean Momentum Balance : Evidence for Topographic Effects from Numerical Model Output and Altimeter Data. *Journal of Physical Oceanography*, 27(10) :2219–2232. Publisher : American Meteorological Society Section : Journal of Physical Oceanography.

Gille, S. T. (2002). Warming of the Southern Ocean Since the 1950s. *Science*, 295(5558) :1275–1277. Publisher : American Association for the Advancement of Science.

Gille, S. T. (2008). Decadal-Scale Temperature Trends in the Southern Hemisphere Ocean. *Journal of Climate*, 21(18) :4749–4765. Number : 18.

Gille, S. T. (2014). Meridional displacement of the Antarctic Circumpolar Current. *Philosophical Transactions of the Royal Society A : Mathematical, Physical and Engineering Sciences*, 372(2019) :20130273. Publisher : Royal Society.

Gille, S. T., McKee, D. C., and Martinson, D. G. (2016). Temporal Changes in the Antarctic Circumpolar Current : IMPLICATIONS FOR THE ANTARCTIC CONTINENTAL SHELVES. *Oceanography*, 29(4) :96–105. Publisher : Oceanography Society.

Golledge, N. R., Keller, E. D., Gomez, N., Naughten, K. A., Bernales, J., Trusel, L. D., and Edwards, T. L. (2019). Global environmental consequences of twenty-first-century ice-sheet melt. *Nature*, 566(7742) :65–72. Bandiera_abtest : a Cg_type : Nature Research Journals Number : 7742 Primary_atype : Research Publisher : Nature Publishing Group Subject_term : Climate and Earth system modelling ;Cryospheric science ;Projection and prediction Subject_term_id : climate-and-earth-system-modelling ;cryospheric-science ;projection-and-prediction.

Gordon, A. L. and Huber, B. A. (1990). Southern ocean winter mixed layer. *Journal of Geophysical Research : Oceans*, 95(C7) :11655–11672. _eprint : https ://onlinelibrary.wiley.com/doi/pdf/10.1029/JC095iC07p11655.

Gordon, A. L., Huber, B. A., and Abrahamsen, E. P. (2020). Interannual Variability of the Outflow of Weddell Sea Bottom Water. *Geophysical Research Letters*, 47(4) :e2020GL087014. _eprint : https ://onlinelibrary.wiley.com/doi/pdf/10.1029/2020GL087014.

Goyal, R., Gupta, A. S., Jucker, M., and England, M. H. Historical and projected changes in the Southern Hemisphere surface westerlies. *Geophysical Research Letters*, n/a(n/a) :e2020GL090849. _eprint : https ://agupubs.onlinelibrary.wiley.com/doi/pdf/10.1029/2020GL090849.

Gray, A. R., Johnson, K. S., Bushinsky, S. M., Riser, S. C., Russell, J. L., Talley, L. D., Wanninkhof, R., Williams, N. L., and Sarmiento, J. L. (2018). Autonomous Biogeochemical Floats Detect Significant Carbon Dioxide Outgassing in the High-Latitude Southern Ocean. *Geophysical Research Letters*, 45(17) :9049–9057. _eprint : https ://onlinelibrary.wiley.com/doi/pdf/10.1029/2018GL078013.

Gulev, S., Thorne, P., Ahn, J., Dentener, F., Domingues, C., Gerland, S., Gong, D., Kaufman, D., Nnamchi, H., Quaas, J., Rivera, J., Sathyendranath, S., Smith, S., Trewin, B., von Schuckmann, K., and Vose, R. (2021). Changing State of the Climate System. In : IPCC AR6 Climate Change 2021 : The Physical Science Basis.

Hall, A. and Visbeck, M. (2002). Synchronous Variability in the Southern Hemisphere Atmosphere, Sea Ice, and Ocean Resulting from the Annular Mode*. *Journal of Climate*, 15 :3043–3057.

Hallberg, R. and Gnanadesikan, A. (2006). The Role of Eddies in Determining the Structure and Response of the Wind-Driven Southern Hemisphere Overturning : Results from the Modeling Eddies in the Southern Ocean (MESO) Project. *Journal of Physical Oceanography*, 36(12) :2232–2252. Publisher : American Meteorological Society Section : Journal of Physical Oceanography.

Hattermann, T. (2018). Antarctic Thermocline Dynamics along a Narrow Shelf with Easterly Winds. *Journal of Physical Oceanography*, 48(10) :2419–2443. Publisher : American Meteorological Society Section : Journal of Physical Oceanography.

Hattermann, T., Smedsrud, L. H., Nøst, O. A., Lilly, J. M., and Galton-Fenzi, B. K. (2014). Eddy-resolving simulations of the Fimbul Ice Shelf cavity circulation : Basal melting and exchange with open ocean. *Ocean Modelling*, 82 :28–44.

Haumann, F. A., Gruber, N., and Münnich, M. (2020). Sea-Ice Induced Southern Ocean Subsurface Warming and Surface Cooling in a Warming Climate. *AGU Advances*, 1(2) :e2019AV000132. _eprint : https ://agupubs.onlinelibrary.wiley.com/doi/pdf/10.1029/2019AV000132.

Haumann, F. A., Gruber, N., Münnich, M., Frenger, I., and Kern, S. (2016). Sea-ice transport driving Southern Ocean salinity and its recent trends. *Nature*, 537(7618) :89–92. Number : 7618.

Haumann, F. A., Notz, D., and Schmidt, H. (2014). Anthropogenic influence on recent circulation-driven Antarctic sea ice changes. *Geophysical Research Letters*, 41(23) :8429–8437. _eprint : https ://agupubs.onlinelibrary.wiley.com/doi/pdf/10.1002/2014GL061659.

Held, I. M. and Soden, B. J. (2006). Robust Responses of the Hydrological Cycle to Global Warming. *Journal of Climate*, 19(21) :5686–5699. Publisher : American Meteorological Society Section : Journal of Climate.

Hellmer, H. H., Kauker, F., Timmermann, R., Determann, J., and Rae, J. (2012). Twenty-first-century warming of a large Antarctic ice-shelf cavity by a redirected coastal current. *Nature*, 485(7397) :225–228. Bandiera_abtest : a Cg_type : Nature Research Journals Number : 7397 Primary_atype : Research Publisher : Nature Publishing Group Subject_term : Climate sciences Subject_term_id : climate-sciences.

Hellmer, H. H., Kauker, F., Timmermann, R., and Hattermann, T. (2017). The Fate of the Southern Weddell Sea Continental Shelf in a Warming Climate. *Journal of Climate*, 30(12) :4337–4350. Publisher : American Meteorological Society Section : Journal of Climate.

Helm, V., Humbert, A., and Miller, H. (2014). Elevation and elevation change of Greenland and Antarctica derived from CryoSat-2. *The Cryosphere*, 8(4) :1539–1559. Publisher : Copernicus GmbH.

Heywood, K. and King, B. (2002). Water masses and baroclinic transports in the South Atlantic and Southern oceans.

Heywood, K. J., Schmidtko, S., Heuzé, C., Kaiser, J., Jickells, T. D., Queste, B. Y., Stevens, D. P., Wadley, M., Thompson, A. F., Fielding, S., Guihen, D., Creed, E., Ridley, J. K., and Smith, W. (2014). Ocean processes at the Antarctic continental slope. *Philosophical Transactions of the Royal Society A : Mathematical, Physical and Engineering Sciences*, 372(2019) :20130047. Publisher : Royal Society.

Hobbs, W. R., Roach, C., Roy, T., Sallée, J.-B., and Bindoff, N. (2021). Anthropogenic Temperature and Salinity Changes in the Southern Ocean. *Journal of Climate*, 34(1) :215–228. Publisher : American Meteorological Society Section : Journal of Climate.

Hodel, F., Grespan, R., de Rafélis, M., Dera, G., Lezin, C., Nardin, E., Rouby, D., Aretz, M., Steinnman, M., Buatier, M., Lacan, F., Jeandel, C., and Chavagnac, V. (2021). Drake Passage gateway opening and Antarctic Circumpolar Current onset 31 Ma ago : The message of foraminifera and reconsideration of the Neodymium isotope record. *Chemical Geology*, 570 :120171.

Hogg, A. M. (2010). An Antarctic Circumpolar Current driven by surface buoyancy forcing. *Geophysical Research Letters*, 37(23). _eprint : https ://onlinelibrary.wiley.com/doi/pdf/10.1029/2010GL044777.

Hogg, A. M., Meredith, M. P., Chambers, D. P., Abrahamsen, E. P., Hughes, C. W., and Morrison, A. K. (2015). Recent trends in the Southern Ocean eddy field. *Journal of Geophysical Research : Oceans*, 120(1) :257–267. _eprint : https ://onlinelibrary.wiley.com/doi/pdf/10.1002/2014JC010470.

Hogg, A. M., Spence, P., Saenko, O. A., and Downes, S. M. (2017). The Energetics of Southern Ocean Upwelling. *Journal of Physical Oceanography*, 47(1) :135–153. Publisher : American Meteorological Society Section : Journal of Physical Oceanography.

Holland, P. R. (2014). The seasonality of Antarctic sea ice trends. *Geophysical Research Letters*, 41(12) :4230–4237. _eprint : https ://agupubs.onlinelibrary.wiley.com/doi/pdf/10.1002/2014GL060172.

Holland, P. R. and Kwok, R. (2012). Wind-driven trends in Antarctic sea-ice drift. *Nature Geoscience*, 5(12) :872–875. Bandiera_abtest : a Cg_type : Nature Research Journals Number : 12 Primary_atype : Research Publisher : Nature Publishing Group Subject_term : Atmospheric dynamics ;Cryospheric science ;Ocean sciences Subject_term_id : atmospheric-dynamics ;cryospheric-science ;ocean-sciences.

Hoppema, M., Bakker, K., van Heuven, S. M. A. C., van Ooijen, J. C., and de Baar, H. J. W. (2015). Distributions, trends and inter-annual variability of nutrients along a repeat section through the Weddell Sea (1996–2011). *Marine Chemistry*, 177 :545–553.

Horvat, C., Tziperman, E., and Campin, J.-M. (2016). Interaction of sea ice floe size, ocean eddies, and sea ice melting. *Geophysical Research Letters*, 43(15) :8083–8090. _eprint : https ://agupubs.onlinelibrary.wiley.com/doi/pdf/10.1002/2016GL069742.

Hughes, C. W. and Ash, E. R. (2001). Eddy forcing of the mean flow in the Southern Ocean. *Journal of Geophysical Research : Oceans*, 106(C2) :2713–2722. _eprint : https ://onlinelibrary.wiley.com/doi/pdf/10.1029/2000JC900332.

Hughes, C. W., Meredith, M. P., and Heywood, K. J. (1999). Wind-Driven Transport Fluctuations through Drake Passage : A Southern Mode. *Journal of Physical Oceanography*, 29(8) :1971–1992. Publisher : American Meteorological Society Section : Journal of Physical Oceanography.

Hughes, C. W., Woodworth, P. L., Meredith, M. P., Stepanov, V., Whitworth, T., and Pyne, A. R. (2003). Coherence of Antarctic sea levels, Southern Hemisphere Annular Mode, and flow through Drake Passage. *Geophysical Research Letters*, 30(9). _eprint : https ://agupubs.onlinelibrary.wiley.com/doi/pdf/10.1029/2003GL017240.

Häkkinen, S. (1986). Coupled ice-ocean dynamics in the marginal ice zones : Upwelling/downwelling and eddy generation. *Journal of Geophysical Research : Oceans*, 91(C1) :819–832. _eprint : https ://onlinelibrary.wiley.com/doi/pdf/10.1029/JC091iC01p00819.

Häkkinen, S., Rhines, P. B., and Worthen, D. L. (2016). Warming of the Global Ocean : Spatial Structure and Water-Mass Trends. *Journal of Climate*, 29(13) :4949–4963. Number : 13.

Ice, J. E. T. o. S. (2009). WMO Sea-ice Nomenclature, WMO/OMM/ - No.259 Suppl.No.5. Linguistic equivalents. Accepted : 2014-02-14T11 :16 :57Z Publisher : JCOMM Expert Team on Sea Ice.

Iijima, B. A., Harris, I. L., Ho, C. M., Lindqwister, U. J., Mannucci, A. J., Pi, X., Reyes, M. J., Sparks, L. C., and Wilson, B. D. (1999). Automated daily process for global ionospheric total electron content maps and satellite ocean altimeter ionospheric calibration based on Global Positioning System data. *Journal of Atmospheric and Solar-Terrestrial Physics*, 61(16) :1205–1218.

Ivchenko, V. O., Danilov, S., and Olbers, D. (2008). Eddies in Numerical Models of the Southern Ocean. In *Ocean Modeling in an Eddying Regime*, pages 177–198. American Geophysical Union (AGU). _eprint : https ://agupubs.onlinelibrary.wiley.com/doi/pdf/10.1029/177GM13.

Jackson, J. (2005). Glossary of Geology. *Glossary of Geology, by J. A. Jackson. 2005 Approx. 900 p. 5th revised and enlarged ed. ISBN 3-540-27951-2. Berlin : Springer, 2005.*, -1.

Jacobs, S. S. (1991). On the nature and significance of the Antarctic Slope Front. *Marine Chemistry*, 35(1) :9–24.

Jacobs, S. S. and Giulivi, C. F. (2010). Large Multidecadal Salinity Trends near the Pacific–Antarctic Continental Margin. *Journal of Climate*, 23(17) :4508–4524. Publisher : American Meteorological Society Section : Journal of Climate.

Jayne, S. R. and Marotzke, J. (2002). The Oceanic Eddy Heat Transport. *Journal of Physical Oceanography*, 32(12) :3328–3345. Publisher : American Meteorological Society Section : Journal of Physical Oceanography.

Johnson, G. C. (2008). Quantifying Antarctic Bottom Water and North Atlantic Deep Water volumes. *Journal of Geophysical Research : Oceans*, 113(C5). _eprint : https ://onlinelibrary.wiley.com/doi/pdf/10.1029/2007JC004477.

Johnson, G. C., Hosoda, S., Jayne, S. R., Oke, P. R., Riser, S. C., Roemmich, D., Suga, T., Thierry, V., Wijffels, S. E., and Xu, J. (2022). ArgoTwo Decades : Global Oceanography, Revolutionized. *Annual Review of Marine Science*, 14(1) :null. _eprint : https ://doi.org/10.1146/annurev-marine-022521-102008.

Jones, J. M., Gille, S. T., Goosse, H., Abram, N. J., Canziani, P. O., Charman, D. J., Clem, K. R., Crosta, X., de Lavergne, C., Eisenman, I., England, M. H., Fogt, R. L., Frankcombe, L. M., Marshall, G. J., Masson-Delmotte, V., Morrison, A. K., Orsi, A. J., Raphael, M. N., Renwick, J. A., Schneider, D. P., Simpkins, G. R., Steig, E. J., Stenni, B., Swingedouw, D., and Vance, T. R. (2016). Assessing recent trends in high-latitude Southern Hemisphere surface climate. *Nature Climate Change*, 6(10) :917–926. Number : 10.

Jullion, L., Garabato, A. C. N., Meredith, M. P., Holland, P. R., Courtois, P., and King, B. A. (2013). Decadal Freshening of the Antarctic Bottom Water Exported from the Weddell Sea. *Journal of Climate*, 26(20) :8111–8125. Publisher : American Meteorological Society Section : Journal of Climate.

Karoly, D. J. (1989). Southern Hemisphere Circulation Features Associated with El Niño-Southern Oscillation Events. *Journal of Climate*, 2(11) :1239–1252. Publisher : American Meteorological Society Section : Journal of Climate.

Klatt, O., Boebel, O., and Fahrbach, E. (2007). A Profiling Float's Sense of Ice. *Journal of Atmospheric and Oceanic Technology*, 24(7) :1301–1308. Publisher : American Meteorological Society Section : Journal of Atmospheric and Oceanic Technology.

Klatt, O., Fahrbach, E., Hoppema, M., and Rohardt, G. (2005). The transport of the Weddell Gyre across the Prime Meridian. *Deep Sea Research Part II : Topical Studies in Oceanography*, 52(3) :513–528.

Koenig, Z., Provost, C., Ferrari, R., Sennéchael, N., and Rio, M.-H. (2014). Volume transport of the Antarctic Circumpolar Current : Production and validation of a 20 year long time series obtained from in situ and satellite observations. *Journal of Geophysical Research : Oceans*, 119(8) :5407–5433. _eprint : https ://agupubs.onlinelibrary.wiley.com/doi/pdf/10.1002/2014JC009966.

Kozlov, I. E., Artamonova, A. V., Manucharyan, G. E., and Kubryakov, A. A. (2019). Eddies in the Western Arctic Ocean From Spaceborne SAR Observations Over Open Ocean and Marginal Ice Zones. *Journal of Geophysical Research : Oceans*, 124(9) :6601–6616. _eprint : https ://agupubs.onlinelibrary.wiley.com/doi/pdf/10.1029/2019JC015113.

Kusahara, K. and Ohshima, K. I. (2009). Dynamics of the Wind-Driven Sea Level Variation around Antarctica. *Journal of Physical Oceanography*, 39(3) :658–674. Publisher : American Meteorological Society Section : Journal of Physical Oceanography.

Kwok, R. and Morison, J. (2016). Sea surface height and dynamic topography of the ice-covered oceans from CryoSat-2 : 2011–2014. *Journal of Geophysical Research : Oceans*, 121(1) :674–692. _eprint : https ://agupubs.onlinelibrary.wiley.com/doi/pdf/10.1002/2015JC011357.

Lago, V. and England, M. H. (2019). Projected Slowdown of Antarctic Bottom Water Formation in Response to Amplified Meltwater Contributions. *Journal of Climate*, 32(19) :6319–6335. Publisher : American Meteorological Society Section : Journal of Climate.

Laxon, S. (1994). Sea ice altimeter processing scheme at the EODC. *International Journal of Remote Sensing*, 15(4) :915–924. Publisher : Taylor & Francis _eprint : https ://-doi.org/10.1080/01431169408954124.

Le Quéré, C., Rödenbeck, C., Buitenhuis, E. T., Conway, T. J., Langenfelds, R., Gomez, A., Labuschagne, C., Ramonet, M., Nakazawa, T., Metzl, N., Gillett, N., and Heimann, M. (2007). Saturation of the southern ocean CO2 sink due to recent climate change. *Science (New York, N.Y.)*, 316(5832) :1735–1738.

Le Traon, P. Y., Faugère, Y., Hernandez, F., Dorandeu, J., Mertz, F., and Ablain, M. (2003). Can We Merge GEOSAT Follow-On with TOPEX/Poseidon and ERS-2 for an Improved Description of the Ocean Circulation ? *Journal of Atmospheric and Oceanic Technology*, 20(6) :889–895. Publisher : American Meteorological Society Section : Journal of Atmospheric and Oceanic Technology.

Le Traon, P. Y., Nadal, F., and Ducet, N. (1998). An Improved Mapping Method of Multisatellite Altimeter Data. *Journal of Atmospheric and Oceanic Technology*, 15(2) :522–534. Publisher : American Meteorological Society Section : Journal of Atmospheric and Oceanic Technology.

Le Traon, P.-Y. and Ogor, F. (1998). ERS-1/2 orbit improvement using TOPEX/POSEIDON : The 2 cm challenge. *Journal of Geophysical Research : Oceans*, 103(C4) :8045–8057. _eprint : https ://agupubs.onlinelibrary.wiley.com/doi/pdf/10.1029/97JC01917.

Lee, J.-Y., Marotzke, J., Bala, G., Cao, L., Corti, S., Dunne, J., Engelbrecht, F., Fischer, E., Fyfe, J., Jones, C., Maycock, A., Mutemi, J., Ndiaye, O., Panickal, S., and Zhou, T. (2021). Future Global Climate : Scenario-Based Projections and Near-Term Information. In : IPCC AR6 Climate Change 2021 : The Physical Science Basis.

Li, X., Cai, W., Meehl, G. A., Chen, D., Yuan, X., Raphael, M., Holland, D. M., Ding, Q., Fogt, R. L., Markle, B. R., Wang, G., Bromwich, D. H., Turner, J., Xie, S.-P., Steig, E. J., Gille, S. T., Xiao, C., Wu, B., Lazzara, M. A., Chen, X., Stammerjohn, S., Holland, P. R., Holland, M. M., Cheng, X., Price, S. F., Wang, Z., Bitz, C. M., Shi, J., Gerber, E. P., Liang, X., Goosse, H., Yoo, C., Ding, M., Geng, L., Xin, M., Li, C., Dou, T., Liu, C., Sun, W., Wang, X., and Song, C. (2021). Tropical teleconnection impacts on Antarctic climate changes. *Nature Reviews Earth & Environment*, 2(10) :680–698. Bandiera_abtest : a Cg_type : Nature Research Journals Number : 10 Primary_atype : Reviews Publisher : Nature Publishing Group Subject_term : Atmospheric dynamics ;Attribution ;Cryospheric science ;Physical oceanography Subject_term_id : atmospheric-dynamics ;attribution ;cryospheric-science ;physical-oceanography.

Llovel, W. and Terray, L. (2016). Observed southern upper-ocean warming over 2005–2014 and associated mechanisms. *Environmental Research Letters*, 11(12) :124023. Publisher : IOP Publishing.

Longépé, N., Thibaut, P., Vadaine, R., Poisson, J., Guillot, A., Boy, F., Picot, N., and Borde, F. (2019). Comparative Evaluation of Sea Ice Lead Detection Based on SAR Imagery and Altimeter Data. *IEEE Transactions on Geoscience and Remote Sensing*, 57(6) :4050–4061. Conference Name : IEEE Transactions on Geoscience and Remote Sensing.

Lu, K., Weingartner, T., Danielson, S., Winsor, P., Dobbins, E., Martini, K., and Statscewich, H. (2015). Lateral mixing across ice meltwater fronts of the Chukchi Sea shelf. *Geophysical Research Letters*, 42(16) :6754–6761. _eprint : https ://onlinelibrary.wiley.com/doi/pdf/10.1002/2015GL064967.

Lyard, F. H., Allain, D. J., Cancet, M., Carrère, L., and Picot, N. (2021). FES2014 global ocean tide atlas : design and performance. *Ocean Science*, 17(3) :615–649. Publisher : Copernicus GmbH.

Lüpkes, C. and Birnbaum, G. (2005). 'Surface Drag in the Arctic Marginal Sea-ice Zone : A Comparison of Different Parameterisation Concepts'. *Boundary-Layer Meteorology*, 117(2) :179–211.

MacGilchrist, G. A., Naveira Garabato, A. C., Brown, P. J., Jullion, L., Bacon, S., Bakker, D. C. E., Hoppema, M., Meredith, M. P., and Torres-Valdés, S. (2019). Reframing the carbon cycle of the subpolar Southern Ocean. *Science Advances*, 5(8) :eaav6410. Publisher : American Association for the Advancement of Science.

Maksym, T. (2016). Southern Ocean freshened by sea ice. *Nature*, 537(7618) :40–41. Number : 7618 Publisher : Nature Publishing Group.

Manucharyan, G. E. and Thompson, A. F. (2017). Submesoscale Sea Ice-Ocean Interactions in Marginal Ice Zones. *Journal of Geophysical Research : Oceans*, 122(12) :9455–9475. _eprint : https ://onlinelibrary.wiley.com/doi/pdf/10.1002/2017JC012895.

Manucharyan, G. E. and Timmermans, M.-L. (2013). Generation and Separation of Mesoscale Eddies from Surface Ocean Fronts. *Journal of Physical Oceanography*, 43(12) :2545–2562. Publisher : American Meteorological Society Section : Journal of Physical Oceanography.

Marshall, G. J. (2003). Trends in the Southern Annular Mode from Observations and Reanalyses. *Journal of Climate*, 16(24) :4134–4143. Publisher : American Meteorological Society Section : Journal of Climate.

Marshall, J. and Radko, T. (2003). Residual-Mean Solutions for the Antarctic Circumpolar Current and Its Associated Overturning Circulation. *Journal of Physical Oceanography*, 33(11) :2341–2354. Publisher : American Meteorological Society Section : Journal of Physical Oceanography.

Marshall, J. and Speer, K. (2012). Closure of the meridional overturning circulation through Southern Ocean upwelling. *Nature Geoscience*, 5(3) :171–180. Bandiera_abtest : a Cg_type : Nature Research Journals Number : 3 Primary_atype : Reviews Publisher : Nature Publishing Group Subject_term : Physical oceanography Subject_term_id : physical-oceanography.

Martin, T., Tsamados, M., Schroeder, D., and Feltham, D. L. (2016). The impact of variable sea ice roughness on changes in Arctic Ocean surface stress : A model study. *Journal of Geophysical Research : Oceans*, 121(3) :1931–1952. _eprint : https ://agupubs.onlinelibrary.wiley.com/doi/pdf/10.1002/2015JC011186.

Martínez Moreno, J., Hogg, A., England, M., Constantinou, N., Kiss, A., and Morrison, A. (2020). *Global changes in oceanic mesoscale currents over the satellite altimetry record.*

Mashayek, A., Ferrari, R., Merrifield, S., Ledwell, J. R., St Laurent, L., and Garabato, A. N. (2017). Topographic enhancement of vertical turbulent mixing in the Southern Ocean. *Nature Communications*, 8(1) :14197. Bandiera_abtest : a Cc_license_type : cc_by Cg_type : Nature Research Journals Number : 1 Primary_atype : Research Publisher : Nature Publishing Group Subject_term : Fluid dynamics ;Physical oceanography Subject_term_id : fluid-dynamics ;physical-oceanography.

Mason, E., Pascual, A., Gaube, P., Ruiz, S., Pelegrí, J. L., and Delepoulle, A. (2017). Subregional characterization of mesoscale eddies across the Brazil-Malvinas Confluence. *Journal of Geophysical Research : Oceans*, 122(4) :3329–3357. _eprint : https ://onlinelibrary.wiley.com/doi/pdf/10.1002/2016JC012611.

Mason, E., Pascual, A., and McWilliams, J. C. (2014). A New Sea Surface Height–Based Code for Oceanic Mesoscale Eddy Tracking. *Journal of Atmospheric and Oceanic Technology*, 31(5) :1181–1188. Publisher : American Meteorological Society Section : Journal of Atmospheric and Oceanic Technology.

Masson-Delmotte, V., Zhai, P., Pirani, A., Connors, S. L., Péan, C., Berger, C., Caud, N., Chen, Y., Goldfarb, L., Gomis, M. I., Huang, M., Leitzell, K., Lonnoy, E., Matthews, J., Maycock, T., Waterfield, T., Yelekçi, O., Yu, R., and Zhou, B. (2021). Climate Change 2021 : The Physical Science Basis. Contribution of Working Group I to the Sixth Assessment Report of the Intergovernmental Panel on Climate Change. Technical report, IPCC.

Mathiot, P., Goosse, H., Fichefet, T., Barnier, B., and Gallée, H. (2011). Modelling the seasonal variability of the Antarctic Slope Current. *Ocean Science*, 7(4) :455–470. Publisher : Copernicus GmbH.

Matsumura, Y. and Hasumi, H. (2008). Brine-Driven Eddies under Sea Ice Leads and Their Impact on the Arctic Ocean Mixed Layer. *Journal of Physical Oceanography - J PHYS OCEANOGR*, 38.

McCartney, M. S. and Donohue, K. A. (2007). A deep cyclonic gyre in the Australian–Antarctic Basin. *Progress in Oceanography*, 75(4) :675–750.

McWilliams, J. C. (1985). Submesoscale, coherent vortices in the ocean. *Reviews of Geophysics*, 23(2) :165–182. _eprint : https ://agupubs.onlinelibrary.wiley.com/doi/pdf/10.1029/RG023i002p00165.

Meehl, G. A., Arblaster, J. M., Chung, C. T. Y., Holland, M. M., DuVivier, A., Thompson, L., Yang, D., and Bitz, C. M. (2019). Sustained ocean changes contributed to sudden Antarctic sea ice retreat in late 2016. *Nature Communications*, 10(1) :14. Bandiera_abtest : a Cc_license_type : cc_by Cg_type : Nature Research Journals Number : 1 Primary_atype : Research Publisher : Nature Publishing Group Subject_term : Climate sciences ;Ocean sciences Subject_term_id : climate-sciences ;ocean-sciences.

Meier, W. N. ; Fetterer, F. S. M. M. S. D. R. A. S. J. (2017). NOAA/NSIDC Climate Data Record of Passive Microwave Sea Ice Concentration, Version 3. Type : dataset.

Meijers, A. J. S., Klocker, A., Bindoff, N. L., Williams, G. D., and Marsland, S. J. (2010). The circulation and water masses of the Antarctic shelf and continental slope between 30 and 80E. *Deep Sea Research Part II : Topical Studies in Oceanography*, 57(9) :723–737.

Meneghello, G., Marshall, J., Lique, C., Isachsen, P. E., Doddridge, E., Campin, J.-M., Regan, H., and Talandier, C. (2020). Genesis and Decay of Mesoscale Baroclinic Eddies in the Seasonally Ice-Covered Interior Arctic Ocean. *Journal of Physical Oceanography*, 51(1) :115–129. Publisher : American Meteorological Society Section : Journal of Physical Oceanography.

Meredith, M., Sommerkorn, M., Cassotta, S., Derksen, C., Ekaykin, A., and Hollowed, A. (2019). Polar Regions. In : IPCC Special Report on the Ocean and Cryosphere in a Changing Climate.

Meredith, M. P. (2016). Understanding the structure of changes in the Southern Ocean eddy field. *Geophysical Research Letters*, 43(11) :5829–5832. _eprint : https ://onlinelibrary.wiley.com/doi/pdf/10.1002/2016GL069677.

Meredith, M. P. and Hogg, A. M. (2006). Circumpolar response of Southern Ocean eddy activity to a change in the Southern Annular Mode. *Geophysical Research Letters*, 33(16). _eprint : https ://agupubs.onlinelibrary.wiley.com/doi/pdf/10.1029/2006GL026499.

Meredith, M. P., Jullion, L., Brown, P. J., Naveira Garabato, A. C., and Couldrey, M. P. (2014). Dense waters of the Weddell and Scotia Seas : recent changes in properties and circulation. *Philosophical Transactions of the Royal Society A : Mathematical, Physical and Engineering Sciences*, 372(2019) :20130041. Publisher : Royal Society.

Milillo, P., Rignot, E., Rizzoli, P., Scheuchl, B., Mouginot, J., Bueso-Bello, J., and Prats-Iraola, P. (2019). Heterogeneous retreat and ice melt of Thwaites Glacier, West Antarctica. *Science Advances*, 5(1) :eaau3433. Publisher : American Association for the Advancement of Science Section : Research Article.

Mizobata, K., Watanabe, E., and Kimura, N. (2016). Wintertime variability of the Beaufort gyre in the Arctic Ocean derived from CryoSat-2/SIRAL observations. *Journal of Geophysical Research : Oceans*, 121(3) :1685–1699. _eprint : https ://agupubs.onlinelibrary.wiley.com/doi/pdf/10.1002/2015JC011218.

Moffat, C. and Meredith, M. (2018). Shelf-ocean exchange and hydrography west of the Antarctic Peninsula : a review. *Philosophical Transactions. Series A, Mathematical, Physical, and Engineering Sciences*, 376(2122) :20170164.

Moorman, R., Morrison, A. K., and Hogg, A. M. (2020). Thermal Responses to Antarctic Ice Shelf Melt in an Eddy-Rich Global Ocean–Sea Ice Model. *Journal of Climate*, 33(15) :6599–6620. Publisher : American Meteorological Society Section : Journal of Climate.

Morales Maqueda, M. A., Willmott, A. J., and Biggs, N. R. T. (2004). Polynya Dynamics : a Review of Observations and Modeling. *Reviews of Geophysics*, 42(1). _eprint : https ://onlinelibrary.wiley.com/doi/pdf/10.1029/2002RG000116.

Morrison, A. K., Hogg, A. M., England, M. H., and Spence, P. (2020). Warm Circumpolar Deep Water transport toward Antarctica driven by local dense water export in canyons. *Science Advances*, 6(18) :eaav2516. Publisher : American Association for the Advancement of Science.

Morrow, R., Fu, L.-L., Ardhuin, F., Benkiran, M., Chapron, B., Cosme, E., d'Ovidio, F., Farrar, J. T., Gille, S. T., Lapeyre, G., Le Traon, P.-Y., Pascual, A., Ponte, A., Qiu, B., Rascle, N., Ubelmann, C., Wang, J., and Zaron, E. D. (2019). Global Observations of Fine-Scale Ocean Surface Topography With the Surface Water and Ocean Topography (SWOT) Mission. *Frontiers in Marine Science*, 6 :232.

Morrow, R. and Kestenare, E. (2014). Nineteen-year changes in surface salinity in the Southern Ocean south of Australia. *Journal of Marine Systems*, 129 :472–483.

Morrow, R. and Kestenare, E. (2017). 22-year surface salinity changes in the Seasonal Ice Zone near 140 degrees E off Antarctica. *Journal of Marine Systems*, 175 :46–62.

Morrow, R. and Le Traon, P.-Y. (2012). Recent advances in observing mesoscale ocean dynamics with satellite altimetry. *Advances in Space Research*, 50(8) :1062–1076.

Mouginot, J., Rignot, E., and Scheuchl, B. (2014). Sustained increase in ice discharge from the Amundsen Sea Embayment, West Antarctica, from 1973 to 2013. *Geophysical Research Letters*, 41(5) :1576–1584. _eprint : https ://agupubs.onlinelibrary.wiley.com/doi/pdf/10.1002/2013GL059069.

Nakayama, Y., Menemenlis, D., Zhang, H., Schodlok, M., and Rignot, E. (2018). Origin of Circumpolar Deep Water intruding onto the Amundsen and Bellingshausen Sea continental shelves. *Nature Communications*, 9(1) :3403. Bandiera_abtest : a Cc_license_type : cc_by Cg_type : Nature Research Journals Number : 1 Primary_atype : Research Publisher : Nature Publishing Group Subject_term : Cryospheric science ;Physical oceanography Subject_term_id : cryospheric-science ;physical-oceanography.

Nakayama, Y., Ohshima, K. I., Matsumura, Y., Fukamachi, Y., and Hasumi, H. (2014). A Numerical Investigation of Formation and Variability of Antarctic Bottom Water off Cape Darnley, East Antarctica. *Journal of Physical Oceanography*, 44(11) :2921–2937. Publisher : American Meteorological Society Section : Journal of Physical Oceanography.

Naughten, K. A., Meissner, K. J., Galton-Fenzi, B. K., England, M. H., Timmermann, R., and Hellmer, H. H. (2018). Future Projections of Antarctic Ice Shelf Melting Based on CMIP5 Scenarios. *Journal of Climate*, 31(13) :5243–5261. Publisher : American Meteorological Society Section : Journal of Climate.

Naveira Garabato, A. C., Williams, A. P., and Bacon, S. (2014). The three-dimensional overturning circulation of the Southern Ocean during the WOCE era. *Progress in Oceanography*, 120 :41–78.

Newman, L., Heil, P., Trebilco, R., Katsumata, K., Constable, A., van Wijk, E., Assmann, K., Beja, J., Bricher, P., Coleman, R., Costa, D., Diggs, S., Farneti, R., Fawcett, S., Gille, S. T., Hendry, K. R., Henley, S., Hofmann, E., Maksym, T., Mazloff, M., Meijers, A., Meredith, M. M., Moreau, S., Ozsoy, B., Robertson, R., Schloss, I., Schofield, O., Shi, J., Sikes, E., Smith, I. J., Swart, S., Wahlin, A., Williams, G., Williams, M. J. M., Herraiz-Borreguero, L., Kern, S., Lieser, J., Massom, R. A., Melbourne-Thomas, J., Miloslavich, P., and Spreen, G. (2019). Delivering Sustained, Coordinated, and Integrated Observations of the Southern Ocean for Global Impact. *Frontiers in Marine Science*, 6.

Nicholls, K. W., Østerhus, S., Makinson, K., Gammelsrød, T., and Fahrbach, E. (2009). Ice-ocean processes over the continental shelf of the southern Weddell Sea, Antarctica : A review. *Reviews of Geophysics*, 47(3). _eprint : https ://onlinelibrary.wiley.com/doi/pdf/10.1029/2007RG000250.

Nøst, O. A., Biuw, M., Tverberg, V., Lydersen, C., Hattermann, T., Zhou, Q., Smedsrud, L. H., and Kovacs, K. M. (2011). Eddy overturning of the Antarctic Slope Front controls glacial melting in the Eastern Weddell Sea. *Journal of Geophysical Research : Oceans*, 116(C11). _eprint : https ://agupubs.onlinelibrary.wiley.com/doi/pdf/10.1029/2011JC006965.

Núñez-Riboni, I. and Fahrbach, E. (2009). Seasonal variability of the Antarctic Coastal Current and its driving mechanisms in the Weddell Sea. *Deep Sea Research I*, 56(11) :1927–1941. Number : 11.

Ohshima, K. I., Fukamachi, Y., Williams, G. D., Nihashi, S., Roquet, F., Kitade, Y., Tamura, T., Hirano, D., Herraiz-Borreguero, L., Field, I., Hindell, M., Aoki, S., and Wakatsuchi, M. (2013). Antarctic Bottom Water production by intense sea-ice formation in the Cape Darnley polynya. *Nature Geoscience*, 6(3) :235–240. Bandiera_abtest : a Cg_type : Nature Research Journals Number : 3 Primary_atype : Research Publisher : Nature Publishing Group Subject_term : Cryospheric science ;Ocean sciences Subject_term_id : cryospheric-science ;ocean-sciences.

Ollivier, A., Phillips, S., Couhert, A., and Picot, N. Assessment of Orbit Quality through the SSH calculation : POE-E orbit standards.

Orsi, A. H. (2010). Recycling bottom waters. *Nature Geoscience*, 3(5) :307–309. Bandiera_abtest : a Cg_type : Nature Research Journals Number : 5 Primary_atype : News & Views Publisher : Nature Publishing Group Subject_term : Physical oceanography Subject_term_id : physical-oceanography.

Orsi, A. H., Johnson, G. C., and Bullister, J. L. (1999). Circulation, mixing, and production of Antarctic Bottom Water. *Progress in Oceanography*, 43(1) :55–109.

Orsi, A. H. and Whitworth, T. (2005). *Hydrographic Atlas of the World Ocean Circulation Experiment (WOCE) Volume 1 : Southern Ocean*.

Orsi, A. H., Whitworth, T., and Nowlin, W. D. (1995). On the meridional extent and fronts of the Antarctic Circumpolar Current. *Deep Sea Research Part I : Oceanographic Research Papers*, 42(5) :641–673. Number : 5.

Palmer, M. D., Durack, P. J., Chidichimo, M. P., Church, J. A., Cravatte, S., Hill, K., Johannessen, J. A., Karstensen, J., Lee, T., Legler, D., Mazloff, M., Oka, E., Purkey, S., Rabe, B., Sallée, J.-B., Sloyan, B. M., Speich, S., von Schuckmann, K., Willis, J., and Wijffels, S. (2019). Adequacy of the Ocean Observation System for Quantifying Regional Heat and Freshwater Storage and Change. *Frontiers in Marine Science*, 6 :416.

Paolo, F. S., Fricker, H. A., and Padman, L. (2015). Volume loss from Antarctic ice shelves is accelerating. *Science*, 348(6232) :327–331. Publisher : American Association for the Advancement of Science Section : Report.

Park, Y.-H., Charriaud, E., Craneguy, P., and Kartavtseff, A. (2001). Fronts, transport, and Weddell Gyre at 30°E between Africa and Antarctica. *Journal of Geophysical Research : Oceans*, 106(C2) :2857–2879. _eprint : https ://agupubs.onlinelibrary.wiley.com/doi/pdf/10.1029/2000JC900087.

Parkinson, C. L. (2019). A 40-y record reveals gradual Antarctic sea ice increases followed by decreases at rates far exceeding the rates seen in the Arctic. *Proceedings of the National Academy of Sciences*, 116(29) :14414–14423.

Parkinson, C. L. and Cavalieri, D. J. (2012). Antarctic sea ice variability and trends, 1979&ndash ;2010. *The Cryosphere*, 6(4) :871–880. Publisher : Copernicus GmbH.

Patara, L., Böning, C. W., and Biastoch, A. (2016). Variability and trends in Southern Ocean eddy activity in 1/12° ocean model simulations. *Geophysical Research Letters*, 43(9) :4517–4523. _eprint : https ://onlinelibrary.wiley.com/doi/pdf/10.1002/2016GL069026.

Pauthenet, E., Sallée, J.-b., Schmidtko, S., and Nerini, D. (2021). Seasonal Variation of the Antarctic Slope Front Occurrence and Position Estimated from an Interpolated Hydrographic Climatology. *Journal of Physical Oceanography*, 51.

Peacock, N. R. and Laxon, S. W. (2004). Sea surface height determination in the Arctic Ocean from ERS altimetry. *Journal of Geophysical Research : Oceans*, 109(C7). _eprint : https ://agupubs.onlinelibrary.wiley.com/doi/pdf/10.1029/2001JC001026.

Pedlosky, J. (2013). *Geophysical Fluid Dynamics*. Springer Science & Business Media. Google-Books-ID : iIbTBwAAQBAJ.

Pegliasco, C., Chaigneau, A., and Morrow, R. (2015). Main eddy vertical structures observed in the four major Eastern Boundary Upwelling Systems. *Journal of Geophysical Research : Oceans*, 120(9) :6008–6033. _eprint : https ://onlinelibrary.wiley.com/doi/pdf/10.1002/2015JC010950.

Pegliasco, C., Delepoulle, A., Morrow, R., Faugère, Y., and Dibarboure, G. (2021). META3.1exp : A new Global Mesoscale Eddy Trajectories Atlas derived from altimetry. *Earth System Science Data Discussions*, pages 1–31. Publisher : Copernicus GmbH.

Pellichero, V., Sallée, J.-B., Chapman, C. C., and Downes, S. M. (2018). The southern ocean meridional overturning in the sea-ice sector is driven by freshwater fluxes. *Nature Communications*, 9(1) :1789. Bandiera_abtest : a Cc_license_type : cc_by Cg_type : Nature Research Journals Number : 1 Primary_atype : Research Publisher : Nature Publishing Group Subject_term : Cryospheric science ;Physical oceanography Subject_term_id : cryospheric-science ;physical-oceanography.

Pellichero, V., Sallée, J.-B., Schmidtko, S., Roquet, F., and Charrassin, J.-B. (2017a). The ocean mixed layer under Southern Ocean sea-ice : Seasonal cycle and forcing. *Journal of Geophysical Research : Oceans*, 122(2) :1608–1633. _eprint : https ://agupubs.onlinelibrary.wiley.com/doi/pdf/10.1002/2016JC011970.

Pellichero, V., Sallée, J.-B., Schmidtko, S., Roquet, F., and Charrassin, J.-B. (2017b). The ocean mixed layer under Southern Ocean sea-ice : Seasonal cycle and forcing. *Journal of Geophysical Research : Oceans*, 122(2) :1608–1633. _eprint : https ://agupubs.onlinelibrary.wiley.com/doi/pdf/10.1002/2016JC011970.

Peng, G., Meier, W. N., Scott, D. J., and Savoie, M. H. (2013). A long-term and reproducible passive microwave sea ice concentration data record for climate studies and monitoring. *Earth System Science Data*, 5(2) :311–318.

Peterson, R. G. (1988). On the transport of the Antarctic Circumpolar Current through Drake Passage and its relation to wind. *Journal of Geophysical Research : Oceans*, 93(C11) :13993–14004. _eprint : https ://agupubs.onlinelibrary.wiley.com/doi/pdf/10.1029/JC093iC11p13993.

Poisson, J., Quartly, G. D., Kurekin, A. A., Thibaut, P., Hoang, D., and Nencioli, F. (2018). Development of an ENVISAT Altimetry Processor Providing Sea Level Continuity Between Open Ocean and Arctic Leads. *IEEE Transactions on Geoscience and Remote Sensing*, 56(9) :5299–5319. Conference Name : IEEE Transactions on Geoscience and Remote Sensing.

Prandi, P. (2020). multi-mission sea level in the Arctic Ocean. Technical Report CLS-ENV-NT-20-0126, CLS.

Prandi, P., Ablain, M., Cazenave, A., and Picot, N. (2012). Sea level variability in the Arctic Ocean observed by satellite altimetry. *Ocean Science Discussions*, 9(4) :2375–2401. Publisher : Copernicus GmbH.

Price, M. R., Heywood, K. J., and Nicholls, K. W. (2008). Ice-shelf? ocean interactions at Fimbul Ice Shelf, Antarctica from oxygen isotope ratio measurements. *Ocean Science*, 4(1) :89–98. Publisher : European Geosciences Union.

Pujol, M.-I., Faugère, Y., Taburet, G., Dupuy, S., Pelloquin, C., Ablain, M., and Picot, N. (2016). DUACS DT2014 : the new multi-mission altimeter data set reprocessed over 20 years. *Ocean Science*, 12(5) :1067–1090. Publisher : Copernicus GmbH.

Pujol, M.-I., Schaeffer, P., Faugère, Y., Raynal, M., Dibarboure, G., and Picot, N. (2018). Gauging the Improvement of Recent Mean Sea Surface Models : A New Approach for Identifying and Quantifying Their Errors. *Journal of Geophysical Research : Oceans*, 123(8) :5889–5911. _eprint : https ://agupubs.onlinelibrary.wiley.com/doi/pdf/10.1029/2017JC013503.

Purich, A., England, M. H., Cai, W., Sullivan, A., and Durack, P. J. (2018). Impacts of Broad-Scale Surface Freshening of the Southern Ocean in a Coupled Climate Model. *Journal of Climate*, 31(7) :2613–2632. Publisher : American Meteorological Society Section : Journal of Climate.

Purkey, S. G. and Johnson, G. C. (2012). Global Contraction of Antarctic Bottom Water between the 1980s and 2000s. *Journal of Climate*, 25(17) :5830–5844. Publisher : American Meteorological Society Section : Journal of Climate.

Purkey, S. G. and Johnson, G. C. (2013). Antarctic Bottom Water Warming and Freshening : Contributions to Sea Level Rise, Ocean Freshwater Budgets, and Global Heat Gain. *Journal of Climate*, 26(16) :6105–6122. Publisher : American Meteorological Society Section : Journal of Climate.

Quartly, G. D., Rinne, E., Passaro, M., Andersen, O. B., Dinardo, S., Fleury, S., Guillot, A., Hendricks, S., Kurekin, A. A., Müller, F. L., Ricker, R., Skourup, H., and Tsamados, M. (2019). Retrieving Sea Level and Freeboard in the Arctic : A Review of Current Radar Altimetry Methodologies and Future Perspectives. *Remote Sensing*, 11(7) :881. Number : 7 Publisher : Multidisciplinary Digital Publishing Institute.

Ray, R. D. (2013). Precise comparisons of bottom-pressure and altimetric ocean tides. *Journal of Geophysical Research : Oceans*, 118(9) :4570–4584. _eprint : https ://agupubs.onlinelibrary.wiley.com/doi/pdf/10.1002/jgrc.20336.

Rignot, E., Mouginot, J., Scheuchl, B., van den Broeke, M., van Wessem, M. J., and Morlighem, M. (2019). Four decades of Antarctic Ice Sheet mass balance from 1979–2017. *Proceedings of the National Academy of Sciences*, 116(4) :1095.

Rintoul, S., Hughes, C., and Olbers, D. (2001). The Antarctic Circumpolar Current system. *International Geophysics*, 77.

Rintoul, S. R. (2007). Rapid freshening of Antarctic Bottom Water formed in the Indian and Pacific oceans. *Geophysical Research Letters*, 34(6). _eprint : https ://agupubs.onlinelibrary.wiley.com/doi/pdf/10.1029/2006GL028550.

Rintoul, S. R. (2018). The global influence of localized dynamics in the Southern Ocean. *Nature*, 558(7709) :209–218. Bandiera_abtest : a Cg_type : Nature Research Journals Number : 7709 Primary_atype : Reviews Publisher : Nature Publishing Group Subject_term : Physical oceanography Subject_term_id : physical-oceanography.

Rintoul, S. R. and Naveira Garabato, A. C. (2013). Dynamics of the Southern Ocean circulation. pages 471–492. Academic Press. Num Pages : 898.

Riser, S. C., Freeland, H. J., Roemmich, D., Wijffels, S., Troisi, A., Belbéoch, M., Gilbert, D., Xu, J., Pouliquen, S., Thresher, A., Le Traon, P.-Y., Maze, G., Klein, B., Ravichandran, M., Grant, F., Poulain, P.-M., Suga, T., Lim, B., Sterl, A., Sutton, P., Mork, K.-A., Vélez-Belchí, P. J., Ansorge, I., King, B., Turton, J., Baringer, M., and Jayne, S. R. (2016). Fifteen years of ocean observations with the global Argo array. *Nature Climate Change*, 6(2) :145–153. Bandiera_abtest : a Cg_type : Nature Research Journals Number : 2 Primary_atype : Reviews Publisher : Nature Publishing Group Subject_term : Climate change ;Ocean sciences Subject_term_id : climate-change ;ocean-sciences.

Roach, L. A., Dörr, J., Holmes, C. R., Massonnet, F., Blockley, E. W., Notz, D., Rackow, T., Raphael, M. N., O'Farrell, S. P., Bailey, D. A., and Bitz, C. M. (2020). Antarctic Sea Ice Area in CMIP6. *Geophysical Research Letters*, 47(9) :e2019GL086729. _eprint : https ://onlinelibrary.wiley.com/doi/pdf/10.1029/2019GL086729.

Roemmich, D. and Gilson, J. (2009). The 2004–2008 mean and annual cycle of temperature, salinity, and steric height in the global ocean from the Argo Program. *Progress in Oceanography*, 82(2) :81–100.

Roquet, F., Williams, G., Hindell, M. A., Harcourt, R., McMahon, C., Guinet, C., Charrassin, J.-B., Reverdin, G., Boehme, L., Lovell, P., and Fedak, M. (2014). A Southern Indian Ocean database of hydrographic profiles obtained with instrumented elephant seals. *Scientific Data*, 1(1) :140028. Bandiera_abtest : a Cg_type : Nature Research Journals Number : 1 Primary_atype : Research Publisher : Nature Publishing Group Subject_term : Marine biology ;Physical oceanography Subject_term_id : marine-biology ;physical-oceanography.

Rye, C. D., Marshall, J., Kelley, M., Russell, G., Nazarenko, L. S., Kostov, Y., Schmidt, G. A., and Hansen, J. (2020). Antarctic Glacial Melt as a Driver of Recent Southern Ocean Climate Trends. *Geophysical Research Letters*, n/a(n/a) :e2019GL086892. Number : n/a.

Sadai, S., Condron, A., DeConto, R., and Pollard, D. (2020). Future climate response to Antarctic Ice Sheet melt caused by anthropogenic warming. *Science Advances*, 6(39) :eaaz1169. Publisher : American Association for the Advancement of Science.

Sallée, J.-B. (2018). Southern Ocean Warming. *Oceanography*, 31(2). Number : 2.

Sallée, J.-B., Matear, R. J., Rintoul, S. R., and Lenton, A. (2012). Localized subduction of anthropogenic carbon dioxide in the Southern Hemisphere oceans. *Nature Geoscience*, 5(8) :579–584. Bandiera_abtest : a Cg_type : Nature Research Journals Number : 8 Primary_atype : Research Publisher : Nature Publishing Group Subject_term : Atmospheric chemistry ;Marine chemistry Subject_term_id : atmospheric-chemistry ;marine-chemistry.

Sallée, J.-B., Morrow, R., and Speer, K. (2008). Eddy heat diffusion and Subantarctic Mode Water formation. *Geophysical Research Letters*, 35(5). _eprint : https ://onlinelibrary.wiley.com/doi/pdf/10.1029/2007GL032827.

Sallée, J.-B., Pellichero, V., Akhoudas, C., Pauthenet, E., Vignes, L., Schmidtko, S., Garabato, A. N., Sutherland, P., and Kuusela, M. (2021). Summertime increases in upper-ocean stratification and mixed-layer depth. *Nature*, 591(7851) :592–598. Bandiera_abtest : a Cg_type : Nature Research Journals Number : 7851 Primary_atype : Research Publisher : Nature Publishing Group Subject_term : Physical oceanography Subject_term_id : physical-oceanography.

Sandwell, D. T. and Smith, W. H. F. (1997). Marine gravity anomaly from Geosat and ERS 1 satellite altimetry. *Journal of Geophysical Research : Solid Earth*, 102(B5) :10039–10054. _eprint : https ://agupubs.onlinelibrary.wiley.com/doi/pdf/10.1029/96JB03223.

Sarmiento, J. L., Gruber, N., Brzezinski, M. A., and Dunne, J. P. (2004). High-latitude controls of thermocline nutrients and low latitude biological productivity. *Nature*, 427(6969) :56–60. Number : 6969 Publisher : Nature Publishing Group.

Scagliola, M., Tagliani, N., and Fornari, M. (2013). *MEASURING THE EFFECTIVE ALONG-TRACK RESOLUTION OF CRYOSAT*.

Schaffer, J., Timmermann, R., Arndt, J. E., Kristensen, S. S., Mayer, C., Morlighem, M., and Steinhage, D. (2016). A global, high-resolution data set of ice sheet topography, cavity geometry, and ocean bathymetry. *Earth System Science Data*, 8(2) :543–557. Publisher : Copernicus GmbH.

Schmidtko, S., Heywood, K. J., Thompson, A. F., and Aoki, S. (2014). Multidecadal warming of Antarctic waters. *Science*, 346(6214) :1227–1231. Publisher : American Association for the Advancement of Science Section : Report.

Schubert, R., Thompson, A., Speer, K., Chretien, L., and Bebieva, Y. (2021). The Antarctic Coastal Current in the Bellingshausen Sea. *The Cryosphere*, 15 :4179–4199.

Schulze Chretien, L. M., Thompson, A. F., Flexas, M. M., Speer, K., Swaim, N., Oelerich, R., Ruan, X., Schubert, R., and LoBuglio, C. (2021). The Shelf Circulation of the Bellingshausen Sea. *Journal of Geophysical Research : Oceans*, 126(5) :e2020JC016871. _eprint : https ://onlinelibrary.wiley.com/doi/pdf/10.1029/2020JC016871.

Shen, Q., Wang, H., Shum, C. K., Jiang, L., Hsu, H. T., and Dong, J. (2018). Recent high-resolution Antarctic ice velocity maps reveal increased mass loss in Wilkes Land, East Antarctica. *Scientific Reports*, 8(1) :4477. Number : 1.

Shi, J.-R., Talley, L. D., Xie, S.-P., Liu, W., and Gille, S. T. (2020). Effects of Buoyancy and Wind Forcing on Southern Ocean Climate Change. *Journal of Climate*, 33(23) :10003–10020. Publisher : American Meteorological Society Section : Journal of Climate.

Shimada, K., Aoki, S., Ohshima, K. I., and Rintoul, S. R. (2012). Influence of Ross Sea Bottom Water changes on the warming and freshening of the Antarctic Bottom Water in the Australian-Antarctic Basin. *Ocean Science*, 8(4) :419–432. Number : 4.

Sigmond, M. and Fyfe, J. C. (2014). The Antarctic Sea Ice Response to the Ozone Hole in Climate Models. *Journal of Climate*, 27(3) :1336–1342. Publisher : American Meteorological Society Section : Journal of Climate.

Silvano, A., Foppert, A., Rintoul, S. R., Holland, P. R., Tamura, T., Kimura, N., Castagno, P., Falco, P., Budillon, G., Haumann, F. A., Naveira Garabato, A. C., and Macdonald, A. M. (2020). Recent recovery of Antarctic Bottom Water formation in the Ross Sea driven by climate anomalies. *Nature Geoscience*, 13(12) :780–786. Bandiera_abtest : a Cg_type : Nature Research Journals Number : 12 Primary_atype : Research Publisher : Nature Publishing Group Subject_term : Attribution ;Physical oceanography Subject_term_id : attribution ;physical-oceanography.

Silvano, A., Rintoul, S. R., Kusahara, K., Peña-Molino, B., Wijk, E. v., Gwyther, D. E., and Williams, G. D. (2019). Seasonality of Warm Water Intrusions Onto the Continental Shelf Near the Totten Glacier. *Journal of Geophysical Research : Oceans*, 124(6) :4272–4289. _eprint : https ://agupubs.onlinelibrary.wiley.com/doi/pdf/10.1029/2018JC014634.

Sloyan, B. M. and Rintoul, S. R. (2001). Circulation, Renewal, and Modification of Antarctic Mode and Intermediate Water. *Journal of Physical Oceanography*, 31(4) :1005–1030. Publisher : American Meteorological Society Section : Journal of Physical Oceanography.

Sloyan, B. M., Wanninkhof, R., Kramp, M., Johnson, G. C., Talley, L. D., Tanhua, T., McDonagh, E., Cusack, C., O'Rourke, E., McGovern, E., Katsumata, K., Diggs, S., Hummon, J., Ishii, M., Azetsu-Scott, K., Boss, E., Ansorge, I., Perez, F. F., Mercier, H., Williams, M. J. M., Anderson, L., Lee, J. H., Murata, A., Kouketsu, S., Jeansson, E., Hoppema, M., and Campos, E. (2019). The Global Ocean Ship-Based Hydrographic Investigations Program (GO-SHIP) : A Platform for Integrated Multidisciplinary Ocean Science. *Frontiers in Marine Science*, 6 :445.

Smith, D. C., Lavelle, J. W., and Fernando, H. J. S. (2002). Arctic Ocean mixed-layer eddy generation under leads in sea ice. *Journal of Geophysical Research : Oceans*, 107(C8) :17–1–17–17. _eprint : https ://agupubs.onlinelibrary.wiley.com/doi/pdf/10.1029/2001JC000822.

Smith IV, D. C. and Morison, J. H. (1993). A numerical study of haline convection beneath leads in sea ice. *Journal of Geophysical Research : Oceans*, 98(C6) :10069–10083. _eprint : https ://onlinelibrary.wiley.com/doi/pdf/10.1029/93JC00137.

Sokolov, S. and Rintoul, S. R. (2009a). Circumpolar structure and distribution of the Antarctic Circumpolar Current fronts : 1. Mean circumpolar paths. *Journal of Geophysical Research : Oceans*, 114(C11). _eprint : https ://agupubs.onlinelibrary.wiley.com/doi/pdf/10.1029/2008JC005108.

Sokolov, S. and Rintoul, S. R. (2009b). Circumpolar structure and distribution of the Antarctic Circumpolar Current fronts : 2. Variability and relationship to sea surface height. *Journal of Geophysical Research : Oceans*, 114(C11). _eprint : https ://agupubs.onlinelibrary.wiley.com/doi/pdf/10.1029/2008JC005248.

Speer, K. and Marshall, J. (2012). Closure of the meridional overturning circulation through Southern Ocean upwelling. *Nature Geoscience - NAT GEOSCI*, 5 :171–180.

Speer, K., Rintoul, S. R., and Sloyan, B. (2000). The Diabatic Deacon Cell. *Journal of Physical Oceanography*, 30(12) :3212–3222. Publisher : American Meteorological Society Section : Journal of Physical Oceanography.

Spence, P., Griffies, S. M., England, M. H., Hogg, A. M., Saenko, O. A., and Jourdain, N. C. (2014). Rapid subsurface warming and circulation changes of Antarctic coastal waters by poleward shifting winds. *Geophysical Research Letters*, 41(13) :4601–4610. _eprint : https ://agupubs.onlinelibrary.wiley.com/doi/pdf/10.1002/2014GL060613.

Spence, P., Holmes, R. M., Hogg, A. M., Griffies, S. M., Stewart, K. D., and England, M. H. (2017). Localized rapid warming of West Antarctic subsurface waters by remote winds. *Nature Climate Change*, 7(8) :595–603. Bandiera_abtest : a Cg_type : Nature Research Journals Number : 8 Primary_atype : Research Publisher : Nature Publishing Group Subject_term : Atmospheric dynamics ;Climate and Earth system modelling ;Physical oceanography Subject_term_id : atmospheric-dynamics ;climate-and-earth-system-modelling ;physical-oceanography.

Sprintall, J. (2008). Long-term trends and interannual variability of temperature in Drake Passage. *Progress in Oceanography*, 77(4) :316–330.

Stammer, D. (1998). On Eddy Characteristics, Eddy Transports, and Mean Flow Properties. *Journal of Physical Oceanography*, 28(4) :727–739. Publisher : American Meteorological Society Section : Journal of Physical Oceanography.

Stammer, D. and Cazenave, A. (2018). *Satellite altimetry over oceans and land surfaces*. Earth observation of global changes. CRC press, Taylor & Francis Group, Boca Raton, Fla.

Stewart, A. L., Klocker, A., and Menemenlis, D. (2018). Circum-Antarctic Shoreward Heat Transport Derived From an Eddy- and Tide-Resolving Simulation. *Geophysical Research Letters*, 45(2) :834–845. _eprint : https ://agupubs.onlinelibrary.wiley.com/doi/pdf/10.1002/2017GL075677.

Stewart, A. L., Klocker, A., and Menemenlis, D. (2019). Acceleration and Overturning of the Antarctic Slope Current by Winds, Eddies, and Tides. *Journal of Physical Oceanography*, 49(8) :2043–2074. Publisher : American Meteorological Society Section : Journal of Physical Oceanography.

Stewart, A. L. and Thompson, A. F. (2015). Eddy-mediated transport of warm Circumpolar Deep Water across the Antarctic Shelf Break. *Geophysical Research Letters*, 42(2) :432–440. _eprint : https ://agupubs.onlinelibrary.wiley.com/doi/pdf/10.1002/2014GL062281.

Strong, C. and Rigor, I. G. (2013). Arctic marginal ice zone trending wider in summer and narrower in winter. *Geophysical Research Letters*, 40(18) :4864–4868. _eprint : https ://onlinelibrary.wiley.com/doi/pdf/10.1002/grl.50928.

Sverdrup, H. U. (1947). Wind-Driven Currents in a Baroclinic Ocean ; with Application to the Equatorial Currents of the Eastern Pacific. *Proceedings of the National Academy of Sciences*, 33(11) :318–326. Publisher : National Academy of Sciences Section : Geophysics.

Swart, N. C., Gille, S. T., Fyfe, J. C., and Gillett, N. P. (2018). Recent Southern Ocean warming and freshening driven by greenhouse gas emissions and ozone depletion. *Nature Geoscience*, 11(11) :836–841. Number : 11 Publisher : Nature Publishing Group.

Swart, S., Gille, S. T., Delille, B., Josey, S., Mazloff, M., Newman, L., Thompson, A. F., Thomson, J., Ward, B., du Plessis, M. D., Kent, E. C., Girton, J., Gregor, L., Heil, P., Hyder, P., Pezzi, L. P., de Souza, R. B., Tamsitt, V., Weller, R. A., and Zappa, C. J. (2019). Constraining Southern Ocean Air-Sea-Ice Fluxes Through Enhanced Observations. *Frontiers in Marine Science*, 6 :421.

Taburet, G., Sanchez-Roman, A., Ballarotta, M., Pujol, M.-I., Legeais, J.-F., Fournier, F., Faugere, Y., and Dibarboure, G. (2019). DUACS DT2018 : 25 years of reprocessed sea level altimetry products. *Ocean Science*, 15(5) :1207–1224. Publisher : Copernicus GmbH.

Talley, L. D. (2003). Shallow, Intermediate, and Deep Overturning Components of the Global Heat Budget. *Journal of Physical Oceanography*, 33(3) :530–560. Publisher : American Meteorological Society Section : Journal of Physical Oceanography.

Talley, L. D. (2013). Closure of the Global Overturning Circulation Through the Indian, Pacific, and Southern Oceans : Schematics and Transports. *Oceanography*, 26(1) :80–97. Publisher : Oceanography Society.

Tamsitt, V., Drake, H. F., Morrison, A. K., Talley, L. D., Dufour, C. O., Gray, A. R., Griffies, S. M., Mazloff, M. R., Sarmiento, J. L., Wang, J., and Weijer, W. (2017). Spiraling pathways of global deep waters to the surface of the Southern Ocean. *Nature Communications*, 8(1) :172. Bandiera_abtest : a Cc_license_type : cc_by Cg_type : Nature Research Journals Number : 1 Primary_atype : Research Publisher : Nature Publishing Group Subject_term : Physical oceanography Subject_term_id : physical-oceanography.

Thomas, L. N. (2008). Formation of intrathermocline eddies at ocean fronts by wind-driven destruction of potential vorticity. *Dynamics of Atmospheres and Oceans*, 45(3) :252–273.

Thompson, A. and Heywood, K. (2008). Frontal structure and transport in the northwestern Weddell Sea. *Deep-sea Research Part I-oceanographic Research Papers - DEEP-SEA RES PT I-OCEANOG RES*, 55.

Thompson, A. and Youngs, M. K. (2013). Surface exchange between the Weddell and Scotia Seas.

Thompson, A. F., Heywood, K. J., Schmidtko, S., and Stewart, A. L. (2014). Eddy transport as a key component of the Antarctic overturning circulation. *Nature Geoscience*, 7(12) :879–884. Bandiera_abtest : a Cg_type : Nature Research Journals Number : 12 Primary_atype : Research Publisher : Nature Publishing Group Subject_term : Climate change ;Cryospheric science ;Physical oceanography Subject_term_id : climate-change ;cryospheric-science ;physical-oceanography.

Thompson, A. F. and Sallee, J.-B. (2012). Jets and topography : jet transitions and the impact on transport in the Antarctic Circumpolar Current. *Journal of Physical Oceanography*, 42 :956–972. Publisher : American Meteorological Society.

Thompson, A. F., Stewart, A. L., Spence, P., and Heywood, K. J. (2018). The Antarctic Slope Current in a Changing Climate. *Reviews of Geophysics*, 56(4) :741–770. _eprint : https ://agupubs.onlinelibrary.wiley.com/doi/pdf/10.1029/2018RG000624.

Thompson, D. W. J., Solomon, S., Kushner, P. J., England, M. H., Grise, K. M., and Karoly, D. J. (2011). Signatures of the Antarctic ozone hole in Southern Hemisphere surface climate change. *Nature Geoscience*, 4(11) :741–749. Bandiera_abtest : a Cg_type : Nature Research Journals Number : 11 Primary_atype : Reviews Publisher : Nature Publishing Group Subject_term : Atmospheric science ;Climate change ;Climate-change impacts Subject_term_id : atmospheric-science ;climate-change ;climate-change-impacts.

Thompson, D. W. J. and Wallace, J. M. (2000). Annular Modes in the Extratropical Circulation. Part I : Month-to-Month Variability. *Journal of Climate*, 13(5) :1000–1016. Publisher : American Meteorological Society Section : Journal of Climate.

Thorpe, S., Heywood, K., Stevens, D., and Brandon, M. (2004). Tracking passive drifters in a high resolution ocean model : implications for interannual variability of larval krill transport to South Georgia. *Deep Sea Research Part I : Oceanographic Research Papers*, 51(7) :909–920.

Tilling, R. L., Ridout, A., and Shepherd, A. (2018). Estimating Arctic sea ice thickness and volume using CryoSat-2 radar altimeter data. *Advances in Space Research*, 62(6) :1203–1225.

Timmermans, M.-L., Toole, J., Proshutinsky, A., Krishfield, R., and Plueddemann, A. (2008). Eddies in the Canada Basin, Arctic Ocean, Observed from Ice-Tethered Profilers. *Journal of Physical Oceanography*, 38(1) :133–145. Publisher : American Meteorological Society Section : Journal of Physical Oceanography.

Tran, N., Philipps, S., Poisson, J.-C., Urien, S., Bronner, E., and Picot, N. (2012). Impact of GDR_d standards on SSB corrections.

Treasure, A. M., Roquet, F., Ansorge, I. J., Bester, M. N., Boehme, L., Bornemann, H., Charrassin, J.-B., Chevallier, D., Costa, D. P., Fedak, M. A., Guinet, C., Hammill, M. O., Harcourt, R. G., Hindell, M. A., Kovacs, K. M., Lea, M.-A., Lovell, P., Lowther, A. D., Lydersen, C., McIntyre, T., McMahon, C. R., Muelbert, M. M., Nicholls, K., Picard, B., Reverdin, G., Trites, A. W., Williams,

G. D., and de Bruyn, P. N. (2017). Marine Mammals Exploring the Oceans Pole to Pole : A Review of the MEOP Consortium. *Oceanography*, 30(2) :132–138. Publisher : Oceanography Society.

Trenberth, K. E. (2011). Changes in precipitation with climate change. *Climate Research*, 47(1-2) :123–138.

Trenberth, K. E., Large, W. G., and Olson, J. G. (1990). The Mean Annual Cycle in Global Ocean Wind Stress. *Journal of Physical Oceanography*, 20(11) :1742–1760. Publisher : American Meteorological Society Section : Journal of Physical Oceanography.

Tsamados, M., Feltham, D. L., Schroeder, D., Flocco, D., Farrell, S. L., Kurtz, N., Laxon, S. W., and Bacon, S. (2014). Impact of Variable Atmospheric and Oceanic Form Drag on Simulations of Arctic Sea Ice. *Journal of Physical Oceanography*, 44(5) :1329–1353. Publisher : American Meteorological Society Section : Journal of Physical Oceanography.

Tschudi, M. and CO, U. O. (2016). Polar Pathfinder Daily 25 km EASE-Grid Sea Ice Motion Vectors, Version 3. Type : dataset.

Turner, J., Phillips, T., Hosking, J. S., Marshall, G. J., and Orr, A. (2013). The Amundsen Sea low. *International Journal of Climatology*, 33(7) :1818–1829. _eprint : https ://rmets.onlinelibrary.wiley.com/doi/pdf/10.1002/joc.3558.

Turner, J., Phillips, T., Marshall, G. J., Hosking, J. S., Pope, J. O., Bracegirdle, T. J., and Deb, P. (2017). Unprecedented springtime retreat of Antarctic sea ice in 2016. *Geophysical Research Letters*, 44(13) :6868–6875. _eprint : https ://agupubs.onlinelibrary.wiley.com/doi/pdf/10.1002/2017GL073656.

Ubelmann, C., Fu, L.-L., Brown, S., Peral, E., and Esteban-Fernandez, D. (2014). The Effect of Atmospheric Water Vapor Content on the Performance of Future Wide-Swath Ocean Altimetry Measurement. *Journal of Atmospheric and Oceanic Technology*, 31(6) :1446–1454. Publisher : American Meteorological Society Section : Journal of Atmospheric and Oceanic Technology.

Vernet, M., Geibert, W., Hoppema, M., Brown, P. J., Haas, C., Hellmer, H. H., Jokat, W., Jullion, L., Mazloff, M., Bakker, D. C. E., Brearley, J. A., Croot, P., Hattermann, T., Hauck, J., Hillenbrand, C.-D., Hoppe, C. J. M., Huhn, O., Koch, B. P., Lechtenfeld, O. J., Meredith, M. P., Garabato, A. C. N., Nöthig, E.-M., Peeken, I., Loeff, M. M. R. v. d., Schmidtko, S., Schröder, M., Strass, V. H., Torres-Valdés, S., and Verdy, A. (2019). The Weddell Gyre, Southern Ocean : Present Knowledge and Future Challenges. *Reviews of Geophysics*, 57(3) :623–708. _eprint : https ://agupubs.onlinelibrary.wiley.com/doi/pdf/10.1029/2018RG000604.

Verron, J., Sengenes, P., Lambin, J., Noubel, J., Steunou, N., Guillot, A., Picot, N., Coutin-Faye, S., Sharma, R., Gairola, R. M., Murthy, D. V. A. R., Richman, J. G., Griffin, D., Pascual, A., Rémy, F., and Gupta, P. K. (2015). The SARAL/AltiKa Altimetry Satellite Mission. *Marine Geodesy*, 38(sup1) :2–21. Publisher : Taylor & Francis _eprint : https ://doi.org/10.1080/01490419.2014.1000471.

Vignudelli, S., Kostianoy, A. G., Cipollini, P., and Benveniste, J., editors (2011). *Coastal Altimetry*. Springer-Verlag, Berlin Heidelberg.

Visbeck, M., Marshall, J., Haine, T., and Spall, M. (1997). Specification of Eddy Transfer Coefficients in Coarse-Resolution Ocean Circulation Models. *Journal of Physical Oceanography*, 27(3) :381–402. Publisher : American Meteorological Society Section : Journal of Physical Oceanography.

Wang, G., Hendon, H. H., Arblaster, J. M., Lim, E.-P., Abhik, S., and van Rensch, P. (2019). Compounding tropical and stratospheric forcing of the record low Antarctic sea-ice in 2016. *Nature Communications*, 10(1) :13. Bandiera_abtest : a Cc_license_type : cc_by Cg_type : Nature Research Journals Number : 1 Primary_atype : Research Publisher : Nature Publishing Group Subject_term : Atmospheric science ;Climate sciences ;Cryospheric science Subject_term_id : atmospheric-science ;climate-sciences ;cryospheric-science.

Waugh, D. W., Hogg, A. M., Spence, P., England, M. H., and Haine, T. W. N. (2019). Response of Southern Ocean Ventilation to Changes in Midlatitude Westerly Winds. *Journal of Climate*, 32(17) :5345–5361. Publisher : American Meteorological Society Section : Journal of Climate.

Weatherall, P., Marks, K. M., Jakobsson, M., Schmitt, T., Tani, S., Arndt, J. E., Rovere, M., Chayes, D., Ferrini, V., and Wigley, R. (2015). A new digital bathymetric model of the world's oceans. *Earth and Space Science*, 2(8) :331–345. _eprint : https ://onlinelibrary.wiley.com/doi/pdf/10.1002/2015EA000107.

Whitworth, T., Orsi, A. H., Kim, S.-J., Nowlin, W. D., and Locarnini, R. A. (1985). Water Masses and Mixing Near the Antarctic Slope Front. In *Ocean, Ice, and Atmosphere : Interactions at the Antarctic Continental Margin*, pages 1–27. American Geophysical Union (AGU). _eprint : https ://agupubs.onlinelibrary.wiley.com/doi/pdf/10.1029/AR075p0001.

Williams, G. D., Bindoff, N. L., Marsland, S. J., and Rintoul, S. R. (2008). Formation and export of dense shelf water from the Adélie Depression, East Antarctica. *Journal of Geophysical Research : Oceans*, 113(C4). _eprint : https ://onlinelibrary.wiley.com/doi/pdf/10.1029/2007JC004346.

Wingham, D. J., Francis, C. R., Baker, S., Bouzinac, C., Brockley, D., Cullen, R., de Chateau-Thierry, P., Laxon, S. W., Mallow, U., Mavrocordatos, C., Phalippou, L., Ratier, G., Rey, L., Rostan, F., Viau, P., and Wallis, D. W. (2006). CryoSat : A mission to determine the fluctuations in Earth's land and marine ice fields. *Advances in Space Research*, 37(4) :841–871.

Winton, M., Adcroft, A., Griffies, S. M., Hallberg, R. W., Horowitz, L. W., and Stouffer, R. J. (2013). Influence of Ocean and Atmosphere Components on Simulated Climate Sensitivities. *Journal of Climate*, 26(1) :231–245. Publisher : American Meteorological Society Section : Journal of Climate.

Wouters, B., Martin-Español, A., Helm, V., Flament, T., Wessem, J. M. v., Ligtenberg, S. R. M., Broeke, M. R. v. d., and Bamber, J. L. (2015). Dynamic thinning of glaciers on the Southern Antarctic Peninsula. *Science*, 348(6237) :899–903. Publisher : American Association for the Advancement of Science Section : Report.

Wynn, R. B., Huvenne, V. A. I., Le Bas, T. P., Murton, B. J., Connelly, D. P., Bett, B. J., Ruhl, H. A., Morris, K. J., Peakall, J., Parsons, D. R., Sumner, E. J., Darby, S. E., Dorrell, R. M., and Hunt, J. E. (2014). Autonomous Underwater Vehicles (AUVs) : Their past, present and future contributions to the advancement of marine geoscience. *Marine Geology*, 352 :451–468.

Wåhlin, A. K., Yuan, X., Björk, G., and Nohr, C. (2010). Inflow of Warm Circumpolar Deep Water in the Central Amundsen Shelf. *Journal of Physical Oceanography*, 40(6) :1427–1434. Publisher : American Meteorological Society Section : Journal of Physical Oceanography.

Yamazaki, K., Aoki, S., Shimada, K., Kobayashi, T., and Kitade, Y. (2020). Structure of the Subpolar Gyre in the Australian-Antarctic Basin Derived From Argo Floats. *Journal of Geophysical Research : Oceans*, 125(8) :e2019JC015406. _eprint : https ://onlinelibrary.wiley.com/doi/pdf/10.1029/2019JC015406.

Youngs, M. K., Thompson, A. F., Flexas, M. M., and Heywood, K. J. (2015). Weddell Sea Export Pathways from Surface Drifters. *Journal of Physical Oceanography*, 45(4) :1068–1085. Publisher : American Meteorological Society Section : Journal of Physical Oceanography.

Zhang, Y., Chambers, D., and Liang, X. (2021). Regional Trends in Southern Ocean Eddy Kinetic Energy. *Journal of Geophysical Research : Oceans*, 126(6) :e2020JC016973. _eprint : https ://agupubs.onlinelibrary.wiley.com/doi/pdf/10.1029/2020JC016973.

Zhang, Z., Wang, W., and Qiu, B. (2014). Oceanic mass transport by mesoscale eddies. *Science*, 345(6194) :322–324. Publisher : American Association for the Advancement of Science.

Zhao, M., Timmermans, M.-L., Cole, S., Krishfield, R., Proshutinsky, A., and Toole, J. (2014). Characterizing the eddy field in the Arctic Ocean halocline. *Journal of Geophysical Research : Oceans*, 119(12) :8800–8817. _eprint : https ://onlinelibrary.wiley.com/doi/pdf/10.1002/2014JC010488.

Zhao, M., Timmermans, M.-L., Cole, S., Krishfield, R., and Toole, J. (2016). Evolution of the eddy field in the Arctic Ocean's Canada Basin, 2005–2015. *Geophysical Research Letters*, 43(15) :8106–8114. _eprint : https ://onlinelibrary.wiley.com/doi/pdf/10.1002/2016GL069671.

Zika, J. D., Gregory, J. M., McDonagh, E. L., Marzocchi, A., and Clément, L. (2021). Recent Water Mass Changes Reveal Mechanisms of Ocean Warming. *Journal of Climate*, 34(9) :3461–3479. Publisher : American Meteorological Society Section : Journal of Climate.